Acta Universitatis Tamperensis 2227

ANNI SORKIO

Biomaterial Substrates and Transplantation Materials for Human Embryonic Stem Cell Derived Retinal Pigment Epithelial Cells

Biomimetic approaches for retinal tissue engineering

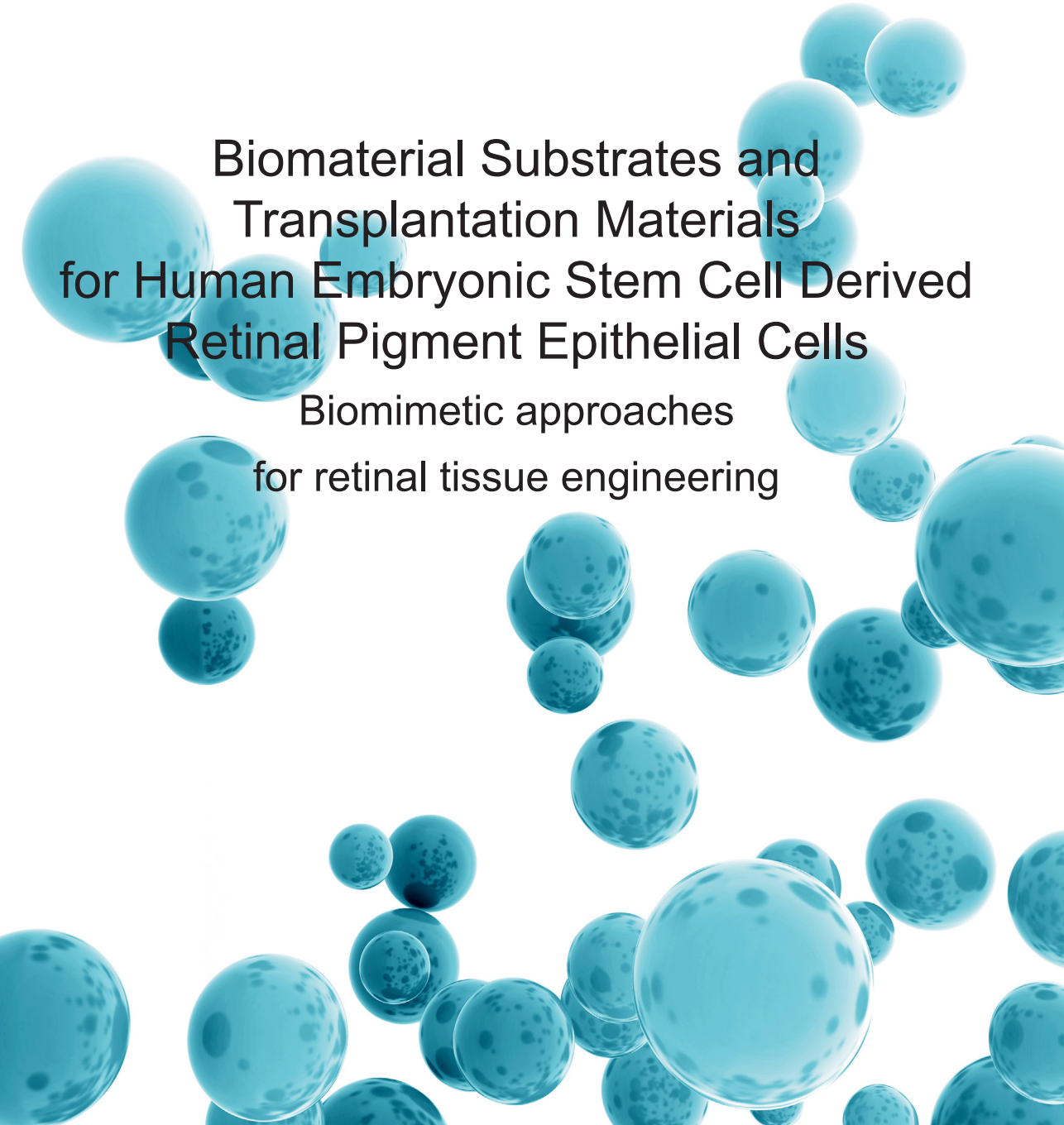

ANNI SORKIO

Biomaterial Substrates and Transplantation Materials for Human Embryonic Stem Cell Derived Retinal Pigment Epithelial Cells

Biomimetic approaches for retinal tissue engineering

■

ACADEMIC DISSERTATION
To be presented, with the permission of
the Board of the BioMediTech of the University of Tampere,
for public discussion in the auditorium F114 of the Arvo building,
Lääkärinkatu 1, Tampere,
on 2 December 2016, at 12 o'clock.

UNIVERSITY OF TAMPERE

ANNI SORKIO

Biomaterial Substrates and Transplantation Materials for Human Embryonic Stem Cell Derived Retinal Pigment Epithelial Cells

Biomimetic approaches for retinal tissue engineering

Acta Universitatis Tamperensis 2227
Tampere University Press
Tampere 2016

UNIVERSITY OF TAMPERE

ACADEMIC DISSERTATION
University of Tampere, BioMediTech
Finland

Supervised by
Associate Professor Heli Skottman
University of Tampere
Finland
Docent Kati Juuti-Uusitalo
University of Tampere
Finland

Reviewed by
Adjuct Professor Joachim Loo
Nanyang Technological University
Singapore
Adjuct Professor Aki Manninen
University of Oulu
Finland

The originality of this thesis has been checked using the Turnitin OriginalityCheck service in accordance with the quality management system of the University of Tampere.

Cover design by
Mikko Reinikka

Acta Universitatis Tamperensis 2227
ISBN 978-952-03-0266-5 (print)
ISSN-L 1455-1616
ISSN 1455-1616

Acta Electronica Universitatis Tamperensis 1727
ISBN 978-952-03-0267-2 (pdf)
ISSN 1456-954X
http://tampub.uta.fi

Suomen Yliopistopaino Oy – Juvenes Print
Tampere 2016

Table of contents

Abstract

The retinal pigment epithelium (RPE) is a monolayer of polarized and pigmented cells that resides between the neural retina and the choroid. Together with the underlying Bruch's membrane, the RPE has a pivotal role in the proper function, homeostasis and survival of the adjacent retinal photoreceptors. Irreversible damage and loss of the RPE is a fundamental factor in the development of degenerative retinal diseases such as age-related macular degeneration (AMD). In AMD, degeneration of the RPE and photoreceptors in the macular area of central vision lead to a gradual loss of visual acuity and eventually blindness. Currently, there is no treatment for the dry form of AMD. However, replacement of the dysfunctional and damaged RPE with a population of healthy cells is considered as a potential therapeutic strategy for AMD and related diseases. Cell transplants of human embryonic stem cell derived RPE (hESC-RPE) cells have shown potential for these cell therapies in animal models and are currently investigated in clinical setting.

An approach where cells are delivered to the subretinal space as a sheet on a biomaterial substrate, has shown improved cell survival upon transplantation. Several biomaterial substrates have been investigated as prospective carriers for RPE, but they often fail to fulfill the requirements set for subretinal implantation. Importantly, these substrates do not mimic the composition and structure of Bruch's membrane, the natural environment of the RPE, which might affect their capacity to differentiate *in vitro* and subsequent performance in cell transplantation. Moreover, the majority of currently used biomaterial substrates contain animal-derived products. In addition, testing of these substrates is usually carried out with immortalized cells lines under culture conditions not suitable for clinical production.

The work presented in this dissertation aimed at finding and developing biomaterial substrates for hESC-RPE cells that bear a resemblance to the native microenvironment of the RPE. A special focus was paid to exploring biomaterial substrates of human or synthetic origin that would support the formation of mature hESC-RPE in serum-free culture conditions. Consequently, three approaches were developed to fabricate a biomimetic environment for hESC-RPE *in vitro*. To begin with, the role of several human extracellular matrix (ECM) proteins found in the Bruch's membrane and commercial basement membrane matrices was evaluated in

adherent hESC-RPE cell differentiation and maturation cultures under serum-free conditions. Although there were no significant differences between the studied protein coatings in early-stage differentiation, the protein coatings had a major effect on the structure, function and basal lamina production of hESC-RPE cells upon further maturation of the cultures.

Thereafter, a biomimetic microenvironment simulating the layered structure of the Bruch's membrane was fabricated with Langmuir-Schaefer technology from human derived collagens for the production of hESC-RPE cells. Only biocompatible components were involved in the manufacturing process. A thorough characterization of the substrate demonstrated that the fabricated collagen films had a layered structure with oriented fibers resembling the architecture of the two uppermost layers of Bruch's membrane. Furthermore, the fabricated collagen films were superior in supporting hESC-RPE cell maturation and functionality compared to collagen IV dip-coated controls in serum-free culture conditions.

Finally, biodegradable biomaterial substrates were fabricated from synthetic polymer with an electrospinning method. The substrates were surface modified and coated with an additional collagen layer to increase hESC-RPE cell adhesion and maturation. The fabricated substrates consisted of unaligned fibers and were permeable for small molecular weight substance. Thus, these substrates bore a resemblance to the fibrous structure of Bruch's membrane. Moreover, these biodegradable surface modified biomaterial substrates supported the formation of functional hESC-RPE in serum-free culture medium, therefore demonstrating the potential of biomaterial substrates for subretinal transplantation.

In conclusion, this dissertation has increased understanding of hESC-RPE cell interaction and performance on biomaterial substrates. Moreover, the results of this dissertation offer a range of methods to provide a biomimetic environment for the *in vitro* production of hESC-RPE cells without the use of animal-derived substrates and serum. These results can be exploited in future applications and biomaterial design for the retinal tissue engineering field.

Tiivistelmä

Verkkokalvon pigmenttiepiteeli (retinal pigment epithelium, RPE) on tiivis yksikerroksinen epiteelisolukerros, joka sijaitsee silmän takaosassa verkkokalvon ja suonikalvon välissä. RPE:llä ja sen alapuolella sijaitsevalla tukirakenteella, Bruchin kalvolla, on merkittävä tehtävä ylläpitää verkkokalvon toimintoja. Peruuttamattomat vauriot RPE:n toiminnassa johtavat asteittaiseen näkökyvyn heikkenemiseen ja lopulta sokeutumiseen verkkokalvon rappeumasairauksissa kuten verkkokalvon ikärappeumassa. Tällä hetkellä verkkokalvon ikärappeuman kuivaan muotoon ei ole olemassa parantavaa hoitokeinoa. Solusiirtoa, jossa vaurioituneet RPE-solut korvataan terveillä toiminnallisilla soluilla, pidetään mahdollisena tulevaisuuden hoitokeinona verkkokalvon rappeumasairauksiin. Ihmisen alkion kantasoluista erilaistetut RPE-solut (hESC-RPE) ovat osoittautuneet lupaavaksi solulähteeksi näihin solusiirtoihin eläinkokeissa ja ovat parhaillaan tutkimuksen kohteena ensimmäisissä kliinisissä hoitokokeissa.

RPE-solujen siirtämisen tiiviinä yksisolukerroksena tukirakenteen päällä on todettu auttavan solusiirteen selviytymistä ja sopeutumista vaurioituneelle verkkokalvon alueella. Useita biomateriaali-kasvualustoja on tutkittu mahdollisina tukirakenteina RPE-soluille, mutta nämä aiemmin ehdotetut rakenteet harvoin täyttävät tukirakenteelle asetettuja vaatimuksia. Lisäksi, nämä kasvualustat eivät muistuta koostumukseltaan RPE-solujen luontaista ympäristöä, Bruchin kalvoa, mikä saattaa vaikuttaa solujen tuotantoon laboratoriossa sekä solujen toimintakykyyn solusiirroissa. Useat tutkituista kasvualuista sisältävät myös ihmiselle vieraita aineita, ja kasvualustojen testaukset tehdään pääosin kaupallisilla kuolemattomiksi tehdyillä solulinjoilla kliiniseen käyttöön soveltumattomissa olosuhteissa.

Tämän väitöskirjatutkimuksen tavoitteena oli kehittää biomateriaalipohjaisia kasvualustoja hESC-RPE soluille. Tutkimuksessa keskityttiin kehittämään ihmisperäisiä ja synteettisiä kasvualustoja, jotka muistuttavat RPE-solujen luontaista ympäristöä silmässä ja tukevat hESC-RPE solujen kasvua seerumittomissa viljelyolosuhteissa. Tavoitetta lähestyttiin kolmella eri tavalla. Ensiksi tutkittiin useita ihmisen Bruchin kalvon luontaisia proteiinipinnoitteita sekä kaupallisia soluviljelypinnoitteita hESC-RPE solujen kasvatusalustana solujen erilaistuksessa sekä kypsymisessä. Siitä huolimatta, että hESC-RPE solujen alkuvaiheen

erilaistuksessa ei löydetty eroja eri proteiinipinnoitteiden välillä, solujen kypsyessä proteiinipinnoitteiden huomattiin vaikuttavan merkittävästi solujen rakenteeseen, toimintaan sekä soluväliaineproteiinien tuotantoon.

Seuraavaksi Bruchin kalvon rakennetta ja koostumusta jäljittelevä kasvualusta tehtiin ihmisperäisistä kollageeneista Langmuir-Schaefer (LS) tekniikalla. Valmistuksessa käytettiin vain bioyhteensopivia ainesosia. LS-kalvojen kerroksittainen ja kuitumainen rakenne muistutti Bruchin kalvon RPE:n läheisen kerroksen rakennetta. Lisäksi LS-kalvot tukivat paremmin hESC-RPE solujen kypsymistä ja toiminnallisuutta seerumittomissa viljelyolosuhteissa pelkkään proteiinipinnoitteiseen verrattuna.

Viimeiseksi tässä väitöskirjatyössä valmistettiin biohajoava siirtomateriaali hESC-RPE soluille synteettisestä polymeeristä sähkökehruutekniikalla. Valmistettu siirtomateriaali pintakäsiteltiin ja päällystettiin kollageeni-proteiinipinnoituksella hESC-RPE solujen kiinnittymisen ja kypsymisen edistämiseksi. Nämä biohajoavat siirtomateriaalit koostuivat satunnaisesti järjestäytyneistä säikeistä ja läpäisivät pienimolekyylistä yhdistettä. Materiaalien säiemäinen ja huokoinen rakenne muistutti Bruchin kalvon rakennetta. Pintamuokatut ja proteiini pinnoitetut biohajoavat siirtomateriaalit tukivat toiminnallisen hESC-RPE:n muodostumista seerumittomassa viljely-ympäristössä, minkä vuoksi nämä ovat lupaavia tukirakenteita verkkokalvon kudosteknologisiin sovelluksiin.

Tämä väitöskirjatyö on tuonut merkittävästi lisätietoa hESC-RPE solujen vuorovaikutuksesta biomateriaali-kasvualustoilla. Tässä työssä esitetään useita lupaavia tekniikoita biomimeettisen ympäristön valmistukseen hESC-RPE solujen *in vitro*-tuotantoa varten. Lisäksi, tässä väitöskirjassa esiteltyjen töiden tuloksia voidaan hyödyntää biomateriaalirakenteiden suunnittelussa ja soluterapia sovelluksissa verkkokalvon kudosteknologiassa.

List of original publications

The present thesis is based on the following publications, which are referred to in the text by their Roman numerals (**I-III**)

I **Sorkio A**, Hongisto H, Kaarniranta K, Uusitalo H, Juuti-Uusitalo K, Skottman H. Structure and barrier properties of human embryonic stem cell-derived retinal pigment epithelial cells are affected by extracellular matrix protein coating. Tissue Engineering Part A 2014, 20(3):622-634.

II **Sorkio A**, Vuorimaa-Laukkanen E, Hakola H, Liang H, Ujula T, Valle-Delgado J, Österberg M, Yliperttula M, Skottman H. Biomimetic collagen I and IV double layer Langmuir-Schaefer films as microenvironment for human pluripotent stem cell derived retinal pigment epithelial cells. Biomaterials 2015, 51:257-269.

III **Sorkio A***, Porter P*, Juuti-Uusitalo K, Meenan B, Skottman H, Burke G. Surface modified biodegradable electrospun membranes as a carrier for human embryonic stem cell derived retinal pigment epithelial cells. Tissue Engineering Part A 2015, 21(17-18):2301-14.

*Authors contributed equally

This dissertation contains unpublished data, indicated separately in the text.

List of abbreviations

AFM	Atomic force microscopy
AMD	Age-related macular degeneration
BAM	Brewster angle microscopy
BEST	Bestrophin
bFGF	Basic fibroblast growth factor
BRB	Blood retinal barrier
cGMP	Current good manufacturing practice
Col I	Collagen I
Col IV	Collagen IV
CS	CELLStart™
CRALBP	Retinaldehyde binding protein 1
DAPI	4´, 6´diamidino-2-phenylidole
DBD	Dielectric barrier discharge
DPBS	Dulbecco's phosphate buffered saline
EB	Embryoid body
ECM	Extracellular matrix
ELISA	Enzyme-linked immunosorbent assay
ELR-RGD	Bioactive RGD-containing elastin-like recombinamer
ERK/MAPK	Extracellular signal-related-kinase/mitogen-activated protein kinase
ePTFE	Expanded polytetrafluoroethylene
FAK	Focal adhesion kinase
FDA	Food and drug administration
FN	Fibronectin protein coating
FTIR	Fourier Transform Infrared Spectroscopy
GAPDH	Glyceraldehyde 3-phosphate dehydrogenase
hESC	Human embryonic stem cell
hESC-RPE	Human embryonic stem cell derived retinal pigment epithelium
hiPSC	Human induced pluripotent stem cell

hiPSC-RPE	Human induced pluripotent stem cell derived retinal pigment epithelium
hPSC	Human pluripotent stem cell
IF	Immunofluorescence
IPAAm	N-isopropylacrylamide monomer
KO-SR	KnockOut™ Serum replacement
LB	Langmuir-Blodgett
LN	Laminin protein coating
LS	Langmuir-Schaefer
MERTK	Mer tyrosine kinase receptor
MITF	Microphthalmia-associated transcription factor
MG	Matrigel™ coating
Na^+/K^+ATPase	Sodium/Potassium-transporting ATPase
Nanog	Nanog homeobox
NC-1	Non-collagenous1 domain
OCT3/4	Octamer-binding transcription factor
PAX6	Paired box gene 6
PEDF	Pigment epithelium derived factor
PCL	Poly(ε-caprolactone)
PEG	Poly(ethylene glycol)
PET	Polyethylene terephthalate
PHBV8	Poly(hydroxybutyrate-co-hydroxyvaleric acid)
PDLLA	Poly(D,L-lactic acid)
PDMS	Polydimethylsiloxane
PI	Polyimide
PLA	Polylactide
PLDLA	Poly L-lactide/D-lactide copolymer
PLGA	Poly(D,L-lactic-co-glycolic acid)
PLLA	Poly(L-lactic acid)
PLCL	Poly(L-lactide-co-caprolactone)
P(MMA-co-PEG)	Poly(ethylene glycol) methacrylate
POS	Photoreceptor outer segments
PTMC	Poly(trimethylene carbonate)
qPCR	Quantitative real-time polymerase chain reaction
RPE	Retinal pigment epithelium
rhLN-521	Recombinant human laminin-521
RhoA/ROCK	Rho-associated coiled-coil protein kinase

RPE65	Retinal pigment epithelium-specific protein 65 kDa
RT	Room temperature
RT-PCR	Reverse transcription-polymerase chain reaction
SEM	Scanning electron microscopy
SPR	Surface plasmon resonance
TEM	Transmission electron microscopy
TER	Transepithelial resistance
TYR	Tyrosinase
VEGF	Vascular endothelial growth factor
VN	Vitronectin protein coating
WB	Western blotting
XPS	X-ray photoelectron spectroscopy
ZO-1	Zonula occludens protein 1

1 Introduction

Vision is a prerequisite for a good life quality and independence. Diseases affecting vision substantially reduce the patient's quality of life and cause an economic burden for society. The retinal pigment epithelium (RPE) is a monolayer of densely pigmented cells located at the interface between the neural retina and choroid. The RPE has a vital role for the healthy homeostasis and proper function of the retina. Dysfunction and irreversible damage of the RPE leads to death of photoreceptors and gradual loss of central vision in retinal degenerative diseases, such as age-related macular degeneration (AMD). At present, there is no cure for the dry form of AMD. (Ambati & Fowler, 2012; Simo et al., 2010)

A cell therapy approach wherein diseased and degenerated RPE cells are replaced with a population of healthy cells is considered a promising treatment for degenerative retinal diseases. Human pluripotent stem cells (hPSCs), including human embryonic stem cells (hESCs) and human induced pluripotent stem cells (hiPSCs), provide an excellent cell source for these therapies due to their limitless supply and ability to differentiate towards functional RPE cells (Idelson et al., 2009; Klimanskaya et al., 2004; Plaza Reyes et al., 2016). Cell transplants of hESC- and hiPSC-RPE cells are currently undergoing clinical trials to treat AMD and related diseases (Kamao et al., 2014; Nazari et al., 2015; Schwartz et al., 2012; Schwartz et al., 2016).

Cells in tissues are influenced by their surrounding microenvironment (Barthes et al., 2014). Successful manufacturing of RPE cells requires reproducing their natural environment as closely as possible (Hotaling et al., 2016). Moreover, efficient production of functional and mature hPSC-RPE cells *in vitro* is necessary for their further clinical use (Hu et al., 2012). A tissue engineering approach where hPSC-RPE cells are delivered to the subretinal space as a monolayer sheet on a supportive biomaterial substrate has shown improved cell survival compared to transplantation of cells in suspension (Diniz et al., 2013). Several natural and synthetic biomaterial substrates have been studied as potential substrates for the production of RPE cells and subsequent transplantation (Lu et al., 2014; Subrizi et al., 2012; Thumann et al., 2009; Treharne et al., 2012). However, the biomaterial substrates currently used *in vitro* and *in vivo* for the most part fail to mimic the natural environment of the RPE.

Thus, the environmental cues received by the cells *in vitro* differ from the cues they receive *in vivo*, which could possibly affect the performance of the produced cells in transplantations (McCarthy et al., 1996).

As the field of retinal tissue engineering progresses, so will the demand for hPSC-RPE production to be carried out under defined conditions devoid of animal derived products (Pennington & Clegg, 2016). Especially the use of xenomaterial such as bovine serum and Matrigel™ is of particular concern when developing cellular therapies for retinal degenerative diseases (Bharti et al., 2014). Yet, testing of the potential biomaterial substrates for RPE production and transplantation is frequently carried out with animal-derived biomaterial components in serum-containing culture environment (Lu et al., 2014; Xiang et al., 2014).

The work presented in this dissertation aimed at finding and developing biomaterial substrates and transplantation materials for hESC-RPE cells that bear a resemblance to the native microenvironment of the RPE. A special focus was paid on finding biomaterial substrates with human or synthetic origin that would support the formation of hESC-RPE in serum-free culture conditions. The hypothesis throughout the studies was that substrates mimicking the composition and structure of Bruch's membrane, the natural environment of the RPE, would be superior for efficient production of hESC-RPE cells.

2 Literature review

2.1 The retinal pigment epithelium

The human eye is a complex and highly organized organ with several layers of distinct cells from epithelial, mesenchymal, connective and neural tissue. The lens focuses light to the back of the eye to the light-sensitive retina, which converts energy from the absorbed photons into neural activity (Bharti et al., 2011) (Figure 1).

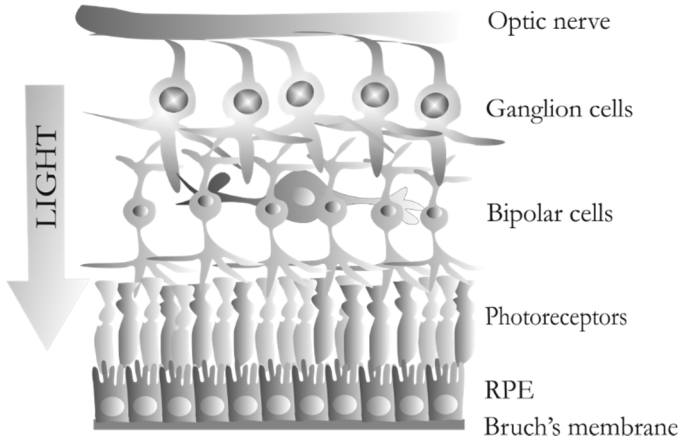

Figure 1. Structure of the human retina.

The retinal pigment epithelium (RPE) is a monolayer of densely pigmented cells located at the interface between the neural retina and choroid (Figure 2). It originates from the neuroectoderm and is therefore considered to be part of the retina (Fuhrmann et al., 2014). The RPE has an essential role in the maintenance of visual function. Together with Bruch's membrane and the choriocapillaris it forms the outer blood retinal barrier (BRB) (Rizzolo, 2014). The RPE displays anatomic features of a typical epithelium with hexagonal cell morphology in surface view and tightly packed columnar cells. Moreover, organelles and cytoskeletal elements are localized to specific sub-cellular positions along the apico-basal axis. Long apical microvilli of the RPE interact with the photoreceptor outer segments (POS) whereas

the folded basolateral membrane is attached to the Bruch's membrane (Burke, 2008; Simo et al., 2010; Strauss, 2005).

The principal function of the RPE is to form a dynamic barrier: it controls the reciprocal exchange of ions, nutrients, water and metabolites between the neural retina and the underlying choroid (Rizzolo et al., 2011; Rizzolo, 2014). RPE is classified as a tight epithelium due to the junctions between the RPE cells that form high paracellular resistance (Strauss, 2005). These tight junctions are fundamental components of the BRB and regulate diffusion through paracellular space in a semi-selective manner. Apart from paracellular diffusion, solutes can enter via transcellular facilitated diffusion, transcellular active transport, transcytosis and metabolic processing (Rizzolo, 2014; Wimmers et al., 2007). Sodium/Potassium-transporting ATPase (Na^+/K^+ATPase) provides energy for the transcellular transport and it is located in the apical membrane of the RPE (Rizzolo, 1999; Wimmers et al., 2007). Tight junctions form an apical junctional complex which encircles the cells throughout the epithelium. In RPE, the main components of these tight junctions include zonula occludens protein 1 (ZO-1), Claudin-19, Claudin-3 and N-cadherin (Peng et al., 2011; Peng et al., 2013).

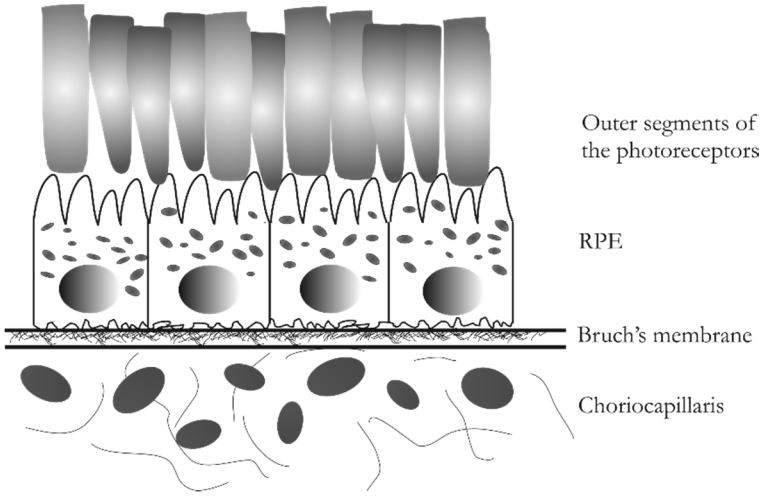

Figure 2. The human retinal pigment epithelium.

The RPE increases the optical quality of the eye by absorption of the scattered light. For this, RPE cells contain various pigments, such as melanin and lipofuscin, which are specialized to different wavelengths. Moreover, general light absorption in the RPE is mediated via melanin in pigmented granules referred to as melanosomes (Strauss, 2005). In human retina, vision is initiated and maintained by

light sensitive photoreceptors. However, the cyclical process involved in visual cycle highly depends on the interaction between the photoreceptors and the RPE. Photoreceptors lack *cis-trans* isomerase function for retinal and are unable to regenerate all-*trans*-retinal into 11-*cis*-retinal. This reisomerization of 11-cis-retinal is performed by the RPE. The retinal pigment epithelium-specific protein 65 kDa (RPE65) mediates this regeneration of all-*trans*-retinal back to its photoactive 11-*cis*-retinal form inside RPE (Simo et al., 2010; Strauss, 2005).

POS undergo a constant renewal to maintain light transduction capacity of the photoreceptors. One of the key functions of the RPE is to phagocytose shed POS (Mazzoni et al., 2014). In the RPE, these POS are digested to essential molecules and redelivered to the photoreceptors for further use and new POS formation (Simo et al., 2010). Phagocytosis in RPE is regulated by Mer tyrosine kinase (MERTK) and αVβ5-integrin receptors, both of which reside on the apical membrane of the RPE (D'Cruz et al., 2000; Nandrot et al., 2012). Besides phagocytic activity, the RPE secretes numerous vital factors for the maintenance of the healthy homeostasis and structure of the retina, such as pigment-epithelium-derived factor (PEDF) and vascular endothelial growth factor (VEGF). PEDF has been shown to have neuroprotective as well as antiangiogenic properties, whereas VEGF is a vasoactive factor preventing endothelial cell apoptosis. According to their functions, PEDF is secreted mainly from the apical side of the RPE, whereas most of the VEGF secretion is basal. (Becerra et al., 2004; Blaauwgeers et al., 1999)

Due to RPE's significant role in the proper functioning of the retina, a failure of one or more of these functions can result in retinal degeneration and visual impairment. Age-related macular degeneration (AMD) is the leading cause of visual loss among the elderly population worldwide (Lim et al., 2012). AMD is a progressive eye disease with two phenotypes: dry (atrophic) and wet (neovascular) form (Ambati & Fowler, 2012). Dry form of AMD is characterized by progressive atrophy of the RPE, choriocapillaris and photoreceptors, whereas in neovascular AMD choroidal neovascularisation breaks through to the neural retina causing leaking of fluid, lipids, and blood, as well as fibrous scarring (Ambati & Fowler, 2012; Lim et al., 2012). Degeneration of RPE and adjacent photoreceptors in the macular area leads to the loss of central vision (Carr et al., 2013). The pathology behind AMD is a combination of multiple factors: changes in the Bruch's membrane structure, drusen formation, and degeneration of the RPE result in loss of function in the photoreceptor cells and gradual decrease in vision acuity (Lim et al., 2012).

The current treatments for AMD, including laser photocoagulation, photodynamic therapy and anti-VEGF therapy, are mostly palliative and aim to delay

disease progression of the neovascular form of AMD (Gehrs et al., 2006). Even though anti-VEGF therapies with therapeutic agents such as ranibizumab have been shown to significantly reduce vision loss in patients suffering from neovascular AMD (Rosenfeld et al., 2006), there are currently no effective treatments or cures for the atrophic form of AMD (Ambati & Fowler, 2012).

2.2 Bruch's membrane

In the eye, RPE cells rest on a thin pentalaminar extracellular matrix (ECM) structure called Bruch's membrane (Figure 2). Bruch's membrane is strategically located between the RPE and the underlying choroid and has a thickness of 2-4 μm in the young. Histologically, Bruch's membrane is composed of five different layers with unique structure and composition (Booij et al., 2010) (Figure 3). The outermost layer of Bruch's membrane is called the basement membrane of the RPE. This 0.14-0.15 μm thick fiber mesh network contains mainly collagen IV, laminin, fibronectin, heparan sulfate and chondroitin sulfate. Inner collagenous layer of Bruch's membrane consists of 60-70 nm diameter striated fibers of Collagens I, III and V, which are organized in a grid-like manner. Besides collagens, this 1.4 μm thick layer is embedded with interacting biomolecules, such as negatively charged proteoglycans heparan sulfate and chondroitin/dermatan sulfate (Curcio & Johnson, 2013). Thereafter, the 0.8 μm thick elastin layer is formed by stacked layers of elastin together with collagen VI, fibronectin and other proteins. The outer collagenous layer has a similar molecular composition to its inner equivalent, but is only 0.7 μm thick. The final layer of Bruch's membrane, the basement membrane of the choroid, is a discontinuous structure which is mainly composed of laminin, heparan sulfate and collagens type IV, V and VI (Booij et al., 2010). The schematic illustration of Bruch's membrane structure is presented in Figure 3.

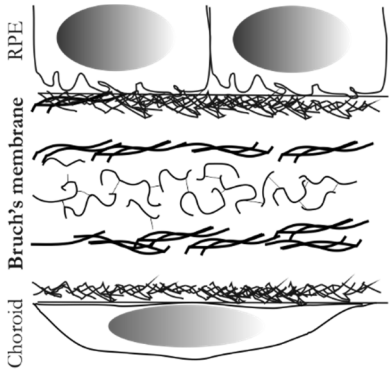

Layer:	Main components:
Basement membrane of the RPE	Collagen IV, laminin, fibronectin
Inner collagenous layer	Collagen I, III, V
Elastin layer	Elastin, collagen VI, fibronectin
Outer collagenous layer	Collagen I, III, V
Basement membrane of the choroid	Laminin, heparan sulphate, collagen IV, V, VI

Figure 3. A schematic illustration of the structure and main components of the human Bruch's membrane layers.

Bruch's membrane has a remarkable role in the proper function and homeostasis of the retina. Firstly, Bruch's membrane acts as a semi-permeable filter for the reciprocal exchange of biomolecules, nutrients, oxygen, fluids and metabolic waste products between the retina and the underlying choroid. Diffusion across the Bruch's membrane is mainly passive, and depends on the composition of the membrane, hydrostatic pressure, as well as the concentration, size and lipophilicity of the biomolecules (Booij et al., 2010; Zayas-Santiago et al., 2011). Secondly, Bruch's membrane provides structural support for RPE cell attachment, migration and differentiation (Del Priore & Tezel, 1998; Gong et al., 2008). Lastly, Bruch's membrane forms a division barrier, preventing cell migration between the retina and the choroid (Booij et al., 2010).

The structure and composition of Bruch's membrane undergo changes with increasing age. Thickening of the membrane, lower filtration capacity, increased crosslinking of collagen fibers, calcification of elastic fibers, lipid accumulation, as well as higher turnover of glycosaminoglycans have been associated with Bruch's membrane during ageing (Curcio & Johnson, 2013; Ramrattan et al., 1994). These age-related structural changes can further progress into AMD pathology through complement activation or neovascularization (Booij et al., 2010; Heller & Martin, 2014). In addition to changes in the Bruch's membrane structure, drusen deposits, accumulate between RPE and Bruch's membrane (Crabb et al., 2002). Moreover, studies have revealed that old or damaged Bruch's membrane does not support RPE cell attachment and proper function (Gullapalli et al., 2005). In AMD patients, Bruch's membrane no longer supports the normal functions of RPE cells, resulting in degeneration of the adjacent photoreceptors and the retina (Del Priore et al., 2006).

2.3 Human pluripotent stem cell derived RPE

Human pluripotent stem cells (hPSCs) have outstanding proliferative and developmental capacity and therefore show great promise for cell therapies, disease modelling and drug discovery. Human embryonic stem cells (hESCs) can be derived from the inner cell mass of the preimplantation embryos (Thomson et al., 1998), whereas human induced pluripotent stem cells (hiPSCs) are generated by reprogramming human somatic cells by transcription factors (Takahashi et al., 2007). Both hESCs and hiPSCs can be expanded indefinitely *in vitro* and have the capability to differentiate towards mature cell types of any germ layer (Takahashi et al., 2007; Thomson et al., 1998).

Two fundamentally different approaches have been introduced for RPE differentiation from hPSCs: spontaneous differentiation and directed differentiation (Pennington & Clegg, 2016). Several studies have demonstrated spontaneous differentiation of hPSCs into RPE in adherent cultures as well as in 3-dimensional suspension cultures as embryoid bodies (Carr et al., 2009; Klimanskaya et al., 2004; Lund et al., 2006; Rowland et al., 2013). Spontaneous differentiation is induced by altering the molecular cues, for example removing basic fibroblast growth factor (bFGF), that are essential for maintenance of hPSC pluripotency *in vitro*. Thereafter, pigmented patches of RPE appear in cultures and can be further manually selected and enriched to obtain a purer population of RPE cells. However, this method requires from several weeks up to a few months of culture to obtain sufficient amounts of pigmented cells and suffers from poor efficiency (Rowland et al., 2012; Vaajasaari et al., 2011).

Directed differentiation of RPE cells from hPSCs recapitulates the natural signaling mechanisms occurring during *in vivo* development of the RPE. First, stem cell differentiation is guided towards neuroectoderm using factors such as nicotinamide, dickkopf-related protein 1, Lefty-A, noggin, N2 and B27 (Buchholz et al., 2013; Idelson et al., 2009; Lane et al., 2014; Reh et al., 2010; Vaajasaari et al., 2011). Thereafter, molecules such as Activin-A and a fibroblast growth factor inhibitor SU5402 promote differentiation towards RPE instead of neural retina (Buchholz et al., 2013; Idelson et al., 2009). In a recent study, directed differentiation was shown to be a more reliable method to differentiate RPE cells from various hPSC sources when compared with spontaneous differentiation (Leach et al., 2016).

Specific concerns exist with the use of animal-derived xenomaterial such as fetal bovine serum, Matrigel™, feeder cells, and growth factors in clinical settings (Bharti et al., 2014). Incorporating animal-derived products for hPSC-RPE cell production

contains a risk of transmitting non-human factors and virus components that can elicit an immune response upon transplantation (O'Connor, 2013; Vukicevic et al., 1992). Nevertheless, in clinical applications most of the current hPSC-RPE differentiation methods involve xeno-derived substrates such as Matrigel™ or porcine gelatin (Kamao et al., 2014; Schwartz et al., 2012). Recently, a xeno-free and defined differentiation method of hESC-RPE cells has been developed. This protocol uses recombinant human laminins as a substrate for differentiation. Nevertheless, also here Matrigel™ was used for maintaining undifferentiated hESCs (Plaza Reyes et al., 2016). In addition, a xeno-free commercial substrate Synthemax II-SC has been shown to support hESC maintenance as well as hESC-RPE differentiation and thus provides a potential alternative for the use of Matrigel™ in retinal tissue engineering applications (Pennington et al., 2015).

Several recent studies have demonstrated that hPSC-RPE cells express characteristics and function similar to the native RPE (Buchholz et al., 2013; Kamao et al., 2014; Leach et al., 2016). Previous comparative studies have reported that hPSC-RPE cells demonstrate a closer resemblance to human fetal RPE cells compared to human adult RPE cells (Klimanskaya et al., 2004; Liao et al., 2010). In contrast, in one study hiPSC-RPE cells showed gene expression profile closer to human adult RPE cells rather than to human fetal RPE cells (Kamao et al., 2014). Even though evident similarities in cell morphology and function have been displayed between hPSC-RPE and its native counterpart, hPSC-RPE cells have shown lower expression of genes involved in visual perception and eye development compared to human fetal RPE cells (Liao et al., 2010). Moreover, hiPSC-RPE cells were shown to maintain expression of cell cycle markers on day 30 at passage 3, which could suggest incomplete maturation of these cells. These findings in gene expression profiles are indicative of an immature hPSC-RPE differentiation status when compared to human fetal RPE (Leach et al., 2016; Liao et al., 2010).

2.4 Tissue engineering for macular degeneration

The human eye is an attractive target organ for tissue engineering applications and cell therapy due to four main features. Firstly, a healthy eye has an ability to tolerate foreign antigens and cells without eliciting an immune response, hence, it has an immunoprivileged nature (Kimbrel & Lanza, 2015; Schwartz et al., 2016). Secondly, it is a secluded environment for the transplanted cells, without direct contact to the systemic circulation. Thirdly, it is accessible with minimal invasive surgery and,

finally, it can be monitored through the lens whenever necessary by using basic ophthalmic instruments (Carr et al., 2013; Kimbrel & Lanza, 2015).

A potential therapeutic approach for AMD and related diseases is to replace the damaged RPE cells in the macular area of central vision with a population of healthy cells. These transplanted cells could thereafter reconnect to the remaining neural retina and restore vision (Hynes & Lavik, 2010). A definite prerequisite for the transplanted cells is that they are capable of functionally re-establishing the degenerated cells. Moreover, the cells must integrate to the host retina. Allogeneic human fetal RPE cells and human adult RPE cells and cell sheets, autologous RPE cells as well as autologous RPE-choroid tissue grafts have been intensively investigated as cell sources for RPE cell transplantation (Algvere et al., 1999; Binder et al., 2004; Castellarin et al., 1998). However, the majority of these trials resulted in limited cell survival and poor integration of the grafts to the host retina. Moreover, long-term improvement in the visual acuity was not observed. Merely autologous RPE-choroid tissue grafts have been shown to increase visual function in AMD patients in long-term assessment (van Zeeburg et al., 2012). Nonetheless, these autologous cell sources suffer from limited availability and contain the equivalent genetic risk factors as the damaged cells in the macular area (John et al., 2013).

The hPSC-RPE cells are an attracting cell source for retinal tissue engineering. Transplantation of hESC-RPE cells to the subretinal space in animal models exhibited improved vision acuity and enhanced function of the degenerating photoreceptors (Lu et al., 2009; Lund et al., 2006). Similar outcome was detected after subretinal transplantation of hiPSC-RPE cells (Carr et al., 2009; Li et al., 2012). Two approaches have been suggested for the hPSC-RPE delivery to the subretinal space: transplanting the cells in suspension or transplanting polarized hPSC-RPE sheets. In the cell suspension approach, cells are dissociated, suspended in saline solution and thereafter injected to the subretinal space in the macular area (Carr et al., 2013). This technique is fast and easy to administer, and has resulted in improved visual acuity (Plaza Reyes et al., 2016). Nevertheless, in suspension the cells lose their polarized and mature monolayer structure. Moreover, injected cells in suspension do not adhere well on the aged and diseased Bruch's membrane and suffer from poor viability and functionality (Sugino, Sun et al., 2011; Tezel & Del Priore, 1999).

Consequently, the tissue engineering approach where hPSC-RPE cells are transplanted as a polarized monolayer sheet on a supportive biomaterial substrate is considered attractive. Here, hPSC-RPE cells are grown *in vitro* on a biomaterial substrate and the graft consisting of cells and the substrate is transplanted to the subretinal space (Figure 4). These biomaterial substrates facilitate the surgical

handling of the graft, provide structural support for the cells upon transplantation and allow the cells to be transplanted as a polarized, and therefore functional sheet (Hynes & Lavik, 2010). Additionally, the biomaterial substrate can replace the lost function of the damaged Bruch's membrane associated with ageing and retinal degenerative diseases. In a comparative study, polarized hESC-RPE cell sheets on a biomaterial substrate revealed improved graft survival compared to cells delivered in suspension (Diniz et al., 2013). In addition to delivering hPSC-RPE cells on a biomaterial supportive structure, an approach where hiPSC-RPE cell sheets are fabricated without an artificial biomaterial substrate has been introduced (Kamao et al., 2014). Several recent studies have shown the feasibility of hPSC-RPE sheet delivery in animal models (Brant Fernandes et al., 2016; Kamao et al., 2014; Koss et al., 2016; Thomas et al., 2016).

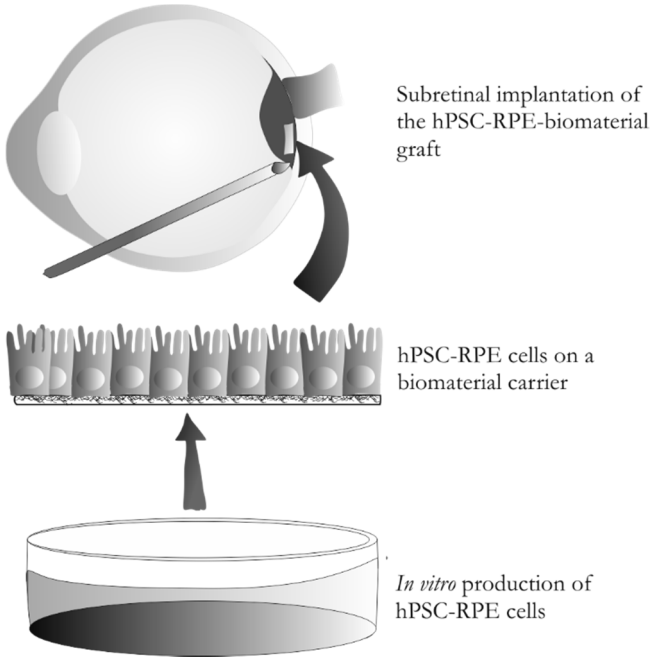

Figure 4. A schematic illustration of the hPSC-RPE-biomaterial substrate production and transplantation. First, functional RPE cells are differentiated from hPSCs. Thereafter, hPSC-RPE cells are cultured on a biomaterial substrate as polarized monolayer. Finally, the hPSC-RPE cell sheet in combination with the biomaterial substrate is implanted to the subretinal space in the macular area of central vision.

The first clinical trials with hESC-RPE cells delivered as suspensions involved the safety and tolerability testing of the cells (Schwartz et al., 2012). The results of these trials have been encouraging: no signs of adverse proliferation, rejection, or

serious ocular or systemic safety issues related to the transplanted tissue were detected (Schwartz et al., 2012). In addition, more than half of the patients experienced sustained improvements in visual acuity (Schwartz et al., 2016). Adverse reactions were associated with vitreoretinal surgery and immunosuppression (Schwartz et al., 2015). At present, multiple clinical trials are ongoing for hPSC-RPE cells to treat AMD and related diseases, such as Stargardt's disease (Kimbrel & Lanza, 2015). The majority of these ongoing and prospective studies transplant hESC-RPE cells in suspension. However, a few approaches where hESC-RPE cells are transplanted to the subretinal space on stabile biomaterial substrates are heading to the clinics (Carr et al., 2013; Coffey et al., 2009; Koss et al., 2016; Thomas et al., 2016). In addition, hiPSC-RPE cell sheets are currently under clinical trials to treat neovascular AMD (Kamao et al., 2014).

2.5 Biomimetic environment

A design or a system that mimic biological structures and phenomena are referred to as biomimetics (Bhushan, 2009; Han et al., 2014). Controlling cellular microenvironment by imitating nature is a fundamental aspect in tissue engineering applications. The cellular microenvironment is a combination of multiple factors, which have a direct or indirect effect on cells via biophysical, biochemical or other routes. *In vivo*, this microenvironment is composed of ECM, surrounding cells, secretory bioactive factors, physical and topographical cues as well as mechanical forces (Barthes et al., 2014; Han et al., 2014). The design of new biomaterial substrates focuses on revealing cell-substrate interactions as well as mimicking the structure and function of ECM (Williams, 2009; Yao et al., 2013).

2.5.1 Cell-biomaterial interaction

The cellular response on biomaterial substrates is unlikely a result of direct biomaterial-cell interaction. Rather, proteins from the surrounding environment, such as serum from culture medium, rapidly adsorb onto the biomaterial surface and interact with cells (Wilson et al., 2005). When a biomaterial substrate comes in contact with a biological aqueous environment, a hydration layer is formed on the biomaterial surface within nanoseconds. The integrity of this hydration layer determines the nature of the subsequent adlayer of proteins. Thereafter, the

composition and concentration of this formed protein adlayer determines the cellular responses on biomaterials (Kasemo, 2002).

Protein adsorption to the biomaterial surface is a complex process determined by a number of enthalpic and entropic changes within the biomaterial surface-hydration layer-protein system (Haynes & Norde, 1994). The composition of the protein adlayer will commonly change over time as faster diffusing proteins such as albumin are displaced by proteins with a higher affinity to the surface. This phenomenon is referred to as the Vroman effect (Vroman & Adams, 1986). The properties of the protein adlayer are influenced by modifications in biomaterial substrate characteristics such as surface chemistry, surface charge, wettability as well as topography (D'Sa et al., 2010b; Wilson et al., 2005). Not only the amount and composition of the protein adlayer, but also the conformation of the proteins has an immense impact on cellular response thereon (Lewandowska et al., 1992).

2.5.2 Integrins

Interactions of cells with their surrounding ECM or substrate can be directly mediated via integrins. Apart from direct integrin-mediated interactions with the cells, the ECM regulates cellular function via growth factor presentation. ECM components bind growth factors, regulate their local availability and generate biochemical gradients (Gattazzo et al., 2014). Integrins are heterodimeric transmembrane proteins, consisting of α- and β-subunits that bind to a number of ECM components such as laminins and collagens (Humphries et al., 2006; Walters & Gentleman, 2015). To date, 18 α-subunits and 8 β-subunits have been identified in mammals and shown to form at least 24 different αβ-heterodimers (Hynes, 2002). Each of these integrins has specific signaling properties and binding selectivity (Campbell & Humphries, 2011). Heterodimerization of the subunits is essential for the proper function of integrins (Afshari & Fawcett, 2009).

Cell attachment to the ECM is commenced by integrins binding to specific amino acid sequences on ECM proteins. Integrin receptor engagement and clustering leads to the formation of focal adhesions where integrins link to the intracellular actin cytoskeleton via large multiprotein complexes. The cytoplasmic tail of integrins interacts with several actin-associated proteins including talin and paxillin (Zhao et al., 2013). The cytoplasmic tail of the integrin β subunit, either directly or via other integrin-binding proteins, recruits a central regulator of integrin-mediated signaling called focal adhesion kinase (FAK) and vinculin to focal adhesions (Mitra et al., 2005). FAK-recruited to integrin-mediated adhesions undergoes

autophosphorylation that coincides with activation of another kinase, c-Src belonging to Src family kinases (Cary & Guan, 1999). This dual kinase comlex in turn activates extracellular signal-related-kinase/mitogen-activated protein kinase (ERK/MAPK) and Rho-associated coiled-coil protein kinase (RhoA/ROCK) pathways, which mediate the signals from the ECM to the nucleus (Figure 5). The ERK/MAPK signaling pathway upregulates gene transcription stimulating cell growth and proliferation, whereas the RhoA/ROCK pathway induces formation of contractile stress fibers to regulate actin dynamics and maturation of focal adhesions (Zhao et al., 2013).

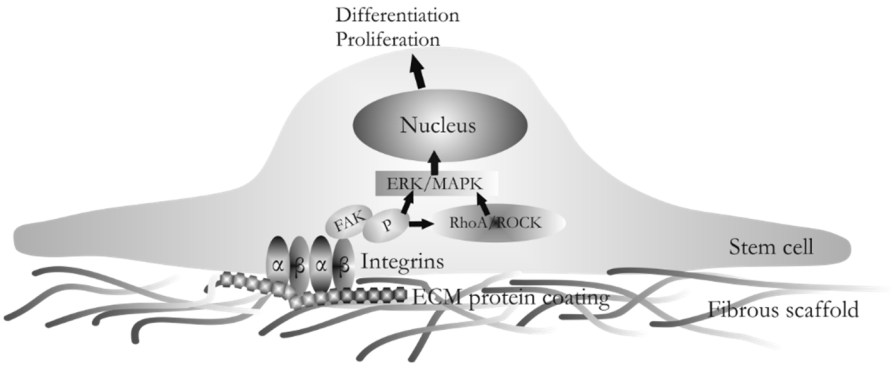

Figure 5. Interaction of cells and substrates. Modified from (Zhao et al., 2013).

Several studies have demonstrated integrin expression in human RPE cells. Human RPE *in situ* have shown to express α4 and β2 integrin subunits. In addition, blocking β1 integrin subunit binding in human RPE decreases cell adhesion to RPE derived matrix as well as to Bruch's membrane, indicating that β1 integrins have a significant role for the attachment of human RPE cells (Chu & Grunwald, 1991). Human fetal and adult RPE cells have been shown to express α1, α2, α3, α4, α5, αV, α6, α7, α11, β1, β4, β5 and β8 subunits on the cell surface (Aisenbrey et al., 2006; Proulx et al., 2004; Rowland et al., 2013; Zarbin, 2003). ARPE-19 cells have been demonstrated to bind to laminin-111 via α6β1, to laminin-332 via α6β4 and to laminin-511/521 via α3β1 and α6β1 heterodimers (Aisenbrey et al., 2006; Fang et al., 2009). The fibronectin receptor α5β1 is also found from the basal surface of human RPE cells (Anderson et al., 1990). Furthermore, hESC-RPE cells have been shown to express integrins α1-5 and β1 on mRNA level (Rowland et al., 2013; Sugino et al., 2011). However, freshly isolated human RPE cells and cultured human RPE cells have been shown to express different amounts of integrins. Culturing of RPE cells *in vitro* upregulates integrin expression and promotes more efficient RPE attachment

and survival on aged Bruch's membrane (Gullapalli et al., 2008; Tian et al., 2004; Zarbin, 2003). Furthermore, hESC-RPE cells with prolonged *in vitro* culture period and higher degree of pigmentation showed increased integrin expression levels (Sugino et al., 2011).

2.5.3 Extracellular matrix components

The ECM where cells reside provides cells with structural support, binds soluble factors and regulates their distribution and presentation to the cells. Moreover, ECM has a fundamental role in cell morphology, migration, differentiation and maturation (Shapira et al., 2014). The basement membrane supporting the epithelial cells is a specialized ECM network that protects tissues from disruptive physical stresses, and forms an interface between the cells and their surrounding environment (Yurchenco, 2011). The large insoluble ECM components of the basement membranes gather together to form a sheet-like structure via self-assembly (Kalluri, 2003). Interaction between cells and surrounding ECM is reciprocal and dynamic: cells receive cues from the ECM while ECM is constantly remodeled by the cells. Epithelial cell basement membranes are assembled from two major ECM proteins -laminin and collagen IV. Primary animal and human RPE cells produce ECM components, including fibronectin, laminin, elastin, heparan sulfate proteoglycan, and collagen types I, III, and IV *in vivo* and *in vitro* (Campochiaro et al., 1986; Kamei et al., 1998).

Laminins are heterotrimeric glycoproteins that consists of α-, β- and γ-chains in a coiled-coiled cross-like structure. Overall, 16 different laminin isoforms have been found in humans (Aumailley, 2013). The RPE basement membrane contains four laminins, laminin-111, laminin-332, laminin-511 and laminin-521, that adhere to the RPE via specific integrins (Aisenbrey et al., 2006). The self-assembly of basement membranes, including RPE basement membrane, is initiated by laminin polymerization to the basolateral side of the cells. Cell surface proteins such as integrins facilitate the initial deposition of laminin polymers, via site-specific interactions. Thereafter, the laminin network interacts with the collagen IV network directly or via nidogen/entactin and heparan sulfate proteoglycan perlecan (Figure 6). The covalently polymerized collagen IV network stabilizes the basement membrane structure. The other basement membrane components interact with laminin and collagen IV complex (Kalluri, 2003; Yurchenco, 2011).

Collagen IV is the main component of the RPE basement membrane in Bruch's membrane. Six genetically different collagen IV isoforms have been identified in

humans. Collagen IV molecule is a trimer, which consist of three α-chains assembling into heterotrimeric molecules of α1α1α2, α3α4α5 and α5α5α6 chains. These collagen IV molecules have been shown to have distinct topographical locations and function. Unlike collagens in fibrous tissue, collagen IV molecules do not aggregate parallel into fibrous bundles. Instead, collagen IV molecules form a loose network in the basement membranes by end-to-end and lateral interactions (Yurchenco et al., 2004). The α-chains of collagen IV are separated into three domains: an amino-terminal 7S domain, a triplehelical domain in the middle of the chain, and, finally, a carboxy-terminal non-collagenous (NC)-1 domain. First, three α-chains form a helical trimer, which is initiated by the gathering of the NC-1 domains of the chains. Next, two heterotrimeric collagen IV molecules form a dimer via the NC-1 domains. Thereafter, two collagen dimers interact at the amino-terminal 7S region to form the collagenous network (Kalluri, 2003). Previously, the RPE basement membrane in Bruch's membrane has shown positive expression of both α1α1α2 and α5α5α6 molecules of collagen IV (Chen et al., 2003).

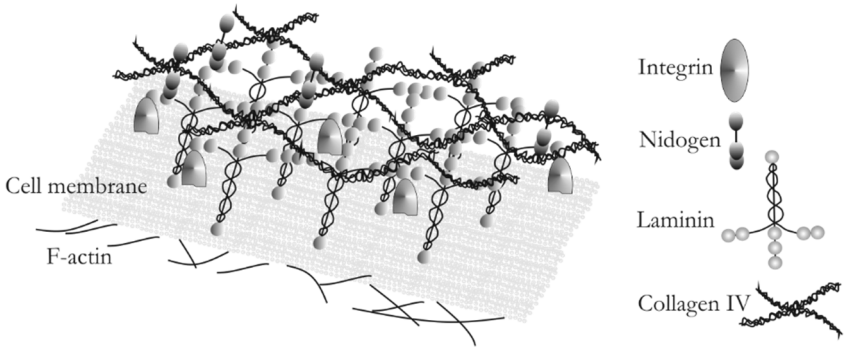

Figure 6. Schematic illustration of the ECM protein network in the basement membranes. Modified from (Yurchenco, 2011).

Collagen I is the most abundant protein in humans and a major component in the inner collagenous layer of Bruch's membrane. Similar to collagen IV, collagen I contains three α-chains, which form an α-helical structure of 300 nm in length and 1.5 nm in diameter with a molecular mass of 270–300 kDa. These triple helices coil together to form collagen I fibrils. Thereafter, fibrils combine with other collagenous and non-collagenous molecules including proteoglycans, to form fibers. (Abraham et al., 2008; Varma et al., 2016)

Collagens have been widely investigated as biomaterial substrates in tissue engineering applications (Antoine et al., 2014; Hapach et al., 2015). Collagen I films

derived from equine, bovine, porcine and human tissues have been studied as a potential substrate for human primary RPE cells and ARPE-19 cells (Bhatt et al., 1994; Lu et al., 2007; Thumann et al., 2009; Warnke et al., 2013). In addition, porcine collagen I gels are in use to develop hiPSC-RPE cell sheets for clinical settings (Kamao et al., 2014). However, collagen IV has been used in tissue engineering applications as well as with RPE cells merely in the form of protein coating (Rowland et al., 2013; Subrizi et al., 2012). Regardless of the extensive use of collagens in biomedical applications, reproducing the intrinsic architecture and fiber orientation of collagens *in vitro* is challenging (Friess, 1998; Tenboll et al., 2010).

2.6 Biomaterials for retinal tissue engineering

A biomaterial is defined as a substance that alone or as part of a complex system is engineered to interact with living biological systems for a medical purpose (Williams, 2009). Various requirements have been set for designing optimal biomaterial substrates for the production and transplantation of clinically relevant hESC-RPE cells. Above all, the biomaterial substrates have to be biocompatible *in vivo*. These substrates must also support the formation of a mature and functional hESC-RPE monolayer *in vitro*. Moreover, these substrates should be thin enough to fit the subretinal space; a thickness similar to the native Bruch's membrane is preferred. A successful supportive biomaterial should also have sufficient mechanical properties and flexibility to withstand the surgical handling as well as transplantation to the subretinal space. In addition, biodegradable substrates must not form toxic by-products during biodegradation. Finally, permeability to fluids and biomolecules is a definite prerequisite for these substrates to restore the function of damaged Bruch's membrane as a semipermeable barrier. (Binder, 2011; Hynes & Lavik, 2010; Jha & Bharti, 2015; Lee & MacLaren, 2011; Pennington & Clegg, 2016)

Natural decellularized ECM scaffolds as well as substrates fabricated from polymers of biological origin have been extensively investigated in the aspiration of finding potential biomaterial substrates for RPE (Table 1). Decellularized natural ECM scaffolds, such as amniotic membrane, Bruch's membrane and anterior lens capsules, have previously gained interest as prospective substrates in retinal tissue engineering applications (Akrami et al., 2011; Nicolini et al., 2000; Sugino et al., 2011). These natural decellularized ECM scaffolds provide a significant advantage in retaining the complex structure and organization of the ECM while possessing tissue specific micro- and nanotopography (Hynes & Lavik, 2010; Walters & Gentleman,

2015). Besides decellularized natural scaffolds, natural polymers such as collagen, alginate, and fibroin can be utilized as biocompatible substrate sources for retinal tissue engineering. Similar to natural decellularized scaffolds, substrates fabricated from natural polymers closely mimic the native ECM and possess innate biological activity (Hynes & Lavik, 2010; Rahmany & Van Dyke, 2013). However, major disadvantages have been associated with the use of natural biomaterials including poor mechanical properties, batch to batch variation as well as concerns with immunogenicity and pathogen transmission (Lynn et al., 2004; Rahmany & Van Dyke, 2013).

Synthetic polymers have multiple attractive characteristics that make them an appealing source of biomaterials for tissue engineering applications. Controlled chemical and physical structure, predictable properties, high degree of processing flexibility, superior mechanical properties and high reproducibility in commercial-scale manufacturing processes are evident advantages of synthetic polymers compared to naturally derived biomaterials (Hotaling et al., 2016; Hynes & Lavik, 2010). The most commonly used synthetic polymers in retinal tissue engineering include the food and drug administration (FDA)-approved poly-α-hydroxy-acid-based polymers such as poly(L-lactic acid) (PLLA), poly(lactic-co-glycolic acid) (PLGA) and poly(ε-caprolactone) (PCL) (Hynes & Lavik, 2010). The possibility to combine these materials as co-polymers, such as poly(L-lactide-co-caprolactone) (PLCL), provides a range of important tunable features (Lee et al., 2008). Even though synthetic polymers overcome the common drawbacks associated with natural polymers, synthetic polymers as such lack cell binding ligands on the scaffold surface, which results in poor cell attachment (Desmet et al., 2009). Moreover, synthetic polymers frequently used in tissue engineering applications are highly hydrophobic, which can decrease the cellular response on these materials (D'Sa et al., 2010b; Wang et al., 2005). Various synthetic biomaterial substrates with distinct architecture have been investigated as potential substrates for RPE by several groups (Table 2). Apart from substrates fabricated either from natural or synthetic polymers, hybrid materials incorporate the beneficial aspects of both biologically active natural polymers and structurally flexible synthetic polymers (Wang et al., 1999). Several recent studies have introduced hybrid biomaterials as potential substrates for RPE as well (Table 3).

Table 1. Natural scaffolds for RPE cell transplantation.

Material	Substrate architecture	Cell type	Stability	Reference
Anterior lens capsule	Decellularized natural scaffolds of porcine, bovine or human origin	Porcine RPE, ARPE-19 cells	Biodegradable	(Hartmann et al., 1999; Kiilgaard et al., 2012; Lee et al., 2007; Nicolini et al., 2000; Singh et al., 2001)
Acetylated bacterial cellulose	41.6 ± 2.2 μm thick heat-dried films with surface modification, coated with urinary bladder matrix	Human RPE cells	Biodegradable	(Goncalves et al., 2015; Goncalves et al., 2016)
Alginate	3D beads, films, 3D matrix	RPE, porcine RPE, ARPE-19 cells	Biodegradable	(Eurell et al., 2003; Heidari et al., 2015; Jeong et al., 2011; Najafabadi et al., 2015)
Amniotic membrane	Decellularized natural scaffold	Human RPE cells	Biodegradable	(Akrami et al., 2011; Capeans et al., 2003; Ohno-Matsui et al., 2005; Singhal & Vemuganti, 2005; Stanzel et al., 2005)
Chitosan		ARPE-19 cells	Biodegradable	(Lai et al., 2010)
Col I	Col I from rat tail tendon, crosslinked or non-crosslinked	Human fetal RPE cells	Biodegradable	(Bhatt et al., 1994)
	Thin films of 2.4 μm thickness	ARPE-19 cells		(Lu et al., 2007)
	7 μm thick film of equine Col I	ARPE-19 cells		(Thumann et al., 2009)
Descemet's membrane	Decellularized natural scaffold of 10-12 μm thickness	Porcine and bovine RPE cells	Biodegradable	(Thumann et al., 1997)
Fibrinogen	Microspheres	Human fetal RPE cells	Biodegradable	(Oganesian et al., 1999)
Gelatin	50 % gelatin	Porcine RPE cells, ARPE-19 cells	Biodegradable	(Del Priore et al., 2004; Lai, 2009)
Human Bruch's membrane	Decellularized natural scaffold as such or with additional ECM modifications	Human fetal RPE cells, ARPE-19 cells	Biodegradable	(Del Priore et al., 2002; Gullapalli et al., 2008; Sugino et al., 2011; Sugino, Gullapalli et al., 2011; Tezel & Del Priore, 1999; Tezel et al., 1999)
Human inner limiting membrane	Decellularized natural scaffold	Human RPE cells, ARPE-19 cells	Biodegradable	(Beutel et al., 2007)
Silk fibroin	Membranes of 3 μm thickness	ARPE-19 cells	Biodegradable	(Shadforth et al., 2012; Shadforth et al., 2015)

Table 2. Biomaterial substrates fabricated from synthetic polymers for RPE cell transplantation.

Material	Substrate architechture	Cell type	Stability	Reference
ELR-RGD	Solvent cast films	Human RPE	Biodegradable	(Singh et al., 2014; Srivastava et al., 2011)
ePTFE	Plasma-treated 100 μm thick commercial porous films	ARPE-19 cells	Stabile	(Krishna et al., 2011)
IPAAm	Temperature sensitive hydrogels for cell sheet production *in vitro*	ARPE-19 cells, human D407 cells	Stabile	(Kubota et al., 2006; von Recum et al., 1998; von Recum et al., 1999)
Methacrylate and (meth)acrylamide	Hydrogel coated with poly-D-lysine and fibronectin	Pig and human RPE cells	Stabile	(Singh et al., 2001)
Montmorillonite clay based polyurethane	Solvent cast 30-50 μm thick films	ARPE-19 cells	Biodegradable	(Da Silva et al., 2013)
PA	Electrospun nanofibers	Human fetal RPE and adult RPE cells	Biodegradable	(Thieltges et al., 2011)
PCL	Thin film, with 0.5 μm pores	Human fetal RPE	Biodegradable	(McHugh et al., 2014)
PCL	Electrospun nanofibers, 130 nm in diameter	ARPE-19 cells	Biodegradable	(Da Silva et al., 2015)
PHBV8	Solvent cast films of 5-10 μm thickness	human D407 cells	Biodegradable	(Tezcaner et al., 2003)
PDLLA	A frame-supported 4 μm thick electrospun film with 640 nm thick fibers	Human RPE cells	Biodegradable	(Popelka et al., 2015)
PLCL	Electrospun substrates, fiber diameters of 200-1000 nm	Human fetal RPE cells	Biodegradable	(Liu et al., 2014)
PLGA	Thin films	ARPE-19 cells	Biodegradable	(Lu et al., 2001)
	Thickness <10 μm	human D407 cells		(Lu et al., 1998)
PLGA a and PEG/PLA	Solvent cast films with micropatterned surfaces	human D407 cells	Biodegradable	(Lu et al., 1999; Lu et al., 2001)
PLGA and PLLA	Solvent cast solid films	Porcine RPE, human fetal RPE	Biodegradable	(Giordano et al., 1997; Hadlock et al., 1999; Thomson et al., 1996)
	Microcarriers	ARPE-19 cells		(Thomson et al., 2010)
P(MMA-co-PEG)	50 μm thick electrospun film, fiber diameter of 1.9 μm	ARPE-19 cells	Stabile	(Treharne et al., 2012)
Polyethylene Terephthalate (PET)	Commercial cell culture insert with 1 μm pores	Human fetal and adult RPE cells	Stabile	(Stanzel et al., 2014)
	10 μm thick film, 0.4 μm pores	Human fetal RPE cells		
	Electrospun films with fiber diameters of 200-1000 nm	Human fetal RPE cells		(Stanzel et al., 2012)
Polyether urethanes	Commercially available Pellethane®, Tecoflex® and Zytar®, thickness 100-1000 μm	ARPE-19 cells	Stabile	(Williams et al., 2005)
PDMS	Micropatterned surface	ARPE-19 cells	Stabile	(Lim et al., 2004)

Abbreviations: Col I=Collagen I, PA=Polyamide, PHBV8= poly(hydroxybutyrate-co-hydroxyvaleric acid), PLGA-PHBV8=Poly(L-lactic acid-co-glycolic acid)/poly(hydroxybutyrate-co-hydroxyvaleric acid, PCL=Poly(ε-caprolactone) , PEG=poly(ethylene glycol), PET=Polyethylene terephthalate, PDLLA= Poly(DL-lactic acid), PLLA=Poly(L-lactic acid) , PDMS=Polydimethylsiloxane, ePTFE=Expanded polytetrafluoroethylene, IPAAm=N-isopropylacrylamide monomer, PLCL= Poly(L-lactide-co-ε-caprolactone), PLGA= poly(D,L-lactic-co-glycolic acid), ELR-RGD=Bioactive RGD-containing elastin-like recombinamers, P(MMA-co-PEG)=Poly(ethylene glycol) methacrylate.

Table 3. Hybrid biomaterial substrates for human RPE cells.

Material	Substrate architechture	Cell type	Stability	Reference
Combined silk fibroin, PCL and gelatin	Electrospun thin film 3-5 μm with 166 nm fibers	ARPE-19 cells	Biodegradable	(Xiang et al., 2014)
Bovine Col I and PLGA	Electrospun fibers with average diameter of 300 nm on a PET cell culture insert	Human primary RPE cells	Biodegradable fibres on top of stabile PET film	(Warnke et al., 2013)
Human lens capsules with PDMS stamps	Decellularized natural scaffod with micropatterned PDMS wafer	ARPE-19 cells	Biodegradable lens capsule with stabile PDMS	(Lee et al., 2002)

Abbreviations: Col I=Collagen I, PLGA=Poly(L-lactic acid-co-glycolic acid), PCL=Poly(ε-caprolactone) , PEG=poly(ethylene glycol), PET=Polyethylene terephthalate, PDMS=Polydimethylsiloxane.

The initial attachment and survival of hESC-RPE cells on biomaterial substrates has been shown to be severely impaired compared to human fetal RPE cells (Sugino et al., 2011). Even though hESC- and hiPSC-derived RPE cells hold great promise for RPE cell transplantation therapies, the majority of biomaterial studies in retinal tissue engineering field have been conducted with primary RPE cells, fetal RPE cells or immortalized cell lines (Tables 1-3). Merely a few of the recent studies have focused on investigating cell-biomaterial interactions with clinically relevant hESC-RPE and hiPSC-RPE cells (Table 4). The performance of only two potential transplantation materials, polymide (PI) (Ilmarinen et al., 2015) and Parylene C (Koss et al., 2016; Thomas et al., 2016), have been assessed for hESC-RPE *in vivo*. Parylene C is a biostabile and chemically inert polymer that have been used in biomedical applications. Parylene C membranes have been fabricated with two step photolithography technology to obtain 300 nm thick permeable membranes with a 6 μm thick supporting mesh frame. When combined with Matrigel™ or human vitronectin, these stabile ultrathin films were able to support hESC-RPE growth and functionality both *in vitro* and *in vivo* (Brant Fernandes et al., 2016; Diniz et al., 2013; Hu et al., 2012; Koss et al., 2016; Lu et al., 2014; Thomas et al., 2016). Although several biodegradable substrates have been investigated with primary RPE cells, only a few of these have been shown to result in adequate cellular response with hESC-RPE.

Table 4. Biomaterial substrates for hESC-RPE cells.

Biomaterial	Architecture	Cell type	Stability	Culture conditions	Clinical status	Reference
Self-assembled ECM	Self-assembled ECM by hiPSC-RPE consisting mainly of ollagen IV and laminin	hiPSC -RPE	Biodegradable	Porcine Col I- gel used for RPE sheet preparation, cell sheet transplanted as such. Fetal bovine serum included in culture medium.	Clinical trial	(Kamao et al., 2014)
rhLN-521	Laminin protein coating	hESC-RPE	Biodegradable	Xeno-free medium. Laminin coatings in *in vitro* production of hESC-RPE, *in vivo* studies as single cell suspension.	*In vitro/in vivo* (rabbits)	(Plaza Reyes et al., 2016)
Parylene-C	Mesh-supported parylene C membrane with ultrathin 0.3 μm regions	hESC-RPE	Stabile	Matrigel™- or human vitronectin coating, serum-free medium	Clinical trial	(Brant Fernandes et al., 2016; Diniz et al., 2013; Hu et al., 2012; Koss et al., 2016; Lu et al., 2014)
PLDLA	Porous honeycomb films of 20 μm thickness	hESC-RPE	Biodegradable	Human Col IV-coating, serum-free medium	*In vitro*	(Calejo et al., 2016)
PET	Commercially available 10 μm thick film, with 0.4 μm pores	hESC-RPE	Stabile	Matrigel™- or human laminin	Clinical trial	(Carr et al., 2013; Coffey et al., 2009)
PI	7.6 μm thick sheet with 1 μm pores	hESC-RPE	Stabile	Human laminin-coating, serum-free medium	*In vivo* (rabbits)	(Ilmarinen et al., 2015)
	24 μm thick sheet with 1 μm pores	hESC-RPE	Stabile	Additional protein coatings used, serum-free medium	*In vitro*	(Subrizi et al., 2012)
PTMC	Compression molded nonporous elastic films with 100 μm thickness	hESC-RPE	Biodegradable	Human Col IV-coating, serum-free medium	*In vitro*	(Sorkio et al., 2016)
Synthemax II-SC	Commercial synthetic xenofree, RGD peptide-containing copolymer coating	hESC-RPE	Stabile	Serum-free medium	*In vitro*	(Pennington et al., 2015)

Abbreviations: rhLN-521=Recombinant human laminin-521, PET=Polyethylene Terephthalate, PI=Polyimide, PLDLA= Poly L-lactide/D-lactide copolymer, PTMC=Poly(trimethylene carbonate)

2.7 Methods for fibrous biomaterial substrate fabrication

The environmental cues that cells receive from biomaterial substrates *in vitro* differ drastically from those they receive in their natural microenvironment *in vivo* (McCarthy et al., 1996). A range of approaches has been introduced to mimic the surrounding ECM *in vitro* (Figure 7) (Hotaling et al., 2016; Rahmany & Van Dyke, 2013; Shapira et al., 2014; Zhao et al., 2013). Moreover, various fabrication techniques have been developed to manufacture fibrous scaffolds to mimic ECM structure in the field of tissue engineering. Methods, such as phase separation, self-assembly and electrospinning have been used for the production of porous substrates from natural or synthetic materials (Wang et al., 2013). These biomaterial substrates can be further processed for enhanced cellular attachment and proliferation by surface modification (Wang et al., 2005).

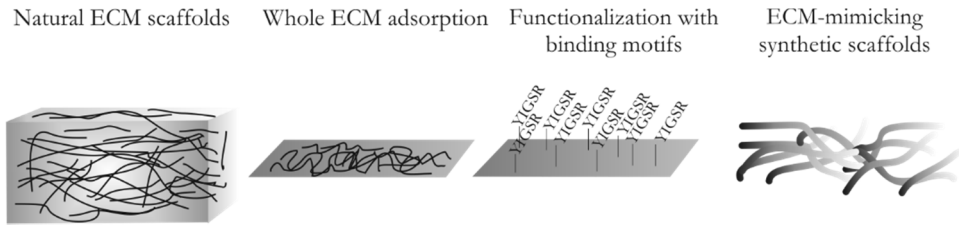

Figure 7. Examples of approaches for creating biomimetic substrates *in vitro*.

2.7.1 Functionalization of biomaterials with ECM proteins

ECM protein adsorption on biomaterial substrates has been in use in tissue engineering since 1980's, when fibronectin-coated glass demonstrated improved cell attachment compared to uncoated glass (Seitz et al., 1982). This adsorption is dictated by both the proteins characteristics and the biomaterial substrate surface properties (Rahmany & Van Dyke, 2013; Wilson et al., 2005). Previously, coating aged Bruch's membrane explants with Bruch's membrane components have resulted in increased RPE cell attachment (Del Priore et al., 2002). Furthermore, the majority of biomaterial substrates investigated in retinal tissue engineering applications are carried out either in culture medium supplemented with serum or with various protein coatings from animal or human derived sources (Hynes & Lavik, 2010; Jha & Bharti, 2015; Rowland et al., 2013). In previous studies, it has been shown that ECM protein coatings have an effect on the early stage differentiation of hESCs into

neural progenitors and neurons (Ma et al., 2008), retinal progenitor cells (Gong et al., 2008), and RPE (Rowland et al., 2013). Xeno-derived protein coatings, such as Matrigel™ (Hu et al., 2012; Lu et al., 2014) and gelatin (Schwartz et al., 2012), and xeno-free ECM proteins collagen IV (Calejo et al., 2016; Ilmarinen et al., 2015; Subrizi et al., 2012), laminins (Subrizi et al., 2012) and vitronectin (Diniz et al., 2013; Koss et al., 2016; Thomas et al., 2016) are currently in use for coating biomaterial substrates to increase hESC- and hiPSC-RPE cell attachment and maturation for *in vitro* and *in vivo* applications. Moreover, successful differentiation and maturation of hESC-RPE has been demonstrated on recombinant human laminin proteins (Plaza Reyes et al., 2016). Despite their frequent use in retinal tissue engineering, the effects of protein coatings on the maturation and functionality of differentiating hESC-RPE have not been assessed thoroughly.

Apart from ECM proteins, biomaterial surfaces have been functionalized with integrin binding motifs to enhance cellular response (Mateos-Timoneda et al., 2015; Rahmany & Van Dyke, 2013). Various integrin binding motifs found in ECM proteins have been characterized and can be synthetisized as short linear peptides. Among these bioadhesive motifs, the most commonly used peptides are derived from fibronectin (RGD), laminin (IKVAV, YIGSR, PDGSR) and collagen (DGEA, GFOGER). Recently, RGD-peptide containing xeno-free copolymer substrate has been used for hESC-RPE differentiation (Pennington et al., 2015). In addition, RGD-modified synthetic elastin-like substrate has been found to support the immortalized ARPE-19 cell line (Srivastava et al., 2011). Moreover, RGD- and YIGSR-modifications on electrospun methacrylate-based substrates resulted in significant improvement in ARPE-19 cell adhesion (Treharne et al., 2012). Additionally, activation of these integrins could improve cell-biomaterial interaction (Heller & Martin, 2014; Olsen & Ffrench-Constant, 2005; Strachan & Condic, 2008). For instance, manganese (Mn^{2+}) replaces the calcium (Ca^{2+}) in the integrin ligand-binding domain, which results in conformational changes and subsequent integrin activation (Gailit & Ruoslahti, 1988; Olsen & Ffrench-Constant, 2005). Addition of Mn^{2+} to the culture medium has been shown to stimulate integrin activation in ARPE-19 cells leading to enhanced adhesion and migration of ARPE-19 cells on Bruch's membrane components and Bruch's membrane explants (Afshari et al., 2010).

2.7.2 Self-assembly of ECM matrix components

Native RPE cells are capable of abundant secretion of Bruch's membrane key components such as laminin-111, laminin-332, laminin-511, laminin-521, collagen IV, collagen I and fibronectin (Aisenbrey et al., 2006; Campochiaro et al., 1986; Kigasawa et al., 1998). Furthermore, hESC-RPE cells grown on Matrigel™ have demonstrated basal assembly of collagen IV, laminin and fibronectin (Vugler et al., 2008), whereas hiPSC-RPE cultured on porcine collagen I gel assembled basal lamina mainly consisting of collagen IV and laminin (Kamao et al., 2014). This ability of RPE cells to secrete Bruch's membrane components has been previously employed to fabricate hiPSC-RPE cell sheets for subretinal transplantation. These hiPSC-RPE cell sheets were generated on porcine collagen I gel, where the cells assembled their own basal lamina. The collagen I gel used for cell sheet production was subsequently dissolved prior to transplantation (Kamao et al., 2014). In addition, temperature-responsive hydrogels have been developed for human RPE monolayer transplantation with their own deposited ECM. In order to harvest the cell sheets from these temperature-responsive hydrogels, the temperature was decreased from 37 °C to 20 °C resulting in increased hydrophobicity of the substrate and cell sheet detachment (Kubota et al., 2006; von Recum et al., 1998; von Recum et al., 1999). While the cell sheet approach with self-assembled ECM shows great promise for the retinal tissue engineering transplantation and has progressed towards clinical settings (Kamao et al., 2014), the effects of the biomaterial substrate on hPSC-RPE ECM protein deposition remain to be investigated.

2.7.3 Electrospinning

Electrospun substrates have been shown to mimic the structural cues and properties of the native ECM. Moreover, they provide porous substrates that allow for the transportation of nutrients and metabolic waste (Hotaling et al., 2016; Zhang et al., 2007). Electrospinning technology enables the fabrication of fibers ranging from nanometer to micrometer scale. For electrospinning, polymers are dissolved in an appropriate solvent and loaded into a syringe. The polymer solution is expelled from the syringe through a metallic needle at a constant rate controlled via a syringe pump. A high voltage is applied to the metallic needle, which results in charging of the polymer. The electric field strength overcomes the surface tension of the polymer solution and generates a charged liquid jet. This liquid jet is deposited on the grounded collector. The solvent evaporates on the way and a non-woven fibrous

substrate is formed on the collector (Wang et al., 2013; Zhang et al., 2007). Previously, electrospun substrates fabricated from poly(DL-lactide) (PLA), polyamide (PA), polyethylene terephthalate (PET), PLCL, bovine collagen type I and PLGA, poly(ethylene glycol) methacrylate P(MMA-co-PEGM) and silk fibroin, PCL and gelatin have been studied as potential substrates for human RPE cells, human fetal RPE cells and ARPE-19 cells (Liu et al., 2014; Popelka et al., 2015; Thieltges et al., 2011; Treharne et al., 2012; Warnke et al., 2013; Xiang et al., 2014). However, the suitability of these fibrous substrates for hPSC-RPE has not been assessed yet.

2.7.4 Langmuir-Blodgett technology

Langmuir-Blodgett (LB) technology is a versatile fabrication method for thin films traditionally used for modelling biomembranes, organic and inorganic coatings, electronic industry and sensors. Recently, LB technology has gained interest among tissue engineering applications (Goffin et al., 2010; Higuchi et al., 2002; Pastorino et al., 2014; Tenboll et al., 2010). This method provides an attractive approach for creating highly organized and well-characterized biomimetic substrates without the use of additives and bio-incompatible substances (Chen et al., 2007; Tenboll et al., 2010). The LB technology is based on certain properties of organic molecules, such as phospholipids, to orient at an air-subphase interface and minimize their free energy and subsequently form an insoluble monolayer referred to as Langmuir film. The classical molecules used in LB technology are amphiphilic molecules which means that molecules have a hydrophilic and a hydrophobic tail. These amphiphilic molecules orient at the air-subphase interface according to their hydrophilicity: the hydrophilic tail seeks to the aqueous subphase, whereas the hydrophobic tail orients towards air (Langmuir, 1938).

The monolayer film formation on air-subphase interface interferes with the surface pressure of the liquid. As the surface area of the monolayer film is compressed, the surface pressure increases. Compression of the monolayer film at the air-subphase interface is achieved by moving barriers across the interface. In the course of compression, the molecules on the interface self-organize and the film undergoes several phase transitions eventually forming an organized floating film. Subsequently, this floating film can be deposited from the subphase surface onto a solid substrate (Girard-Egrot et al., 2005; Langmuir, 1938). When this deposition is carried out by moving the solid substrate vertically through the monolayer, the film

is referred to as Langmuir-Blodgett film, whereas in case of Langmuir-Schaefer (LS) films the deposition occurs horizontally (Langmuir, 1938).

Most proteins are large polarized amphiphilic molecules (Hlady & Buijs, 1996). Additionally, collagens are present in their molecular form in acidic solutions and form fibers as a result of increase in solvent pH (Jiang et al., 2004) (Figure 8). In LB technique, this process is forced to take place at the air-subphase interface. The interface can be rapidly compressed to orient the assembled fibers and deposited on a solid substrate (Goffin et al., 2010). Previously, collagen I LB films have been fabricated from rat and calf collagens. These collagen I LB films showed favorable cellular response and attachment of human fibroblasts, 3T3 mouse fibroblastic cells and adipose-derived stem cells (Goffin et al., 2010; Pastorino et al., 2014; Tenboll et al., 2010). Apart from collagen I, LB films have been previously fabricated from laminin, fibronectin and vitronectin (Higuchi et al., 2002). To my best knowledge, collagen IV films have not been previously produced with LB technology. Moreover, the suitability of the LB technique to fabricate structures resembling the basement membrane structure of the epithelial cells has not been assessed yet.

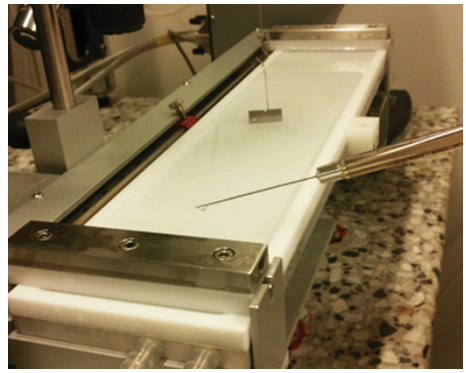

Figure 8. Application of acidic collagen solution at air-subphase interface in Langmuir trough.

2.7.5 Atmospheric plasma surface treatment

The lack of cell binding ligands as well as high hydrophobicity of the synthetic polymer substrates commonly used in tissue engineering result in a poor cellular response (D'Sa et al., 2010b; Zhang et al., 2007). Gaseous plasma discharges are a common means to modify the biomaterial surface properties without affecting its bulk properties. The surface chemistry as well as micro- and nanostructure of a

variety of polymers can be tuned by using atmospheric pressure dielectric barrier discharge (DBD) (Balzer et al., 2015; Borges et al., 2013; Jacobs et al., 2013). Moreover, DBD is a fast, versatile and cost-effective surface modification technique. For up-scaled manufacturing processes the use of plasma in atmospheric pressure is preferred over vacuum conditions (Desmet et al., 2009).

Plasma is partly ionized gas, which contains ions and electrons as free carriers (Heinlin et al., 2011). In plasma treatment, inert gases, such as argon, helium, nitrogen and oxygen are used. In DBD treatment, a high AC voltage is applied between parallel electrodes covered with dielectric material. DBD produces high-energy electrons, which are able to produce radicals and electronically excited particles (Desmet et al., 2009). The function of the dielectric layer on electrodes is to stabilize the discharge and to hinder electric arc formation by restricting the current (Jacobs et al., 2013). Plasma treatment induces chemical functionalities and free radicals onto the surfaces, this in turn increases appearance of functional groups, wettability groups and surface roughness. The introduced surface modifications can be subsequently used to bind proteins or ligands with biological activity (Desmet et al., 2009). The final surface properties of a biomaterial substrate after plasma treatment are a result of intricate interactions between the biomaterial, gases and processing parameters. In addition, the biomaterial surfaces typically undergo surface adaptation after the plasma treatment when surfaces tend to minimize the interfacial energy (Desmet et al., 2009; D'Sa et al., 2010b).

Previously DBD plasma treatment has been demonstrated result in increased protein adsorption and cell attachment of human lens epithelial cells and fibroblasts on various biomaterial substrates (D'Sa et al., 2010a; D'Sa et al., 2012; Jacobs et al., 2013). Furthermore, surface modification of biomaterial substrates with plasma treatment improved the cellular response of ARPE-19 cells and human primary RPE cells on various substrates (Kearns et al., 2012; Krishna et al., 2011; Tezcaner et al., 2003; Williams et al., 2005). Moreover, the hydrophobic Parylene C membranes investigated as prospective substrates for hESC-RPE transplantation are oxygen plasma treated for improved biocompatibility (Song et al., 2009).

3 Aims of the study

The objective of this dissertation was to develop and modify biomaterials as culture substrates and transplantation materials and to test them with clinically relevant hESC-RPE cells in serum-free culture conditions. Special focus and attention was paid to finding substrates and structures that resemble the native environment of the RPE in the eye, Bruch's membrane. The hESC-RPE cell-substrate interaction as well as the ability of these substrates to support formation of functional hESC-RPE was studied. The specific aims of the studies are outlined below:

I. To study the effect of several human-sourced ECM proteins found in the native Bruch's membrane as well as a xeno-derived substrate on hESC-RPE cell differentiation, maturation and functionality in adherent serum-free cultures. The ultimate goal was to find an optimal substrate for the clinical production of hESC-RPE cells.

II. To manufacture a biomimetic microenvironment from human origin biomaterials that bears a resemblance to the structure and organization of native Bruch's membrane for the *in vitro* production of the clinically relevant hESC-RPE cells.

III. To investigate and modify a biodegradable membrane mimicking the fibrous structure of the Bruch's membrane as a potential transplantation material for hESC-RPE cell delivery for retinal applications.

4 Materials and methods

4.1 Biomaterial substrates

4.1.1 Dip-coating

In **Study I**, purified human ECM proteins as well as basement membrane matrices were investigated as biomaterial substrates in differentiation and maturation of hESC-RPE cells. These purified human ECM proteins were chosen as they all are present in the native Bruch's membrane (Booij et al., 2010) and provide xeno-free, clinically suitable matrices for hESC-RPE support. CELLstart™ is a xeno-free current good manufacturing practice (cGMP)-produced commercial hPSC matrix, whereas commercial mouse-tumor-derived Matrigel™ was included in the study as it is commonly used for hPSC-RPE differentiation and maintenance (Lane et al., 2014). The protein coatings and studied concentrations in this dissertation are listed in Table 5. Commercial cell culture inserts with 1 μm pore size dip-coated with collagen IV (Col IV) were chosen as a control and a reference susbtrate in cell culture studies as Col IV has been previously routinely used for enrichment and maturation of hPSC-RPE cells in our laboratory (Vaajasaari et al., 2011) (**Studies I**, **II** and **III**).

In this dissertation, full-length proteins were applied on substrates using dip-coating. That is the substrates were immersed in ECM protein solution, and the proteins were adsorbed on the biomaterial substrate surface via physicochemical interactions between the substrate surface and applied protein solutions (Wilson et al., 2005). Detailed dip-coating protocol is described in the original publications (**Studies I**, **II** and **III**).

Table 5. ECM protein coatings applied by dip-coating.

Protein coating	Abbre-viation	Source	Manufacturer	Concentration	Study
CELLstart™	CS	Human	Life Technologies, Carlsbad, CA	1:50	**I**
Collagen I	Col I	Human placenta	Sigma-Aldrich, St. Louis, MO	5 μgcm^{-2}	**I**
Collagen IV	Col IV	Human placenta	Sigma-Aldrich, St. Louis, MO	5 μgcm^{-2} 10 μgcm^{-2}	**I, II** **III**
Fibronectin	FN	Human plasma	Sigma-Aldrich, St. Louis, MO	5 μgcm^{-2}	**I**
Laminin	LN	Human placenta	Sigma-Aldrich, St. Louis, MO	5 μgcm^{-2}	**I**
Matrigel	MG	Mouse	BD Biosciences, San Jose, CA	30 μgcm^{-2}	**I**
Vitronectin	VN	Human plasma	Sigma-Aldrich, St. Louis, MO	0.5 μgcm^{-2}	**I**

4.1.2 Langmuir-Schaefer films

In **Study II**, LS technique was used to manufacture a biomaterial substrate mimicking the structure and organization of Bruch's membrane for the production of clinically relevant hESC-RPE cells. A layered collagen film of human placental collagen type I (Col I) and Col IV (Sigma-Aldrich St. Louis, MO, USA) was manufactured using biocompatible substances of human origin using the KSV minitrough Langmuir film balance (KSV Instruments). Briefly, both collagens were dissolved in dilute acetic acid (Merck, Germany) to a concentration of 1 $mgml^{-1}$ and pH 3. Collagen solution was applied onto a subphase, two-fold Dulbecco's phosphate buffered saline (DPBS), and allowed to equilibrate for 30 min. Thereafter, the LS film was compressed to a deposition pressure of 12 mNm^{-1} for Col I and 30 mNm^{-1} for Col IV. The LS films were deposited onto substrates by touch-and-lift method. For the double layer LS film, Col IV LS film was deposited on top of a dried Col I LS film. The manufacturing process of the collagen LS films is illustrated in **Study II**/Supplementary Figure 1 and described in detail in the original publication (**Study II**). Before cell seeding, the double layer LS films were sterilized with UV light and hydrated in culture medium for 1 hour.

4.1.3 Electrospun biodegradable membranes

In **Study III**, fibrous electrospun membranes were studied as potential substrates for hESC-RPE. These membranes were manufactured from PLCL (PURAC). Briefly, a 10 % (w/v) solution of PLCL was prepared in chloroform/dimethylformamide (Sigma-Aldrich) solution. The prepared polymer solution was fed into electrospinning chamber system at a flow rate of 1 mlh^{-1}. High

voltage DC current of 18 kV was applied to a 21 G dispensing needle, and formed fibers were collected at 15 cm distance.

The electrospun PLCL membranes were modified with DBD plasma processing technique to enhance hESC-RPE cell growth and maturation in serum-free culture conditions. This procedure was carried out at atmospheric surface pressure using a laboratory scale DBD system (Arcojet Gmbh, Germany). Two different plasma powers, 500 W and 750 W, were studied. Transit speed (v) through the active plasma zone was set at 0.48 ms^{-1} and 10 cycles were run for all samples. Each cycle responded to two periods of exposure (i.e. forward and backward). Exposure of the polymer samples to the atmospheric pressure plasma discharge was described quantitatively by the power density (P_d) and residence time (R). Thus, the total energy delivered by the plasma to the electrospun membrane per unit area was given as the dose D = 2NPd/vl (Jcm^{-2}), where l is the length of the discharge region and N is the number of cycles. The DBD plasma treatment parameters for the studied samples are summarized in Table 6. Electrospun PLCL membranes without the DBD plasma treatment were used as reference material and denoted as untreated samples. Before cell seeding, the various electrospun PLCL membranes were sterilized in 70 % ethanol for 1 h at RT and washed thoroughly with DPBS. The electrospun PLCL membranes were studied with and without additional Col IV dip-coating.

Table 6. DBD plasma surface treatment parameters.

Sample name	Cycles	Plasma power (W)	P_d (Wcm^{-2})	R (s)	D (Jcm^{-2})
ES 5/10	10	500	52.91	0.19	9.92
ES 7/10	10	750	79.37	0.19	14.88

4.2 Biomaterial characterization

The structure and properties of the fabricated collagen LS films (**Study II**) and electrospun plasma-treated PLCL membranes (**Study III**) were analyzed in detail. Moreover, effects of the DBD plasma treatment on the surface properties of the electrospun PLCL membranes were evaluated (**Study III**). The biomaterial characterization methods used in this dissertation are summarized in Table 7. In brief, the microstructure of the fabricated substrates was observed with scanning electron microscopy (SEM), whereas atomic force microscopy (AFM) was used to analyze the nanostructure of the films and fiber topographies. Indirect

immunofluorescence (IF) stainings were carried out to visualize ECM protein coatings (**Study I**), distribution of Col IV coating on electrospun PLCL membranes, the fiber-like structure of the LS films and the conformation of Col I and Col IV therein. The ability of fabricated substrates to act as a semipermeable barrier was studied with a permeability assay. Brewster angle microscopy (BAM) was used to detect the Col I and Col IV Langmuir film formation, whereas surface plasmon resonance (SPR) measurements were performed to determine LS film thickness. The effects of the DBD plasma treatment on the surface chemistry of electrospun PLCL membranes were evaluated with contact angle measurements and X-ray photoelectron spectroscopy (XPS). The chemical composition of the electrospun PLCL membranes was confirmed with Fourier Transform Infrared Spectroscopy (FTIR). The above mentioned biomaterial characterization protocols are described in detail in the original publications **I**-**III**.

Table 7. Biomaterial characterization.

Biomaterial substrate	IF	SEM	AFM	Permeability	BAM	Contact angle	XPS	SPR	FTIR
ECM protein coatings (**I**)	X								
Collagen LS film (**II**)	X	X	X	X	X			X	
Electrospun PLCL membrane (**III**)	X	X	X	X		X	X		X

4.3 Culture of hESC lines

Two hESC lines were used in the original publications. Both hESC lines Regea 08/023 (46, XY) (**Studies I**, **II** and **III**) and Regea 11/013 (46, XY) (**Studies II** and **III**) were previously derived and regularly characterized as described in prior publication (Skottman, 2010). Undifferentiated hESCs were maintained on γ-irradiated (40 Gy) (**Study I**) or Mitomycin C-treated (Sigma-Aldrich) (**Studies II** and **III**) mitocally inactivated human foreskin fibroblast feeder cells (CRL-2429™, ATCC, Manassas, VA, USA) in serum-free culture conditions. The serum-free hESC culture medium consisted of KnockOut™ Dulbecco's Modified Eagle Medium containing 20 % KnockOut™ Serum Replacement (KO-SR), 2 mM Glutamax, 0.1 mM 2-mercaptoethanol (all from Invtirogen, Carlsbad, CA), 1 % Minimum Essential Medium non-essential amino acids, 50 Uml^{-1} penicillin/streptomycin (Cambrex Bio Science, Walkersville, MD) and 8 $ngml^{-1}$ human bFGF (PeproTech). Undifferentiated hESCs were passaged either manually once a week (**Study I**) or

enzymatically using TrypLE Select (Invitrogen, UK) at ten-day intervals (**Studies II** and **III**).

4.4 hESC-RPE differentiation and culture

Human ESCs were differentiated into RPE either in adherent differentiation on protein coatings (**Study I**) or as embryoid bodies (EBs) in suspension cultures on low cell bind well plates (Nunc, Tokyo, Japan) (**Studies II** and **III**). The protein coatings used for adherent differentiation in **Study I** are shown in Table 5. To prompt differentiation, undifferentiated hESC colonies were manually cut into small pieces and transferred either on a protein coating or onto low cell bind well plates for suspension culture. Importantly, KO-SR concentration was reduced to 15 % and bFGF was removed completely from the culture medium to induce spontaneous differentiation. Thereafter, the culture medium was changed three times a week.

Pigmented areas were manually cut under a light microscope with a lancet into pieces. The selected pigmented cells were enriched in adherent cultures on appropriate protein coatings (Table 5). In **Studies II** and **III**, Col IV-coated (5 μgcm^{-2}) well plates (Corning® CellBIND®, Corning, Inc., NY) were used for hESC-RPE enrichment. Finally, hESC-RPE cells were seeded on investigated biomaterial substrates for maturation. For this, hESC-RPE cells were dissociated with TrypLE Select (Invitrogen), filtered through BD Falcon cell strainers (BD BioSciences) and seeded onto biomaterial substrates. The differentiation and maturation steps to produce hESC-RPE cells in this dissertation are illustrated in Figure 9.

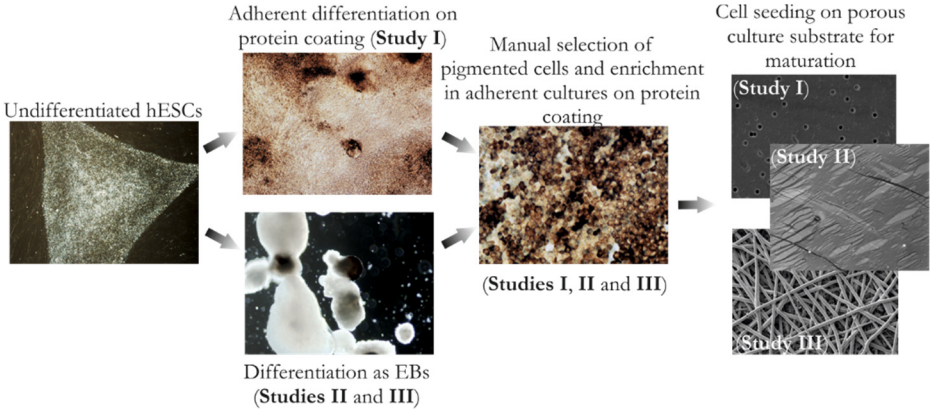

Figure 9. hESC-RPE differentiation and enrichment.

4.5 Characterization of hESC-RPE cells on biomaterial substrates

4.5.1 Analysis of pigmentation

In **Study I**, appearance of the first pigmentation during adherent differentiation of hESCs on the different protein coatings was observed daily using Nikon Eclipse TE200S phase-contrast microscope (Nikon Instruments, The Netherlands). After 42 days of culture on protein coated cell culture inserts and altogether 140 days of differentiation, degree of pigmentation was evaluated further with image analysis of phase-contrast microscope images from randomly selected locations on cell culture inserts. The degree of pigmentation was quantified with Image J Image Processing and Analysis Software and presented as inverse of pixel intensities normalized against Col IV.

4.5.2 Analysis of cell number and proliferation

In **Study III**, the attachment and proliferation of hESC-RPE cells on untreated and DBD plasma-treated electrospun PLCL membranes was studied by cell counts. Images of 4´, 6´diamidino-2-phenylidole (DAPI)-stained nuclei were captured with AxioScope A1 fluorescence microscope and analyzed with the Cell Counter plugin in Image J Image Processing and Analysis Software. Detailed protocol is presented in the original publication (**Study III**). The hESC-RPE cell proliferation on various electrospun PLCL membranes was examined further using AlamarBlue® assay (Invitrogen) according to the manufacturer's instructions. This assay is based on its active ingredient, resazurin, which is a non-toxic cell permeable compound that converts to red-fluorescent resofurin. The change from non-fluorescent molecule to a compound with bright fluorescence is due to a reduction reaction by metabolically active cells. The amount of fluorescence is proportional to the amount of number of living cells. In **Study III**, the measured fluorescence values were normalized against the hESC-RPE cells cultured on untreated electrospun PLCL membranes to study the effect of DBD plasma surface treatment on hESC-RPE cell proliferation on these membranes.

4.5.3 Gene expression analysis

Gene expression of RPE specific markers as well as markers for pluripotency was assessed with reverse transcription-polymerase chain reaction (RT-PCR) (**Studies I**, **II** and **III)**. RNA was extracted using NucleoSpin XS and NucleoSpin® RNA II kits (Macherey-Nagel, GmbH & Co) in accordance with the manufacturer's instructions. The RNA concentration and quality were determined with NanoDrop 1000 spectrophotometer (NanoDrop Technologies, Wilmington, DE). 40 ng of the isolated RNA was reverse transcribed with MultiScribe Reverse Transcriptase (Applied Biosystems, Foster City CA) according to the manufacturer's guidelines. The cDNA synthesis was performed in the following conditions: 10 min at 25 ºC, 120 min at 37 ºC and 5 min at 85 ºC. PCR reaction was performed using 1 µl of cDNA as a template and 5 $U\mu l^{-1}$ Taq DNA Polymerase (Fermentas, Thermo Fisher Scientific INc., Leicestershire, UK) with 5 µM primers (Biomers.net Gmbh, Söflinger, Germany) specific for the target genes. Studied genes, their primer sequences and annealing temperatures are listed in Table 8. Water was included as a control in RT-PCR analysis to detect any impurities in the procedure and reagents. Glyceraldehyde 3-phosphate dehydrogenase (GAPDH) was used as an endogenous control. Undifferentiated hESCs were used as a control for hESC-RPE cells cultured on various substrates.

Table 8. RT-PCR genes, primer sequences and annealing temperatures.

Gene symbol	Forward (5'>3')	Reverse (5'>3')	Tann (C°)	Study
BEST	GAATTTGCAGGTGTCCCTGT	ATCCTCCTCGTCCTCCTG AT	55	**II, III**
GAPDH	GTTCGACAGTCAGCCGCATC	GGAATTTGCCATGGGTGGA	55	**I, II, III**
MITF	AAGTCCTGAGCTTGCCATGT	GGCAGACCT TGGTTTCCAA	52	**II, III**
NANOG	TGAAATGTCTTCTGCTGAGAT	GTTCAGGATGTTGGAGAGTTC	55	**I, II**
OCT3/4	CGTGAAGCTGGAGAAGGAGAAGC TG	AAGGGCCGCAGCTTACACATGT TC	62	**I, II, III**
PEDF	AGCTCGCCAGGTCCACAAAG	TGGGCAATCTTGCAGCTGAG	60	**II, III**
RPE65	TCCCCAATACAACTGCCACT	CACCACCACACTCAGAACTA	52	**II, III**
TYR	TGCCAACGATCCTATCTTCC	GACACAGCAAGCTCACAAGC	52	**II, III**

Abbreviations: *BEST*=bestrophin, *GAPDH*=glyceraldehyde 3-phosphate dehydrogenase, *MITF*=microphthalmia-associated transcription factor, *NANOG*=nanog homeobox, *OCT3/4*=octamer-binding transcription factor, *PEDF*=pigment epithelium-derived factor, *RPE65*=retinal pigment epithelium specific protein 65 kD, *TYR*=tyrosinase

PCR reactions were carried out in PCR MasterCycler as follows: 3 min at 95 ºC, 38 cycles at 95 ºC for 30 s, annealing temperature 30 s and 1 min at 72 ºC. Final extensions were run at 72 ºC for 5 min. PCR products were visualized on 2.0 %

agarose gels with a 50 bp DNA ladder (MassRuler™ DNA Ladder Mix; Fermentas). The bands were imaged with Quantity one 4.5.2. Basic program (Bio-Rad Laboratories, Inc., Hercules, CA).

Differences in gene expression levels were studied further with quantitative real-time PCR (qPCR) (**Studies I** and **II**). The studied genes as well as corresponding TaqMan primers are listed in Table 9. For details of the qPCR protocol, see the original publication (**Study I**).

Table 9. The expression levels of genes studied with qPCR.

Gene symbol	Gene name	TaqMan assay	Study
BEST	bestrophin	Hs00959251_m1	**I**
COL4A1	collagen type IV alpha-1	Hs00266237_m1	**I**
CRALBP	cellular retinaldehyde-binding protein	Hs00165632_m1	**I**
FN1	fibronectin 1	Hs00365052_m1	**I**
GAPDH	glyceraldehyde 3-phosphate dehydrogenase	Hs99999905_m1	**I, II**
LAMA1	laminin subunit alpha-1	Hs00300550_m1	**I**
LAMA5	laminin subunit alpha-5	Hs00245699_m1	**I**
MERTK	Mer tyrosinase kinase receptor	Hs00179024_m1	**I**
MITF	microphthalmia-associated transcription factor	Hs01115553_m1	**I**
PAX6	paired box gene 6	Hs00240871_m1	**I**
RPE65	retinal pigment epithelium specific protein	Hs01071462_m1	**I, II**

4.5.4 Indirect immunofluorescence staining

Protein expression and localization in hESC-RPE cells grown on different substrates was examined with IF staining (**Studies I**, **II** and **III**). The structure of the manufactured collagen LS films was verified with IF staining in **Study II**. Moreover, IF analysis was established to evaluate the distribution of Col IV on electrospun PLCL membranes in **Study III**. The primary antibodies used for IF staining in this dissertation are listed in Table 10. In addition, phalloidin-tetramethylrhodamine B isothiocyanate (Sigma-Aldrich) was used to visualize the filamentous actin cytoskeleton in hESC-RPE cells grown on investigated substrates. The entire IF protocol is described in detail in the original publications (**Studies I**, **II**, and **III**).

Table 10. Protein expression and localization examined with IF staining.

Antibody	Host	Manufacturer	Dilution	Study
Bestrophin	Rabbit	Abcam, Cambridge, UK	1:200-1:400	**I, II, III**
Collagen I	Rabbit	Millipore	1:200	**II**
Collagen IV	Mouse	Neomarkers	1:100	**I**
Collagen IV	Mouse	Merck Millipore	1:200	**II, III**
CRALBP	Mouse	Abcam, Cambridge, UK	1:200-1:600	**I, II, III**
Fibronectin	Mouse	Chemicon	1:500	**I**
Laminin	Rabbit	Abcam, Cambridge, UK	1:200	**I**
MERTK	Mouse	Abnova	1:50	**II, III**
MITF	Rabbit	Abcam, Cambridge, UK	1:350	**II, III**
Na^+/K^+ATPase	Mouse	Abcam, Cambridge, UK	1:100-1:200	**I, II, III**
OCT3/4	Goat	R&D Systems Inc., Minneapolis, MN	1:200	**II**
ZO-1	Mouse	Invitrogen, Carlsbad, CA	1:250	**I, II, III**

4.5.5 Western blotting

The ECM protein expression in hESC-RPE cells grown on Col IV, FN, LN and MG coatings was quantified with Western blotting (WB) (**Study I**). Furthermore, the expression of RPE specific protein RPE65 in hESC-RPE cells cultured on double layer collagen LS films and controls was determined with WB (**Study II)**. The primary antibodies are presented in Table 11. β-actin was used as a loading control in all WB analyses in the studies carried out as a part of this dissertation. Detailed WB protocol is reported in the original publication (**Study I**).

Table 11. Protein expression investigated with western blotting.

Antibody	Host	Manufacturer	Dilution	Study
β-actin	Mouse	Santa Cruz	1:5000	**I, II**
Collagen IV	Mouse	Merck Millipore	1:1000	**I**
Fibronectin	Mouse	Merck Millipore	1:8000	**I**
Laminin	Rabbit	Abcam, Cambridge, UK	1:1000	**I**
RPE65	Mouse	Merck Millipore	1:5000	**II**

4.5.6 Transmission electron microscopy

Transmission electron microscopy (TEM) was used to evaluate the fine structure of maturated hESC-RPE cells on different protein coatings (**Study I**). Sample preparation for TEM analysis is described in detail in the original publication (**Study I**). Samples were imaged with JEM-2100F transmission electron microscope (Jeol Ltd., Tokyo, Japan).

4.5.7 Transepithelial resistance

Transepithelial resistance (TER) measurements were used to assess the integrity and barrier function of hESC-RPE on various biomaterial substrates (**Study I**, **II** and **III**). Measurements were carried out with a Millicell electrical resistance system volt-ohm meter (Merck Millipore, Darmstad, Germany) in DPBS. In **Studies II** and **III**, samples were clamped to a P2307 slider (Physiologic Instruments) and placed in a custom-made Teflon chamber (Juuti-Uusitalo et al., 2013). TER values of similarly treated empty substrates without cells were subtracted from the original values. Final values were calculated multiplying the result by the surface area of the substrate (Ωcm^2).

4.5.8 Permeability assay

The ability of manufactured biomaterial substrates to act as a semipermeable barrier was determined by measuring the flux of small molecular weight (700 Da) Alexa Fluor® 568 Hydrazide sodium salt (Life Technologies) (**Studies II** and **III**). In **Study II**, the integrity of hESC-RPE monolayer on collagen LS films was also assessed with the permeability assay. This assay was carried out in Ussing chamber system (Physiologic Instruments, San Diego, CA) and culture medium without KO-SR was used as diffusion medium. The detailed protocol is described in the original publications.

4.5.9 Phagocytosis

The phagocytic properties of hESC-RPE cells grown on biomaterial substrates were investigated with *in vitro* phagocytosis assay (**Studies I**, **II** and **III**). In **Study I**, rat retinal explants were used, whereas in **Studies II** and **III** the assay was carried out with isolated porcine POS. Both protocols are described in detail in the original publications (see **Study I** for the rat retina explant protocol and **Study II** for the isolated porcine POS protocol). In **Study III**, human foreskin fibroblasts were used as a negative control. Additionally, hESC-RPE cell controls were blocked with anti-MERTK antibody to demonstrate that the phagocytic activity in hESC-RPE is MERTK dependent and RPE-specific. The images of hESC-RPE cells with internalized POS fragments in both cases were taken with a Zeiss LSM 700 confocal microscope (Carl Zeiss) using sectional scanning.

4.5.10 Enzyme-linked immunosorbent assay

The functionality of hESC-RPE cells grown on double layer collagen LS films was evaluated by their PEDF secretion (**Study II**). PEDF concentration was quantified with Chemikine PEDF Sandwich Enzyme-linked immunosorbent assay (ELISA) Kit (Millipore) according to the manufacturer's instructions. The PEDF concentrations were determined from conditioned medium after 24 h incubation with hESC-RPE cells cultured on double layer LS films and dip-coated controls. PEDF concentrations were normalized to cell densities on each investigated substrate.

4.6 Statistical analyses

Mann-Whitney *U*-test in the IBM SPSS Statistics software was used for determining statistical significance in cell characterization studies on all investigated biomaterial substrates established as part of this dissertation. In **Study III**, one-way analysis of variance (ANOVA) and Tukey's multiple comparison test were used to assess statistical differences in surface properties between the various electrospun PLCL membranes under investigation. P-values <0.05 were considered significant.

4.7 Ethical considerations

The National Authority for Medicolegal Affairs in Finland has authorized The Institute of Biosciences and Medical Technology (BioMediTech) to conduct research with human embryos (Dnro 1426/32/300/05). In addition, the local ethics committee of the Pirkanmaa hospital district Finland has given the institute a supportive statement to derive and expand hESC lines and use these cell lines for research purposes (Skottman/R05116). No new cell lines were derived for the studies carried out in this dissertation.

5 Summary of the results

5.1 Protein coatings as hESC-RPE cell biomaterial substrates

The aim of **Study I** was to investigate the effect of several xeno-free ECM proteins as well as a xeno-derived substrate Matrigel™ on hESC-RPE cell differentiation, maturation and functionality in serum-free adherent cultures. All investigated protein coatings resulted in successful hESC-RPE differentiation with no eminent biologically relevant differences in the early stages of differentiation (**Study I**/Figure 1).

Pigmented areas were selected for further maturation and enrichment on all coatings. After 140 days of differentiation, confluent hESC-RPE with hexagonal RPE cell morphology were seen on all substrates. Moreover, all protein coatings promoted the growth of hESC-RPE as monolayer (**Study I**/Supplementary Figure 4). However, non-uniform epithelia were at times detected on LN and VN coatings in visual inspection by phase-contrast microscopy and TER measurements. In addition, hESC-RPE cells on all studied protein coatings showed positive expression of RPE specific proteins bestrophin and CRALBP as well as correct polarization with apical expression of Na^+/K^+ATPase in IF staining (**Study I**/Figure 1). Importantly, RT-PCR analysis revealed no expression of pluripotency markers *OCT3/4* and *Nanog* on protein coatings (**Study I**/Supplementary Figure 1). Further, comparison of gene expression levels with qPCR did not show any significant differences in mature RPE marker gene expression between the protein coatings (**Study I**/Supplementary Figure 2). The phagocytic properties of hESC-RPE cells were investigated on Col IV, FN, LN, CS and MG coatings with rat explant *in vitro* phagocytosis assay. Internalized POS were seen in hESC-RPE on all protein coatings (**Study I**/Supplementary Figure 3).

Significant differences were found in hESC-RPE cell phenotype and functionality between protein coatings in long-term differentiation. Visual microscopic inspection as well as pigmentation analysis showed abundant pigmentation on LN, whereas FN and MG showed lower levels of pigmentation (**Study I**/Figure 2). Intermediate pigmentation levels were detected on Col IV. Moreover, TEM analysis revealed variation in the morphology and height of hESC-RPE cells cultured on different

protein coatings (**Study I**/ Figure 3). Human ESC-RPE cells on MG showed cuboidal morphology, whereas more columnar cells were seen on other investigated protein coatings. Human ESC-RPE cells had the highest cell thickness on LN, whereas substantially thinner cells were seen on MG. In addition, the structure and density of the apical microvilli varied between the studied protein coatings. The effects of protein coatings on hESC-RPE cell differentiation and maturation are summarized in Table 12.

Table 12. Summary of the effects of ECM protein coatings on hESC-RPE cells.

Protein coating	Col IV	Col I	LN	FN	VN	CS	MG
Appearance of pigmentation (days)	12±2	12±1	14±3	16±4	13±3	14±4	16±5
Degree of pigmentation	++	+++	++++	+	+ +	+++	+
Gene exression of early eye field markers	+	+	+	+	+	+	+
hESC-RPE monolayer	++	++	+	++	+	++	++
hESC-RPE cell morphology	+	+	+	+	+	+	+
RPE gene expression	+	+	+	+	+	+	+
RPE protein expression	+	+	+	+	+	+	+
Polarization	+	+	+	+	+	+	+
TER (Ωcm^2)	247±35	183±72	128±25	552±56	122±64	275±77	473±53
Presence of tight junctions	+	+	+	+	+	+	+
Phagocytosis	+	NA	+	+	NA	+	+
Cell thickness (μm)	13.2±2.4	13.8±0.1	14.7±1.3	12.5±1.1	10.8±1.4	10.9±0.5	7.6±0.4
Basal lamina thickness (μm)	0.31±0.08	0.70±0.07	0.82±0.28	0.27±0.08	0.32±0.06	0.22±0.05	0.33±0.06
ECM protein secretion	High	High	High	Low	High	Low	High
- Collagen IV	+ ++	+ +	+ +	+	+	+	+
- Fibronectin	+++	++	++	-	++	-	+
- Laminin	++	++	++	+	++	+	+++

NA=Not analyzed.

The ECM protein secretion by hESC-RPE cells cultured on different protein coatings was thoroughly characterized with qPCR, IF, TEM and WB. qPCR revealed no clear differences in the expression levels of genes encoding ECM proteins. However, IF staining showed abundant secretion of collagen IV, fibronectin and laminin fibers on Col IV, Col I, LN, VN and MG (**Study I**/Figure 4). On the contrary, low amounts of collagen IV and laminin were seen on FN and CS coatings,

and fibronectin fibers were not detected at all. IF stainings additionally confirmed the basal localization of secreted collagen IV and fibronectin (Figure 10) (unpublished images). Laminin fibers were mainly localized basally, but some were also observed at intercellular spaces.

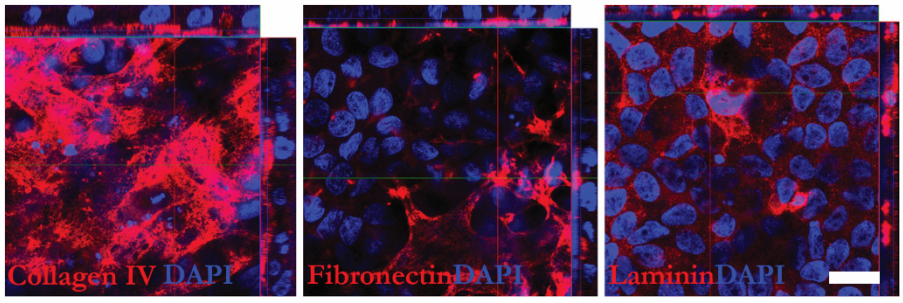

Figure 10. Localization of the secreted ECM proteins on LN coating. Scale bar 10 µm.

Furthermore, TEM analysis revealed differences in self-assembled basal lamina thickness of hESC-RPE cells on protein coatings (**Study I**/Figure 3). In WB analysis, the highest laminin deposition was found on MG, whereas the highest fibronectin and collagen secretion was detected on Col IV (**Study I**/Figure 5). Unlike the IF staining, WB analysis confirmed fibronectin to be deposited on FN coating.

5.2 Biomimetic microenvironment for hESC-RPE cells

In **Study II**, a biomimetic microenvironment was fabricated for the *in vitro* production of hESC-RPE cells in serum-free culture conditions. The LS technique was applied to create a biomaterial substrate resembling the structure and organization of the native Bruch's membrane. The suitability of the LS fabrication method for Col I and Col IV was evaluated with surface pressure-area isotherms. These measurements demonstrated an increase in surface pressure when collagens were applied to the DPBS air-subphase interface. Moreover, for both collagens the surface pressure increased steadily upon compression of the air-subphase interface. During LS film fabrication, BAM was used to detect the film and fiber formation at the air-subphase interface. The density of collagens at the air-subphase interface increased during compression, and fiber-like structures were observed. The

fabricated LS films had a fiber-like microstructure, and the substrates were fully covered with collagens (**Study II**/Figure 1).

The structure and organization of the LS films was analyzed with SEM, AFM, IF, SPR and permeability assay. Col I LS films consisted of well-oriented fibers, whereas Col IV LS films had more net-like structure. On the contrary, fiber-like organized structures were not detected on dip-coated controls. Double layer LS films, with Col I and Col IV layers, were highly permeable for small molecular weight marker (**Study II**/Figure 1). However, the double layer LS film restricted the flow of the small molecular weight marker compared to an empty substrate therefore forming a barrier. For Col I, average width of the small fibrils was 4.5 nm, while widths of up to 65 nm were observed for larger fibrils. Widths of 12.5 nm and 140 nm were measured for smaller and larger Col IV fibrils, respectively. The double layer LS films had an average thickness of 27.1±3.0 nm, whereas for the dip-coated Col IV controls thickness of only 5.4±0.22 nm was measured (**Study II**/Figure 3).

The stability of the collagen LS films was evaluated in water flow with MP-SPR, and merely small changes in the angle were detected (**Study II**/Supplementary Figure 3 and Supplementary Table 1). In addition, the stability of the double layer LS films *in vitro* was evaluated (Figure 11, not reported in the original publication). The fabricated films were kept in culture medium at +37 °C and analyzed with IF. After 14 days of incubation, some degradation was observed on the film surface. After 63 days of incubation, the double layer LS film was still present on the substrate surface. However, clear thinning of the film was seen compared to the earlier time points.

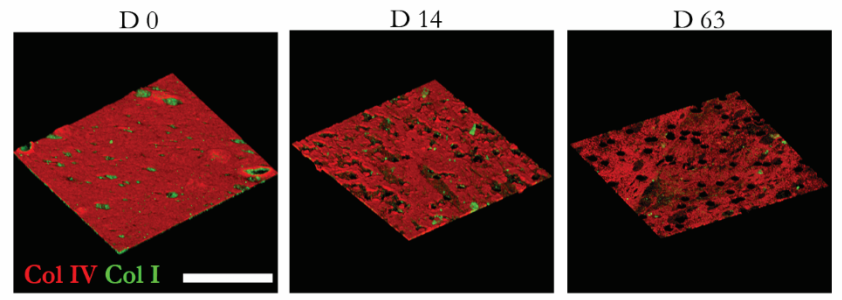

Figure 11. *In vitro* degradation of double layer LS films in culture medium before (D0) and after 14 days (D14) and 63 days (D63) of incubation. 3D images from vertical confocal sections. Scale bar 50 µm.

The double layer collagen LS films supported the formation of confluent, polarized, and uniform hESC-RPE with abundant pigmentation and RPE cell

morphology. A clear difference was seen in the monolayer homogeneity between LS film and dip-coated control; more uniform and smoother epithelium was formed on LS film (**Study II**/Figure 4, Supplementary Figure 4). Human ESC-RPE on both LS films as well as dip-coated controls exhibited expression of RPE specific markers on both gene and protein level. However, expression of *RPE65* in hESC-RPE on LS films was increased compared to the dip-coated controls, as demonstrated using qPCR. In addition, hESC-RPE cells grown on LS film expressed RPE65 at higher levels compared to the dip-coated controls (**Study II**/Figure 4).

The barrier properties of hESC-RPE on LS films and dip-coated controls were thoroughly examined with IF, TER measurements, and permeability assay. Human ESC-RPE cells on LS films showed uniform expression of ZO-1, whereas more discontinuous labeling was detected on dip-coated controls. Moreover, hESC-RPE cells on LS films had significantly higher epithelial integrity seen in TER measurements compared to the controls in both investigated cell lines. Furthermore, hESC-RPE cells on LS films resulted in significantly lower permeability for a small molecular weight marker compared to the dip-coated controls (**Study II**/Figure 5). Human ESC-RPE cells from both cell lines on all investigated substrates demonstrated phagocytic activity with internalized POS detected with confocal microscopy. However, major differences were found in PEDF secretion between LS films and dip-coated controls. Human ESC-RPE cells on double layer LS films showed notably increased PEDF secretion levels compared to the dip-coated controls (**Study II**/Figure 6). The maturation and functionality of hESC-RPE cells on biomimetic LS films and dip-coated controls is summarized in Table 13.

Table 13. Summary of the results of hESC-RPE cell maturation and functionality on LS films and dip-coated controls.

	Cell line	Regea 08/023		Regea 11/013	
Feature	**Method**	**LS film**	**Dip-coated control**	**LS film**	**Dip-coated control**
Pigmentation	Light microscopy	+	+	+	+
RPE cell morphology	Light microscopy, IF	+	+	+	+
RPE monolayer	Light microscopy, IF	+++	+	+++	+
Polarization	IF	+	+	+	+
RPE gene expression	RT-PCR	+	+	+	+
	qPCR	++	+	++	+
Expression of pluripotency genes	RT-PCR	-	-	-	-
RPE-related proteins	IF	+	+	+	+
	WB	+++	+	++	+
Tight junctions	IF	++	+	++	+
Barrier properties	TER	++	+	++	+
	Permeability (P_{app}, cm^2s^{-1})	1.76×10^{-6}	3.86×10^{-6}	2.48×10^{-6}	4.93×10^{-6}
Phagocytosis	Phagocytosis assay	+	+	+	+
Growth factor secretion	PEDF ELISA ($ngml^{-1}$)	1682±167	274±118	853±146	207±155

5.3 Biodegradable fibrous transplantation material for hESC-RPE

In **Study III**, porous biodegradable electrospun PLCL membranes were fabricated. The aim was to create a substrate that mimics the fibrous structure of the native Bruch's membrane. The electrospun PLCL membranes had an average fiber diameter of 3.1±0.14 μm, and the formed fibers had an unaligned orientation (**Study III**/Figure 1). These membranes had an average thickness of 43.2±1.95 μm and were permeable for small molecular weight substance.

The electrospun PLCL membranes were surface modified with DBD plasma treatment to promote hESC-RPE cellular response. The effects of the DBD plasma treatment on the surface properties and chemical composition of the fabricated membranes were evaluated with SEM, AFM, XPS, contact angle measurements and IF staining. The surface-treated membranes had increased surface roughness

compared to the untreated samples (**Study III**/Figure 1). Moreover, an eminent reduction was seen in contact angle measurements of the surface-treated membranes indicating increased hydrophilicity of the surface (**Study III**/Figure 2). XPS analysis revealed a significant increase in oxygen content of the surface-treated PLCL membranes, which was dependent on the DBD plasma dose applied on the surfaces (**Study III/**Figure 3, Table 1). Furthermore, DBD plasma treatment before additional Col IV-coating increased the atomic concentration of nitrogen in XPS analysis. The amount of nitrogen on Col IV-coated surface-treated PLCL membranes was significantly higher compared to the untreated PLCL membranes with additional Col IV-coating (**Study III**/table 2). In addition, Col IV-coating had distributed in uniform manner on all investigated PLCL membranes (**Study III**/Figure 4).

Without additional Col IV-coating, hESC-RPE cells did not grow on any of the fabricated electrospun PLCL membranes. In addition, hESC-RPE cell attachment and proliferation were poor on untreated Col IV-coated electrospun PLCL membranes (**Study III**/Figure 5, Supplementary Figure 2). DBD plasma treatment significantly increased the cell attachment and proliferation on electrospun PLCL membranes when combined with additional Col IV-coating (**Study III**/Figure 5). Moreover, the DBD plasma surface modified PLCL membranes with Col IV-coating supported the formation of confluent and uniform hESC-RPE layer in serum-free culture conditions (**Study III**/Figure 5). Human ESC-RPE cells on these surface modified membranes expressed mature RPE marker genes and morphologically correct and homogeneous localization of the RPE-specific proteins in IF stainings (**Study III/** Figures 5 and 6). Likewise, Col IV-coated DBD plasma treated PLCL membranes supported the formation of polarized epithelium with apical expression of Na^+/K^+ATPase, MERTK and ZO-1. In addition, hESC-RPE on Col IV-coated DBD treated PLCL membranes showed improved epithelial integrity and barrier properties compared to the untreated membranes in TER measurements. Finally, hESC-RPE functionality on these films was verified with phagocytosis assay where internalized POS were seen in both studied hESC-RPE cell lines (**Study III**/Figure 7).

6 Discussion

Human ESC-RPE cells show great potential as a cell source for retinal tissue engineering applications (Schwartz et al., 2015). Therefore, efficient production of mature and functional hESC-RPE monolayer sheets is essential for their future use in clinical applications (Hu et al., 2012; Koss et al., 2016). However, the current *in vitro* and *in vivo* intended biomaterial substrates and transplantation materials fail to mimic the natural environment of the RPE (Jha & Bharti, 2015), which could possibly affect the performance of the produced cells in transplantations (McCarthy et al., 1996). Thus special attention must be paid in to biomaterial design and optimization for retinal tissue engineering applications.

6.1 Protein coatings as hESC-RPE cell biomaterial substrates

The ECM proteins adsorbed to the biomaterial substrate affect the differentiation fate of hESCs (Laperle et al., 2015). Previously, ECM protein coatings have been demonstrated to influence early stage differentiation of hPSCs into neural progenitors and neurons (Ma et al., 2008), retinal progenitor cells (Gong et al., 2008), and RPE (Rowland et al., 2013). In previous studies, human RPE cells have shown improved attachment to RPE basement membrane and its proteins compared to the other layers and components of Bruch's membrane (Tezel et al., 1999; Tezel & Del Priore, 1999). Thus, the first aim of this dissertation was to evaluate the effect of selected ECM proteins found in Bruch's membrane on production of hESC-RPE cells for clinical purposes. Human ESCs were differentiated to RPE on several xeno-free human-derived ECM proteins as well as on xeno-derived Matrigel™ in adherent cultures. Here, in **Study I**, we hypothesized that abundant components of the native RPE basement membrane, namely Col IV and LN, would result in improved performance during hESC-RPE differentiation and further maturation.

Unexpectedly in **Study I,** no eminent differences were detected between the investigated protein coatings in hESC-RPE differentiation when assessing its early stages. These results are in line with a previous study, where hiPSC-RPE differentiated on several different ECM proteins demonstrated RPE cell

morphology and expression of key RPE genes (Rowland et al., 2013). However, the effect of full-length ECM proteins was previously evaluated only on hiPSC-RPE differentiation by analysing the cell morphology, pigmentation frequency and RPE gene expression on ECM substrates (Rowland et al., 2013). In **Study I**, evident disparities were found when assessing the fine structure and functionality of these cells. Remarkable differences were detected in the degree of pigmentation, basal lamina secretion as well as barrier properties between hESC-RPE cells maturated on different protein coatings. To compare, significant differences were previously reported in pigmentation density after 5 weeks of initial differentiation between hiPSC-RPE generated on different ECM substrates (Rowland et al., 2013). Thus, the results of **Study I** indicate that the choice of substrate in hESC-RPE differentiation and maturation is of high importance when producing cells for clinical purposes. Regardless of the extensive use of full-length protein coatings in retinal tissue engineering applications, the effects of different ECM proteins on the maturation and functionality of hESC-RPE have not been previously thoroughly assessed. Hence, **Study I** is the first to show an extensive comparative analysis of hESC-RPE differentiated and further maturated on several ECM substrates.

While significant progress has been made with hPSC-RPE differentiation, the criteria for the generated RPE cells to be used in clinical settings have not been validated yet (Jha & Bharti, 2015). The hexagonal RPE cell morphology, expression of RPE specific proteins on gene and protein level, polarization of the RPE monolayer, abundant pigmentation, phagocytic properties and formation of tight barrier are generally considered as hallmarks of mature RPE (Bharti et al., 2011; Binder et al., 2007; Burke, 2008; Jha & Bharti, 2015; Rizzolo et al., 2011). When assessing all the above mentioned criteria in **Study I**, Col IV was the golden mean coating. Surprisingly, the degree of pigmentation showed an inverse relation to the epithelial resistance: heavily pigmented hESC-RPE on LN demonstrated low TER values whereas low degree of pigmentation and highest TER values were observed on hESC-RPE cultured on FN and MG coatings. Previously, mouse laminin-111 and Matrigel™ have been suggested as suitable matrices for hPSC-RPE differentiation due to relatively high degree of pigmentation (Rowland et al., 2013). In contrast, less pigmented hESC-RPE cells were chosen for the first clinical trial over heavily pigmented cells as they demonstrated improved cell attachment and migration (Schwartz et al., 2012). Additionally, in a recent study evaluation of cellular function, in particular epithelial integrity and electrical activity, were suggested as potential tools for testing hiPSC-RPE quality for clinical applications (Miyagishima et al., 2016). Thus, the aspect of epithelium maturation and selection criteria of

hPSC-RPE cells for clinical applications needs to be clarified and further assessed with respect to *in vivo* functionality of the cells.

Several concerns, such as pathogen transmission and immunogenicity, have been associated with animal-derived components and their use in tissue engineering applications (Sakamoto et al., 2007). Yet, xenogeneic components, such as gelatin and Matrigel™, are commonly in use during hPSC-RPE differentiation and enrichment (Kamao et al., 2014; Lu et al., 2014; Rowland et al., 2013; Schwartz et al., 2012). Matrigel™ is extracted from the Engelbreth-Holm-Swarm mouse sarcoma and it is rich in ECM proteins including laminin, collagen IV, heparan sulfate proteoglycans, and entactin/nidogen. Previously, Matrigel™ has been shown to contain over 1800 proteins that vary from batch to batch (Hughes et al., 2010; Hughes et al., 2011). Gelatin is denaturated collagen that has been processed to remove its higher order structure and it is generally extracted from animal sources such as porcine and bovine skin and bone (Malafaya et al., 2007; Veis & Cohen, 1960). In **Study I**, hESC-RPE cells were successfully differentiated and maturated on the xeno-free fully defined cGMP-produced matrix CS. Additionally, several xeno-free human-derived proteins supported the formation of functional hESC-RPE and therefore are more suitable substrate choices compared to Matrigel™ and other animal-derived protein coatings in hESC-RPE production for clinical applications.

Biomaterial substrates of natural origin have the advantage of mimicking the intrinsic architecture of the native ECM (Rahmany & Van Dyke, 2013). However, several limitations have been associated with the use of full-length protein coatings such as batch to batch variations and limited scalability of the manufacturing process (Hotaling et al., 2016; Villa-Diaz et al., 2013). Moreover, upon adsorption, the large proteins tend to fold randomly and thus the binding domains for integrins may not be available for the cells (Lewandowska et al., 1992). In addition, full-length proteins have been shown to elicitan immune response upon transplantation. In contrast, shorter peptides containing the binding motifs have been shown to be less antigenic compared to their full-length proteins (Rudensky et al., 1991; Yewdell & Bennink, 2001). Many of these obstacles encountered with xenogeneic material and full-length ECM protein coatings could be circumvented by using synthetic substrates and peptide motifs or full-length engineered proteins obtained by recombinant DNA technology (Plaza Reyes et al., 2016; Villa-Diaz et al., 2013).

The coating success of biomaterial substrates is based on physicochemical adsorption of the proteins on material surface, and thus depends on the substrate surface properties and its interaction with ECM protein in question (Wilson et al.,

2005). In **Study I**, polystyrene cell culture well plate wells and commercial PET cell culture inserts were coated with various protein coatings. The coating success in this study was evaluated solely by their ability to support hESC-RPE differentiation and maturation, and the amount of adsorbed proteins and their conformations on the substrate were not analyzed. Thus, it should be emphasized that on distinct biomaterial substrates these full-length protein coatings can adsorb differently and possess various conformations affecting the cellular response thereon (Hlady & Buijs, 1996). Further studies are needed to investigate the success of full-length protein coating, the protein conformation, and interaction with biomaterial substrates in order to fully understand their role in hESC-RPE differentiation and maturation.

Sufficient ECM production by hESC-RPE is important in respect to their use in clinical applications to ensure adequate cell attachment, proper integration to the host tissue and remodeling of the damaged Bruch's membrane in AMD (Sugino et al., 2011). Previously, ECM protein composition on the biomaterial substrate was shown to affect ECM deposition by the differentiating hESCs (Laperle et al., 2015). In **Study I**, the qPCR analysis, IF staining, WB analysis as well as TEM showed that hESC-RPE cells assemble their own basal lamina. Previously, hESC-RPE cells grown on Matrigel™ showed secretion of basement membrane components in TEM and IF analysis (Vugler et al., 2008). Yet, a comparison elucidating the ECM secretion by hESC-RPE cells grown on different substrates has not been reported previously. In **Study I**, qPCR analysis was carried out after a total of 140 days of differentiation and maturation. Even though other analyses revealed differences in ECM composition secreted by hESC-RPE between the investigated protein coatings, no clear differences were found on gene expression level. Most likely, this time point was too late after cell seeding on protein coatings, and earlier inspection of ECM protein gene expression levels could be more relevant. Moreover, gene expression of only one Col IV isomer was assessed. Thus, a more thorough analysis of different ECM protein isomers should be conducted to evaluate the ECM secretion of hESC-RPE in more detail. IF staining of the hESC-RPE cells on substrates showed fiber-like ECM proteins, whereas IF staining of the protein coated substrates without cells did not have a fiber-like structure. This is in line with previous studies showing the distribution of dip-coated full-length proteins in IF staining on biomaterial substrates (Calejo et al., 2016; Subrizi et al., 2012). Thus, the fiber-like ECM proteins seen in IF staining were produced or modified by the cells. To my knowledge, **Study I** was the first to exhibit that self-assembly of ECM proteins by hESC-RPE is influenced by their substrate.

Laminins in the basement membranes have an important role for cell adhesion (Kalluri, 2003) and they have been shown to support the derivation and culture of hESCs (Rodin et al., 2014) as well as RPE differentiation (Plaza Reyes et al., 2016; Rowland et al., 2013). In **Study I**, hESC-RPE cells were successfully differentiated on LN coating. Even though hESC-RPE cells on LN were superior in all other studied aspects, they demonstrated low TER values. Recently, mouse laminin-111 was suggested as a potential substrate for hiPSC-RPE differentiation due to a high degree of pigmentation (Rowland et al., 2013). However, the integrity of the epithelium on laminin was not assessed in that study. Since Col IV supported the formation of mature and functional hESC-RPE with good epithelial integrity and average degree of pigmentation in **Study I,** and due the structural role of collagens in basement membranes, Col IV was chosen as the starting material and protein coating for the **Studies II** and **III**. Nevertheless, further studies are required to find the optimal protein coating and biomaterial substrate combination for hESC-RPE cell production for clinical applications.

6.2 Biomimetic microenvironment for hESC-RPE cells

After initial cell attachment to a substrate, cells undergo several processes that can be directed by the stimuli provided by the ECM in the native environment. However, recapitulating all these signals for biomaterial substrates remains a challenge in biomaterial design: the classic cell culture substrates do not provide the native cell microenvironment existing naturally *in vivo*, potentially affecting the clinical performance of the cells in tissue engineering applications (Alamdari et al., 2013). The aim of **Study II** was to fabricate a biomimetic microenvironment simulating the layered structure and composition of the two uppermost layers of Bruch's membrane. Human placental Col I and IV were used in the manufacturing process without additional bioincompatible substances.

The collagen film fabricated with LS technology had a layered and fibrous structure with Col I layer below and Col IV layer on top to mimic the inner collagenous layer and basement membrane of Bruch's membrane, respectively. Apart from layered structure, the Col I layer consisted of fiber-like structures with diameters ranging from 4.5 nm up to 65 nm suggesting that it contains Col I tropocollagen, microfibrils and fibers. In a previous study mimicking the inner collagenous layer of Bruch's membrane, the electrospun Col I fibers with diameters ranging from 200 to 500 nm were fabricated (Warnke et al., 2013). Thus, LS

technology allows the fabrication of collagen I fibers closer to their native equivalent in inner collagenous layer compared to the electrospinning method. Previously, Col IV has been used in tissue engineering applications merely in the form of protein coating (Calejo et al., 2016; Subrizi et al., 2012). In **Study II**, the Col IV layer of the LS film demonstrated a net-like surface topography formed by 12.5 nm and 140 nm thick fibrils, mimicking the Col IV network found in the native RPE basement membrane. These results indicate that LS technology is a valid, low-cost and simple method to fabricate especially Col IV substrates with delicate architecture for tissue engineering applications.

It is important to note that ECM is only one factor among several others within the *in vivo* microenvironment of the cells (Barthes et al., 2014). For cell production in tissue engineering field, the cells are commonly placed on plastic substrate in the presence of vast amounts of salt water, additives and serum (Chen et al., 2011). However, the demand for hPSC-RPE production to be carried out under fully defined conditions and devoid of animal derived products for clinical use of the cells (Bharti et al., 2014; Pennington et al., 2015) brings up further limitations to the soluble environment of hPSC-RPE cells *in vitro*. Thus, the importance of a supportive biomaterial substrate mimicking the ECM structure for the production of functional hPSC-RPE is emphasized. In this dissertation, it was hypothesized that substrates resembling the native environment of the cells would result in improved cellular response compared to conventional cell culture substrates in serum-free medium. Indeed, extensive characterization confirmed that the double layer collagen LS films were superior in supporting hESC-RPE maturation and functionality compared to the dip-coated controls. Thus, the results presented in **Study II** suggest that double layer LS films provide optimal cues for hESC-RPE cell production and provide a biomimetic environment for the efficient production of hESC-RPE cells, potentially increasing their performance in retinal tissue engineering applications.

Individual hESC and hiPSC lines have remarkable differences in their capacity and rate to differentiate towards mature RPE (Leach et al., 2016; Toivonen et al., 2013). Regardless of the cell line dependent differences detected on LS films between the two investigated hESC lines, the hESC-RPE cells produced from both cell lines demonstrated increased functionality on double layer LS films compared to the dip-coated controls. Previous studies have shown that LB films made of ECM proteins increased NB1-RGB cell growth and growth factor secretion compared to solvent cast ECM protein films (Higuchi et al., 2002). Apart from the lack of fiber-like surface topography on the dip-coated controls, SPR measurements demonstrated that their thickness was significantly lower compared to the thickness of the double

layer LS films. Thus, the improvement in cellular response on biomimetic substrate is likely due to multiple factors, including formation of fiber-like collagen networks, as well as increase in the amount of collagens and thus integrin binding motifs on the surface. Hence, not only the primary structure of proteins but also the fabrication methods of the films are a strong factor affecting cell growth on a biomaterial substrate (Higuchi et al., 2002).

In the native Bruch's membrane, the two uppermost layers have a combined thickness of 1.5 μm (Booij et al., 2010). Thus, the double layer LS film with average thickness of 27 nm is far off from this. Nevertheless, by depositing multiple layers of both collagens, the thickness of the film could be increased. Importantly, the layer by layer deposition of collagens in **Study II**, with Col I deposited below and Col IV on top as in the native Bruch's membrane, influenced the overall stucture. Therefore, the Col IV layer on Col I had a different surface topography compared to Col IV deposited directly onto substrate. This result is in line with a common phenomenon seen in the LB film field, where the first layer affects the structure of the next layer (Lotta et al., 1988). Owing to the extremely low thickness of the LS films, they need an additional supportive structure, such as porous and thin PET, to withstand handling. Hence, these films are not suitable for further use in *in vivo* applications as such. However, in **Study II** we were able to deposit double layer LS films on multiple substrates. Therefore, these films could be used to coat biomaterial substrates fabricated from synthetic polymers that have a thin but mechanically durable and permeable structure, yet lack cell binding ligands on the scaffold surface. Thus, the results reported in **Study II** indicate that these LS films show potential as a biomaterial substrate for the *in vitro* production of the clinically relevant hESC-RPE cells under serum-free culture conditions. However, to be able to confirm the suitability of these LS films for subretinal transplantation, *in vivo* studies need to be conducted in the future.

6.3 Biodegradable fibrous transplantation material for hESC-RPE

Transplantation of hESC-RPE to the subretinal space on a supportive biomaterial substrate shows promise for retinal cell therapies (Diniz et al., 2013; Koss et al., 2016). As the double layer LS films developed in **Study II** were too fragile to be transplanted as such, we searched for an alternative biomaterial substrate for hESC-RPE cell transplantations. Synthetic fibrous membranes have a significant advantage

over natural polymeric substrates by possessing favorable characteristics including well-defined and xeno-free substances and tailorable fiber size and porosity (Hotaling et al., 2016). Previous comparative studies between smooth and fibrous substrates have demonstrated that RPE function and maturation is enhanced on electrospun substrates regardless of the polymer composition (Singh et al., 2001; Thieltges et al., 2011; Warnke et al., 2013). The aim of **Study III** was to fabricate a fibrous biodegradable membrane for hESC-RPE transplantation from synthetic polymer that would support hESC-RPE growth in serum-free culture conditions.

Hydrolytically degradable synthetic polymers are commonly chosen as implant material due to their minimal site-to-site and patient-to-patient variations compared to enzymatically degradable polymers (Nair & Laurencin, 2007). FDA approved poly-α-hydroxy-acid-based polymers, including PLLA and PCL, have been tested as potential scaffolds for human primary RPE cells and ARPE-19 cells (McHugh et al., 2014; Thomson et al., 2010; Thomson et al., 1996). Flexibility of the biomaterial substrate is an advantage for subretinal transplantations, as rigid materials might damage surrounding soft tissues (Hynes & Lavik, 2010). Unfortunately, biomaterial substrates fabricated from PLLA alone, have been shown to be extremely rigid and brittle (Thomson et al., 1996). Combining PLLA and PCL materials as co-polymer PLCL offers a range of favorable features. In addition, PLCL nanofibers have shown *in vivo* biocompatibility in subretinal space of rabbits (Liu et al., 2014). Previously, electrospun PLCL membranes have demonstrated elastic properties (Lee et al., 2008) resembling the elasticity of the native Bruch's membrane (Ugarte et al., 2006). However, the elastic properties of the DBD plasma treated PLCL membrane fabricated in **Study III** were not analyzed in this dissertation, and further experiments should be carried out in the future to better address this issue.

Various studies have generated electrospun substrates in an attempt to mimic the fibrous structure of the Col I fibers in the inner collagenous layer of the Bruch's membrane (Liu et al., 2014; Thieltges et al., 2011; Warnke et al., 2013; Xiang et al., 2014). The fabricated electrospun PLCL membranes in **Study III** had unaligned fiber-like morphology with porous structure and uniform fiber diameter of 3.1 μm. DBD plasma surface treatment did not affect the membrane and fiber architecture, and only minor changes in surface topography were detected demonstrating that plasma treatment is a valid method to surface modify biomaterial substrates with delicate structures. Even though these membranes had fibrous appearance, the fiber diameter of the prepared membranes was significantly larger than the fibers found in the basement membrane of Bruch's membrane. In contrast to previous findings in the field with nanoscale fibers (Thieltges et al., 2011; Xiang et al., 2014), the fibrous

morphology of the PLCL membrane alone did not improve hESC-RPE cell attachment and further surface modifications of the membranes were required. This could be due to microscale fiber diameter, and further efforts should be done to fine-tune the fiber-like morphology of these PLCL membranes.

Biodegradability is a desirable feature of a biomaterial substrate, since the primary aim for the biomaterial structure in tissue engineering applications is to provide temporary support for the cells during transplantation and integration to the host tissue until the natural ECM has sufficiently developed (Ulery et al., 2011). In addition, biodegradable substrates allow the incorporation of therapeutic agents and their controlled and local release in subretinal transplantation (Sakai et al., 2001). However, the degradation rate of these biodegradable substrates and the biocompatibility of their degradation products cause a regulatory concern and need to be thoroughly addressed *in vivo*. In contrast, stabile substrates provide permanent support for the transplanted cells. However, these stabile substrates need be highly permeable to allow the reciprocal exchange of nutrients and fluids (Pennington & Clegg, 2016). Previously, PET substrates with 3.0 μm pores resulted in significantly better preservation of outer retinal layers compared to a similar carrier with pores of 0.4 μm (Stanzel et al., 2014). Both biodegradable and synthetic transplantation materials have been suggested for human RPE cells both *in vitro* and *in vivo* (Jha & Bharti, 2015). However, only the stabile biomaterial substrates have shown success with hESC-RPE (Carr et al., 2013; Coffey et al., 2009; Koss et al., 2016; Subrizi et al., 2012). Moreover, none of the biomaterial substrates support the maturation of functional hESC-RPE as such: human proteins such as laminin, vitronectin and collagen IV, as well as animal derived Matrigel™ and gelatin, have been assessed to improve hESC-RPE response on investigated substrates (Ilmarinen et al., 2015; Koss et al., 2016; Lu et al., 2014; Subrizi et al., 2012; Thomas et al., 2016). Thorough *in vivo* comparative studies need to be carried out in the future to conclude whether biodegradable or stabile biomaterial substrates are more suitable for retinal tissue engineering applications.

Various synthetic polymers in their native state lack surface functionality necessary to elicit appropriate cellular responses. The lack of published results and our own extensive empirical testing suggests that substrates fabricated from biodegradable synthetic polymers do not support hESC-RPE attachment and maturation as such in serum-free culture conditions. It is well recognized that in general cells do not directly interact with synthetic biomaterial substrates. Instead, the interaction depends on the adsorption of proteins on the substrate surface (Ngandu Mpoyi et al., 2016; Wang et al., 2005). DBD plasma processing technique

is a commonly used method to fine-tune biomaterial substrate surfaces to enhance cell attachment and maturation (D'Sa et al., 2010b). In **Study III**, this phenomenon was confirmed as the beneficial effects of the DBD plasma surface treatment were only evident with additional protein coating. Without Col IV adlayer DBD plasma surface modified membranes failed to support hESC-RPE cell attachment and monolayer formation in serum-free cultures, whereas identical substrate in similar culture conditions with Col IV coating allowed the formation of functional hESC-RPE. These results imply that the DBD plasma surface treatment and its beneficial properties on cellular response appears to be a secondary effect and is above all caused by improved Col IV adsorption and conformation on the PLCL membrane surface. Moreover, the untreated PLCL membranes, even when combined with Col IV coating, did not support hESC-RPE monolayer formation. Thus, the surface treatment of these synthetic PLCL substrates is essential in obtaining uniform hESC-RPE monolayers in serum-free culture conditions.

It has been widely observed that cell adhesion is commonly increased on hydrophilic surfaces (Wang et al., 2005; Wilson et al., 2005). Likewise, hydrophilic surface has been shown to adsorb more ECM proteins compared to hydrophobic surface (Yang et al., 2002). In **Study III**, the DBD plasma treatment significantly increased the hydrophilicity of the PLCL membranes. Moreover, higher nitrogen content on DBD plasma treated membranes was detected compared to untreated membranes, indicating increased Col IV adsorption on the substrate surface after DBD plasma treatment. The DBD plasma treated PLCL membranes also demonstrated increase in the number of polarized oxygen groups on the surface as well as rougher nanotopography compared to untreated membranes. Both of these surface characteristics have been previously associated with improvements in the surface-free energy and subsequent increase in collagen binding on plasma-treated synthetic membranes (Yang et al., 2002).

For retinal tissue engineering applications, the intended substrate should primarily allow formation of polarized and functional RPE monolayer (Binder et al., 2007). **Study III** was the first to show formation of a functional hESC-RPE monolayer on a porous biodegradable membrane in a serum-free culture environment. Thereafter, successful hESC-RPE maturation was demonstrated on porous honeycomb structured PLDLA films (Calejo et al., 2016) and nonporous elastic poly(trimethylene carbonate) (PTMC) substrates (Sorkio et al., 2016) with additional human-derived protein coating in serum-free medium. Even though a number of studies have used biodegradable scaffolds with primary RPE cells and immortalized cell lines, it seems that these results are not directly translatable for

hESC-RPE cells. Recent findings suggest that the extent of hESC-RPE cell maturity and pigmentation might substantially affect subsequent attachment and growth of the cells *in vitro* (Schwartz et al., 2012). Thus, a comparison of hESC-RPE cell performance on biomaterial substrates between cells with different degree of maturity should be assessed in future studies.

The electrospun DBD plasma surface modified PLCL membranes fulfill the majority of the criteria set for an ideal substrate for subretinal transplantation. These membranes are porous, allowing the reciprocal exchange of biomolecules, support the formation of functional hESC-RPE *in vitro* in serum-free culture conditions without the use of animal-derived substrates, and have physical strength and maneuverability necessary for the surgical procedure. Yet, there are a few limitations including relatively high membrane thickness of 43 μm compared to the 2-4 μm thin native Bruch's membrane. This thickness could be further optimized and significantly reduced. However, wetted electrospun meshes less than 10 μm in thickness are difficult to handle for subretinal transplantation (Popelka et al., 2015). This was the case for electrospun PLGA and PLCL fibers designed for RPE cells, which needed an additional PET film as support, and the fibers merely provided a thin coating on the film surface (Liu et al., 2014; Warnke et al., 2013). One proposed option to transplant thin electrospun membranes used frame-supported 6 μm thick electrospun membranes, where biodegradable surgical sutures were applied to maintain the membrane flat during transplantation (Popelka et al., 2015). Yet another option could be to encapsulate the nanofiber carrier graft in a biodegradable hydrogel (Stanzel et al., 2012). Nevertheless, the suitability of these surgical techniques for thin electrospun membranes needs to be further optimized and investigated thoroughly *in vivo*.

The double layer LS films developed in **Study II** mimicked the fibrillary structure of the uppermost layers of the RPE basement membrane to a great extent, but lacked the mechanical durability as such, limiting the *in vivo* use of the films. On the other hand, the electrospun PLCL membranes fabricated in **Study III** exhibited good durability as well as handling, but had substantially higher fiber diameter compared to their native counterpart in the inner collagenous layer of Bruch's membrane. Combining the double layer LS film with the electrospun PLCL membrane into a biodegradable composite scaffold could potentially result in a combination with the best properties of both constituents. However, the feasibility of these composite scaffolds as biomaterial substrates for retinal tissue engineering applications needs to be further addressed in both *in vitro* and *in vivo* settings.

6.4 Future perspectives

Retinal tissue engineering applications currently dominate the first-in-man clinical trials of hPSC-derived cells with several ongoing clinical trials (Kimbrel & Lanza, 2015; Nazari et al., 2015). Preliminary results of the first clinical trials with hESC-RPE cells delivered in cell suspension were promising: no signs of hyperproliferation, tumorigenicity or clear rejection of the cells were seen (Schwartz et al., 2012). Moreover, long-term safety, graft survival, as well as biological activity of the transplanted cells have been recently reported, which gives promise to hESCs as cell source for retinal tissue engineering applications (Schwartz et al., 2015; Schwartz et al., 2016). Even though successful transplantation of hESC-RPE cells in suspension has been shown *in vivo*, there is growing evidence demonstrating the feasibility of hESC-RPE transplantation as monolayer sheet on a biomaterial substrate (Koss et al., 2016; Thomas et al., 2016). The first clinical trials with hESC-RPE sheets on stabile PET and Parylene-C biomaterial substrates will commence soon (Carr et al., 2013; Coffey et al., 2009; Koss et al., 2016). The outcome of these trials will determine the course for the RPE-biomaterial transplantation and biomaterial substrate design for future retinal tissue engineering applications. Moreover, as the biomaterial substrates will be more often used in clinical applications, special attention must be paid to designing substrates that replace the structure and lost functionality of the damaged ECM in subretinal space.

Patient-specific hiPSC-RPE cells open the door for personalized medicine applications. In addition, autologous hiPSC-RPE cells are considered as a potential cell source for tissue engineering applications as they can potentially avoid the immune rejection commonly associated with allogeneic cells (Riera et al., 2016). In the studies carried out as part of this dissertation, only hESC-derived RPE cells were investigated. Recently, comparable distribution and integration patterns were observed in transplants of RPE cells differentiated either from hESCs or hiPSCs in subretinal space of rats (Riera et al., 2016). Regardless of the cell source, hPSC-RPE cell transplants have shown neuroprotective effects in the subretinal space as well as demonstrated visual acuity. However, hiPSCs are not identical to hESCs (Toivonen et al., 2013) and may harbor genetic mutations and ageing marks brought on by environmental insults to the original somatic cell (Pera, 2011). The majority of the currently ongoing clinical studies are carried out with hESC-RPE cells, whereas the first clinical trial with hiPSC-RPE monolayer sheets (Kamao et al., 2014) was put on hold due to genetic mutations in one patient's hiPSCs (Kimbrel & Lanza, 2015). The feasibility and safety of both cell types, not only hESC-RPE but also hiPSC-RPE,

and their cellular response and performance on biomaterial substrates must be assessed and compared in future studies.

The current cell therapies to treat AMD merely focus on the transplantation of healthy RPE cells to the damaged macular area (Carr et al., 2013; Kamao et al., 2014). However, further disease progression of AMD leads to death and loss of the adjacent photoreceptors (Lim et al., 2012). In these more severe cases, where the neural retina has already undergone degeneration, the transplantation of RPE cells alone might not be sufficient to restore the lost visual acuity (Wright et al., 2014). Therefore, delivery of healthy photoreceptor cells together with functional RPE could potentially provide an alternative cell therapeutic approach for retinal tissue engineering applications (Wu et al., 2016). Recently, hESCs and hiPSCs have been successfully differentiated into photoreceptors and other neural progenitor cells (Homma et al., 2013; Lamba et al., 2009). Moreover, using the hESCs to generate optic cup-like structures, where neural retina and RPE together form a stratified three-dimensional complex, has been demonstrated (Nakano et al., 2012). A transition from two-dimensional sheet-like structure with a single cell type to a three-dimensional approach with multiple incorporated cell types sets new challenges for the future biomaterial design for retinal tissue engineering.

Serum is a major source of undefined factors in culture medium. In addition, lot-to-lot variation is often observed and serum may be contaminated with infectious agents such as mycoplasma, bacteriophages, and viruses. The undefined nature of serum prevents determining the true nutritional and hormonal requirements for the cultured cells. Even though replacing the serum with more defined KO-SR is possible, this medium supplement still contains xeno-derived bovine serum albumin and bovine transferrin (Price et al., 1998). Recent studies have developed protocols to differentiate hESC-RPE cells in defined and xeno-free culture conditions on synthetic substrates including Synthemax (Pennington et al., 2015) and recombinant laminins (Plaza Reyes et al., 2016). In the near future, the biomaterial substrate design and testing should also be carried out under defined and xeno-free environment to meet the clinical requirements set for hESC-RPE monolayer grafts. Moreover, a shift from naturally derived scaffolds and proteins to synthetic polymers, as well as recombinant proteins is in order when designing biomaterial substrates for the *in vitro* production and transplantation of the clinically relevant hESC-RPE.

As the field is rapidly moving towards clinics, not only the hESC-RPE cell-biomaterial graft development but also its transplantation to the subretinal space is of high importance. Recent *in vivo* studies have reported difficulties in surgical procedure and handling of the RPE monolayer grafts and biomaterial substrates

(Diniz et al., 2013; Ilmarinen et al., 2015). Thus, special instrumentation is required for successful transplantation of hPSC-RPE-biomaterial substrate grafts to the subretinal space (Hu et al., 2012; Stanzel et al., 2012; Thumann et al., 2009). In their present form the shooter introduced by Stanzel et al. was not applicable for ultrathin PI membranes for subretinal delivery in rabbits (Ilmarinen et al., 2015). Therefore, modification of these tools and surgical techniques for cell sheet transplantation is a major challenge for the retinal tissue engineering field in the future.

7 Conclusions

This dissertation focused on investigating and fabricating biomaterial substrates and transplantation materials for hESC-RPE. The natural environment of the RPE in the eye was used as a source of inspiration for biomaterial design. Here, we produced novel biomaterial substrates for hESC-RPE cells that resembled the native Bruch's membrane as well as provided new information about hESC-RPE cell-biomaterial interactions in serum-free culture medium. Based on the studies carried out in this dissertation, the following main conclusions can be drawn:

1. Biomaterial substrates mimicking the composition and structure of ECM in the native microenvironment of the RPE cells resulted in improved cellular response and function of hESC-RPE cells compared to conventional cell culture substrates *in vitro*.

2. Single protein substrate in a form of full-length protein coating had a crucial effect on the degree of maturation and functionality of hESC-RPE cells in adherent differentiation cultures.
   - The major component of the RPE basement membrane, Col IV, was the golden mean protein coating in supporting hESC-RPE differentiation and maturation.

3. Double layer collagen LS films mimicked the architecture of the two uppermost layers of the native Bruch's membrane.
   - LS technique shows potential for generating intricate biomimetic substrates for tissue engineering applications without the use of non-biocompatible substances.

4. The fibrous and porous biodegradable PLCL membranes supported the growth and maturation of hESC-RPE cells in serum-free culture medium *in vitro*.
   - This study showed for the first time successful culture of functional hESC-RPE cells on a biodegradable carrier.

- Atmospheric pressure plasma surface treatment of electrospun PLCL increased favorable adsorption of adhesion mediating Col IV and is thus a convenient method to modify synthetic polymer surfaces with delicate structures.
- Nevertheless, the feasibility of these fibrous biomaterial substrates for subretinal transplantation needs to be further evaluated *in vivo*.

Acknowledgements

This study was carried out at the Institute of Biosciences and Medical Technology (BioMediTech), University of Tampere, during the years 2012-2016. I warmly thank the Dean of BioMediTech Hannu Hanhijärvi for providing excellent research facilities and an innovative environment to work in.

I would also like to thank the Finnish Funding agency for Technology and Innovation (TEKES), the Finnish Cultural Foundation Central Fund and Pirkanmaa Regional Fund, the Otto A. Malm Foundation, Emil Aaltonen Foundation, the Finnish foundation to promote technology (TES), the Finnish Concordia Fund, the Tampere Graduate Programme in Biomedicine and Biotechnology (TGPBB) and the City of Tampere for financially enabling my research and international conference journeys.

My deepest gratitude goes to my supervisors Associated Professor Heli Skottman and University lecturer Kati Juuti-Uusitalo. Heli, it has been an honor to work for a distinguished scientist like you. You definitely have proved that women in science rock. I thank you for the freedom and responsibility you have given me as a researcher to pursuit of my dreams. I am deeply grateful to you for always being there for me whenever in need of guidance and encouragement. Kati, thank you for all the help and support during these years, as well as teaching me valuable scientific skills. You are an excellent scientist and I admire your determination in whatever you do.

I wish to sincerely thank the members of my thesis committee Professor Hannu Uusitalo, Professor Minna Kellomäki and Professor Marjo Yliperttula for the encouragement, valuable advice and research ideas during my PhD studies. I am also grateful for Adjunct Professor Joachim Loo and Adjunct Professor Aki Manninen for reviewing this dissertation and providing their constructive criticism to improve the quality of this work. The co-authors George Burke, Hanna Hakola, Kai Kaarniranta, Huamin Liang, Brian Meenan, Patrick Porter, Tiina Ujula, Juan José Valle-Delgado, Elina Vuorimaa-Laukkanen, and Monika Österberg are warmly thanked for their contributions - without your expertise, these publications would not have been possible. I wish to also thank the coworkers in the BioMediTech,

especially the regenerative medicine research groups, for fun times and rewarding scientific and non-scientific conversations.

I could have never reached the heights nor explored the depths without the amazing people working in the Eye Group. Outi Heikkilä, Outi Melin and Hanna Pekkanen – I thank you for your irreplaceable technical assistance during these years and most importantly for your friendship. Heidi Hongisto, I am deeply grateful to you for introducing the fascinating ECM world to me and for all the priceless help and laughter during the years. Tanja Ilmarinen, I wish to thank you for supervising me during my undergraduate studies and spreading your scientific enthusiasm as well as your positive outlook on life. Hanna Hiidenmaa is thanked for the outstanding company and precious peer support. Special thanks goes to the other half of the A-team, Alexandra Mikhailova. Thank you for all the support and help you gave me during these years. You are an amazing friend, and it has been a privilege to share this journey with a talented and warm-hearted person like you.

Thanks to all of my friends for keeping it real and providing truly needed real-life distractions from the scientific scene. I am lucky to have such an amazing group of people around me. Katja, you are my rock. Elina, Kaisa, Karoliina and Veera, I wish to thank you from your friendship and encouragement while going through countless "what am I going to do with my life"-crises during these years as a PhD student. My parents, Vesa and Anneli, thank you for always supporting me in every way loving parents possible can.

Finally, I would like to thank the man in my life, Miikka, for your support and always being there by my side. You are an amazing father to our beautiful daughter Aada and know how to make me laugh every single day. You and Aada mean the world to me.

Tampere, October 2016

Anni

References

Abraham, L. C., Zuena, E., Perez-Ramirez, B., & Kaplan, D. L. (2008). Guide to collagen characterization for biomaterial studies. Journal of Biomedical Materials Research.Part B, Applied Biomaterials, 87(1), 264-285.

Afshari, F. T., & Fawcett, J. W. (2009). Improving RPE adhesion to bruch's membrane. Eye (London, England), 23(10), 1890-1893.

Afshari, F. T., Kwok, J. C., Andrews, M. R., Blits, B., Martin, K. R., Faissner, A., Ffrench-Constant, C., & Fawcett, J. W. (2010). Integrin activation or alpha 9 expression allows retinal pigmented epithelial cell adhesion on bruch's membrane in wet age-related macular degeneration. Brain : A Journal of Neurology, 133(Pt 2), 448-464.

Aisenbrey, S., Zhang, M., Bacher, D., Yee, J., Brunken, W. J., & Hunter, D. D. (2006). Retinal pigment epithelial cells synthesize laminins, including laminin 5, and adhere to them through α3- and α6-containing integrins. Investigative Ophthalmology & Visual Science, 47(12), 5537-5544.

Akrami, H., Soheili, Z. S., Sadeghizadeh, M., Khalooghi, K., Ahmadieh, H., Kanavi, M. R., Samiei, S., & Pakravesh, J. (2011). Evaluation of RPE65, CRALBP, VEGF, CD68, and tyrosinase gene expression in human retinal pigment epithelial cells cultured on amniotic membrane. Biochemical Genetics, 49(5-6), 313-322.

Alamdari, O. G., Seyedjafari, E., Soleimani, M., & Ghaemi, N. (2013). Micropatterning of ECM proteins on glass substrates to regulate cell attachment and proliferation. Avicenna Journal of Medical Biotechnology, 5(4), 234-240.

Algvere, P. V., Gouras, P., & Dafgard Kopp, E. (1999). Long-term outcome of RPE allografts in non-immunosuppressed patients with AMD. European Journal of Ophthalmology, 9(3), 217-230.

Ambati, J., & Fowler, B. J. (2012). Mechanisms of age-related macular degeneration. Neuron, 75(1), 26-39.

Anderson, D. H., Guerin, C. J., Matsumoto, B., & Pfeffer, B. A. (1990). Identification and localization of a beta-1 receptor from the integrin family in mammalian retinal pigment epithelial cells. Investigative Ophthalmology & Visual Science, 31(1), 81-93.

Antoine, E. E., Vlachos, P. P., & Rylander, M. N. (2014). Review of collagen I hydrogels for bioengineered tissue microenvironments: Characterization of mechanics, structure, and transport. Tissue Engineering.Part B, Reviews, 20(6), 683-696.

Aumailley, M. (2013). The laminin family. Cell Adhesion & Migration, 7(1), 48-55.

Balzer, J., Heuer, K., Demir, E., Hoffmanns, M. A., Baldus, S., Fuchs, P. C., Awakowicz, P., Suschek, C. V., & Oplander, C. (2015). Non-thermal dielectric barrier discharge (DBD) effects on proliferation and differentiation of human fibroblasts are primary mediated by hydrogen peroxide. PloS One, 10(12), e0144968.

Barthes, J., Ozcelik, H., Hindie, M., Ndreu-Halili, A., Hasan, A., & Vrana, N. E. (2014). Cell microenvironment engineering and monitoring for tissue engineering and regenerative medicine: The recent advances. BioMed Research International, 2014, 921905.

Becerra, S. P., Fariss, R. N., Wu, Y. Q., Montuenga, L. M., Wong, P., & Pfeffer, B. A. (2004). Pigment epithelium-derived factor in the monkey retinal pigment epithelium and interphotoreceptor matrix: Apical secretion and distribution. Experimental Eye Research, 78(2), 223-234.

Beutel, J., Greulich, L., Luke, M., Ziemssen, F., Szurman, P., Bartz-Schmidt, K. U., & Grisanti, S. (2007). Inner limiting membrane as membranous support in RPE sheet-transplantation. Graefe's Archive for Clinical and Experimental Ophthalmology = Albrecht Von Graefes Archiv Fur Klinische Und Experimentelle Ophthalmologie, 245(10), 1469-1473.

Bharti, K., Miller, S. S., & Arnheiter, H. (2011). The new paradigm: Retinal pigment epithelium cells generated from embryonic or induced pluripotent stem cells. Pigment Cell & Melanoma Research, 24(1), 21-34.

Bharti, K., Rao, M., Hull, S. C., Stroncek, D., Brooks, B. P., Feigal, E., van Meurs, J. C., Huang, C. A., & Miller, S. S. (2014). Developing cellular therapies for retinal degenerative diseases. Investigative Ophthalmology & Visual Science, 55(2), 1191-1202.

Bhatt, N. S., Newsome, D. A., Fenech, T., Hessburg, T. P., Diamond, J. G., Miceli, M. V., Kratz, K. E., & Oliver, P. D. (1994). Experimental transplantation of human retinal pigment epithelial cells on collagen substrates. American Journal of Ophthalmology, 117(2), 214-221.

Bhushan, B. (2009). Biomimetics: Lessons from nature--an overview. Philosophical Transactions.Series A, Mathematical, Physical, and Engineering Sciences, 367(1893), 1445-1486.

Binder, S. (2011). Scaffolds for retinal pigment epithelium (RPE) replacement therapy. The British Journal of Ophthalmology, 95(4), 441-442.

Binder, S., Krebs, I., Hilgers, R. D., Abri, A., Stolba, U., Assadoulina, A., Kellner, L., Stanzel, B. V., Jahn, C., & Feichtinger, H. (2004). Outcome of transplantation of autologous retinal pigment epithelium in age-related macular degeneration: A prospective trial. Investigative Ophthalmology & Visual Science, 45(11), 4151-4160.

Binder, S., Stanzel, B. V., Krebs, I., & Glittenberg, C. (2007). Transplantation of the RPE in AMD. Progress in Retinal and Eye Research, 26(5), 516-554.

Blaauwgeers, H. G., Holtkamp, G. M., Rutten, H., Witmer, A. N., Koolwijk, P., Partanen, T. A., Alitalo, K., Kroon, M. E., Kijlstra, A., van Hinsbergh, V. W., & Schlingemann, R. O. (1999). Polarized vascular endothelial growth factor secretion by human retinal pigment epithelium and localization of vascular endothelial growth factor receptors on the inner choriocapillaris. evidence for a trophic paracrine relation. The American Journal of Pathology, 155(2), 421-428.

Booij, J. C., Baas, D. C., Beisekeeva, J., Gorgels, T. G., & Bergen, A. A. (2010). The dynamic nature of bruch's membrane. Progress in Retinal and Eye Research, 29(1), 1-18.

Borges, A. M., Benetoli, L. O., Licinio, M. A., Zoldan, V. C., Santos-Silva, M. C., Assreuy, J., Pasa, A. A., Debacher, N. A., & Soldi, V. (2013). Polymer films with surfaces

unmodified and modified by non-thermal plasma as new substrates for cell adhesion. Materials Science & Engineering.C, Materials for Biological Applications, 33(3), 1315-1324.

Brant Fernandes, R. A., Koss, M. J., Falabella, P., Stefanini, F. R., Maia, M., Diniz, B., Ribeiro, R., Hu, Y., Hinton, D., Clegg, D. O., Chader, G., & Humayun, M. S. (2016). An innovative surgical technique for subretinal transplantation of human embryonic stem cell-derived retinal pigmented epithelium in yucatan mini pigs: Preliminary results. Ophthalmic Surgery, Lasers & Imaging Retina, 47(4), 342-351.

Buchholz, D. E., Pennington, B. O., Croze, R. H., Hinman, C. R., Coffey, P. J., & Clegg, D. O. (2013). Rapid and efficient directed differentiation of human pluripotent stem cells into retinal pigmented epithelium. Stem Cells Translational Medicine, 2(5), 384-393.

Burke, J. M. (2008). Epithelial phenotype and the RPE: Is the answer blowing in the wnt? Progress in Retinal and Eye Research, 27(6), 579-595.

Calejo, M. T., Ilmarinen, T., Jongprasitkul, H., Skottman, H., & Kellomaki, M. (2016). Honeycomb porous films as permeable scaffold materials for human embryonic stem cell-derived retinal pigment epithelium. Journal of Biomedical Materials Research.Part A, 104(7), 1646-1656.

Campbell, I. D., & Humphries, M. J. (2011). Integrin structure, activation, and interactions. Cold Spring Harbor Perspectives in Biology, 3(3), 10.1101/cshperspect.a004994.

Campochiaro, P. A., Jerdon, J. A., & Glaser, B. M. (1986). The extracellular matrix of human retinal pigment epithelial cells in vivo and its synthesis in vitro. Investigative Ophthalmology & Visual Science, 27(11), 1615-1621.

Capeans, C., Pineiro, A., Pardo, M., Sueiro-Lopez, C., Blanco, M. J., Dominguez, F., & Sanchez-Salorio, M. (2003). Amniotic membrane as support for human retinal pigment epithelium (RPE) cell growth. Acta Ophthalmologica Scandinavica, 81(3), 271-277.

Carr, A. J., Smart, M. J., Ramsden, C. M., Powner, M. B., da Cruz, L., & Coffey, P. J. (2013). Development of human embryonic stem cell therapies for age-related macular degeneration. Trends in Neurosciences, 36(7), 385-395.

Carr, A. J., Vugler, A. A., Hikita, S. T., Lawrence, J. M., Gias, C., Chen, L. L., Buchholz, D. E., Ahmado, A., Semo, M., Smart, M. J., Hasan, S., da Cruz, L., Johnson, L. V., Clegg, D. O., & Coffey, P. J. (2009). Protective effects of human iPS-derived retinal pigment epithelium cell transplantation in the retinal dystrophic rat. PloS One, 4(12), e8152.

Cary, L. A., & Guan, J. L. (1999). Focal adhesion kinase in integrin-mediated signaling. Frontiers in Bioscience : A Journal and Virtual Library, 4, D102-13.

Castellarin, A. A., Sugino, I. K., Vargas, J. A., Parolini, B., Lui, G. M., & Zarbin, M. A. (1998). In vitro transplantation of fetal human retinal pigment epithelial cells onto human cadaver bruch's membrane. Experimental Eye Research, 66(1), 49-67.

Chen, C., Loe, F., Blocki, A., Peng, Y., & Raghunath, M. (2011). Applying macromolecular crowding to enhance extracellular matrix deposition and its remodeling in vitro for tissue engineering and cell-based therapies. Advanced Drug Delivery Reviews, 63(4-5), 277-290.

Chen, L., Miyamura, N., Ninomiya, Y., & Handa, J. T. (2003). Distribution of the collagen IV isoforms in human bruch's membrane. The British Journal of Ophthalmology, 87(2), 212-215.

Chen, Q., Xu, S., Li, R., Liang, X., & Liu, H. (2007). Network structure of collagen layers absorbed on LB film. Journal of Colloid and Interface Science, 316(1), 1-9.

Chu, P. G., & Grunwald, G. B. (1991). Functional inhibition of retinal pigment epithelial cell-substrate adhesion with a monoclonal antibody against the beta 1 subunit of integrin. Investigative Ophthalmology & Visual Science, 32(6), 1763-1769.

Coffey,P., Da Cruz,L. and Cheethan,K. . Membrane. 2009. WO2009127809 (A1).

Crabb, J. W., Miyagi, M., Gu, X., Shadrach, K., West, K. A., Sakaguchi, H., Kamei, M., Hasan, A., Yan, L., Rayborn, M. E., Salomon, R. G., & Hollyfield, J. G. (2002). Drusen proteome analysis: An approach to the etiology of age-related macular degeneration. Proceedings of the National Academy of Sciences of the United States of America, 99(23), 14682-14687.

Curcio, C., & Johnson, M. (2013). Structure, function, and pathology of bruch's membrane. In S. Ryan (Ed.), *Retina* (pp. 465-481) Elsevier Inc.

Da Silva, G. R., Da Silva-Cunha, A.,Jr, Vieira, L. C., Silva, L. M., Ayres, E., Orefice, R. L., Fialho, S. L., Saliba, J. B., & Behar-Cohen, F. (2013). Montmorillonite clay based polyurethane nanocomposite as substrate for retinal pigment epithelial cell growth. Journal of Materials Science.Materials in Medicine, 24(5), 1309-1317.

Da Silva, G. R., Lima, T. H., Orefice, R. L., Fernandes-Cunha, G. M., Silva-Cunha, A., Zhao, M., & Behar-Cohen, F. (2015). In vitro and in vivo ocular biocompatibility of electrospun poly(varepsilon-caprolactone) nanofibers. European Journal of Pharmaceutical Sciences : Official Journal of the European Federation for Pharmaceutical Sciences, 73, 9-19.

D'Cruz, P. M., Yasumura, D., Weir, J., Matthes, M. T., Abderrahim, H., LaVail, M. M., & Vollrath, D. (2000). Mutation of the receptor tyrosine kinase gene mertk in the retinal dystrophic RCS rat. Human Molecular Genetics, 9(4), 645-651.

Del Priore, L. V., Geng, L., Tezel, T. H., & Kaplan, H. J. (2002). Extracellular matrix ligands promote RPE attachment to inner bruch's membrane. Current Eye Research, 25(2), 79-89.

Del Priore, L. V., & Tezel, T. H. (1998). Reattachment rate of human retinal pigment epithelium to layers of human bruch's membrane. Archives of Ophthalmology (Chicago, Ill.: 1960), 116(3), 335-341.

Del Priore, L. V., Tezel, T. H., & Kaplan, H. J. (2004). Survival of allogeneic porcine retinal pigment epithelial sheets after subretinal transplantation. Investigative Ophthalmology & Visual Science, 45(3), 985-992.

Del Priore, L. V., Tezel, T. H., & Kaplan, H. J. (2006). Maculoplasty for age-related macular degeneration: Reengineering bruch's membrane and the human macula. Progress in Retinal and Eye Research, 25(6), 539-562.

Desmet, T., Morent, R., De Geyter, N., Leys, C., Schacht, E., & Dubruel, P. (2009). Nonthermal plasma technology as a versatile strategy for polymeric biomaterials surface modification: A review. Biomacromolecules, 10(9), 2351-2378.

Diniz, B., Thomas, P., Thomas, B., Ribeiro, R., Hu, Y., Brant, R., Ahuja, A., Zhu, D., Liu, L., Koss, M., Maia, M., Chader, G., Hinton, D. R., & Humayun, M. S. (2013). Subretinal implantation of retinal pigment epithelial cells derived from human embryonic stem cells: Improved survival when implanted as a monolayer. Investigative Ophthalmology & Visual Science, 54(7), 5087-5096.

D'Sa, R. A., Burke, G. A., & Meenan, B. J. (2010a). Lens epithelial cell response to atmospheric pressure plasma modified poly(methylmethacrylate) surfaces. Journal of Materials Science.Materials in Medicine, 21(5), 1703-1712.

D'Sa, R. A., Burke, G. A., & Meenan, B. J. (2010b). Protein adhesion and cell response on atmospheric pressure dielectric barrier discharge-modified polymer surfaces. Acta Biomaterialia, 6(7), 2609-2620.

D'Sa, R. A., Raj, J., McMahon, M. A., McDowell, D. A., Burke, G. A., & Meenan, B. J. (2012). Atmospheric pressure plasma induced grafting of poly(ethylene glycol) onto silicone elastomers for controlling biological response. Journal of Colloid and Interface Science, 375(1), 193-202.

Eurell, T. E., Brown, D. R., Gerding, P. A., & Hamor, R. E. (2003). Alginate as a new biomaterial for the growth of porcine retinal pigment epithelium. Veterinary Ophthalmology, 6(3), 237-243.

Fang, I. M., Yang, C. H., Yang, C. M., & Chen, M. S. (2009). Overexpression of integrin alpha6 and beta4 enhances adhesion and proliferation of human retinal pigment epithelial cells on layers of porcine bruch's membrane. Experimental Eye Research, 88(1), 12-21.

Friess, W. (1998). Collagen--biomaterial for drug delivery. European Journal of Pharmaceutics and Biopharmaceutics : Official Journal of Arbeitsgemeinschaft Fur Pharmazeutische Verfahrenstechnik E.V, 45(2), 113-136.

Fuhrmann, S., Zou, C., & Levine, E. M. (2014). Retinal pigment epithelium development, plasticity, and tissue homeostasis. Experimental Eye Research, 123, 141-150.

Gailit, J., & Ruoslahti, E. (1988). Regulation of the fibronectin receptor affinity by divalent cations. The Journal of Biological Chemistry, 263(26), 12927-12932.

Gattazzo, F., Urciuolo, A., & Bonaldo, P. (2014). Extracellular matrix: A dynamic microenvironment for stem cell niche. Biochimica Et Biophysica Acta, 1840(8), 2506-2519.

Gehrs, K. M., Anderson, D. H., Johnson, L. V., & Hageman, G. S. (2006). Age-related macular degeneration--emerging pathogenetic and therapeutic concepts. Annals of Medicine, 38(7), 450-471.

Giordano, G. G., Thomson, R. C., Ishaug, S. L., Mikos, A. G., Cumber, S., Garcia, C. A., & Lahiri-Munir, D. (1997). Retinal pigment epithelium cells cultured on synthetic biodegradable polymers. Journal of Biomedical Materials Research, 34(1), 87-93.

Girard-Egrot, A. P., Godoy, S., & Blum, L. J. (2005). Enzyme association with lipidic langmuir-blodgett films: Interests and applications in nanobioscience. Advances in Colloid and Interface Science, 116(1-3), 205-225.

Goffin, A. J., Rajadas, J., & Fuller, G. G. (2010). Interfacial flow processing of collagen. Langmuir : The ACS Journal of Surfaces and Colloids, 26(5), 3514-3521.

Goncalves, S., Padrao, J., Rodrigues, I. P., Silva, J. P., Sencadas, V., Lanceros-Mendez, S., Girao, H., Dourado, F., & Rodrigues, L. R. (2015). Bacterial cellulose as a support for the growth of retinal pigment epithelium. Biomacromolecules, 16(4), 1341-1351.

Goncalves, S., Rodrigues, I. P., Padrao, J., Silva, J. P., Sencadas, V., Lanceros-Mendez, S., Girao, H., Gama, F. M., Dourado, F., & Rodrigues, L. R. (2016). Acetylated bacterial cellulose coated with urinary bladder matrix as a substrate for retinal pigment epithelium. Colloids and Surfaces.B, Biointerfaces, 139, 1-9.

Gong, J., Sagiv, O., Cai, H., Tsang, S. H., & Del Priore, L. V. (2008). Effects of extracellular matrix and neighboring cells on induction of human embryonic stem cells into retinal or retinal pigment epithelial progenitors. Experimental Eye Research, 86(6), 957-965.

Gullapalli, V. K., Sugino, I. K., Van Patten, Y., Shah, S., & Zarbin, M. A. (2005). Impaired RPE survival on aged submacular human bruch's membrane. Experimental Eye Research, 80(2), 235-248.

Gullapalli, V. K., Sugino, I. K., & Zarbin, M. A. (2008). Culture-induced increase in alpha integrin subunit expression in retinal pigment epithelium is important for improved resurfacing of aged human bruch's membrane. Experimental Eye Research, 86(2), 189-200.

Hadlock, T., Singh, S., Vacanti, J. P., & McLaughlin, B. J. (1999). Ocular cell monolayers cultured on biodegradable substrates. Tissue Engineering, 5(3), 187-196.

Han, Y. L., Wang, S., Zhang, X., Li, Y., Huang, G., Qi, H., Pingguan-Murphy, B., Li, Y., Lu, T. J., & Xu, F. (2014). Engineering physical microenvironment for stem cell based regenerative medicine. Drug Discovery Today, 19(6), 763-773.

Hapach, L. A., VanderBurgh, J. A., Miller, J. P., & Reinhart-King, C. A. (2015). Manipulation of in vitro collagen matrix architecture for scaffolds of improved physiological relevance. Physical Biology, 12(6), 061002-3975/12/6/061002.

Hartmann, U., Sistani, F., & Steinhorst, U. H. (1999). Human and porcine anterior lens capsule as support for growing and grafting retinal pigment epithelium and iris pigment epithelium. Graefe's Archive for Clinical and Experimental Ophthalmology = Albrecht Von Graefes Archiv Fur Klinische Und Experimentelle Ophthalmologie, 237(11), 940-945.

Haynes, C., & Norde, W. (1994). Globular proteins at solid/liquid interfaces. Colloids and Surfaces B: Biointerfaces, 2(29), 517-566.

Heidari, R., Soheili, Z. S., Samiei, S., Ahmadieh, H., Davari, M., Nazemroaya, F., Bagheri, A., & Deezagi, A. (2015). Alginate as a cell culture substrate for growth and differentiation of human retinal pigment epithelial cells. Applied Biochemistry and Biotechnology, 175(5), 2399-2412.

Heinlin, J., Isbary, G., Stolz, W., Morfill, G., Landthaler, M., Shimizu, T., Steffes, B., Nosenko, T., Zimmermann, J., & Karrer, S. (2011). Plasma applications in medicine with

a special focus on dermatology. Journal of the European Academy of Dermatology and Venereology : JEADV, 25(1), 1-11.

Heller, J. P., & Martin, K. R. (2014). Enhancing RPE cell-based therapy outcomes for AMD: The role of bruch's membrane. Translational Vision Science & Technology, 3(3), 11.

Higuchi, A., Takanashi, Y., Ohno, T., Asakura, T., Cho, C. S., Akaike, T., & Hara, M. (2002). Production of interferon-beta by fibroblast cells on membranes prepared by extracellular matrix proteins. Cytotechnology, 39(3), 131-137.

Hlady, V. V., & Buijs, J. (1996). Protein adsorption on solid surfaces. Current Opinion in Biotechnology, 7(1), 72-77.

Homma, K., Okamoto, S., Mandai, M., Gotoh, N., Rajasimha, H. K., Chang, Y. S., Chen, S., Li, W., Cogliati, T., Swaroop, A., & Takahashi, M. (2013). Developing rods transplanted into the degenerating retina of crx-knockout mice exhibit neural activity similar to native photoreceptors. Stem Cells (Dayton, Ohio), 31(6), 1149-1159.

Hotaling, N. A., Khristov, V., Wan, Q., Sharma, R., Jha, B. S., Lotfi, M., Maminishkis, A., Simon, C. G.,Jr, & Bharti, K. (2016). Nanofiber scaffold-based tissue-engineered retinal pigment epithelium to treat degenerative eye diseases. Journal of Ocular Pharmacology and Therapeutics : The Official Journal of the Association for Ocular Pharmacology and Therapeutics, 32(5), 272-285.

Hu, Y., Liu, L., Lu, B., Zhu, D., Ribeiro, R., Diniz, B., Thomas, P. B., Ahuja, A. K., Hinton, D. R., Tai, Y. C., Hikita, S. T., Johnson, L. V., Clegg, D. O., Thomas, B. B., & Humayun, M. S. (2012). A novel approach for subretinal implantation of ultrathin substrates containing stem cell-derived retinal pigment epithelium monolayer. Ophthalmic Research, 48(4), 186-191.

Hughes, C. S., Postovit, L. M., & Lajoie, G. A. (2010). Matrigel: A complex protein mixture required for optimal growth of cell culture. Proteomics, 10(9), 1886-1890.

Hughes, C. S., Radan, L., Betts, D., Postovit, L. M., & Lajoie, G. A. (2011). Proteomic analysis of extracellular matrices used in stem cell culture. Proteomics, 11(20), 3983-3991.

Humphries, J. D., Byron, A., & Humphries, M. J. (2006). Integrin ligands at a glance. Journal of Cell Science, 119(Pt 19), 3901-3903.

Hynes, R. (2002). Integrins: Bidirectional, allosteric signaling machines. Cell, 110(6), 673-687.

Hynes, S. R., & Lavik, E. B. (2010). A tissue-engineered approach towards retinal repair: Scaffolds for cell transplantation to the subretinal space. Graefe's Archive for Clinical and Experimental Ophthalmology = Albrecht Von Graefes Archiv Fur Klinische Und Experimentelle Ophthalmologie, 248(6), 763-778.

Idelson, M., Alper, R., Obolensky, A., Ben-Shushan, E., Hemo, I., Yachimovich-Cohen, N., . . . Reubinoff, B. (2009). Directed differentiation of human embryonic stem cells into functional retinal pigment epithelium cells. Cell Stem Cell, 5(4), 396-408.

Ilmarinen, T., Hiidenmaa, H., Koobi, P., Nymark, S., Sorkio, A., Wang, J. H., Stanzel, B. V., Thieltges, F., Alajuuma, P., Oksala, O., Kataja, M., Uusitalo, H., & Skottman, H. (2015). Ultrathin polyimide membrane as cell carrier for subretinal transplantation of human embryonic stem cell derived retinal pigment epithelium. PloS One, 10(11), e0143669.

Jacobs, T., Declercq, H., De Geyter, N., Cornelissen, R., Dubruel, P., Leys, C., Beaurain, A., Payen, E., & Morent, R. (2013). Plasma surface modification of polylactic acid to promote interaction with fibroblasts. Journal of Materials Science.Materials in Medicine, 24(2), 469-478.

Jeong, S. M., Kim, E. Y., Hwang, J. H., Lee, G. Y., Cho, S. J., Bae, J. Y., Song, J. E., Yoon, K. H., Joo, C. K., Lee, D., & Khang, G. (2011). A study on proliferation and behavior of retinal pigment epithelial cells on purified alginate films. International Journal of Stem Cells, 4(2), 105-112.

Jha, B. S., & Bharti, K. (2015). Regenerating retinal pigment epithelial cells to cure blindness: A road towards personalized artificial tissue. Current Stem Cell Reports, 1(2), 79-91.

Jiang, F., Horber, H., Howard, J., & Muller, D. J. (2004). Assembly of collagen into microribbons: Effects of pH and electrolytes. Journal of Structural Biology, 148(3), 268-278.

John, S., Natarajan, S., Parikumar, P., Shanmugam, P. M., Senthilkumar, R., Green, D. W., & Abraham, S. J. (2013). Choice of cell source in cell-based therapies for retinal damage due to age-related macular degeneration: A review. Journal of Ophthalmology, 2013, 465169.

Juuti-Uusitalo, K., Delporte, C., Gregoire, F., Perret, J., Huhtala, H., Savolainen, V., Nymark, S., Hyttinen, J., Uusitalo, H., Willermain, F., & Skottman, H. (2013). Aquaporin expression and function in human pluripotent stem cell-derived retinal pigmented epithelial cells. Investigative Ophthalmology & Visual Science, 54(5), 3510-3519.

Kalluri, R. (2003). Basement membranes: Structure, assembly and role in tumour angiogenesis. Nature Reviews.Cancer, 3(6), 422-433.

Kamao, H., Mandai, M., Okamoto, S., Sakai, N., Suga, A., Sugita, S., Kiryu, J., & Takahashi, M. (2014). Characterization of human induced pluripotent stem cell-derived retinal pigment epithelium cell sheets aiming for clinical application. Stem Cell Reports, 2(2), 205-218.

Kamei, M., Kawasaki, A., & Tano, Y. (1998). Analysis of extracellular matrix synthesis during wound healing of retinal pigment epithelial cells. Microscopy Research and Technique, 42(5), 311-316.

Kasemo, B. (2002). Biological surface science. Surface Science, 500, 656–677.

Kearns, V., Mistry, A., Mason, S., Krishna, Y., Sheridan, C., Short, R., & Williams, R. L. (2012). Plasma polymer coatings to aid retinal pigment epithelial growth for transplantation in the treatment of age related macular degeneration. Journal of Materials Science.Materials in Medicine, 23(8), 2013-2021.

Kigasawa, K., Ishikawa, H., Obazawa, H., Minamoto, T., Nagai, Y., & Tanaka, Y. (1998). Collagen production by cultured human retinal pigment epithelial cells. The Tokai Journal of Experimental and Clinical Medicine, 23(3), 147-151.

Kiilgaard, J. F., Scherfig, E., Prause, J. U., & la Cour, M. (2012). Transplantation of amniotic membrane to the subretinal space in pigs. Stem Cells International, 2012, 716968.

Kimbrel, E. A., & Lanza, R. (2015). Current status of pluripotent stem cells: Moving the first therapies to the clinic. Nature Reviews.Drug Discovery, 14(10), 681-692.

Klimanskaya, I., Hipp, J., Rezai, K. A., West, M., Atala, A., & Lanza, R. (2004). Derivation and comparative assessment of retinal pigment epithelium from human embryonic stem cells using transcriptomics. Cloning and Stem Cells, 6(3), 217-245.

Koss, M. J., Falabella, P., Stefanini, F. R., Pfister, M., Thomas, B. B., Kashani, A. H., Brant, R., Zhu, D., Clegg, D. O., Hinton, D. R., & Humayun, M. S. (2016). Subretinal implantation of a monolayer of human embryonic stem cell-derived retinal pigment epithelium: A feasibility and safety study in yucatan minipigs. Graefe's Archive for Clinical and Experimental Ophthalmology = Albrecht Von Graefes Archiv Fur Klinische Und Experimentelle Ophthalmologie,

Krishna, Y., Sheridan, C., Kent, D., Kearns, V., Grierson, I., & Williams, R. (2011). Expanded polytetrafluoroethylene as a substrate for retinal pigment epithelial cell growth and transplantation in age-related macular degeneration. The British Journal of Ophthalmology, 95(4), 569-573.

Kubota, A., Nishida, K., Yamato, M., Yang, J., Kikuchi, A., Okano, T., & Tano, Y. (2006). Transplantable retinal pigment epithelial cell sheets for tissue engineering. Biomaterials, 27(19), 3639-3644.

Lai, J. Y. (2009). The role of bloom index of gelatin on the interaction with retinal pigment epithelial cells. International Journal of Molecular Sciences, 10(8), 3442-3456.

Lai, J. Y., Li, Y. T., & Wang, T. P. (2010). In vitro response of retinal pigment epithelial cells exposed to chitosan materials prepared with different cross-linkers. International Journal of Molecular Sciences, 11(12), 5256-5272.

Lamba, D. A., Gust, J., & Reh, T. A. (2009). Transplantation of human embryonic stem cell-derived photoreceptors restores some visual function in crx-deficient mice. Cell Stem Cell, 4(1), 73-79.

Lane, A., Philip, L. R., Ruban, L., Fynes, K., Smart, M., Carr, A., Mason, C., & Coffey, P. (2014). Engineering efficient retinal pigment epithelium differentiation from human pluripotent stem cells. Stem Cells Translational Medicine, 3(11), 1295-1304.

Langmuir, I. (1938). Overturning and anchoring of monolayers. Science (New York, N.Y.), 87(2266), 493-500.

Laperle, A., Masters, K. S., & Palecek, S. P. (2015). Influence of substrate composition on human embryonic stem cell differentiation and extracellular matrix production in embryoid bodies. Biotechnology Progress, 31(1), 212-219.

Leach, L. L., Croze, R. H., Hu, Q., Nadar, V. P., Clevenger, T. N., Pennington, B. O., Gamm, D. M., & Clegg, D. O. (2016). Induced pluripotent stem cell-derived retinal pigmented epithelium: A comparative study between cell lines and differentiation methods. Journal of Ocular Pharmacology and Therapeutics : The Official Journal of the Association for Ocular Pharmacology and Therapeutics, 32(5), 317-330.

Lee, C. J., Fishman, H. A., & Bent, S. F. (2007). Spatial cues for the enhancement of retinal pigment epithelial cell function in potential transplants. Biomaterials, 28(13), 2192-2201.

Lee, C. J., Huie, P., Leng, T., Peterman, M. C., Marmor, M. F., Blumenkranz, M. S., Bent, S. F., & Fishman, H. A. (2002). Microcontact printing on human tissue for retinal cell transplantation. Archives of Ophthalmology (Chicago, Ill.: 1960), 120(12), 1714-1718.

Lee, E., & MacLaren, R. E. (2011). Sources of retinal pigment epithelium (RPE) for replacement therapy. The British Journal of Ophthalmology, 95(4), 445-449.

Lee, J., Tae, G., Kim, Y. H., Park, I. S., Kim, S. H., & Kim, S. H. (2008). The effect of gelatin incorporation into electrospun poly(L-lactide-co-epsilon-caprolactone) fibers on mechanical properties and cytocompatibility. Biomaterials, 29(12), 1872-1879.

Lewandowska, K., Pergament, E., Sukenik, C. N., & Culp, L. A. (1992). Cell-type-specific adhesion mechanisms mediated by fibronectin adsorbed to chemically derivatized substrata. Journal of Biomedical Materials Research, 26(10), 1343-1363.

Li, Y., Tsai, Y. T., Hsu, C. W., Erol, D., Yang, J., Wu, W. H., Davis, R. J., Egli, D., & Tsang, S. H. (2012). Long-term safety and efficacy of human-induced pluripotent stem cell (iPS) grafts in a preclinical model of retinitis pigmentosa. Molecular Medicine (Cambridge, Mass.), 18, 1312-1319.

Liao, J. L., Yu, J., Huang, K., Hu, J., Diemer, T., Ma, Z., Dvash, T., Yang, X. J., Travis, G. H., Williams, D. S., Bok, D., & Fan, G. (2010). Molecular signature of primary retinal pigment epithelium and stem-cell-derived RPE cells. Human Molecular Genetics, 19(21), 4229-4238.

Lim, J. M., Byun, S., Chung, S., Park, T. H., Seo, J. M., Joo, C. K., Chung, H., & Cho, D. I. (2004). Retinal pigment epithelial cell behavior is modulated by alterations in focal cell-substrate contacts. Investigative Ophthalmology & Visual Science, 45(11), 4210-4216.

Lim, L. S., Mitchell, P., Seddon, J. M., Holz, F. G., & Wong, T. Y. (2012). Age-related macular degeneration. Lancet (London, England), 379(9827), 1728-1738.

Liu, Z., Yu, N., Holz, F. G., Yang, F., & Stanzel, B. V. (2014). Enhancement of retinal pigment epithelial culture characteristics and subretinal space tolerance of scaffolds with 200 nm fiber topography. Biomaterials, 35(9), 2837-2850.

Lotta, T. I., Laakkonen, L. J., Virtanen, J. A., & Kinnunen, P. K. (1988). Characterization of langmuir-blodgett films of 1,2-dipalmitoyl-sn-glycero-3-phosphatidylcholine and 1-palmitoyl-2-[10-(pyren-1-yl)decanoyl]-sn-glycero-3-phosphat idylcholine by FTIR-ATR. Chemistry and Physics of Lipids, 46(1), 1-12.

Lu, B., Malcuit, C., Wang, S., Girman, S., Francis, P., Lemieux, L., Lanza, R., & Lund, R. (2009). Long-term safety and function of RPE from human embryonic stem cells in preclinical models of macular degeneration. Stem Cells (Dayton, Ohio), 27(9), 2126-2135.

Lu, B., Tai, Y. C., & Humayun, M. S. (2014). Microdevice-based cell therapy for age-related macular degeneration. Developments in Ophthalmology, 53, 155-166.

Lu, J. T., Lee, C. J., Bent, S. F., Fishman, H. A., & Sabelman, E. E. (2007). Thin collagen film scaffolds for retinal epithelial cell culture. Biomaterials, 28(8), 1486-1494.

Lu, L., Garcia, C. A., & Mikos, A. G. (1998). Retinal pigment epithelium cell culture on thin biodegradable poly(DL-lactic-co-glycolic acid) films. Journal of Biomaterials Science.Polymer Edition, 9(11), 1187-1205.

Lu, L., Kam, L., Hasenbein, M., Nyalakonda, K., Bizios, R., Gopferich, A., Young, J. F., & Mikos, A. G. (1999). Retinal pigment epithelial cell function on substrates with chemically micropatterned surfaces. Biomaterials, 20(23-24), 2351-2361.

Lu, L., Nyalakonda, K., Kam, L., Bizios, R., Gopferich, A., & Mikos, A. G. (2001). Retinal pigment epithelial cell adhesion on novel micropatterned surfaces fabricated from synthetic biodegradable polymers. Biomaterials, 22(3), 291-297.

Lund, R. D., Wang, S., Klimanskaya, I., Holmes, T., Ramos-Kelsey, R., Lu, B., Girman, S., Bischoff, N., Sauve, Y., & Lanza, R. (2006). Human embryonic stem cell-derived cells rescue visual function in dystrophic RCS rats. Cloning and Stem Cells, 8(3), 189-199.

Lynn, A. K., Yannas, I. V., & Bonfield, W. (2004). Antigenicity and immunogenicity of collagen. Journal of Biomedical Materials Research.Part B, Applied Biomaterials, 71(2), 343-354.

Ma, W., Tavakoli, T., Derby, E., Serebryakova, Y., Rao, M. S., & Mattson, M. P. (2008). Cell-extracellular matrix interactions regulate neural differentiation of human embryonic stem cells. BMC Developmental Biology, 8, 90.

Malafaya, P. B., Silva, G. A., & Reis, R. L. (2007). Natural-origin polymers as carriers and scaffolds for biomolecules and cell delivery in tissue engineering applications. Advanced Drug Delivery Reviews, 59(4-5), 207-233.

Mateos-Timoneda, M. A., Levato, R., Punet, X., Cano, I., Castano, O., & Engel, E. (2015). Biofunctionalization of polymeric surfaces. Conference Proceedings : ...Annual International Conference of the IEEE Engineering in Medicine and Biology Society.IEEE Engineering in Medicine and Biology Society.Annual Conference, 2015, 1745-1748.

Mazzoni, F., Safa, H., & Finnemann, S. C. (2014). Understanding photoreceptor outer segment phagocytosis: Use and utility of RPE cells in culture. Experimental Eye Research, 126, 51-60.

McCarthy, J. B., Vachhani, B., & Iida, J. (1996). Cell adhesion to collagenous matrices. Biopolymers, 40(4), 371-381.

McHugh, K. J., Tao, S. L., & Saint-Geniez, M. (2014). Porous poly(epsilon-caprolactone) scaffolds for retinal pigment epithelium transplantation. Investigative Ophthalmology & Visual Science, 55(3), 1754-1762.

Mitra, S. K., Hanson, D. A., & Schlaepfer, D. D. (2005). Focal adhesion kinase: In command and control of cell motility. Nature Reviews.Molecular Cell Biology, 6(1), 56-68.

Miyagishima, K. J., Wan, Q., Corneo, B., Sharma, R., Lotfi, M. R., Boles, N. C., . . . Bharti, K. (2016). In pursuit of authenticity: Induced pluripotent stem cell-derived retinal pigment epithelium for clinical applications. Stem Cells Translational Medicine,

Nair, L. S., & Laurencin, C. T. (2007). Biodegradable polymers as biomaterials. Progress in Polymer Science, 32(8–9), 762-798.

Najafabadi, H. S., Soheili, Z. S., & Ganji, S. M. (2015). Behavior of a spontaneously arising human retinal pigment epithelial cell line cultivated on thin alginate film. Journal of Ophthalmic & Vision Research, 10(3), 286-294.

Nakano, T., Ando, S., Takata, N., Kawada, M., Muguruma, K., Sekiguchi, K., Saito, K., Yonemura, S., Eiraku, M., & Sasai, Y. (2012). Self-formation of optic cups and storable stratified neural retina from human ESCs. Cell Stem Cell, 10(6), 771-785.

Nandrot, E. F., Silva, K. E., Scelfo, C., & Finnemann, S. C. (2012). Retinal pigment epithelial cells use a MerTK-dependent mechanism to limit the phagocytic particle binding activity of alphavbeta5 integrin. Biology of the Cell / Under the Auspices of the European Cell Biology Organization, 104(6), 326-341.

Nazari, H., Zhang, L., Zhu, D., Chader, G. J., Falabella, P., Stefanini, F., Rowland, T., Clegg, D. O., Kashani, A. H., Hinton, D. R., & Humayun, M. S. (2015). Stem cell based therapies for age-related macular degeneration: The promises and the challenges. Progress in Retinal and Eye Research, 48, 1-39.

Ngandu Mpoyi, E., Cantini, M., Reynolds, P. M., Gadegaard, N., Dalby, M. J., & Salmeron-Sanchez, M. (2016). Protein adsorption as a key mediator in the nanotopographical control of cell behavior. ACS Nano, 10(7), 6638-6647.

Nicolini, J., Kiilgaard, J. F., Wiencke, A. K., Heegaard, S., Scherfig, E., Prause, J. U., & la Cour, M. (2000). The anterior lens capsule used as support material in RPE cell-transplantation. Acta Ophthalmologica Scandinavica, 78(5), 527-531.

O'Connor, M. D. (2013). The 3R principle: Advancing clinical application of human pluripotent stem cells. Stem Cell Research & Therapy, 4(2), 21.

Oganesian, A., Gabrielian, K., Ernest, J. T., & Patel, S. C. (1999). A new model of retinal pigment epithelium transplantation with microspheres. Archives of Ophthalmology (Chicago, Ill.: 1960), 117(9), 1192-1200.

Ohno-Matsui, K., Ichinose, S., Nakahama, K., Yoshida, T., Kojima, A., Mochizuki, M., & Morita, I. (2005). The effects of amniotic membrane on retinal pigment epithelial cell differentiation. Molecular Vision, 11, 1-10.

Olsen, I. M., & Ffrench-Constant, C. (2005). Dynamic regulation of integrin activation by intracellular and extracellular signals controls oligodendrocyte morphology. BMC Biology, 3, 25.

Pastorino, L., Dellacasa, E., Scaglione, S., Giulianelli, M., Sbrana, F., Vassalli, M., & Ruggiero, C. (2014). Oriented collagen nanocoatings for tissue engineering. Colloids and Surfaces.B, Biointerfaces, 114, 372-378.

Peng, S., Gan, G., Qiu, C., Zhong, M., An, H., Adelman, R. A., & Rizzolo, L. J. (2013). Engineering a blood-retinal barrier with human embryonic stem cell-derived retinal pigment epithelium: Transcriptome and functional analysis. Stem Cells Translational Medicine, 2(7), 534-544.

Peng, S., Rao, V. S., Adelman, R. A., & Rizzolo, L. J. (2011). Claudin-19 and the barrier properties of the human retinal pigment epithelium. Investigative Ophthalmology & Visual Science, 52(3), 1392-1403.

Pennington, B. O., & Clegg, D. O. (2016). Pluripotent stem cell-based therapies in combination with substrate for the treatment of age-related macular degeneration. Journal of Ocular Pharmacology and Therapeutics : The Official Journal of the Association for Ocular Pharmacology and Therapeutics, 32(5), 261-271.

Pennington, B. O., Clegg, D. O., Melkoumian, Z. K., & Hikita, S. T. (2015). Defined culture of human embryonic stem cells and xeno-free derivation of retinal pigmented epithelial cells on a novel, synthetic substrate. Stem Cells Translational Medicine, 4(2), 165-177.

Pera, M. F. (2011). Stem cells: The dark side of induced pluripotency. Nature, 471(7336), 46-47.

Plaza Reyes, A., Petrus-Reurer, S., Antonsson, L., Stenfelt, S., Bartuma, H., Panula, S., Mader, T., Douagi, I., Andre, H., Hovatta, O., Lanner, F., & Kvanta, A. (2016). Xeno-free and defined human embryonic stem cell-derived retinal pigment epithelial cells functionally integrate in a large-eyed preclinical model. Stem Cell Reports, 6(1), 9-17.

Popelka, S., Studenovska, H., Abelova, L., Ardan, T., Studeny, P., Stranak, Z., Klima, J., Dvorankova, B., Kotek, J., Hodan, J., & Rypacek, F. (2015). A frame-supported ultrathin electrospun polymer membrane for transplantation of retinal pigment epithelial cells. Biomedical Materials (Bristol, England), 10(4), 045022-6041/10/4/045022.

Price,P., Goldsborough,M. and Tilkins,M. . Embryonic stem cell serum replacement. 1998. WO98/30679.

Proulx, S., Landreville, S., Guerin, S. L., & Salesse, C. (2004). Integrin alpha5 expression by the ARPE-19 cell line: Comparison with primary RPE cultures and effect of growth medium on the alpha5 gene promoter strength. Experimental Eye Research, 79(2), 157-165.

Rahmany, M. B., & Van Dyke, M. (2013). Biomimetic approaches to modulate cellular adhesion in biomaterials: A review. Acta Biomaterialia, 9(3), 5431-5437.

Ramrattan, R. S., van der Schaft, T. L., Mooy, C. M., de Bruijn, W. C., Mulder, P. G., & de Jong, P. T. (1994). Morphometric analysis of bruch's membrane, the choriocapillaris,

and the choroid in aging. Investigative Ophthalmology & Visual Science, 35(6), 2857-2864.

Reh, T. A., Lamba, D., & Gust, J. (2010). Directing human embryonic stem cells to a retinal fate. Methods in Molecular Biology (Clifton, N.J.), 636, 139-153.

Riera, M., Fontrodona, L., Albert, S., Ramirez, D. M., Seriola, A., Salas, A., Munoz, Y., Ramos, D., Villegas-Perez, M. P., Zapata, M. A., Raya, A., Ruberte, J., Veiga, A., & Garcia-Arumi, J. (2016). Comparative study of human embryonic stem cells (hESC) and human induced pluripotent stem cells (hiPSC) as a treatment for retinal dystrophies. Molecular Therapy.Methods & Clinical Development, 3, 16010.

Rizzolo, L. J. (1999). Polarization of the na+, K(+)-ATPase in epithelia derived from the neuroepithelium. International Review of Cytology, 185, 195-235.

Rizzolo, L. J. (2014). Barrier properties of cultured retinal pigment epithelium. Experimental Eye Research, 126, 16-26.

Rizzolo, L. J., Peng, S., Luo, Y., & Xiao, W. (2011). Integration of tight junctions and claudins with the barrier functions of the retinal pigment epithelium. Progress in Retinal and Eye Research, 30(5), 296-323.

Rodin, S., Antonsson, L., Niaudet, C., Simonson, O. E., Salmela, E., Hansson, E. M., . . . Tryggvason, K. (2014). Clonal culturing of human embryonic stem cells on laminin-521/E-cadherin matrix in defined and xeno-free environment. Nature Communications, 5, 3195.

Rosenfeld, P. J., Brown, D. M., Heier, J. S., Boyer, D. S., Kaiser, P. K., Chung, C. Y., Kim, R. Y., & MARINA Study Group. (2006). Ranibizumab for neovascular age-related macular degeneration. The New England Journal of Medicine, 355(14), 1419-1431.

Rowland, T. J., Blaschke, A. J., Buchholz, D. E., Hikita, S. T., Johnson, L. V., & Clegg, D. O. (2013). Differentiation of human pluripotent stem cells to retinal pigmented epithelium in defined conditions using purified extracellular matrix proteins. Journal of Tissue Engineering and Regenerative Medicine, 7(8), 642-653.

Rowland, T. J., Buchholz, D. E., & Clegg, D. O. (2012). Pluripotent human stem cells for the treatment of retinal disease. Journal of Cellular Physiology, 227(2), 457-466.

Rudensky, A. Y., Preston-Hurlburt, P., Hong, S. C., Barlow, A., & Janeway, C. A.,Jr. (1991). Sequence analysis of peptides bound to MHC class II molecules. Nature, 353(6345), 622-627.

Sakai, Y., Furukawa, K., Ushida, T., Tateishi, T., & Suzuki, M. (2001). In vitro organization of biohybrid rat liver tissue incorporating growth factor- and hormone-releasing biodegradable polymer microcapsules. Cell Transplantation, 10(4-5), 479-483.

Sakamoto, N., Tsuji, K., Muul, L. M., Lawler, A. M., Petricoin, E. F., Candotti, F., Metcalf, J. A., Tavel, J. A., Lane, H. C., Urba, W. J., Fox, B. A., Varki, A., Lunney, J. K., & Rosenberg, A. S. (2007). Bovine apolipoprotein B-100 is a dominant immunogen in therapeutic cell populations cultured in fetal calf serum in mice and humans. Blood, 110(2), 501-508.

Schwartz, S. D., Hubschman, J. P., Heilwell, G., Franco-Cardenas, V., Pan, C. K., Ostrick, R. M., Mickunas, E., Gay, R., Klimanskaya, I., & Lanza, R. (2012). Embryonic stem cell trials for macular degeneration: A preliminary report. Lancet, 379(9817), 713-720.

Schwartz, S. D., Regillo, C. D., Lam, B. L., Eliott, D., Rosenfeld, P. J., Gregori, N. Z., . . . Lanza, R. (2015). Human embryonic stem cell-derived retinal pigment epithelium in patients with age-related macular degeneration and stargardt's macular dystrophy: Follow-up of two open-label phase 1/2 studies. Lancet (London, England), 385(9967), 509-516.

Schwartz, S. D., Tan, G., Hosseini, H., & Nagiel, A. (2016). Subretinal transplantation of embryonic stem cell-derived retinal pigment epithelium for the treatment of macular degeneration: An assessment at 4 years. Investigative Ophthalmology & Visual Science, 57(5), ORSFc1-9.

Seitz, T. L., Noonan, K. D., Hench, L. L., & Noonan, N. E. (1982). Effect of fibronectin on the adhesion of an established cell line to a surface reactive biomaterial. Journal of Biomedical Materials Research, 16(3), 195-207.

Shadforth, A. M., George, K. A., Kwan, A. S., Chirila, T. V., & Harkin, D. G. (2012). The cultivation of human retinal pigment epithelial cells on bombyx mori silk fibroin. Biomaterials, 33(16), 4110-4117.

Shadforth, A. M., Suzuki, S., Theodoropoulos, C., Richardson, N. A., Chirila, T. V., & Harkin, D. G. (2015). A bruch's membrane substitute fabricated from silk fibroin supports the function of retinal pigment epithelial cells in vitro. Journal of Tissue Engineering and Regenerative Medicine,

Shapira, A., Kim, D. H., & Dvir, T. (2014). Advanced micro- and nanofabrication technologies for tissue engineering. Biofabrication, 6(2), 020301-5082/6/2/020301. Epub 2014 May 30.

Simo, R., Villarroel, M., Corraliza, L., Hernandez, C., & Garcia-Ramirez, M. (2010). The retinal pigment epithelium: Something more than a constituent of the blood-retinal barrier--implications for the pathogenesis of diabetic retinopathy. Journal of Biomedicine & Biotechnology, 2010, 190724.

Singh, A. K., Srivastava, G. K., Martin, L., Alonso, M., & Pastor, J. C. (2014). Bioactive substrates for human retinal pigment epithelial cell growth from elastin-like recombinamers. Journal of Biomedical Materials Research.Part A, 102(3), 639-646.

Singh, S., Woerly, S., & McLaughlin, B. J. (2001). Natural and artificial substrates for retinal pigment epithelial monolayer transplantation. Biomaterials, 22(24), 3337-3343.

Singhal, S., & Vemuganti, G. K. (2005). Primary adult human retinal pigment epithelial cell cultures on human amniotic membranes. Indian Journal of Ophthalmology, 53(2), 109-113.

Skottman, H. (2010). Derivation and characterization of three new human embryonic stem cell lines in finland. In Vitro Cellular & Developmental Biology.Animal, 46(3-4), 206-209.

Song, J.,Sik, Lee,Sukmin, Jung, S.,Hee, Cha, G.,Chan, & Mun, M.,Seong. (2009). Improved biocompatibility of parylene-C films prepared by chemical vapor deposition and the subsequent plasma treatment. Journal of Applied Polymer Science, 112(6), 3677–3685.

Sorkio, A., Haimi, S., Verdoold, V., Juuti-Uusitalo, K., Grijpma, D., & Skottman, H. (2016). Poly(trimethylene carbonate) as an elastic biodegradable film for human embryonic stem cell derived retinal pigment epithelial cells. Journal of Tissue Engineering and Regenerative Medicine,

Srivastava, G. K., Martin, L., Singh, A. K., Fernandez-Bueno, I., Gayoso, M. J., Garcia-Gutierrez, M. T., Girotti, A., Alonso, M., Rodriguez-Cabello, J. C., & Pastor, J. C. (2011). Elastin-like recombinamers as substrates for retinal pigment epithelial cell growth. Journal of Biomedical Materials Research.Part A, 97(3), 243-250.

Stanzel, B. V., Espana, E. M., Grueterich, M., Kawakita, T., Parel, J. M., Tseng, S. C., & Binder, S. (2005). Amniotic membrane maintains the phenotype of rabbit retinal pigment epithelial cells in culture. Experimental Eye Research, 80(1), 103-112.

Stanzel, B. V., Liu, Z., Brinken, R., Braun, N., Holz, F. G., & Eter, N. (2012). Subretinal delivery of ultrathin rigid-elastic cell carriers using a metallic shooter instrument and biodegradable hydrogel encapsulation. Investigative Ophthalmology & Visual Science, 53(1), 490-500.

Stanzel, B. V., Liu, Z., Somboonthanakij, S., Wongsawad, W., Brinken, R., Eter, N., Corneo, B., Holz, F. G., Temple, S., Stern, J. H., & Blenkinsop, T. A. (2014). Human RPE stem cells grown into polarized RPE monolayers on a polyester matrix are maintained after grafting into rabbit subretinal space. Stem Cell Reports, 2(1), 64-77.

Strachan, L. R., & Condic, M. L. (2008). Neural crest motility on fibronectin is regulated by integrin activation. Experimental Cell Research, 314(3), 441-452.

Strauss, O. (2005). The retinal pigment epithelium in visual function. Physiological Reviews, 85(3), 845-881.

Subrizi, A., Hiidenmaa, H., Ilmarinen, T., Nymark, S., Dubruel, P., Uusitalo, H., Yliperttula, M., Urtti, A., & Skottman, H. (2012). Generation of hESC-derived retinal pigment epithelium on biopolymer coated polyimide membranes. Biomaterials, 33(32), 8047-8054.

Sugino, I. K., Gullapalli, V. K., Sun, Q., Wang, J., Nunes, C. F., Cheewatrakoolpong, N., Johnson, A. C., Degner, B. C., Hua, J., Liu, T., Chen, W., Li, H., & Zarbin, M. A. (2011).

Cell-deposited matrix improves retinal pigment epithelium survival on aged submacular human bruch's membrane. Investigative Ophthalmology & Visual Science, 52(3), 1345-1358.

Sugino, I. K., Sun, Q., Wang, J., Nunes, C. F., Cheewatrakoolpong, N., Rapista, A., Johnson, A. C., Malcuit, C., Klimanskaya, I., Lanza, R., & Zarbin, M. A. (2011). Comparison of FRPE and human embryonic stem cell-derived RPE behavior on aged human bruch's membrane. Investigative Ophthalmology & Visual Science, 52(8), 4979-4997.

Takahashi, K., Tanabe, K., Ohnuki, M., Narita, M., Ichisaka, T., Tomoda, K., & Yamanaka, S. (2007). Induction of pluripotent stem cells from adult human fibroblasts by defined factors. Cell, 131(5), 861-872.

Tenboll, A., Darvish, B., Hou, W., Duwez, A. S., Dixon, S. J., Goldberg, H. A., Grohe, B., & Mittler, S. (2010). Controlled deposition of highly oriented type I collagen mimicking in vivo collagen structures. Langmuir : The ACS Journal of Surfaces and Colloids, 26(14), 12165-12172.

Tezcaner, A., Bugra, K., & Hasirci, V. (2003). Retinal pigment epithelium cell culture on surface modified poly(hydroxybutyrate-co-hydroxyvalerate) thin films. Biomaterials, 24(25), 4573-4583.

Tezel, T. H., & Del Priore, L. V. (1999). Repopulation of different layers of host human bruch's membrane by retinal pigment epithelial cell grafts. Investigative Ophthalmology & Visual Science, 40(3), 767-774.

Tezel, T. H., Kaplan, H. J., & Del Priore, L. V. (1999). Fate of human retinal pigment epithelial cells seeded onto layers of human bruch's membrane. Investigative Ophthalmology & Visual Science, 40(2), 467-476.

Thieltges, F., Stanzel, B. V., Liu, Z., & Holz, F. G. (2011). A nanofibrillar surface promotes superior growth characteristics in cultured human retinal pigment epithelium. Ophthalmic Research, 46(3), 133-140.

Thomas, B. B., Zhu, D., Zhang, L., Thomas, P. B., Hu, Y., Nazari, H., Stefanini, F., Falabella, P., Clegg, D. O., Hinton, D. R., & Humayun, M. S. (2016). Survival and

functionality of hESC-derived retinal pigment epithelium cells cultured as a monolayer on polymer substrates transplanted in RCS rats. Investigative Ophthalmology & Visual Science, 57(6), 2877-2887.

Thomson, H. A., Treharne, A. J., Backholer, L. S., Cuda, F., Grossel, M. C., & Lotery, A. J. (2010). Biodegradable poly(alpha-hydroxy ester) blended microspheres as suitable carriers for retinal pigment epithelium cell transplantation. Journal of Biomedical Materials Research.Part A, 95(4), 1233-1243.

Thomson, J. A., Itskovitz-Eldor, J., Shapiro, S. S., Waknitz, M. A., Swiergiel, J. J., Marshall, V. S., & Jones, J. M. (1998). Embryonic stem cell lines derived from human blastocysts. Science (New York, N.Y.), 282(5391), 1145-1147.

Thomson, R. C., Giordano, G. G., Collier, J. H., Ishaug, S. L., Mikos, A. G., Lahiri-Munir, D., & Garcia, C. A. (1996). Manufacture and characterization of poly(alpha-hydroxy ester) thin films as temporary substrates for retinal pigment epithelium cells. Biomaterials, 17(3), 321-327.

Thumann, G., Schraermeyer, U., Bartz-Schmidt, K. U., & Heimann, K. (1997). Descemet's membrane as membranous support in RPE/IPE transplantation. Current Eye Research, 16(12), 1236-1238.

Thumann, G., Viethen, A., Gaebler, A., Walter, P., Kaempf, S., Johnen, S., & Salz, A. K. (2009). The in vitro and in vivo behaviour of retinal pigment epithelial cells cultured on ultrathin collagen membranes. Biomaterials, 30(3), 287-294.

Tian, J., Ishibashi, K., & Handa, J. T. (2004). The expression of native and cultured RPE grown on different matrices. Physiological Genomics, 17(2), 170-182.

Toivonen, S., Ojala, M., Hyysalo, A., Ilmarinen, T., Rajala, K., Pekkanen-Mattila, M., . . . Otonkoski, T. (2013). Comparative analysis of targeted differentiation of human induced pluripotent stem cells (hiPSCs) and human embryonic stem cells reveals variability associated with incomplete transgene silencing in retrovirally derived hiPSC lines. Stem Cells Translational Medicine, 2(2), 83-93.

Treharne, A. J., Thomson, H. A., Grossel, M. C., & Lotery, A. J. (2012). Developing methacrylate-based copolymers as an artificial bruch's membrane substitute. Journal of Biomedical Materials Research.Part A, 100(9), 2358-2364.

Ugarte, M., Hussain, A. A., & Marshall, J. (2006). An experimental study of the elastic properties of the human bruch's membrane-choroid complex: Relevance to ageing. The British Journal of Ophthalmology, 90(5), 621-626.

Ulery, B. D., Nair, L. S., & Laurencin, C. T. (2011). Biomedical applications of biodegradable polymers. Journal of Polymer Science.Part B, Polymer Physics, 49(12), 832-864.

Vaajasaari, H., Ilmarinen, T., Juuti-Uusitalo, K., Rajala, K., Onnela, N., Narkilahti, S., Suuronen, R., Hyttinen, J., Uusitalo, H., & Skottman, H. (2011). Toward the defined and xeno-free differentiation of functional human pluripotent stem cell-derived retinal pigment epithelial cells. Molecular Vision, 17, 558-575.

van Zeeburg, E. J., Maaijwee, K. J., Missotten, T. O., Heimann, H., & van Meurs, J. C. (2012). A free retinal pigment epithelium-choroid graft in patients with exudative age-related macular degeneration: Results up to 7 years. American Journal of Ophthalmology, 153(1), 120-7.e2.

Varma, S., Orgel, J. P., & Schieber, J. D. (2016). Nanomechanics of type I collagen. Biophysical Journal, 111(1), 50-56.

Veis, A., & Cohen, J. (1960). Reversible transformation of gelatin to the collagen structure. Nature, 186, 720-721.

Villa-Diaz, L. G., Ross, A. M., Lahann, J., & Krebsbach, P. H. (2013). Concise review: The evolution of human pluripotent stem cell culture: From feeder cells to synthetic coatings. Stem Cells (Dayton, Ohio), 31(1), 1-7.

von Recum, H., Kikuchi, A., Okuhara, M., Sakurai, Y., Okano, T., & Kim, S. W. (1998). Retinal pigmented epithelium cultures on thermally responsive polymer porous substrates. Journal of Biomaterials Science.Polymer Edition, 9(11), 1241-1253.

von Recum, H., Okano, T., Kim, S. W., & Bernstein, P. S. (1999). Maintenance of retinoid metabolism in human retinal pigment epithelium cell culture. Experimental Eye Research, 69(1), 97-107.

Vroman, L., & Adams, A. (1986). Adsorption of proteins out of plasma and solutions in narrow spaces. Journal of Colloid and Interface Science, 111(2), 391-402.

Vugler, A., Carr, A. J., Lawrence, J., Chen, L. L., Burrell, K., Wright, A., Lundh, P., Semo, M., Ahmado, A., Gias, C., da Cruz, L., Moore, H., Andrews, P., Walsh, J., & Coffey, P. (2008). Elucidating the phenomenon of HESC-derived RPE: Anatomy of cell genesis, expansion and retinal transplantation. Experimental Neurology, 214(2), 347-361.

Vukicevic, S., Kleinman, H. K., Luyten, F. P., Roberts, A. B., Roche, N. S., & Reddi, A. H. (1992). Identification of multiple active growth factors in basement membrane matrigel suggests caution in interpretation of cellular activity related to extracellular matrix components. Experimental Cell Research, 202(1), 1-8.

Walters, N. J., & Gentleman, E. (2015). Evolving insights in cell-matrix interactions: Elucidating how non-soluble properties of the extracellular niche direct stem cell fate. Acta Biomaterialia, 11, 3-16.

Wang, C., Stewart, R. J., & Kopecek, J. (1999). Hybrid hydrogels assembled from synthetic polymers and coiled-coil protein domains. Nature, 397(6718), 417-420.

Wang, S., Cui, W., & Bei, J. (2005). Bulk and surface modifications of polylactide. Analytical and Bioanalytical Chemistry, 381(3), 547-556.

Wang, X., Ding, B., & Li, B. (2013). Biomimetic electrospun nanofibrous structures for tissue engineering. Materials Today (Kidlington, England), 16(6), 229-241.

Warnke, P. H., Alamein, M., Skabo, S., Stephens, S., Bourke, R., Heiner, P., & Liu, Q. (2013). Primordium of an artificial bruch's membrane made of nanofibers for engineering of retinal pigment epithelium cell monolayers. Acta Biomaterialia, 9(12), 9414-9422.

Williams, D. F. (2009). On the nature of biomaterials. Biomaterials, 30(30), 5897-5909.

Williams, R. L., Krishna, Y., Dixon, S., Haridas, A., Grierson, I., & Sheridan, C. (2005). Polyurethanes as potential substrates for sub-retinal retinal pigment epithelial cell transplantation. Journal of Materials Science.Materials in Medicine, 16(12), 1087-1092.

Wilson, C. J., Clegg, R. E., Leavesley, D. I., & Pearcy, M. J. (2005). Mediation of biomaterial-cell interactions by adsorbed proteins: A review. Tissue Engineering, 11(1-2), 1-18.

Wimmers, S., Karl, M. O., & Strauss, O. (2007). Ion channels in the RPE. Progress in Retinal and Eye Research, 26(3), 263-301.

Wright, L. S., Phillips, M. J., Pinilla, I., Hei, D., & Gamm, D. M. (2014). Induced pluripotent stem cells as custom therapeutics for retinal repair: Progress and rationale. Experimental Eye Research, 123, 161-172.

Wu, N., Doorenbos, M., & Chen, D. F. (2016). Induced pluripotent stem cells: Development in the ophthalmologic field. Stem Cells International, 2016, 2361763.

Xiang, P., Wu, K. C., Zhu, Y., Xiang, L., Li, C., Chen, D. L., Chen, F., Xu, G., Wang, A., Li, M., & Jin, Z. B. (2014). A novel bruch's membrane-mimetic electrospun substrate scaffold for human retinal pigment epithelium cells. Biomaterials, 35(37), 9777-9788.

Yang, J., Bei, J., & Wang, S. (2002). Enhanced cell affinity of poly (D,L-lactide) by combining plasma treatment with collagen anchorage. Biomaterials, 23(12), 2607-2614.

Yao, X., Peng, R., & Ding, J. (2013). Cell-material interactions revealed via material techniques of surface patterning. Advanced Materials (Deerfield Beach, Fla.), 25(37), 5257-5286.

Yewdell, J. W., & Bennink, J. R. (2001). Cut and trim: Generating MHC class I peptide ligands. Current Opinion in Immunology, 13(1), 13-18.

Yurchenco, P. D. (2011). Basement membranes: Cell scaffoldings and signaling platforms. Cold Spring Harbor Perspectives in Biology, 3(2), 10.1101/cshperspect.a004911.

Yurchenco, P. D., Amenta, P. S., & Patton, B. L. (2004). Basement membrane assembly, stability and activities observed through a developmental lens. Matrix Biology : Journal of the International Society for Matrix Biology, 22(7), 521-538.

Zarbin, M. A. (2003). Analysis of retinal pigment epithelium integrin expression and adhesion to aged submacular human bruch's membrane. Transactions of the American Ophthalmological Society, 101, 499-520.

Zayas-Santiago, A., Marmorstein, A. D., & Marmorstein, L. Y. (2011). Relationship of stokes radius to the rate of diffusion across bruch's membrane. Investigative Ophthalmology & Visual Science, 52(7), 4907-4913.

Zhang, Y. Z., Su, B., Venugopal, J., Ramakrishna, S., & Lim, C. T. (2007). Biomimetic and bioactive nanofibrous scaffolds from electrospun composite nanofibers. International Journal of Nanomedicine, 2(4), 623-638.

Zhao, C., Tan, A., Pastorin, G., & Ho, H. K. (2013). Nanomaterial scaffolds for stem cell proliferation and differentiation in tissue engineering. Biotechnology Advances, 31(5), 654-668.

Original publications

TISSUE ENGINEERING: Part A
Volume 20, Numbers 3 and 4, 2014

DOI: 10.1089/ten.tea.2013.0049

Original Article

Structure and Barrier Properties of Human Embryonic Stem Cell–Derived Retinal Pigment Epithelial Cells Are Affected by Extracellular Matrix Protein Coating

Anni Sorkio, MSc,[1,2] Heidi Hongisto, PhD, MSc,[1,2] Kai Kaarniranta, MD, PhD, MSc, FEBO,[3] Hannu Uusitalo, MD, PhD, FEBO,[4] Kati Juuti-Uusitalo, PhD, MSc,[1,2] and Heli Skottman, PhD, MSc[1,2]

Extracellular matrix (ECM) interactions play a vital role in cell morphology, migration, proliferation, and differentiation of cells. We investigated the role of ECM proteins on the structure and function of human embryonic stem cell–derived retinal pigment epithelial (hESC-RPE) cells during their differentiation and maturation from hESCs into RPE cells in adherent differentiation cultures on several human ECM proteins found in native human Bruch's membrane, namely, collagen I, collagen IV, laminin, fibronectin, and vitronectin, as well as on commercial substrates of xeno-free CELLstart™ and Matrigel™. Cell pigmentation, expression of RPE-specific proteins, fine structure, as well as the production of basal lamina by hESC-RPE on different protein coatings were evaluated after 140 days of differentiation. The integrity of hESC-RPE epithelium and barrier properties on different coatings were investigated by measuring transepithelial resistance. All coatings supported the differentiation of hESC-RPE cells as demonstrated by early onset of cell pigmentation and further maturation to RPE monolayers after enrichment. Mature RPE phenotype was verified by RPE-specific gene and protein expression, correct epithelial polarization, and phagocytic activity. Significant differences were found in the degree of RPE cell pigmentation and tightness of epithelial barrier between different coatings. Further, the thickness of self-assembled basal lamina and secretion of the key ECM proteins found in the basement membrane of the native RPE varied between hESC-RPE cultured on compared protein coatings. In conclusion, this study shows that the cell culture substrate has a major effect on the structure and basal lamina production during the differentiation and maturation of hESC-RPE potentially influencing the success of cell integrations and survival after cell transplantation.

Introduction

The retinal pigment epithelium (RPE) is a monolayer of polarized and pigmented cells located between the neural retina and the choriocapillaris. RPE plays a central role maintaining the proper function of the retina and its photoreceptors.[1] Dysfunction or irreversible damage of RPE cells leads to impairment and death of photoreceptors leading to progressive loss of vision in degenerative retinal diseases, such as age-related macular degeneration (AMD).[2,3]

AMD is an increasing cause of blindness in the elderly. Phenotypically, AMD can be divided into two main forms: dry (atrophic) and wet (exudative) types and further subdivided into early and late-stage diseases. However, cure for AMD and especially its dry form is lacking.[2,3] Cell transplants of human embryonic stem cell (hESC)–derived RPE (hESC-RPE) cells are currently under clinical trials for the treatment of the dry form of AMD (80% of total AMD cases) and Stargardt's disease.[4] hESCs are considered to be an excellent, reproducible cell source in regenerative medicine due to their differentiation potential and indefinite proliferation capacity.[5] Several research groups have demonstrated differentiation of functional RPE cells from human pluripotent stem cells (hPSCs), including induced pluripotent stem cells (iPSCs).[6–10] Moreover, cell transplantation experiments in animal models of retinal degeneration have demonstrated improvement in visual function after injection of hPSC-RPE cells.[11–13] However, the effect is eventually lost, likely due to inefficient cell attachment and integration of the transplanted cells with the retina and choroid. Grafting of intact and polarized RPE cell sheets,

[1]Institute of Biomedical Technology, University of Tampere, Tampere, Finland.
[2]BioMediTech, Tampere, Finland.
[3]Department of Ophthalmology, University of Eastern Finland, Kuopio University Hospital, Kuopio, Finland.
[4]Department of Ophthalmology, University of Tampere, SILK, TAUH Eye Center, Tampere University Hospital, Tampere, Finland.

instead of cell injections, is considered as a more promising transplantation strategy.[14–17]

Extracellular matrix (ECM) is a dynamic and complex environment that interacts with cells through cell surface receptors such as integrins.[18,19] Apart from the mechanical support and its role in cell adhesion, ECM binds soluble factors and regulates their distribution and presentation to cells.[20] These cell–matrix interactions play an important role in cell morphology, migration, proliferation, and differentiation.[19,21,22] The basal membrane of RPE cells rests on a specific pentalaminar ECM sheet called Bruch's membrane (BM). BM is an elastin- and collagen-rich ECM that regulates the reciprocal exchange of biomolecules, nutrients, oxygen, fluids, and metabolic waste products between the retina and blood circulation. The basement membrane of RPE is the outermost layer of the BM, and it mainly consists of collagen type IV (COL IV) laminin (LN), fibronectin (FN), hyaluronic acid, heparan sulfate, and chondroitin/dermatan sulfate.[23] Primary RPE cells are influenced by their ECM and abnormal ECM assembly can result in altered structure and functions, and engage in disease states.[24–31] The composition of human BM alters with age, and changes in BM structure have also been shown to be associated with pathological processes: cross-linking of collagens, higher collagen I (Col I) expression, increase in thickness, and reduction of elasticity and permeability of the BM have been shown to be related to AMD pathology.[23,31,32] Moreover, there is evidence that BM fragmentation can trigger proinflammatory responses that might accelerate AMD process.[33–35] In addition to BM modifications, drusen deposits, a hallmark of AMD, accumulate between the RPE and BM. Drusens are rich in ECM proteins such as vitronectin (VN) and many inflammatory markers.[23,33,36,37] Thus, one of the important tasks of transplanted hESC-RPE is to produce sufficient ECM to restore the functions of the damaged BM if no BM mimicking non-biodegradable biomaterial is used with cells.[16,17]

Previously, it has been shown that ECM affects the early stage differentiation of hPSCs into neural progenitors and neurons,[38] retinal progenitor cells,[39,40] and RPE cells.[41] In addition, different ECM proteins have been used in differentiation of hESC-RPE.[42] Most of the current hPSC-RPE differentiation protocols utilize either xeno-derived substrates, such as Matrigel™,[43,44] gelatin,[4,12] and human-derived ECM proteins,[10,16] as attachment and culture matrices.[42] However, little is known about the effects of the ECM proteins on maturation of hESC-RPE epithelium, its barrier properties, and fine structure. Moreover, there is lack of knowledge about the self-produced basal lamina of hESC-RPE cells grown on different protein coatings. We hypothesized that ECM proteins abundant in healthy native RPE basement membrane, such as Col IV and LN, would be superior in supporting the differentiation and maturation of hESCs to RPE cells. Therefore, in this study, we compared the effect generated by components found in the native BM on hESC-RPE differentiation and maturation. Our choice of proteins was based on the concept of finding a simple, effective, xeno-free, and eventually good manufacturing practice (GMP)–compatible matrix for hESC-RPE differentiation. hESCs were differentiated and maturated into RPE cells in adherent differentiation cultures on several xeno-free, human-sourced ECM protein coatings. Matrigel (MG) was tested along with the human matrices for comparison as it is so widely used.

Materials and Methods

Human embryonic stem cells

Previously derived hESC line Regea 08/023 (46, XY) was used in this study.[45] The undifferentiated hESCs were cultured on γ-irradiated (40 Gy) human foreskin fibroblast feeder cells (CRL-2429™; ATCC, Manassas, VA) in serum-free conditions described previously.[10] The culture medium was changed five times a week and undifferentiated colonies were manually passaged onto new feeder cells once a week.

Differentiation of hESCs to RPE cells

hESCs were differentiated to RPE cells on following ECM protein and commercially available substrates: Col I, Col IV, and LN from human placenta (all 5 μg/cm^2; Sigma-Aldrich, St. Louis, MO), FN from human plasma (5 μg/cm^2; Sigma-Aldrich), VN from human plasma (0.5 μg/cm^2; Sigma-Aldrich), xeno-free CELLstart™ (CS; 1:50; Life Technologies, Carlsbad, CA), and growth factor reduced BD Matrigel (MG; 30 μg/cm^2; BD Biosciences, San Jose, CA). The purified human ECM proteins were chosen as they are all present in native BM[23] and provide xeno-free, clinically compliant matrices for hPSC-RPE support. We have previously used Col IV for enrichment and maturation of hPSC-RPE[10] and it was thus chosen as reference matrix for comparisons. CS is a xeno-free, defined, and cGMP-produced commercial hPSC matrix, while MG that is a mouse-tumor-derived ECM matrix is commonly used for hPSC-RPE differentiation and maintenance.[39,44,46,47] The substrates were used in concentrations recommended by the manufacturer. The initial coating concentrations recommended for LN (2 μg/cm^2) and VN (0.2 μg/cm^2) were found insufficient in our preliminary tests (data not shown) and thus were used as higher concentrations. Six-well cell culture plates (Corning® CellBIND®; Corning, Inc., Corning, NY) were coated with the substrates for 3 h at 37°C and rinsed twice with Dulbecco's phosphate-buffered saline (DPBS; Lonza Group Ltd., Basel, Switzerland). Undifferentiated hESC colonies were manually plated to the protein coating and allowed to differentiate in RPEbasic medium consisting of the same reagents as the medium used for maintaining hESCs with the modifications of 15% KnockOut™ Serum Replacement (KO-SR) and no basic fibroblast growth factor (bFGF).[10] RPEbasic medium was changed three times a week.

After 45 days of differentiation, the pigmented areas were manually cut under a light microscope with a lancet into small pieces and detached with a needle. The detached pieces were replated to the same coating for enrichment of pigmented cells. For maturation, the hESC-RPE cells were replated after 98 days of differentiation to 0.3-cm^2 BD Falcon cell culture inserts (BD Biosciences), precoated with each substrate. The hESC-RPE cells were dissociated to single cells with 1× Trypsin-EDTA (Lonza Group Ltd.), filtered through BD Falcon cell strainer (BD Biosciences), and seeded at density of 2.0×10^6 cells/cm^2. The cells were cultured on inserts for 42 days (a total of 140 days of differentiation).

Analysis of pigmentation

The appearance of the first pigmentation on each coating was followed daily by microscopic inspection and recorded. The data were collected from five individual differentiation experiments.

The degree of pigmentation after 140 days of differentiation was analyzed by capturing images of randomly selected locations on cell culture inserts with Nikon Eclipse TE200S phase-contrast microscope (Nikon Instruments Europe B.V., Amstelveen, Netherlands). In each experiment, the light exposure settings and illumination were maintained as constant between the coatings. One to three images from four independent differentiation experiments were analyzed. These analyzed images were taken with 20× objective. The degree of pigmentation was quantified with Image J Image Processing and Analysis Software (http://imagej.nih.gov/ij/index.html) through pixel intensity normalization. Inverse of pixel intensities was calculated in order to illustrate the density of pigmentation by subtracting the normalized pixel intensity from the maximum pixel intensity value for 8-bit grayscale images. To eliminate changes in different light exposures between experiments, the inverse pixel intensities in each experiment were normalized against Col IV.

Quantitative real-time polymerase chain reaction

Differences in relative expression levels of paired box gene 6 (*PAX6*) and microphthalmia-associated transcription factor (*MITF*) genes were studied with quantitative real-time polymerase chain reaction (qPCR) after 28 days of differentiation. Further, the expression of genes coding for RPE-specific proteins bestrophin (*BEST*), cellular retinaldehyde-binding protein (*CRALBP*), receptor tyrosine kinase MerTK (*MERTK*), and retinal pigment epithelium specific protein 65 kDa (*RPE65*) and genes encoding for ECM proteins collagen type IV alpha-1 (*COL4A1*), fibronectin 1 (*FN1*), laminin subunit alpha-1 (*LAMA1*), and laminin subunit alpha-5 (*LAMA5*) was analyzed after 140 days of differentiation. hESCs differentiated on each coating were lysed to lysis buffer RA1 with Tris(2-carboxyethyl)phosphine (TCEP) (both from Macherey-Nagel, GmbH & Co, Düren, Germany) or β-mercaptoethanol (Sigma-Aldrich) and stored at −70°C. Samples were collected from four individual differentiation experiments. A sample of undifferentiated hESCs was used as reference.

Total RNA was extracted using NucleoSpin XS and NucleoSpin® RNA II kits (both from Macherey-Nagel, GmbH & Co) according to the manufacturer's instructions. The quality and concentration of RNA were examined with NanoDrop-1000 spectrophotometer (NanoDrop Technologies, Wilmington, DE). Two hundred nanograms of RNA was synthesized to complementary DNA (cDNA) with high-capacity cDNA reverse transcription kit (Applied Biosystems, Inc., Foster City, CA) following the manufacturer's protocol in the presence of a MultiScribe Reverse Transcriptase and an RNase inhibitor. The synthesis was performed in PCR MasterCycler (Eppendorf AG, Hamburg, Germany) with the following cycle: 10 min at 25°C, 120 min at 37°C, 5 min at 85°C, and finally cooled down to 4°C.

TaqMan® gene expression assays (Applied Biosystems, Inc.) with FAM labels were used for PCRs: *PAX6* (Hs00240871_m1), *MITF* (Hs01115553_m1), *BEST* (hs00959251_m1), *CRALBP* (hs00165632_m1), *MERTK* (hs00179024_m1), *RPE65* (hs01071462_m1), *COL4A1* (Hs00266237_m1), *FN1* (Hs00365052_m1), *LAMA1* (Hs00300550_m1), and *LAMA5* (Hs00245699_m1). Glyceraldehyde 3-phosphate dehydrogenase (*GAPDH*; Hs99999905_m1) was used as an endogenous control. cDNA was diluted 1:5 in RNase-free water and 3 μL of dilution was added to the reaction (total reaction volume 15 μL). Samples and no-template controls were run as triplicate reactions using the 7300 Real-Time PCR system (Applied Biosystems, Inc.) as follows: 2 min at 50°C, 10 min at 95°C, and 40 cycles of 15 s at 95°C, and 1 min at 60°C. Results were analyzed using 7300 System SDS Software (Applied Biosystems, Inc.). Based on the Ct values given by the software, the relative quantification of each gene was calculated using the $2^{-\Delta\Delta Ct}$ method.[48] The values for each sample were normalized to expression levels of GAPDH. The expression level of undifferentiated hESC sample was set as the calibrator for the early eye field markers *PAX6* and *MITF*, whereas the expression level of Col IV sample was set as the calibrator for the mature RPE markers and genes coding for ECM proteins (fold change equals 1).

Reverse transcription–polymerase chain reaction

The expression of pluripotency markers octamer-binding transcription factor (*OCT3/4*) and *Nanog* was studied with reverse transcription–polymerase chain reaction (RT-PCR) after 140 days of differentiation. Total RNA was extracted and 40 ng was reverse transcribed to cDNA as described previously. RT-PCR was carried out using 1 μL of cDNA as template. Undifferentiated hESCs (Regea 08/023) were used as positive control. Detailed protocol and primer sequences have been previously published.[10]

Immunofluorescence

The protein expression and localization was investigated with immunofluorescence (IF) staining after 140 days of differentiation as previously described.[10] The following primary antibodies were used: rabbit anti-BEST 1:400, mouse anti-CRALBP 1:600, mouse anti-Na^+/K^+ATPase 1:100, rabbit anti-LN 1:200 (all from Abcam, Cambridge, United Kingdom), mouse anti-FN 1:500 (Chemicon), mouse anti-Col IV 1:100 (Neomarkers), and mouse anti-zonula occludens 1 (ZO-1) 1:250 (Invitrogen, Carlsbad, CA). Secondary antibodies were diluted 1:800: Alexa Fluor 568-conjugated goat anti-mouse IgG and goat anti-rabbit IgG, and Alexa Fluor 488-conjugated donkey anti-rabbit IgG and donkey anti-mouse IgG (all from Molecular Probes, Life Technologies). 4′,6′-Diamidino-2-phenylidole (DAPI) included in the mounting media was used for staining the nuclei (Vector Laboratories, Inc., Burlingame, CA). To verify that the protein detected in IF staining was secreted by the cells, we carried out immunostainings of empty Col IV, FN-, and LN-coated cell culture inserts before seeding cells to distinguish between the newly secreted ECM molecule and the ECM molecules in the coated cell culture insert. Empty cell culture insert without the ECM coating was used as negative control. Images were taken with Olympus BX60 microscope (Olympus, Tokyo, Japan) or LSM 700 confocal microscope (Carl Zeiss, Jena, Germany)

using a 63× oil-immersion objective. Images were edited using ZEN 2011 Light Edition (Carl Zeiss) and Adobe Photoshop CS4.

Transepithelial resistance

Transepithelial resistance (TER) of the hESC-RPE layers cultured on substrate-coated inserts was measured after 140 days of differentiation to study integrity and barrier properties of the epithelium. RPEbasic culture medium was replaced with DPBS and measurements were carried out with a Millicell electrical resistance system volt-ohm meter (Merck Millipore, Darmstad, Germany). TER values ($\Omega \cdot cm^2$) were calculated by subtracting the value of a similarly treated substrate-coated insert without cells from the result, and by multiplying the result by the surface area of the insert. TER values were obtained from five individual differentiation experiments with multiple parallel samples for each coating. All measurements were conducted twice and average values were calculated.

Transmission electron microscopy

After 140 days of differentiation the hESC-RPE cells on substrate-coated inserts were fixed with 2% glutaraldehyde (Electron Microscopy Sciences, Hatfield, PA) prepared in 0.1 M phosphate buffer for 2 h at room temperature (RT) following incubation in 0.1 M phosphate buffer overnight at RT. Thereafter, the samples were postfixed with 1% osmium tetroxide (Ladd Research, Williston, VT) for 1 h at RT and dehydrated through a graded series of acetone (J.T. Baker; Avantor Performance Materials, B.V. Deventer, Netherlands): 70% acetone, 94% acetone, and absolute acetone. The samples were then infiltrated in a 1:1 mixture of absolute acetone and epoxy resin (Ladd Research) for 1.5 h at RT, embedded in pure epoxy resin overnight at RT, and polymerized for 48 h at 60°C. Toluidine blue staining of the semithin sections was used to select the position for making the thin sections. Thin sections were stained with 1% uranyl acetate for 30 min and with 0.4% lead citrate (Fluk, Steinheim, Switzerland) for 5 min. Samples were examined and imaged with JEM-2100F transmission electron microscope (TEM; Jeol Ltd., Tokyo, Japan). Cell and basal lamina thickness on substrates was determined from the TEM images with Image J Image Processing and Analysis Software. The thickness of four to five randomly chosen cells and self-assembled basal lamina underneath these cells was determined from each substrate.

Western blotting

The ECM protein expression was studied further after 140 days of differentiation with western blotting on Col IV, FN, LN, and MG coatings. The samples were washed twice with ice-cold DPBS, and lysed into 2× Laemmli buffer consisting of 62.5 mM Tris-HCl (pH 6.8 at 25°C) (Trixma base; Sigma-Aldrich), 2% w/v sodium dodecyl sulfate (SDS; Bio-Rad Laboratories, Hercules, CA), 17% glycerol (Merck Millipore), 0.01% w/v bromophenol blue (Sigma-Aldrich), and 1.43 M β-mercaptoethanol (Sigma-Aldrich). Complete Mini protease inhibitor (Roche Diagnostics Gmbh, Mannheim, Germany) was added to the samples to prevent degradation. The samples were run in 7.5% SDS–polyacrylamide gel electrophoresis (PAGE) and then blotted to Amersham Hybond™-P PVDF Transfer membranes (GE Healthcare, Buckinghamshire, United Kingdom) in semidry conditions. Blocking was done with 5% fat-free dry milk in 0.05% Tween20 (Sigma-Aldrich) at RT for 1 h. Thereafter, membranes were incubated in primary antibody dilutions rabbit anti-LN (1:1000; Abcam), mouse anti-FN (1:8000; Merck Millipore), and mouse anti-Col IV (1:1000; Merck Millipore) overnight at +4°C. All primary antibodies were diluted in 5% milk solution with 0.05% Tween20. After primary antibody incubation, the membranes were washed in 0.5% Tween20 in tris-buffered saline (TBS), 0.1% Tween in TBS, and 0.05% Tween in TBS. Horseradish peroxidase-conjugated anti-mouse IgG (Santa Cruz, Dallas, TX) and anti-rabbit IgG were diluted in 5% milk solution with 0.05% Tween20 and incubated at RT for 1 h. Protein–antibody complexes were detected using Amersham™ ECL™ Prime Western Blotting Detection Reagent (GE Healthcare). Thereafter, the membranes were stripped in stripping buffer consisting of 0.1 M β-mercaptoethanol, 2% w/v SDS, and 62.5 mM Tris-HCl (pH 6.8 at 25°C) for 30 min at +56°C. Each stripped membrane was blocked and stained with loading control mouse anti-β-actin (1:5000; Santa Cruz) for 1 h at RT. Immunoblotting and detection for stripped membranes was carried out as described previously.

The ECM protein expression on each protein coating was quantified with band area calculation in Image J Image Processing and Analysis Software. The expression of the secreted ECM protein was compared with the loading control β-actin from the same lane in the membrane. These protein/β-actin ratios were calibrated against Col IV samples (protein/β-actin ratio equals 1) in order to carry out relative comparison between the different protein coatings.

Phagocytosis of photoreceptor outer segments from rat retinal explants

The phagocytic properties of hESC-RPE monolayers on Col IV-, FN-, LN-, CS-, and MG-coated surfaces were studied using rat retinal explants after 184 days of differentiation. The use and handling of the animals was conducted according to the Finland Animal Welfare Act of 1986, the ARVO Statement for the Use of Animals in Ophthalmic and Vision Research, and the guidelines of the Animal Experimentation Committee. Non-dystrophic Royal College of Surgeons (RCS) rats at the ages 15 and 18 weeks were euthanized using carbon dioxide inhalation following cervical dislocation. The eyes were detached carefully and immersed in Ames medium (Sigma-Aldrich) buffered with sodium bicarbonate and equilibrated with a gas mixture of 5% CO_2 and 95% O_2, and the retinas were detached from hemisected eyes. The isolated rat retinal explants were placed on the hESC-RPE monolayers with the photoreceptors facing the cells in B27/N2 medium consisting of Neurobasal A, 1% N2, 2% B27, 2 mM glutamax (all from Gibco, Life Technologies), and 100 U/mL penicillin/streptomycin. The retina was transferred on the hESC-RPE monolayers on top of a small piece of lens paper. The retinal explants were cocultured with hESC-RPE monolayers for 2 days at +37°C and 5% CO_2. Medium was added daily to prevent the drying of the explants. After 2 days of coculture, the retinas were gently removed and the hESC-RPE

monolayers were analyzed by IF staining. Rat rhodopsin was visualized using rat anti-Opsin antibody (O48869; Sigma-Aldrich) and actin was detected with 0.02 μg/mL phalloidin-TRITC (P1951; Sigma-Aldrich). Donkey anti-rabbit Alexa 488 (Molecular Probes, Life Technologies) diluted 1:800 was used as secondary antibody. IF staining was performed as described previously. IF images of phagocytosis were visualized with Zeiss LSM 700 confocal microscope using sectional scanning.

Ethical issues

The Institute of Biomedical Technology at University of Tampere has the approval of the National Authority for Medicolegal Affairs Finland (TEO) to study human embryos (Dnro 1426/32/300/05) and a supportive statement of the Ethical Committee of the Pirkanmaa Hospital District to derive, culture, and differentiate hESC lines (R05116). No new lines were derived for this study.

Statistical analysis

Mann–Whitney *U*-test and IBM SPSS Statistics software were used for determining statistical significance. Average (median) values of TER and pixel intensity obtained from cells cultured on each matrix were compared with average (median) values obtained on Col IV (reference) with Mann–Whitney *U*-test. p-Values ≤ 0.05 were considered statistically significant.

Results

All protein coatings supported differentiation of hESC-RPE cells

To study the effects of protein coatings on hESC-RPE differentiation and maturation, we differentiated hESCs to RPE cells as adherent cultures on five human-sourced ECM proteins and two commercially available hPSC culture substrata. All protein coatings allowed for competent differentiation of hESCs to RPE cells with no marked differences in the onset or degree of pigmentation at the early stage of differentiation process. The first pigmentation appeared within the interval of 10–21 days of differentiation (Fig. 1A). After 28 days of differentiation the cells showed increased gene expression of the early eye field marker *PAX6* and RPE precursor marker *MITF* compared with undifferentiated hESCs. The *MITF* expression had increased from 5-fold on CS up to 10-fold on LN (Fig. 1B, C). The expression of *MITF* was significantly higher ($p<0.005$) on LN coating compared with the other tested coatings, except compared with VN ($p=0.031$). In contrast, the *MITF* expression on CS was significantly lower ($p<0.005$) compared with all other tested coatings, except Col IV ($p=0.119$). However, as overall the fold change differences were subtle (over twofold changes are considered biologically relevant) and our aim was to show the common trend of increased gene expression of early eye field and RPE precursor markers, we did not consider these differences biologically relevant. On day 28, an average of 0.9–1.7 pigmented cell clusters/cm^2 ($n=9$–11 replicates) were gained on different coatings.

Sufficient pigmentation for replating was typically reached after 45 days of differentiation and the cells were efficiently enriched to monolayers of pigmented cells on all coatings by 98 days of differentiation. The hESC-RPE cells were further maturated on coated culture inserts up to 140 days of differentiation. Confluent, intact cell layers were produced on all substrates, but on LN and VN more fragile and ruptured epithelia were occasionally observed. All investigated coatings supported the maintenance of hexagonal and cobblestone-like RPE cell morphology (Fig. 1D). Human ESC-RPE cells were positive for mature RPE-related proteins BEST and CRALBP on all coatings and expressed Na^+/K^+ATPase on the apical membrane of the cells, demonstrating polarization of the formed epithelia (Fig. 1E). There was no expression of pluripotency markers *OCT3/4* and *Nanog* on any of the studied protein coatings after 140 days of differentiation (Supplementary Fig. S1; Supplementary Data are available online at www.liebertpub.com/tea). Further, no significant differences were found in gene expression analysis of mature RPE markers *BEST*, *CRALBP*, *MERTK*, and *RPE65* after 140 days of differentiation (Supplementary Fig. S2). The functionality of hESC-RPE on Col IV, FN, LN, CS, and MG coatings was studied with phagocytosis of POS from rat retinal explants after 184 days of differentiation. After 2 days of coculture with the rat retinal explant, rat opsin was internalized inside hESC-RPE cells on all studied five coatings (Supplementary Fig. S3).

Protein coating affects the degree of pigmentation of hESC-RPE cells

The used protein coating significantly affected the degree of pigmentation of the hESC-RPE layers in long-term differentiation. The differences in the densities of pigmentation were evident by visual microscopic inspection and the relative degree of pigmentation was quantified by calculating pixel intensities from phase-contrast images after 140 days of differentiation. On LN the hESC-RPE evinced the highest degree of pigmentation, whereas culture on FN and MG resulted in lower production of pigmentation. On Col IV, hESC-RPE showed intermediate pigmentation (Fig. 2A). The degree of pigmentation on VN varied substantially between the individual differentiation experiments. The relative degree of cell pigmentation was significantly ($p<0.05$) higher on LN, CS, and Col I, while on FN and MG the pigmentation was significantly lower as compared with Col IV ($p<0.05$) (Fig. 2B).

Barrier properties of the forming epithelium are strongly influenced by the protein coating

Development of the barrier properties and integrity of the RPE epithelia on different coatings were examined with TER measurements from cell culture inserts after 140 days of differentiation. We found major differences in TER values between investigated substrates (Fig. 2B). The highest TER values of $552\pm56\ \Omega\cdot cm^2$ and $473\pm53\ \Omega\cdot cm^2$ were measured for FN and MG, respectively. TER values reached $275\pm77\ \Omega\cdot cm^2$ for CS, $247\pm35\ \Omega\cdot cm^2$ for Col IV, and $183\pm72\ \Omega\cdot cm^2$ for Col I. The lowest TER values were obtained for LN ($128\pm25\ \Omega\cdot cm^2$) and VN ($122\pm64\ \Omega\cdot cm^2$). The average TER value for the epithelium on all coatings, except that for CS, significantly ($p<0.05$) differed from the average TER for epithelium on Col IV (Fig. 2B).

We next studied the presence of tight junctions on the epithelia formed. Positivity of ZO-1 label in IF (Fig. 2C) and

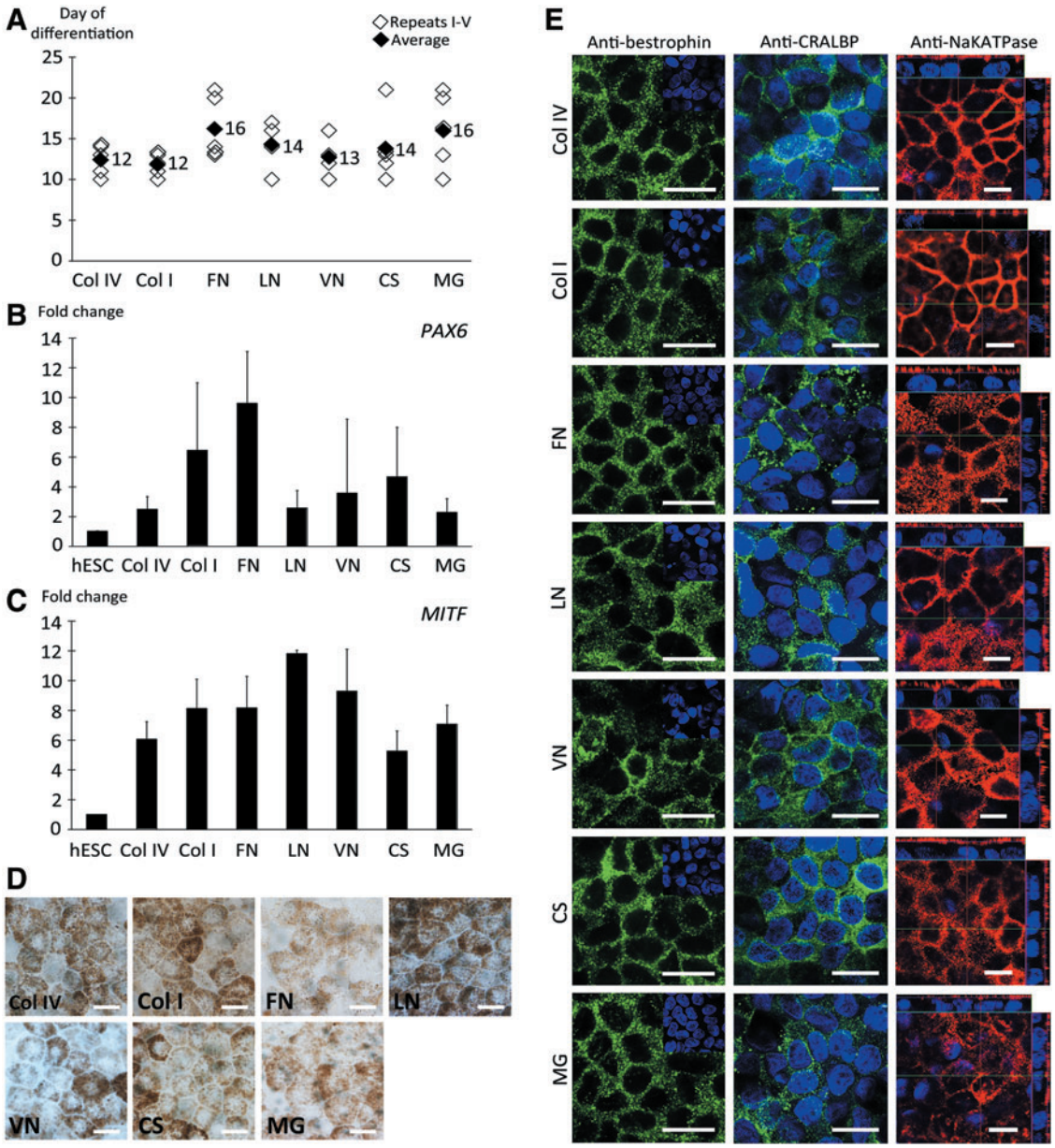

FIG. 1. Characterization of early stage differentiation and maturation of human embryonic stem cell–derived retinal pigment epithelial (hESC-RPE) cells. RPE differentiation and maturation was achieved on all extracellular matrix (ECM) coatings tested. **(A)** Appearance of pigmentation in each differentiation experiment ($n=5$). Relative quantitative real-time polymerase chain reaction (qPCR) analysis of genes involved in retinal development, **(B)** paired box gene 6 (*PAX6*) and **(C)** microphthalmia-associated transcription factor (*MITF*), after 28 days of differentiation ($n=4$ experiments). **(D)** Bright-field images showing mature hESC-RPE with typical pigmented, cobblestone-like RPE morphology and **(E)** immunofluorescence (IF) staining showing correct expression and localization of RPE-specific proteins bestrophin (BEST) and cellular retinaldehyde-binding protein (CRALBP) after 140 days of differentiation. Vertical confocal sections show apical localization of Na^+/K^+ATPase confirming correct polarization of the epithelial monolayers on all coatings. Scale bars = 10 μm. Color images available online at www.liebertpub.com/tea

the electron dense band on apical side of lateral membrane seen in TEM (Fig. 3) confirmed the presence of tight junctions on the apical side of the cells in all of the used coatings.

Protein coating affects the fine structure of the hESC-RPE cells

The fine structure of hESC-RPE cells on different coatings was investigated with TEM. All coatings promoted the growth of the forming epithelium as a monolayer (Supplementary Fig. S4). We discovered variation in structure and thickness of hESC-RPE cells between coatings; cells on human Col I, Col IV, CS, FN, LN, and VN had columnar morphology, whereas hESC-RPE cells on MG showed a more cuboidal structure (Fig. 3 and Supplementary Fig. S4). The hESC-RPE cells had the greatest average cell thickness on LN (14.7 ± 1.3 μm), whereas on Col I and Col IV, the average cell thicknesses reached for 13.8 ± 0.1 μm and

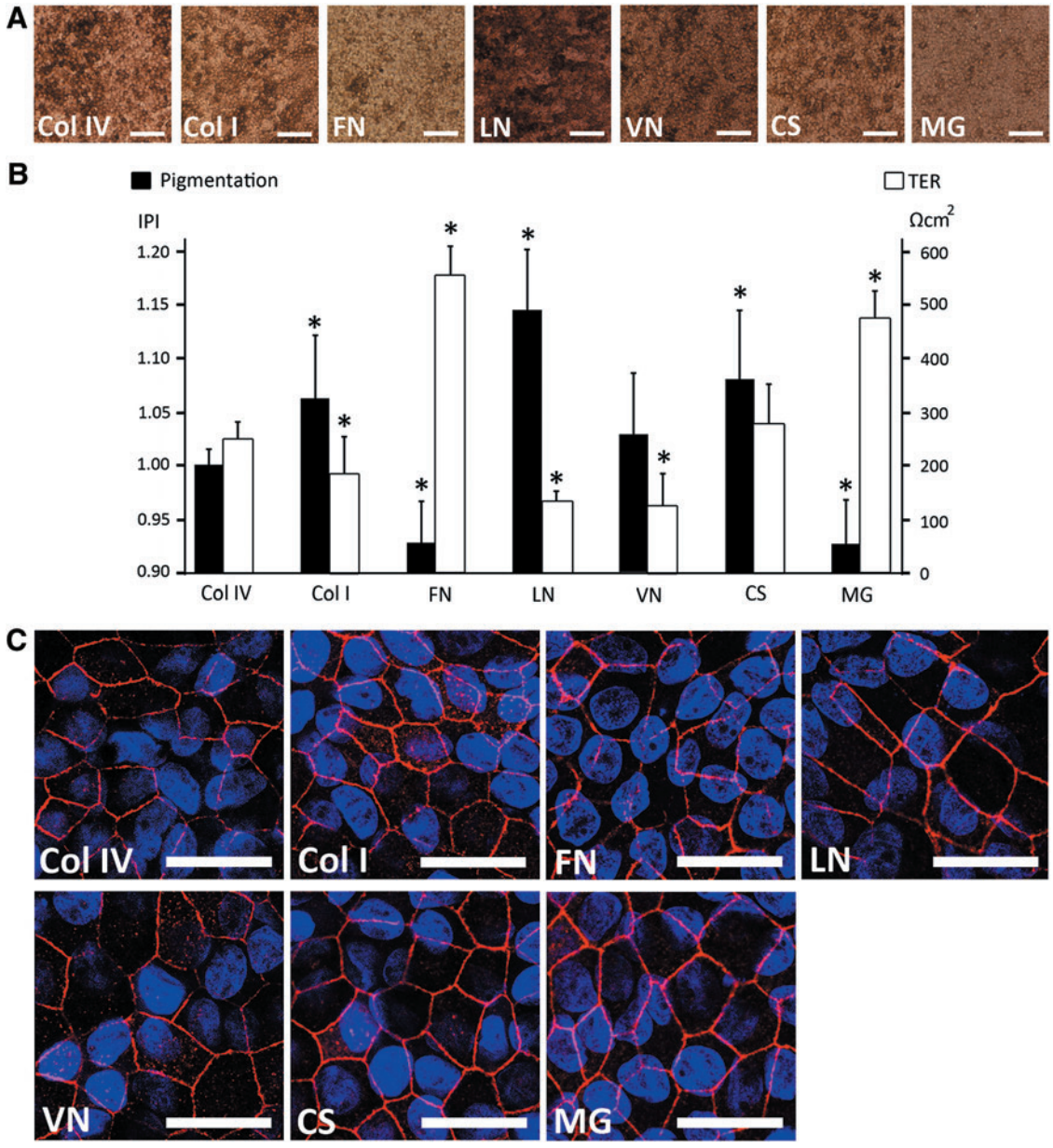

FIG. 2. Degree of pigmentation and barrier properties of maturate hESC-RPE after 140 days of differentiation. **(A)** Phase-contrast images illustrating the degree of pigmentation on different coatings. Scale bars = 100 μm. **(B)** Relative degree of pigmentation quantified by image analysis and presented as inverse of pixel intensity (IPI) ($n = 4$), and transepithelial resistance (TER) measured for human pluripotent stem cell (hPSC)–RPE on different coatings ($n = 5$). *$p < 0.05$ compared with collagen IV (Col IV). **(C)** IF staining of tight junction protein zonula occludens 1 (ZO-1). Scale bars = 10 μm. Color images available online at www.liebertpub.com/tea

13.2 ± 2.4 μm, respectively. Moreover, cell thickness of 12.5 ± 1.1 μm for FN, 10.9 ± 0.5 μm for CS, and 10.8 ± 1.4 μm for VN was found. The hESC-RPE cells were substantially thinner on MG with average cell thickness of 7.6 ± 0.4 μm.

The nuclei of the cells were located basally on all tested coatings, whereas mitochondria and melanosomes were found mainly from the apical side of the cells. Fewer melanosomes were seen in hESC-RPE cells on FN and MG compared with the other coatings. The hESC-RPE cells cultured on FN and MG had rather straight apical borderline whereas hESC-RPE cells cultured on Col IV, Col I, LN, VN, and CS had roundish apical borderline. The apical microvilli of the cells were detected on all coatings, but the structure and density of microvilli differed between tested coatings (Fig. 3). The density of microvilli on VN, LN, and CS was low compared with Col IV, Col I, and FN. Moreover, the apical microvilli were shorter on LN and MG compared with the longer extensions seen on other tested coatings. Tight junctions were visualized at the apical side of the monolayers on all tested coatings. Further, coated pits were associated with both basal and apical membranes of hESC-RPE on all tested coatings.

The hESC-RPE cells assemble their own basal lamina

The ability of the hESC-RPE cells to produce and secrete the key ECM proteins of the basement membrane of the

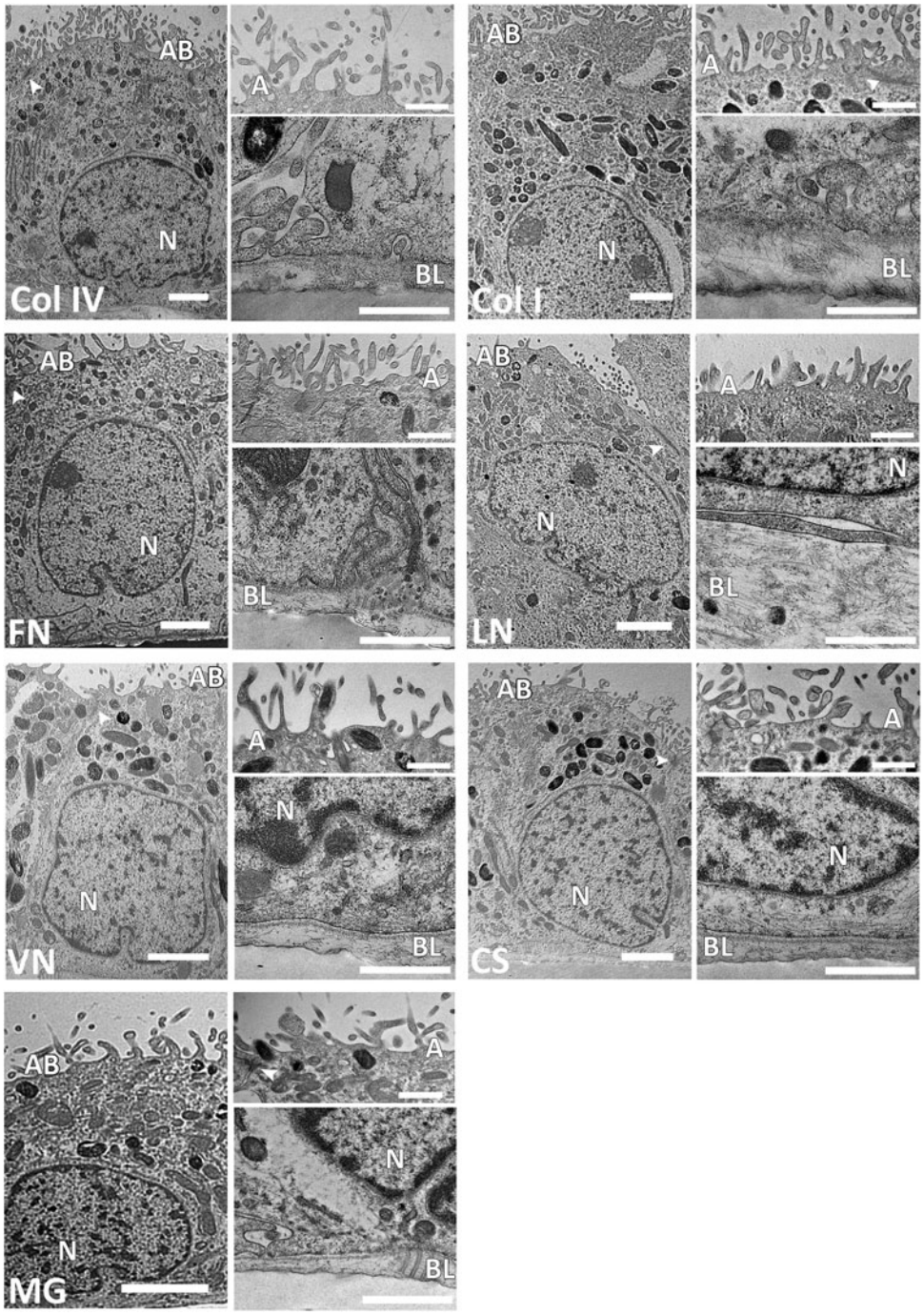

FIG. 3. High-magnification transmission electron microscope (TEM) images showing the fine structure of maturated hESC-RPE on different coatings (scale bars = 2 μm). Apical microvilli (A) and basal lamina (BL) shown in higher magnifications (scale bars = 1 μm). TEM analysis confirmed the presence of tight junctions (arrowheads) on the apical side of the cells in all of the coatings. AB, apical brush border; N, nucleus.

native RPE was investigated with qPCR analysis, IF staining, TEM, and western blotting. qPCR analysis of genes encoding for ECM proteins revealed no clear differences between protein coatings after 140 days of differentiation (Supplementary Fig. S5). However, the gene expression data confirmed that the genes encoding for the key ECM proteins of the basement membrane of the native RPE were transcripted. IF staining showed abundant labeling with Col IV, FN, and LN fibers on Col IV, Col I, LN, VN, and MG (Fig. 4). On FN and CS, cells produced low amounts of Col IV and LN, whereas FN fibers were not detected at all. IF staining confirmed the fiber-like conformation of all secreted basal lamina components and basal localization of Col IV and FN. LN was mostly localized basally, but some fibers were also detected at intercellular spaces. Negative IF control staining of empty inserts and Col IV-, FN-, and LN-coated inserts without cells had dotted-like staining (Supplementary Fig. S6), whereas ECM stainings with cells were in fiber-like form. This confirmed that the fiber-like ECM proteins seen in Figure 4 are being secreted by the cells.

TEM analyses confirmed that the hESC-RPE cells assemble their own basal lamina. Substantial differences in the thickness of the self-assembled basal lamina on the different coatings were found. The hESC-RPE cells assembled the

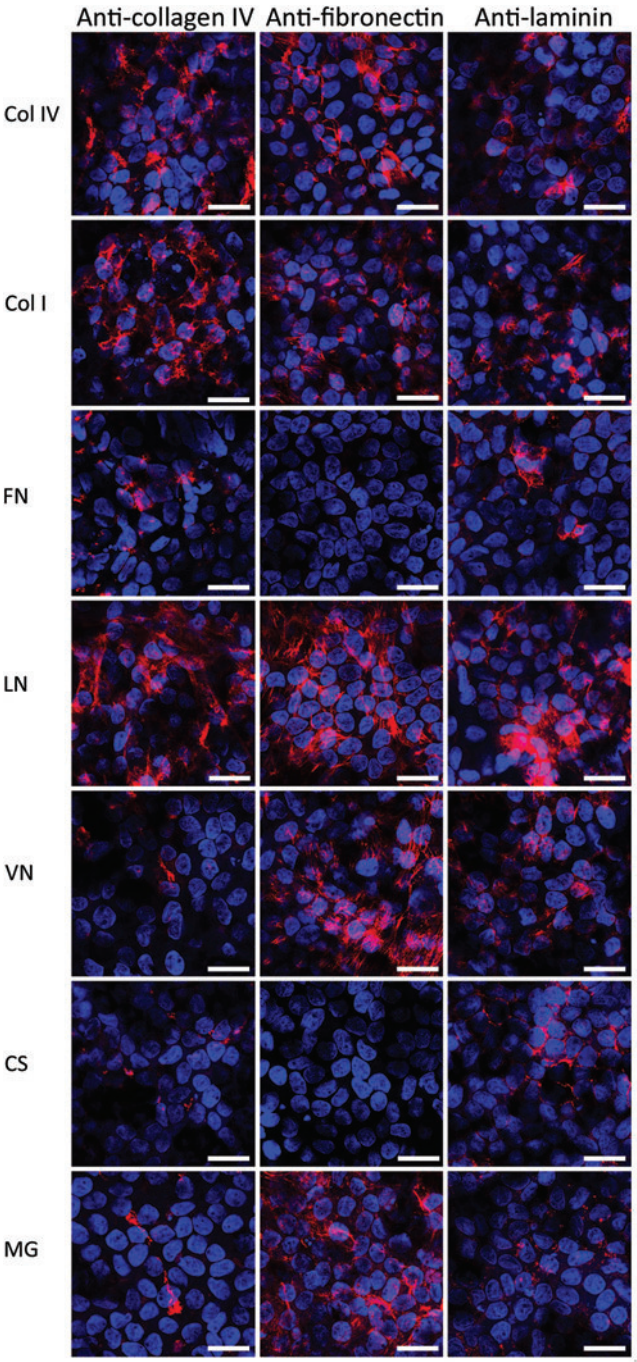

FIG. 4. ECM protein production of maturated hESC-RPE on coatings. Col IV (first column), fibronectin (FN; second column), and laminin (LN; third column) production analyzed by IF stainings on different coatings after 140 days of differentiation. The nuclei were counterstained with 4′,6′-diamidino-2-phenylidole (DAPI). Scale bars = 10 μm. Color images available online at www.liebertpub.com/tea

thickest basal lamina on LN (0.82 ± 0.28 μm) and Col I (0.70 ± 0.07 μm), whereas the thinnest basal lamina was seen on CS (0.22 ± 0.05 μm) (Fig. 3). Moreover, the self-assembled basal lamina thickness was 0.31 ± 0.08 μm for Col IV, 0.27 ± 0.08 μm for FN, 0.33 ± 0.06 μm for MG, and 0.32 ± 0.06 μm for VN.

The effect of protein coating to the ECM production of hESC-RPE on Col IV, FN, LN, and MG coatings was quantified with western blotting (Fig. 5). Highest LN deposition was found on MG, whereas highest FN and Col IV deposition was detected on Col IV. Western blotting also confirmed FN to be deposited on FN coating in contrast to IF staining.

Discussion

Efficient production of intact, mature, and functional sheets of hPSC-RPE cells is considered to be essential for their clinical applications.[17] Most of the current hPSC-RPE differentiation protocols utilize xeno-derived substrates like porcine gelatin, even in the clinical setting.[4] In this study, we compared the effect of xeno-free, human-sourced ECM protein coatings on the differentiation and maturation of hESC-RPE cells with the aim of finding suitable substrate for GMP-quality hESC-RPE production for clinical purposes. To our knowledge, the effects of different ECM proteins on maturation of hESC-RPE epithelium have not been previously studied although it is well acknowledged that primary RPE cells are influenced by their ECM and abnormal ECM can result in altered structure and functions, and engage in disease states.[24–27]

In the present study, we hypothesized that Col IV and LN, abundant components of the native RPE basement membrane, would be superior in supporting the hESC-RPE differentiation. Unexpectedly, all of the investigated protein coatings enabled differentiation of hESC-RPE monolayers in serum-free medium, and no relevant differences in the onset or rate of pigmentation, nor gene expression levels of *PAX6* and *MITF* were found between coatings after 28 days of differentiation. Moreover, after 140 days of culture, the hESC-RPE displayed RPE-specific cobblestone morphology, expression of genes, and correct localization of RPE-specific proteins as well as phagocytic activity, indicating that all used protein coatings support the maturation of hESC toward RPE cell type. However, striking differences were found with structure and epithelial barrier properties, and these were further analyzed.

For RPE, the pigmentation is considered to be an important indicator of phenotypic maturity.[49] In our study, we did not see any notable differences in the amount of pigmented areas after 4 weeks of differentiation between investigated protein coatings. In a study that tested several human- and animal-derived ECM proteins for hiPSC-RPE differentiation, Rowland *et al.* found significant differences in pigmentation density after 5 weeks of initial differentiation but no comparative analyses regarding further maturation with the different ECM proteins were conducted.[41] In their study, mouse LN-111 and Matrigel induced highest degree of pigmentation. Thus, this mouse LN-111 was presented as a suitable matrix for hPSC-RPE differentiation, although monolayers of hiPSC-RPE with correct morphology and similar levels of RPE gene expression were achieved on most ECM protein coatings tested.[41] This is in accordance with our results. Based on our results, it is clear that the early stage hESC-RPE differentiation is not significantly affected by the culture coating when spontaneous differentiation protocol omitting bFGF was used. However, when the long-term effect of culture coating on the degree

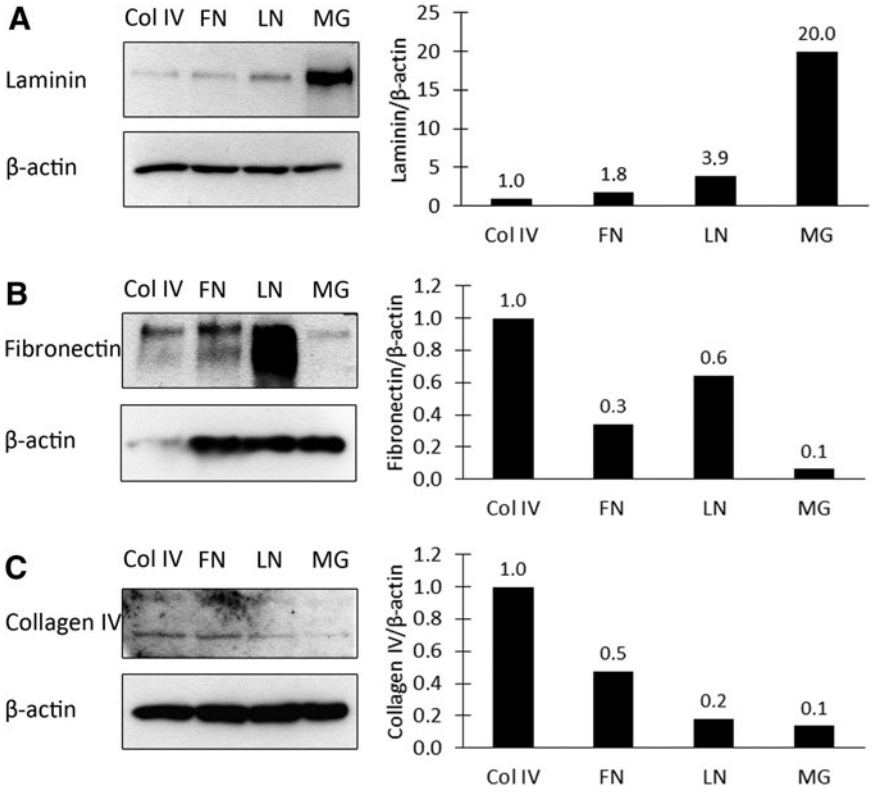

FIG. 5. Western blot analysis of the ECM protein production of matured hESC-RPE on Col IV, FN, LN, and MG coatings. **(A)** LN production, **(B)** FN production, and **(C)** Col IV production after 140 days of differentiation.

of pigmentation (140 days of differentiation) was studied, we found significant differences in the degree of pigmentation between tested coatings. The hESC-RPE cells gained heavily pigmented cells on LN, whereas FN and MG consistently showed lower degree of pigmentation and correspondingly fewer melanosomes detected with TEM analysis.

It is known that ECM influences the polarity of many epithelia[50] and the polarity of the RPE is maintained by the ECM on both the apical and basal sides of the RPE monolayer.[51] In the present study, we saw that all matrices induced formation of polarized monolayer of hESC-RPE cells. There were no marked differences in the polarity of the epithelium on different matrices demonstrated by apical localization of Na^+/K^+ATPase. Moreover, tight junctions were detected on the apical side of the cells on all coatings both in confocal microscopy and TEM. Previously it has been reported that epithelial polarity is linked to formation of tight junctions and consequently to the barrier function of the tissue.[52–54] Rizzolo has reported that individual matrix components influence the distribution of a subset of plasma membrane proteins required for full polarity in the RPE of chicken embryos and that the development of RPE polarity is a gradual process.[55]

Subtle differences in the cell shape or subcellular organization are suggested to have profound consequences for the efficient function of the RPE, and especially for the ability of the RPE to support the survival of photoreceptors.[49] Here, the hESC-RPE cells on all coatings showed high degree of polarity with basally located nuclei with slightly folded nuclear membrane and apical melanosomes, apical tight junctions, coated pits, and high number of mitochondria, consistent with the previous publications that show hESC-RPE ultrastructure.[12,44,46,56] However, the fine structure of hESC-RPE has been previously shown merely on Matrigel[44,46] and on FN.[56] It is noteworthy that in our study, TEM analysis revealed important differences in hESC-RPE ultrastructure between tested coatings; cells on Col IV, Col I, and FN matrices had denser and more homogenous microvilli and the overall thickness of cells was lower than of cells cultured on VN, LN, and CS, which can also reflect the degree of cellular maturation. Despite the lack of exposure the retina or POS,[44,46] the TEM analysis revealed many features of hESC-RPE fine structure associated with proper epithelial maturity gained *in vitro*.

The sufficient ECM production by the hPSC-RPE is important regarding their clinical applications in regenerative medicine to ensure proper cell attachment, survival, and integration of the grafted cells onto damaged BM and possibly also remodeling it in AMD patients.[57] In the present study, we show with TEM, qPCR, IF, and western blotting that the hESC-RPE produce and assemble their own basal lamina on all investigated coatings. Interestingly, marked differences in the thickness of the basal lamina were detected in TEM analysis. Surprisingly, the thickest basal lamina was detected on LN even though more fragile and ruptured epithelia were occasionally observed on LN and VN coatings. This might be due to poor coating success with these matrices. IF staining suggested the secretion of Col IV and LN on all matrices while on FN and CS we did not detect any production of FN. In western blotting, highest LN deposition was found on MG and LN, whereas FN and collagen deposition was most abundant on Col IV. On the contrary to IF stainings, western blotting confirmed FN to be deposited on FN coating. The reason for this discrepancy is not known, but it is repeatable result. Thickness of the

native RPE basement membrane has been reported to be 0.14–0.15 μm.[23] In our study, all investigated protein coatings induced the production of self-assembled ECM with thickness ranging from 0.22 to 0.82 μm. This and the highly organized structure seen in TEM and IF suggests that these studied protein coatings allow proper cues for hESC-RPE to form functional basement membrane. To our knowledge, the assembly of hESC-RPE basal lamina and these key ECM components has previously been shown only for cells cultured on growth factor (e.g., TGFβ)–containing Matrigel[44,46] although it is well acknowledged that native RPE cells secrete the key components of BM.[58–60] To our awareness, the present study is the first to demonstrate that the expression of these secretary ECM proteins in hESC-RPE is clearly influenced by the protein coating.

In vitro, the cobblestone-like RPE cell morphology, expression of RPE-specific proteins, appropriate subcellular localization of polarized proteins, and pigmentation and barrier properties of RPE cells are generally considered to be hallmarks of mature RPE.[49,61] It is vitally important to have valid criteria to define maturity of RPE cells for the stem-cell-based transplantation therapies. RPE cells with high degree of pigmentation are considered to be a golden standard for selection of cells for clinical applications,[4,17] whereas in the experimental series the high TER has been the inclusion criteria.[56,62] Melanin pigment in RPE cells decreases detrimental effects of Fenton reaction and diminish cytotoxic lipid peroxidation, lipofuscin accumulation, and subsequently chronic inflammation involved in AMD pathology.[63–65] In addition, phagocytosis of retinal outer segment promotes tyrosinase biosynthesis, and RPE cell pigmentation is an indication of the cell maturity and functionality.[66] In a recent report, Schwartz *et al.* reported greater attachment and spreading of the hESC-RPE with lower degree of pigmentation compared with darkly pigmented cells after culture. This data suggests that the extent of hESC-RPE maturity and pigmentation *in vitro* might substantially affect the attachment of transplanted cells to BM and their subsequent survival and integration to the host RPE layer.[4] Interestingly in our study, the pigmentation of the epithelium showed an inverse correlation to the epithelial resistance; the heavily pigmented epithelia on LN showed lowest TER values whereas FN and MG resulted in lower production of pigmentation and highest TER values. Even though TER and the degree of pigmentation are not conceptually related, we found the inverse relationship of this hallmarks of maturation unexpected phenomenon. This inverse relationship for hESC-RPE pigmentation and epithelial barrier integrity (TER) has not been described previously and this aspect of the epithelium maturation warrants further investigations in respect of functionality of transplanted cells *in vivo*.

In the beginning we hypothesized that Col IV and LN, both ECM components that reside in the closest proximity of RPE cells in their natural environment, would be superior in inducing differentiation and maturation of hESC-RPE cells. Col IV induced formation of polarized monolayer of cells with the average height of cells, low to average thickness of basal lamina, and average barrier function. LN also induced formation of polarized monolayer of cells with tallest cells, thickest basal lamina, and highest degree of pigmentation but the lowest barrier function. Therefore, we can summarize that Col IV is in the golden midway in all the assessed criteria. LN was superior in all other studied aspects except the barrier function. Still the importance of that factor needs to be elucidated.

Conclusion

In this study, we investigated the effect of seven different protein coatings on differentiation and maturation of hESC-RPE cells. We found single protein substrate to have a crucial effect on the maturation of the RPE epithelium, its pigmentation, barrier properties, and assembly of basal lamina. We produced functional hESC-RPE cells with several xeno-free human-sourced matrices suitable for GMP-quality hESC-RPE production for clinical purposes. This article is the first to report that cell culture coating has a major structural and functional effect on the maturation of hESC-RPE potentially affecting cell integrations and survival after cell transplantation.

Acknowledgments

The authors thank TEKES, the Finnish Funding Agency for Technology and Innovation, the Academy of Finland (grant numbers 218050 and 137801), and Tampere Graduate Program in Biomedicine and Biotechnology for financial support. The funders had no role in study design, data collection, and analysis; decision to publish; or preparation of the article. Outi Melin, Hanna Koskenaho, Elina Konsén, Outi Heikkilä, Raija Hukkila, Soile Nymark, and Johanna Viiri are thanked for technical assistance.

Disclosure Statement

No competing financial interests exist.

References

1. Simo, R., Villarroel, M., Corraliza, L., Hernandez, C., and Garcia-Ramirez, M. The retinal pigment epithelium: something more than a constituent of the blood-retinal barrier—implications for the pathogenesis of diabetic retinopathy. J Biomed Biotechnol **2010,** 190724, 2010.
2. Gehrs, K.M., Anderson, D.H., Johnson, L.V., and Hageman, G.S. Age-related macular degeneration—emerging pathogenetic and therapeutic concepts. Ann Med **38,** 450, 2006.
3. Ambati, J., and Fowler, B.J. Mechanisms of age-related macular degeneration. Neuron **75,** 26, 2012.
4. Schwartz, S.D., Hubschman, J.P., Heilwell, G., Franco-Cardenas, V., Pan, C.K., Ostrick, R.M., Mickunas, E., Gay, R., Klimanskaya, I., and Lanza, R. Embryonic stem cell trials for macular degeneration: a preliminary report. Lancet **379,** 713, 2012.
5. Vazin, T., and Freed, W.J. Human embryonic stem cells: derivation, culture, and differentiation: a review. Restor Neurol Neurosci **28,** 589, 2010.
6. Klimanskaya, I., Hipp, J., Rezai, K.A., West, M., Atala, A., and Lanza, R. Derivation and comparative assessment of retinal pigment epithelium from human embryonic stem cells using transcriptomics. Cloning Stem Cells **6,** 217, 2004.
7. Idelson, M., Alper, R., Obolensky, A., Ben-Shushan, E., Hemo, I., Yachimovich-Cohen, N., Khaner, H., Smith, Y., Wiser, O., Gropp, M., Cohen, M.A., Even-Ram, S., Berman-Zaken,

Y., Matzrafi, L., Rechavi, G., Banin, E., and Reubinoff, B. Directed differentiation of human embryonic stem cells into functional retinal pigment epithelium cells. Cell Stem Cell **5,** 396, 2009.
8. Hirami, Y., Osakada, F., Takahashi, K., Okita, K., Yamanaka, S., Ikeda, H., Yoshimura, N., and Takahashi, M. Generation of retinal cells from mouse and human induced pluripotent stem cells. Neurosci Lett **458,** 126, 2009.
9. Buchholz, D.E., Hikita, S.T., Rowland, T.J., Friedrich, A.M., Hinman, C.R., Johnson, L.V., and Clegg, D.O. Derivation of functional retinal pigmented epithelium from induced pluripotent stem cells. Stem Cells **27,** 2427, 2009.
10. Vaajasaari, H., Ilmarinen, T., Juuti-Uusitalo, K., Rajala, K., Onnela, N., Narkilahti, S., Suuronen, R., Hyttinen, J., Uusitalo, H., and Skottman, H. Toward the defined and xeno-free differentiation of functional human pluripotent stem cell-derived retinal pigment epithelial cells. Mol Vis **17,** 558, 2011.
11. Lu, B., Malcuit, C., Wang, S., Girman, S., Francis, P., Lemieux, L., Lanza, R., and Lund, R. Long-term safety and function of RPE from human embryonic stem cells in preclinical models of macular degeneration. Stem Cells **27,** 2126, 2009.
12. Carr, A.J., Vugler, A.A., Hikita, S.T., Lawrence, J.M., Gias, C., Chen, L.L., Buchholz, D.E., Ahmado, A., Semo, M., Smart, M.J., Hasan, S., da Cruz, L., Johnson, L.V., Clegg, D.O., and Coffey, P.J. Protective effects of human iPS-derived retinal pigment epithelium cell transplantation in the retinal dystrophic rat. PLoS One **4,** e8152, 2009.
13. Li, Y., Tsai, Y.T., Hsu, C.W., Erol, D., Yang, J., Wu, W.H., Davis, R.J., Egli, D., and Tsang, S.H. Long-term safety and efficacy of human induced pluripotent stem cell (iPS) grafts in a preclinical model of retinitis pigmentosa. Mol Med **18,** 1312, 2012.
14. Thumann, G., Viethen, A., Gaebler, A., Walter, P., Kaempf, S., Johnen, S., and Salz, A.K. The *in vitro* and *in vivo* behaviour of retinal pigment epithelial cells cultured on ultrathin collagen membranes. Biomaterials **30,** 287, 2009.
15. Lu, B., Zhu, D., Hinton, D., Humayun, M.S., and Tai, Y.C. Mesh-supported submicron parylene-C membranes for culturing retinal pigment epithelial cells. Biomed Microdevices **14,** 659, 2012.
16. Subrizi, A., Hiidenmaa, H., Ilmarinen, T., Nymark, S., Dubruel, P., Uusitalo, H., Yliperttula, M., Urtti, A., and Skottman, H. Generation of hESC-derived retinal pigment epithelium on biopolymer coated polyimide membranes. Biomaterials **33,** 8047, 2012.
17. Hu, Y., Liu, L., Lu, B., Zhu, D., Ribeiro, R., Diniz, B., Thomas, P.B., Ahuja, A.K., Hinton, D.R., Tai, Y.C., Hikita, S.T., Johnson, L.V., Clegg, D.O., Thomas, B.B., and Humayun, M.S. A novel approach for subretinal implantation of ultrathin substrates containing stem cell-derived retinal pigment epithelium monolayer. Ophthalmic Res **48,** 186, 2012.
18. Zarbin, M.A. Analysis of retinal pigment epithelium integrin expression and adhesion to aged submacular human Bruch's membrane. Trans Am Ophthalmol Soc **101,** 499, 2003.
19. Labat-Robert, J. Cell-Matrix interactions, the role of fibronectin and integrins. A survey. Pathol Biol (Paris) **60,** 15, 2012.
20. Hynes, R.O. The extracellular matrix: not just pretty fibrils. Science **326,** 1216, 2009.
21. Prowse, A.B., Chong, F., Gray, P.P., and Munro, T.P. Stem cell integrins: implications for *ex-vivo* culture and cellular therapies. Stem Cell Res **6,** 1, 2011.
22. Kim, D.H., Provenzano, P.P., Smith, C.L., and Levchenko, A. Matrix nanotopography as a regulator of cell function. J Cell Biol **197,** 351, 2012.
23. Booij, J.C., Baas, D.C., Beisekeeva, J., Gorgels, T.G., and Bergen, A.A. The dynamic nature of Bruch's membrane. Prog Retin Eye Res **29,** 1, 2010.
24. Ho, T.C., and Del Priore, L.V. Reattachment of cultured human retinal pigment epithelium to extracellular matrix and human Bruch's membrane. Invest Ophthalmol Vis Sci **38,** 1110, 1997.
25. Tezel, T.H., and Del Priore, L.V. Serum-free media for culturing and serial-passaging of adult human retinal pigment epithelium. Exp Eye Res **66,** 807, 1998.
26. Mousa, S.A., Lorelli, W., and Campochiaro, P.A. Role of hypoxia and extracellular matrix-integrin binding in the modulation of angiogenic growth factors secretion by retinal pigmented epithelial cells. J Cell Biochem **74,** 135, 1999.
27. Smith-Thomas, L., Richardson, P., Parsons, M.A., Rennie, I.G., Benson, M., and MacNeil, S. Additive effects of extra cellular matrix proteins and platelet derived mitogens on human retinal pigment epithelial cell proliferation and contraction. Curr Eye Res **15,** 739, 1996.
28. Hiscott, P., Sheridan, C., Magee, R.M., and Grierson, I. Matrix and the retinal pigment epithelium in proliferative retinal disease. Prog Retin Eye Res **18,** 167, 1999.
29. Hageman, G.S., Mullins, R.F., Russell, S.R., Johnson, L.V., and Anderson, D.H. Vitronectin is a constituent of ocular drusen and the vitronectin gene is expressed in human retinal pigmented epithelial cells. FASEB J **13,** 477, 1999.
30. Hurt, E.M., Chan, K., Serrat, M.A., Thomas, S.B., Veenstra, T.D., and Farrar, W.L. Identification of vitronectin as an extrinsic inducer of cancer stem cell differentiation and tumor formation. Stem Cells **28,** 390, 2010.
31. Donoso, L.A., Kim, D., Frost, A., Callahan, A., and Hageman, G. The role of inflammation in the pathogenesis of age-related macular degeneration. Surv Ophthalmol **51,** 137, 2006.
32. Alcazar, O., Cousins, S.W., Striker, G.E., and Marin-Castano, M.E. (Pro)renin receptor is expressed in human retinal pigment epithelium and participates in extracellular matrix remodeling. Exp Eye Res **89,** 638, 2009.
33. Newsome, D.A., Huh, W., and Green, W.R. Bruch's membrane age-related changes vary by region. Curr Eye Res **6,** 1211, 1987.
34. Hollyfield, J.G., and Rayborn, M.E. Hyaluronan localization in tissues of the mouse posterior eye wall: absence in the interphotoreceptor matrix. Exp Eye Res **65,** 603, 1997.
35. Termeer, C., Benedix, F., Sleeman, J., Fieber, C., Voith, U., Ahrens, T., Miyake, K., Freudenberg, M., Galanos, C., and Simon, J.C. Oligosaccharides of Hyaluronan activate dendritic cells via toll-like receptor 4. J Exp Med **195,** 99, 2002.
36. Hageman, G.S., Luthert, P.J., Victor Chong, N.H., Johnson, L.V., Anderson, D.H., and Mullins, R.F. An integrated hypothesis that considers drusen as biomarkers of immune-mediated processes at the RPE-Bruch's membrane interface in aging and age-related macular degeneration. Prog Retin Eye Res **20,** 705, 2001.
37. Crabb, J.W., Miyagi, M., Gu, X., Shadrach, K., West, K.A., Sakaguchi, H., Kamei, M., Hasan, A., Yan, L., Rayborn, M.E., Salomon, R.G., and Hollyfield, J.G. Drusen proteome analysis: an approach to the etiology of age-related macular degeneration. Proc Natl Acad Sci U S A **99,** 14682, 2002.
38. Ma, W., Tavakoli, T., Derby, E., Serebryakova, Y., Rao, M.S., and Mattson, M.P. Cell-extracellular matrix interactions

regulate neural differentiation of human embryonic stem cells. BMC Dev Biol **8,** 90, 2008.
39. Gong, J., Sagiv, O., Cai, H., Tsang, S.H., and Del Priore, L.V. Effects of extracellular matrix and neighboring cells on induction of human embryonic stem cells into retinal or retinal pigment epithelial progenitors. Exp Eye Res **86,** 957, 2008.
40. Boucherie, C., Mukherjee, S., Henckaerts, E., Thrasher, A.J., Sowden, J.C., and Ali, R.R. Self-organising neuroepithelium from human pluripotent stem cells facilitates derivation of photoreceptors. Stem Cells **31,** 408, 2012.
41. Rowland, T.J., Blaschke, A.J., Buchholz, D.E., Hikita, S.T., Johnson, L.V., and Clegg, D.O. Differentiation of human pluripotent stem cells to retinal pigmented epithelium in defined conditions using purified extracellular matrix proteins. J Tissue Eng Regen Med **7,** 642, 2012.
42. Rowland, T.J., Buchholz, D.E., and Clegg, D.O. Pluripotent human stem cells for the treatment of retinal disease. J Cell Physiol **227,** 457, 2012.
43. Buchholz, D.E., Pennington, B.O., Croze, R.H., Hinman, C.R., Coffey, P.J., and Clegg, D.O. Rapid and efficient directed differentiation of human pluripotent stem cells into retinal pigmented epithelium. Stem Cells Transl Med **2,** 384, 2013.
44. Vugler, A., Carr, A.J., Lawrence, J., Chen, L.L., Burrell, K., Wright, A., Lundh, P., Semo, M., Ahmado, A., Gias, C., da Cruz, L., Moore, H., Andrews, P., Walsh, J., and Coffey, P. Elucidating the phenomenon of HESC-derived RPE: anatomy of cell genesis, expansion and retinal transplantation. Exp Neurol **214,** 347, 2008.
45. Skottman, H. Derivation and characterization of three new human embryonic stem cell lines in Finland. In Vitro Cell Dev Biol Anim **46,** 206, 2010.
46. Carr, A.J., Vugler, A., Lawrence, J., Chen, L.L., Ahmado, A., Chen, F.K., Semo, M., Gias, C., da Cruz, L., Moore, H.D., Walsh, J., and Coffey, P.J. Molecular characterization and functional analysis of phagocytosis by human embryonic stem cell-derived RPE cells using a novel human retinal assay. Mol Vis **15,** 283, 2009.
47. Zahabi, A., Shahbazi, E., Ahmadieh, H., Hassani, S.N., Totonchi, M., Taei, A., Masoudi, N., Ebrahimi, M., Aghdami, N., Seifinejad, A., Mehrnejad, F., Daftarian, N., Salekdeh, G.H., and Baharvand, H. A new efficient protocol for directed differentiation of retinal pigmented epithelial cells from normal and retinal disease induced pluripotent stem cells. Stem Cells Dev **21,** 2262, 2012.
48. Livak, K.J., and Schmittgen, T.D. Analysis of relative gene expression data using real-time quantitative PCR and the 2(-Delta Delta C(T)) method. Methods **25,** 402, 2001.
49. Burke, J.M. Epithelial phenotype and the RPE: is the answer blowing in the Wnt? Prog Retin Eye Res **27,** 579, 2008.
50. Stoker, A.W., Streuli, C.H., Martins-Green, M., and Bissell, M.J. Designer microenvironments for the analysis of cell and tissue function. Curr Opin Cell Biol **2,** 864, 1990.
51. Crawford, B.J. Some factors controlling cell polarity in chick retinal pigment epithelial cells in clonal culture. Tissue Cell **15,** 993, 1983.
52. Gonzalez-Mariscal, L., Betanzos, A., Nava, P., and Jaramillo, B.E. Tight junction proteins. Prog Biophys Mol Biol **81,** 1, 2003.
53. Jensen, A.M., and Westerfield, M. Zebrafish mosaic eyes is a novel FERM protein required for retinal lamination and retinal pigmented epithelial tight junction formation. Curr Biol **14,** 711, 2004.
54. Schneeberger, E.E., and Lynch, R.D. The tight junction: a multifunctional complex. American journal of physiology. Cell Physiol **286,** C1213, 2004.
55. Rizzolo, L.J. Basement membrane stimulates the polarized distribution of integrins but not the Na, K-ATPase in the retinal pigment epithelium. Cell Regul **2,** 939, 1991.
56. Zhu, D., Deng, X., Spee, C., Sonoda, S., Hsieh, C.L., Barron, E., Pera, M., and Hinton, D.R. Polarized secretion of PEDF from human embryonic stem cell-derived RPE promotes retinal progenitor cell survival. Invest Ophthalmol Vis Sci **52,** 1573, 2011.
57. Sugino, I.K., Gullapalli, V.K., Sun, Q., Wang, J., Nunes, C.F., Cheewatrakoolpong, N., Johnson, A.C., Degner, B.C., Hua, J., Liu, T., Chen, W., Li, H., and Zarbin, M.A. Cell-deposited matrix improves retinal pigment epithelium survival on aged submacular human Bruch's membrane. Invest Ophthal Vis Sci **52,** 1345, 2011.
58. Campochiaro, P.A., Jerdon, J.A., and Glaser, B.M. The extracellular matrix of human retinal pigment epithelial cells *in vivo* and its synthesis *in vitro*. Invest Ophthal Vis Sci **27,** 1615, 1986.
59. Kamei, M., Kawasaki, A., and Tano, Y. Analysis of extracellular matrix synthesis during wound healing of retinal pigment epithelial cells. Microsc Res Tech **42,** 311, 1998.
60. Kigasawa, K., Ishikawa, H., Obazawa, H., Minamoto, T., Nagai, Y., and Tanaka, Y. Collagen production by cultured human retinal pigment epithelial cells. Tokai J Exp Clin Med **23,** 147, 1998.
61. Binder, S., Stanzel, B.V., Krebs, I., and Glittenberg, C. Transplantation of the RPE in AMD. Prog Retin Eye Res **26,** 516, 2007.
62. Savolainen, V., Juuti-Uusitalo, K., Onnela, N., Vaajasaari, H., Narkilahti, S., Suuronen, R., Skottman, H., and Hyttinen, J. Impedance spectroscopy in monitoring the maturation of stem cell-derived retinal pigment epithelium. Ann Biomed Eng **39,** 3055, 2011.
63. Burke, J.M., Kaczara, P., Skumatz, C.M., Zareba, M., Raciti, M.W., and Sarna, T. Dynamic analyses reveal cytoprotection by RPE melanosomes against non-photic stress. Mol Vis **17,** 2864, 2011.
64. Kaczara, P., Zareba, M., Herrnreiter, A., Skumatz, C.M., Zadlo, A., Sarna, T., and Burke, J.M. Melanosome-iron interactions within retinal pigment epithelium-derived cells. Pigment Cell Melanoma Res **25,** 804, 2012.
65. Peters, S., and Schraermeyer, U. Characteristics and functions of melanin in retinal pigment epithelium. Ophthalmologe **98,** 1181, 2001.
66. Schraermeyer, U., Kopitz, J., Peters, S., Henke-Fahle, S., Blitgen-Heinecke, P., Kokkinou, D., Schwarz, T., and Bartz-Schmidt, K.U. Tyrosinase biosynthesis in adult mammalian retinal pigment epithelial cells. Exp Eye Res **83,** 315, 2006.

Address correspondence to:
Heli Skottman, PhD
Institute of Biomedical Technology
University of Tampere
Biokatu 12, 33014
Tampere 33520
Finland

E-mail: heli.skottman@uta.fi

Received: January 24, 2013
Accepted: September 10, 2013
Online Publication Date: January 21, 2014

Biomaterials 51 (2015) 257–269

Contents lists available at ScienceDirect

Biomaterials

journal homepage: www.elsevier.com/locate/biomaterials

Biomimetic collagen I and IV double layer Langmuir–Schaefer films as microenvironment for human pluripotent stem cell derived retinal pigment epithelial cells

Anni E. Sorkio [a, *], Elina P. Vuorimaa-Laukkanen [b], Hanna M. Hakola [b], Huamin Liang [b], Tiina A. Ujula [c], Juan José Valle-Delgado [c], Monika Österberg [c], Marjo L. Yliperttula [d], Heli Skottman [a]

[a] BioMediTech, University of Tampere FM5/BMT, 33014 University of Tampere, Finland
[b] Department of Chemistry and Bioengineering, Tampere University of Technology, Korkeakoulunkatu 8, 33720 Tampere, Finland
[c] Department of Forest Products Technology, School of Chemical Technology, Aalto University, P.O. Box 16300, 00076 Aalto, Finland
[d] Division of Biopharmaceutical Sciences, Centre for Drug Research, Faculty of Pharmacy, University of Helsinki, Viikinkaari 5, 00790 Helsinki, Finland

ARTICLE INFO

Article history:
Received 23 September 2014
Received in revised form
26 January 2015
Accepted 1 February 2015
Available online

Keywords:
Biomimetic material
Collagen structure
Langmuir Blodgett film
Retinal pigment epithelial cell
Retina
Human embryonic stem cell

ABSTRACT

The environmental cues received by the cells from synthetic substrates *in vitro* are very different from those they receive *in vivo*. In this study, we applied the Langmuir–Schaefer (LS) deposition, a variant of Langmuir–Blodgett technique, to fabricate a biomimetic microenvironment mimicking the structure and organization of native Bruch's membrane for the production of the functional human embryonic stem cell derived retinal pigment epithelial (hESC-RPE) cells. Surface pressure-area isotherms were measured simultaneously with Brewster angle microscopy to investigate the self-assembly of human collagens type I and IV on air-subphase interface. Furthermore, the structure of the prepared collagen LS films was characterized with scanning electron microscopy, atomic force microscopy, surface plasmon resonance measurements and immunofluorescent staining. The integrity of hESC-RPE on double layer LS films was investigated by measuring transepithelial resistance and permeability of small molecular weight substance. Maturation and functionality of hESC-RPE cells on double layer collagen LS films was further assessed by RPE-specific gene and protein expression, growth factor secretion, and phagocytic activity. Here, we demonstrated that the prepared collagen LS films have layered structure with oriented fibers corresponding to architecture of the uppermost layers of Bruch's membrane and result in increased barrier properties and functionality of hESC-RPE cells as compared to the commonly used dip-coated controls.

1. Introduction

Cells in tissues are influenced by the extracellular matrix (ECM) in which they reside [1,2]. Apart from the mechanical support, ECM binds soluble factors and regulates their distribution and presentation to cells, as well as plays an important role in cell morphology, migration, proliferation, differentiation and maturation [3–5]. While synthetic scaffolds made of biocompatible materials have been shown to closely mimic the ECM structure, they still lack much of the fine, intricate architecture and biochemical cues that can be found in the native ECM [6]. Thus, the environmental cues received by the cells from these substrates *in vitro* are very different from those they receive *in vivo* [7].

Dysfunction and irreversible damage of the retinal pigment epithelium (RPE) layer is a fundamental factor in the progression of degenerative retinal diseases, such as age-related macular degeneration (AMD) [8,9]. Human embryonic stem cells (hESCs) are an attractive cell source for cell transplantation therapies to treat AMD due to their limitless supply [10] and ability to differentiate towards functional RPE cells [11,12]. Cell transplants of hESC–derived RPE (hESC-RPE) cells are currently under clinical trials for the treatment of the dry form of AMD and Stargardt's disease [13] and clinical trials with autologous human induced pluripotent stem cell (hiPSC)-derived RPE cell sheets for the wet type of AMD have also started [14].

In vivo, the RPE cells rest on a specific pentalaminar 1–4 μm thick ECM sheet called Bruch's membrane. Bruch's membrane is

* Corresponding author. Tel.: +358 40 1901790; fax: +358 33 5518498.
E-mail address: anni.sorkio@uta.fi (A.E. Sorkio).

http://dx.doi.org/10.1016/j.biomaterials.2015.02.005
0142-9612/

located between the RPE and the underlying choroid, where it provides structural support for the RPE cells as well as operates as a biological filter to allow for the reciprocal exchange of nutrients, biomolecules and metabolic waste products. Histologically, Bruch's membrane composes of five different layers with distinguishable structure and composition. The basement membrane of RPE forms the outermost layer of the Bruch's membrane, and it mainly consists of collagen type IV, laminin, fibronectin, hyaluronic acid, heparan sulfate and chondroitin/dermatan sulfate whereas the inner collagenous layer comprises of collagen type I, III, and V [15].

Collagen has been extensively examined as a supportive structure for a variety of tissues such as skin, cartilage, bone, corneal and nerve tissues [16–18]. Human primary RPE cells and the immortalized ARPE-19 cell line have been previously cultured on equine, bovine and rat collagen type I membranes [19–22] as well as on human collagen type I thin films [23]. Furthermore, porcine collagen type I gels have been used for the maturation of hiPSC-RPE cells in studies aiming for clinical applications [14]. In addition, gelatin, which is collagen that has been processed to remove its higher organized structure, has been widely studied with RPE [24–26]. To the best of our knowledge, collagen type IV has been assessed with RPE cells and hESC-RPE cells merely in the form of protein coating [27–29]. Despite the success with collagen in biomedical applications, mimicking the natural fiber orientation and structure remains a major challenge [30–32].

The Langmuir–Blodgett (LB) technique is an attractive approach for obtaining artificial biomimetic models with a well-characterized molecular organization without the use of additives and bio-incompatible materials [30,33,34]. This approach is based on the presence of collagen in its molecular form in acidic solution and its ability to form fibers resulting from the increase of the solvent pH when it is spread onto the subphase surface [35]. In the LB technique, this process is forced to take place at the air-subphase interface in a Langmuir trough. The interface is subsequently compressed to obtain oriented collagen fibers and deposited onto a solid substrate [34]. When the deposition of the floating monolayer from the subphase surface onto a solid support occurs horizontally, the technique is referred to as Langmuir–Schaefer (LS) deposition [36]. In previous studies, human fibroblasts, 3T3 mouse fibroblastic cells and adipose-derived stem cells have been shown to respond favorably to the oriented rat and calf collagen I films prepared with LB technique [34,37]. Along with collagen I, laminin, fibronectin and vitronectin thin LB films have been previously manufactured [38].

In this study, we have applied the LS technique to fabricate a biomimetic microenvironment mimicking the structure and organization of native Bruch's membrane for the production of the clinically relevant hESC-RPE cells. A layered and oriented collagen film from human collagen types I and IV was manufactured only based on human origin biomaterials. The constructed film had two separate layers, collagen type I layer underneath and collagen type IV layer above corresponding the inner collagenous layer and the basement membrane of Bruch's membrane, respectively. Here, we demonstrate that the prepared LS films have layered structure with oriented fibers and result in increased barrier properties and functionality of hESC-RPE cells as compared to commonly used dip-coated controls.

2. Experimental methods

2.1. Preparation of collagen solutions

The human collagen I (Col I) and human collagen IV (Col IV) from human placenta (Sigma–Aldrich St. Louis, MO, USA) were treated according to the protocol described by Goffin et al. [34]. Briefly, both collagens were dissolved into dilute acetic acid (Merck, Germany) to obtain a solution of 1 mg ml^{-1} and pH ~ 3. Prior to Langmuir-film preparation, collagen solutions were sonicated in water bath on ice for two 10 min periods with a 10 min rest period in between. These solutions were prepared fresh right before use.

2.2. Langmuir isotherms and Brewster angle microscopy (BAM)

The full isotherms and Brewster angle microscopy (BAM) images were measured simultaneously with a KSV OPTREL BAM300 mounted on a KSV minitrough Langmuir film balance (KSV Instruments) equipped with a double barrier system. Dulbecco's phosphate buffered saline (DPBS) (Lonza Group Ltd., Basel, Switzerland) was used as a subphase: two-fold DPBS solutions were prepared in Milli-Q water. The temperature of the subphase was 20.8 ± 0.5 °C and the compression speed for the isotherms and Langmuir-film preparation was 65 mm min^{-1} i.e. 48.75 cm^2 min^{-1} 180 μl of the 1 mg ml^{-1} collagen solution was spread drop-wise onto the subphase using a glass microsyringe. The film was allowed to equilibrate for 30 min before compression. The BAM instrument was equipped with a 10 mW HeNe laser (633 nm) linearly polarized in the plane of incidence by a Glan-Thompson polarizer. The reflection from the interface passes through a second Glan-Thompson polarizer and was collected by a CCD camera. The microscope was adjusted so that the background reflection from the bare air–water interface was minimal. The spatial resolution of the system was approximately 2 μm.

2.3. Langmuir–Schaefer (LS) films

The LS films were prepared using the KSV minitrough system. The Langmuir-film was prepared as described above. The film was compressed to the deposition pressure of 12 mN m^{-1} for Col I and 30 mN m^{-1} for Col IV and allowed to stabilize for 15 min before deposition on substrates. The compression of the LS films took place symmetrically and horizontally. Several types of substrates were used for LS-transfer: silicon wafers for scanning electron microscopy (SEM) studies, freshly cleaved mica for atomic force microscopy (AFM) measurements, SPR sensor substrates (ca. 50 nm gold with a chromium adhesion layer of ca. 2 nm coated on glass slides) for SPR, borosilicate glass coverslips (0.13 mm thickness, VWR Collection, VWR, Finland) for immunofluorescence stainings and commercial polyethylene terephthalate (PET) cell culture inserts with 5 μm pore size (Millipore) for cell culture and permeability studies. Prior to the deposition the glass substrates were cleaned by 10 min sonication in chloroform and chromic sulfuric acid. After careful rinsing with water the glass substrates were kept 30 min in 1 mM NaOH (Merck KGaA, Germany) and subsequently dried in an oven at 120 °C. The silicon wafers were cleaned by sonicating 1 min in isopropanol and rinsing with chloroform followed by drying in nitrogen flow. Before deposition, the SPR sensor substrates were first cleaned by boiling them in the cleaning solution of NH_4OH (30%) (Merck KGaA): H_2O_2 (30%) (Merck Schuchardt OHG, Germany): Milli-Q H_2O (1:1:5) for 10 min. The LS films were transferred onto substrates manually by touch-and-lift method. Thereafter, the deposited LS films were dried in a desiccator for a minimum of 24 h to evaporate any remaining of the subphase. Subsequently, the samples were washed twice with Milli-Q H_2O to remove the formed salt crystals and dried again before measurements or the deposition of a second layer. For the double layer Col I and Col IV LS films, Col IV LS film was deposited on top of a dried Col I LS film as described above. The manufacturing process of the LS films is illustrated in Supplementary Fig. 1.

2.4. Dip-coating

For control samples, substrates were dip-coated with collagen protein solutions as described previously [11,27]. Briefly, substrates were rinsed with DPBS, and immersed in collagen protein solution at a concentration of 5 μg cm^{-2} for 3 h at +37 °C. The following substrates were used for dip-coating: freshly cleaved mica for AFM measurements, SPR sensor substrates for SPR, borosilicate glass coverslips for immunofluorescence stainings and commercial PET cell culture inserts with 1 μm pore size for cell culture studies. The pH of collagen solution during coating procedure was 7. Prior to material characterization and cell seeding, the dip-coated control samples were rinsed twice with DPBS to remove any remaining of unbound protein.

2.5. Scanning electron microscopy (SEM)

The microstructure of the LS films deposited on silicon substrates was observed using field-emission scanning electron microscope (FE-SEM, Carl Zeiss Ultra 55).

2.6. Atomic force microscopy (AFM)

A MultiMode 8 atomic force microscope (Bruker Corporation, Massachusetts, USA) equipped with a J scanner and Nanoscope V controller was used to characterize the nanostructure of different collagen LS films. Images were obtained in air using silicon NSC15/AlBS cantilevers (MicroMasch, Tallinn, Estonia) with a tip radius below 10 nm, operating in tapping mode. Research NanoScope 8.15 software (Bruker Corporation) was utilized for image analysis.

2.7. Surface plasmon resonance (SPR)

Surface plasmon resonance (SPR) measurements were performed with an MP-SPR Navi 200-L instrument equipped with two light source pairs providing 654 and 782 nm, as well as 668 and 783 nm, wavelengths (BioNavis Ltd., Tampere, Finland). Before the deposition of the collagen films, all pre-cleaned MP-SPR sensors were measured in air and water to acquire the backgrounds. Thereafter, the MP-SPR sensor substrates with deposited collagen layers were measured in water and then in air. All SPR measurements were performed at the wavelengths of 654 and 782 nm, and 668 and 783 nm at 20 °C. The original SPR data were processed using the BioNavis Data viewer software. The measured MP-SPR spectra for pure SPR sensors were fitted with a free Fresnel equation based program Winspall 3.02 in order to extract the thickness (d) and refractive index (n). During the fitting, the optical parameters from the pure gold fitting were used as backgrounds for multilayer modeling. The refractive index was kept constant but the thickness of the layers was fitted. This fitting procedure was repeated for the n-values with an increment of 0.2 between 1.4 and 1.6. Thus, the d-n continuum solutions were acquired. In order to investigate the stability of deposited collagen LS layers on the gold surface they were monitored in real time with SPR at 782 nm under. The water flow flush was running at 30 μl/min at 20 °C for up to 10 h. The measured SPR sensograms were processed using the BioNavis Data viewer software.

2.8. Human embryonic stem cell derived retinal pigment epithelial cells

In this study, we investigated two hESC lines, Regea 08/023 (46, XY) and Regea 11/013 (46, XY), which were previously derived in our laboratory [39]. The undifferentiated hESCs were maintained on Mitomycin C-treated (Sigma–Aldrich) mitocally inactivated human foreskin fibroblast feeder cells (CRL-2429TM, ATCC, Manassas, VA, USA) in serum-free conditions and enzymatically passaged using TrypLE Select (Invitrogen, UK) onto fresh feeder cells at ten-day intervals. Undifferentiated hESCs were differentiated into RPE cells as described previously [11].

After 55–132 days of differentiation in suspension culture, the pigmented areas of the floating aggregates were manually selected and cut with a lancet, dissociated with Trypsin–EDTA (Lonza, Walkersville, MD) and replated to Col IV-coated 24-well culture plates (Corning® CellBIND®, Corning Inc., NY, USA). Thereafter, the pigmented cells were enriched in adherent cultures for 180–209 days. The hESC-RPE maturation and functionality was investigated on Col I-Col IV double layer LS films. The double layer LS films were sterilized under ultra violet light for 10 min per each side of the film and hydrated in culture medium for 1 h before cell seeding. For plating cells on LS films, the hESC-RPE cells were dissociated with TrypLE Select (Invitrogen), filtered through BD Falcon cell strainer (BD Biosciences) and seeded on LS films at density of 1.2×10^5 cells cm^{-2}. Commercial cell culture inserts with 1 μm pore size (Millipore) dip-coated with collagen IV (5 μg cm^{-2}) were selected as control in cell culture studies as we have previously used Col IV for enrichment and maturation of hPSC-RPE cells [11,27].

2.9. Gene expression analysis

After 42 days of culture, the gene expression of RPE-specific proteins bestrophin (*BEST*), microphthalmia-associated transcription factor (*MITF*), pigment epithelium-derived factor (*PEDF*), retinal pigment epithelium specific protein 65 kDa (*RPE65*) and tyrosinase (*TYR*) as well as pluripotency marker octamer-binding transcription factor (*OCT*)3/4 was assessed with reverse transcription–polymerase chain reaction (RT-PCR). Glyceraldehyde 3-phosphate dehydrogenase (*GAPDH*) was used as an endogenous control. RNA was extracted using NucleoSpin RNA II kit (Macherey-Nagel, GmbH & Co) according to the manufacturer's instructions. Water was used as a negative control in RT-PCR analysis to detect any impurities in the reagents and procedure. The gene expression of pluripotency markers *OCT3/4* and *Nanog* and RPE-specific proteins *RPE65* and *TYR* were also examined for undifferentiated hESCs in both investigated cell lines. Detailed RT-PCR protocol and primer sequences have been previously reported [11].

Differences in relative expression level of *RPE65* gene were studied further with quantitative real-time PCR (qPCR) as described previously [27]. Samples were collected from two individual experiments. TaqMan® Gene Expression Assays (Applied Biosystems Inc.) with FAM-labels were used for PCR reaction: *RPE65* (Hs01071462_m1) and *GAPDH* (Hs99999905_m1). The results were analyzed using 7300 System SDS Software (Applied Biosystems Inc.). The relative quantification of *RPE65* was calculated using the 2-ΔΔCt method [40]. The values for each sample were normalized to expression levels of *GAPDH*. The expression level of cells on dip-coated control was set as the calibrator in both investigated cell lines (fold change equals 1).

2.10. Immunocytochemistry

The fiber-like structure of Col I, Col IV and double layer Collagen LS films as well as the protein expression and localization of hESC-RPE cells on double layer LS films was examined with immunofluorescence (IF) staining. In addition, the expression of pluripotency marker OCT3/4 was investigated for the undifferentiated hESCs. Samples were washed twice with DPBS, fixed with 4% paraformaldehyde (Sigma–Aldrich) for 10 min at room temperature (RT), washed with DPBS and permeabilized with 0.1% Triton X-

100 in DPBS (Sigma–Aldrich) at RT for 10 min. Next, unspecific binding sites were blocked with 3% BSA (Sigma–Aldrich) at RT for 1 h. Thereafter, samples were incubated with primary antibodies overnight in 4 °C: rabbit anti-bestrophin 1:400, mouse anti-CRALBP 1:600, mouse anti-Na^+/K^+ATPase 1:100, rabbit anti-MITF 1:350 (all from Abcam, Cambridge, UK), mouse anti-collagen IV, rabbit anti-collagen I 1:200 (both from Millipore), mouse anti-MERTK 1:50 (Abnova), mouse anti-zonula occludens 1 (ZO-1) 1:250 (Invitrogen) and goat anti-OCT3/4 1:200 (R & D Systems Inc., Minneapolis, MN). Cells were washed several times with DPBS. Secondary antibodies were diluted in ratio of 1:800 with 0.5% BSA-DPBS: Alexa Fluor 568-conjugated goat anti-mouse IgG and goat anti-rabbit Ig G, and Alexa Fluor 488-conjugated donkey anti-rabbit IgG, donkey anti-mouse IgG and donkey anti-goat IgG (all from Molecular Probes, Life Technologies). In addition, Phalloidin–Tetramethylrhodamine B isothiocyanate 1:400 (Sigma–Aldrich) was used for labeling filamentous actin. Samples were incubated in secondary antibody dilutions for 1 h in RT following repeated washes in DPBS. 4′,6′ diamidino-2-phenylidole (DAPI) included in the mounting media was used for staining the nuclei (Vector Laboratories Inc., Burlingame, CA). To verify that the fiber-like organized structure of the LS films is due to the organization of collagen to the air-subphase interface and compression of the surface, we carried out immunostainings of Col I- and Col IV-dip-coated samples (coating concentration for both 5 μg cm^{-2}). Images were taken with Olympus BX60 microscope (Olympus, Tokyo, Japan) or LSM 700 confocal microscope (Carl Zeiss, Jena, Germany) using a 63× oil immersion objective. Images were edited using ZEN 2011 Light Edition (Carl Zeiss) and Adobe Photoshop CS4.

2.11. Western blotting

The RPE65 protein expression was studied further after 42 days of culture on double layer LS films with Western blotting as previously described [27]. Mouse anti-RPE65 (1:5000, Millipore) and mouse anti-β-actin (1:5000, Santa Cruz) primary antibodies were used. The RPE65 protein expression was quantified with band area calculation in Image J Image Processing and Analysis Software and compared to the loading control β-actin from the same lane in the membrane. These RPE65/β-actin ratios were calibrated against dip-coated control samples in both investigated cell lines (RPE65/β-actin ratio for controls equals 1) in order to carry out relative comparison between controls and LS films.

2.12. Transepithelial resistance

The integrity and barrier function of the forming hESC-RPE on LS films were studied with transepithelial resistance (TER) measurements after 42 days of culture. Samples were tightly clamped to a P2307 slider (Physiologic Instruments, San Diego, CA), and assembled to a custom-made Teflon chamber as previously described [41]. Measurements were carried out in DPBS with a Millicell electrical resistance system volt-ohm meter (Merck Millipore, Darmstad, Germany). TER-values (Ω cm^2) were calculated by subtracting the value of empty material sheet without cells from the result, and by multiplying the result by the surface area of the substrate. Calculated TER-values were normalized against the dip-coated controls in both investigated cell lines. TER-values were obtained from three individual experiments with four parallel samples for each condition.

2.13. Permeability study

The ability of LS films to act as semipermeable barrier and the integrity of hESC-RPE monolayer on double layer LS films was assessed by measuring the flux of a small molecular weight (700 Da) Alexa Fluor® 568 Hydrazide sodium salt (Life Technologies) at a concentration of 0.0065 mM. The permeability of hESC-RPE cells on LS films was studied after 64 days of culture. The study was carried out in Ussing chamber system (Physiologic Instruments, San Diego, CA) with P2300 chambers and P2307 sliders and culture medium without KnockOut™ Serum Replacement (KO-SR) was used as a diffusion medium. The chambers were maintained at 37 °C by using a circulating water bath and gas inflow was applied to the chambers. The donor chamber was filled with 2.1 ml of diffusion medium with fluorescent marker, whereas equal volume of diffusion medium without fluorescent marker was applied on the receptor chamber. Volumes of 100 μl were sampled from the receptor chamber at 60, 120, 180, 240 and 300 min and replaced with fresh diffusion medium. The fluorescence of the samples was analyzed in 96-well plates using the Wallac Victor2™ 1420 Multilabel counter (Perkin Elmer–Wallace, Norton, OH) at 590 nm excitation and 642 nm emission wavelengths. The diffusion of Alexa Fluor® 568 Hydrazide sodium salt across the LS films and hESC-RPE monolayers was characterized by calculating the apparent permeability coefficient (P_{app}, cm^2 s^{-1}) as $P_{app} = dC/dt/(60C_0A)$, where dC/dt is the slope of the linear portion of the permeability curve, C_0 is the initial concentration in the donor chamber, and A is the exposed surface area of the RPE monolayer (0.031 cm^2). Furthermore, the data is presented as cumulative permeability illustrating the percentage of diffused fluorescent marker in the receptor chamber compared to initial concentration in the donor chamber over time. Permeability data for hESC-RPE cells on double layer LS films were obtained from three individual experiments with four parallel samples for each condition.

2.14. Phagocytosis

The phagocytic properties of hESC-RPE monolayers on double layer LS films were investigated using isolated porcine photoreceptor outer segments (POS) after 56 days of culture. The POS were isolated as described previously [11]. POS were labeled with fluorescein isothiocyanate (FITC) (0.04 μg/μl; Sigma–Aldrich) in 0.1 M $NaHCO_3$ (pH 9) for 1 h at RT, following washing three times with PBS and resuspended in culture medium supplemented with 10% fetal bovine serum (FBS, Sigma–Aldrich). HESC-RPE cells on LS films were incubated with POS for 2 h at 37 °C. Thereafter, the cells were washed twice with PBS and fixed with 4% paraformaldehyde for 10 min at RT following repeated PBS washings. Subsequently, the cells were permeabilized using 0.1% Triton X-100 for 10 min at RT followed by repeated PBS washings. Filamentous actin was stained with phalloidin (Sigma–Aldrich) by incubating for 30 min at RT following several PBS washings. The nuclei were counterstained with DAPI that was in the mounting media. The images of the hESC-RPE cells with internalized POS fragments were taken using a confocal microscope (LSM 700, Carl Zeiss, 63× oil immersion objective).

2.15. Enzyme-linked immunosorbent assay

The functionality of hESC-RPE cells on LS films was evaluated by their PEDF secretion after 21 days of culture. Culture medium was conditioned with hESC-RPE cells on double layer LS films and dip-coated controls for 24 h before collecting samples for analysis. PEDF concentration was determined from the conditioned medium using Chemikine PEDF Sandwich ELISA Kit (Millipore) according to the manufacturer's instructions. Cell density on LS films and controls at day 21 was taken into consideration in PEDF concentration calculations.

2.16. Ethical issues

The National Authority for Medicolegal Affairs Finland has approved our research with human embryos (Dnro 1426/32/300/05). We also have a supportive statement from the local ethics committee of the Pirkanmaa hospital district Finland to derive and expand hESC lines from surplus embryos not used in the treatment of infertility by the donating couples, and to use these cell lines for research purposes (R05116). No new lines were derived for this study.

2.17. Statistical analysis

Mann–Whitney U-test and IBM SPSS Statistics software were used for determining statistical significance. Average (median) values of relative TER, P_{app}, and PEDF secretion on LS films were compared to average (median) values obtained on dip-coated controls with Mann–Whitney U-test. P-values $\leq$ 0.05 were considered statistically significant.

3. Results

3.1. Surface pressure-area isotherms

Isotherms of Col I and Col IV were measured to investigate whether the collagen molecules remain on the DPBS air-subphase interface or enter the subphase instead. During the 30 min stabilization period, the surface pressure increased 0.4 ± 0.2 mN m^{-1} for Col I and 1.4 ± 0.4 mN m^{-1} for Col IV (Fig. 1(a)). The initial surface pressure after spreading of the collagen solution was 1 mN m^{-1} higher for Col IV compared to Col I although the same amount (in mass) of collagens were used. The pressure versus surface area isotherms for Col I and Col IV are illustrated in Fig. 1(b). For Col I the surface pressure did not reach 20 mN m^{-1} before the trough space between the barriers ran out. Instead, the surface pressure of 40 mN m^{-1} was attained for Col IV. Spreading more Col I only led to a shift of the isotherm to higher areas per gram. For both collagens, a steady increase in surface pressure was detected upon compression of the interface between the barriers. For deposition of LS films and for further analysis and cell culture studies, the surface pressures of 12 and 30 mN m^{-1} were used for Col I and Col IV, respectively.

3.2. Fiber formation, orientation and structure of collagen LS films

BAM was used to detect the Col I and Col IV Langmuir film formation and fiber orientation in the DPBS-air interface during compression. Both Col I and Col IV covered the surface evenly and no pure subphase surface was observed after spreading. At low surface pressures the collagen molecules floated loosely on the surface, and neither orientation nor fiber-like structures were observed. As the surface pressure increased, during both stabilization and compression periods, the images got brighter as the density of collagen on the air-subphase interface increased. For Col I, the fiber formation was clearly observed during compression as nearly vertical 10 μm thick and 50 μm long structures were visible already 27 s after the compression was started (Fig. 1(c)). At this point, the pressure had increased only 1 mN m^{-1} from that measured after the 30 min stabilization period. For Col IV, darker domains with lower collagen density or thickness were observed (Fig. 1(d)). The domains differed in size from small nearly circular areas with 10 μm diameter to larger 200 μm × 100 μm areas. At 10–20 mN m^{-1} the shape of the domains changed from irregular to elongated ellipses which were oriented according to the compression direction. Highly organized structures oriented parallel to the barriers were observed with both collagens (Fig. 1(c,d)). At all pressures the BAM images of Col IV were brighter than those of Col I.

The microstructure of LS films was assessed with SEM. In the SEM images, a thin film with a fiber-like structure similar to those observed in BAM figures were detected (Fig. 1(e,f)). The substrates were completely covered by both Col I and Col IV LS films. During deposition of the second layer of the double layer LS film, the angle of the substrate towards compression direction was changed. Thus, the presence of both Col I and Col IV layers can be clearly seen as ordered structures of different angles (Fig. 1(g)). IF stainings for the empty substrates were negative for collagen I and collagen IV (data not shown) confirming that the fiber-like collagen structures seen in Fig. 1 are deposited collagens and not background from the substrates.

The fiber formation and structure was studied further with IF staining. Beautiful oriented fibers were observed with Col I LS films (Fig. 1(i)) whereas the structure of Col IV LS films appeared more net-like (Fig. 1(k)). These results are similar to those seen in both BAM and SEM images. The dip-coated controls had neither fiber-like nor organized structure (Fig. 1(j–l)). The IF images of the double layer LS film confirmed the presence of both Col I and Col IV layers (Fig. 1(h)). As detected with SEM, the Col I and Col IV films in double layer LS films had organized structure and the layers were oriented at different angles, with Col I LS film deposited underneath the net-like Col IV LS layer.

The barrier properties of LS films were assessed using a small molecular weight (700Da) fluorescent marker. The P_{app} for Col I LS films was $21 \times 10^{-5} \pm 8 \times 10^{-5}$ cm^2 s^{-1} and for Col IV $26 \times 10^{-5} \pm 5 \times 10^{-5}$ cm^2 s^{-1}, whereas a slightly smaller value of $15 \times 10^{-5} \pm 5 \times 10^{-5}$ cm^2 s^{-1} was detected for double layer LS film (Fig. 1(m)). For empty PET insert P_{app}-value of $17 \times 10^{-5} \pm 2 \times 10^{-5}$ cm^2 s^{-1} was recorded. The cumulative permeability for Col I and Col IV LS films is shown in Fig. 1(n) and for double layer LS film and empty PET insert in Fig. 1(o). Compared to the empty PET insert, Col I LS film did not form a barrier for the small molecular weight marker. Instead, decrease in the cumulative permeability of Col IV LS films was detected. However, after 300 min exposure, this barrier was disturbed. A similar decrease in cumulative permeability was observed for double layer LS film as detected for Col IV LS film. Instead, no sudden changes and disturbance in barrier property was noticed during 300 min exposure time for the double layer LS film.

3.3. Nanostructure and the stability of the collagen LS films

The nanostructure of the collagen LS films was investigated with AFM (Fig. 2(a–h)). The width of the collagen fibers was determined from the analysis of the height topographic profiles of AFM images (Fig. 2(i–l)) Average values of about 4.5 nm and 12.5 nm were obtained for the fibrils of Col I and Col IV LS films, respectively. Widths up to 65 nm and 140 nm were also observed for larger fibers of collagen I and IV, respectively. The Col IV LS films had more of a net-like structure. Interestingly, the surface topography of the double layer LS film was different from the monolayer Col IV LS film even though Col IV LS film was the uppermost layer of both samples.

The deposited LS films were further characterized with two-media (air and water) MP-SPR measurements in order to extract the unique solution of refractive index (d) and thickness (n) [42]. Examples of the Winspall fitting in air and water at 782 nm for washed collagen LS films are shown in Fig. 3(a) and for unwashed films in Supplementary Fig. 2. Good fits and clear angle shifts between the collagen layers and the background were observed both in air and in water. The gathered d and n continuum solutions were then plotted in order to find the intersection of air and water, which is the actual thickness and refractive index (an example illustrated

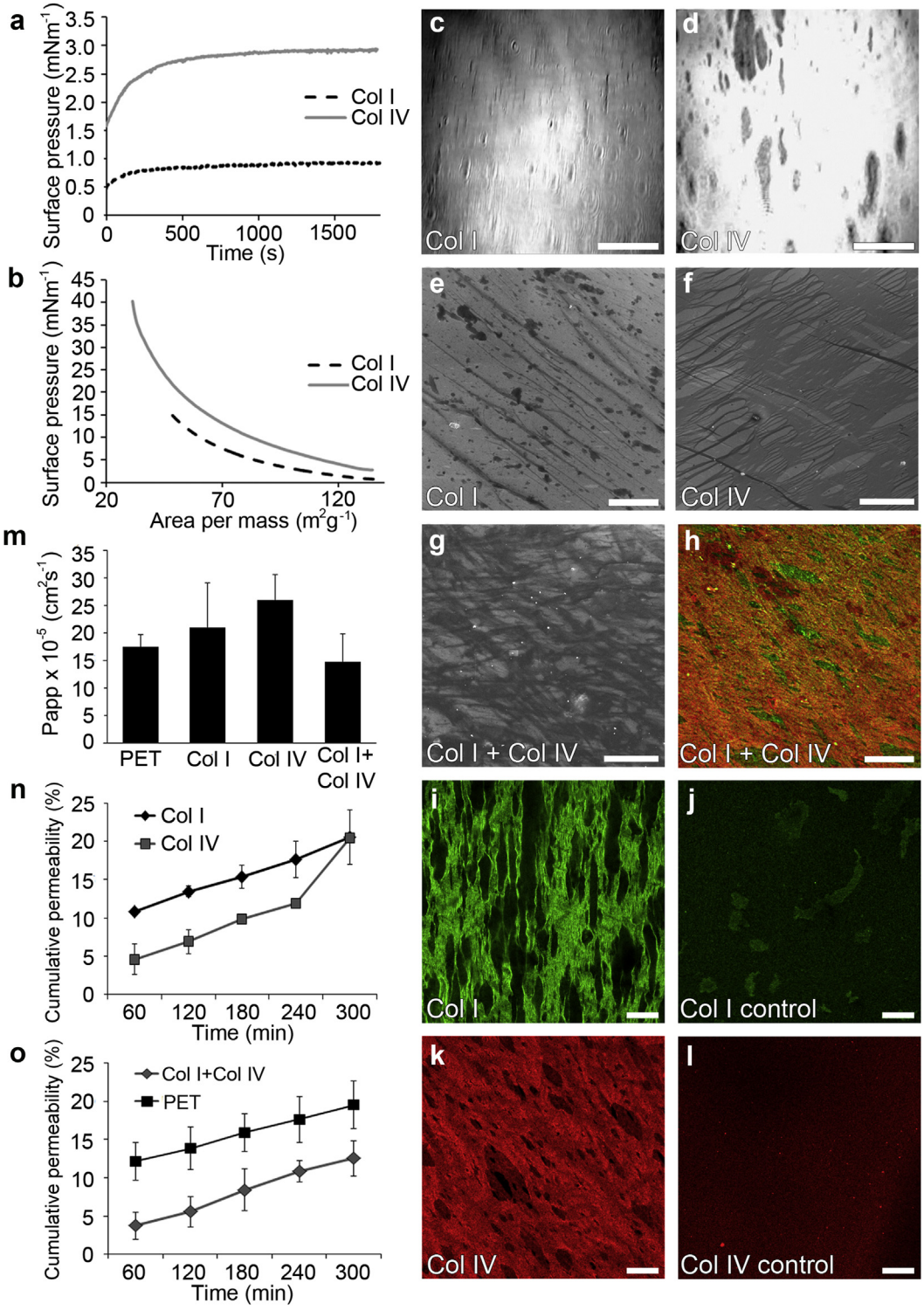

Fig. 1. Fiber formation, orientation and structure of collagen Langmuir and LS films. a) Surface pressure during stabilization after spreading of collagen on subphase and b) surface pressure-area isotherms for Col I and Col IV. BAM images demonstrating the fiber formation during compression of c) Col I and d) Col IV Langmuir films. Scale bars c–d) 100 μm. SEM images of e) Col I, f) Col IV and g) double layer LS films show the microstructure and orientation of prepared LS films. Scale bars e) 40 μm and f-g) 20 μm. Immunofluorescence images of h) double layer LS film, i) Col I LS films, j) Col I dip-coated control, k) Col IV LS film and l) Col IV dip-coated control. Collagen I (green) and collagen IV (red). Scale bars h) 20 μm and i–l) 50 μm. (m) The apparent permeability coefficient P_{app} and the cumulative permeability of small molecular weight fluorescent marker for n) Col I and Col IV LS films and o) for double layer LS film.

in Fig. 3(b)). Thicknesses of different collagen LS films measured by MP-SPR are summarized in Fig. 3(c). The average thickness of the unwashed Col I LS films was less than 11 nm whereas the Col IV LS films showed much higher values reaching up to 31 nm. The thickness of the double layer LS film, 27 nm, was significantly lower than the sum of Col I and Col IV monolayer LS films. The thickness of Col I LS film reduced during washing procedure down to 7 nm. Instead, for Col IV and double layer LS films the difference between

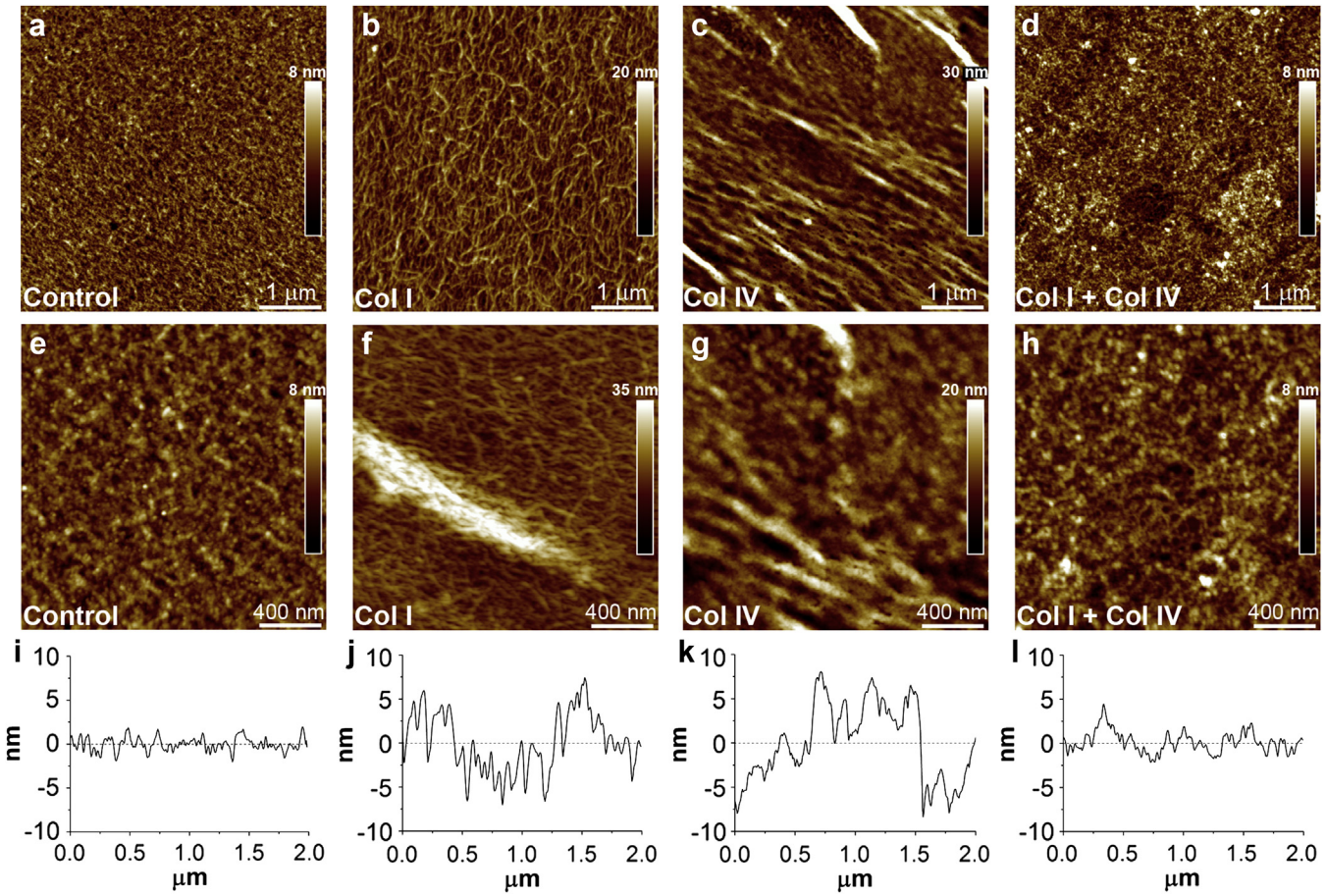

Fig. 2. AFM height images illustrating the nanostructures of different collagen films: a,e) control sample; b,f) Col I LS film; c,g) Col IV LS film; d,h) double layer collagen LS film. e–h) Demonstrate representative higher magnification images of the prepared samples. i–l) Show the height topographic profiles corresponding to the lines marked in panels e–h), respectively.

unwashed and washed samples was insignificant. The thickness of the dip-coated collagen IV control was only 5 nm.

The stability of the deposited collagen layers in the water flow was evaluated by monitoring the real-time signal change with MP-SPR. Merely small changes in the angle were observed (Supplementary Fig. 3): the highest angle decrease was 0.08°, which is much less than the angle shifts induced by the deposited layers (between 0.9 and 2.7°, Supplementary Table 1). Furthermore, the SPR signals became constant after about 6000 s. In all cases, the largest shifts were detected for unwashed samples and the highest changes were observed for Col IV LS films.

3.4. Human ESC-RPE growth on collagen LS films

Undifferentiated hESCs of both cell lines grew as colonies with defined borders (Supplementary Fig. 4(a)), were positive for pluripotency marker OCT3/4 in IF stainings (Supplementary Fig. 4(b)) and also expressed pluripotency markers *OCT3/4* and *Nanog* on gene expression level. The expression of RPE-specific proteins *RPE65* and *TYR* was negative for the undifferentiated cells (Supplementary Fig. 4(c)). hESC-RPE cell adhesion and maturation on LS films was evaluated with light microscopy imaging, immunofluorescent staining, gene expression analysis and western blotting after 42 days of culture (Fig. 4). By this time point, polarization and correct localization of RPE specific proteins is usually achieved [27]. Both investigated hESC-RPE cell lines had formed confluent and uniform RPE monolayer throughout the entire double layer LS films with abundant pigmentation and typical hexagonal RPE cell morphology (Fig. 4(a,b)). Furthermore, the hESC-RPE cells on LS films formed more uniform and smoother epithelium compared to the dip-coated controls (Supplementary Fig. 5). hESC-RPE cells from both used cell lines showed expression of Na^+/K^+ATPase on the apical membrane, demonstrating polarization of the formed epithelia (Fig. 4(c)). Moreover, hESC-RPE cells were positive for mature RPE-related proteins bestrophin, CRALBP, MITF, MERTK and RPE65 (Supplementary Fig. 6) on all investigated substrates.

Gene expression analysis confirmed the expression of mature RPE markers *BEST*, *MITF*, *PEDF*, *RPE65* and *TYR* on double layer LS films as well as on controls (Fig. 4(d)). Furthermore, there was no expression of the pluripotency marker *OCT3/4* in cells on double layer LS films and on dip-coated controls (Supplementary Fig. 7). However, hESC-RPE cells on double layer LS films showed increased gene expression of *RPE65* compared to the dip-coated control samples in qPCR analysis (Fig. 4(e)). The *RPE65* expression on LS films increased up to 2.1-fold in Regea 08/023 hESC-RPE cells, whereas 2.4-fold expression was seen with Regea 11/013 hESC-RPE cells. However, the increase in expression level of *RPE65* was significantly higher on LS film only with Regea 08/023 hESC-RPE cells ($p < 0.05$). Similar trend in RPE65 synthesis was also detected in protein expression level with western blot analysis. In both investigated cell lines, hESC-RPE cells on LS films showed higher expression of RPE65

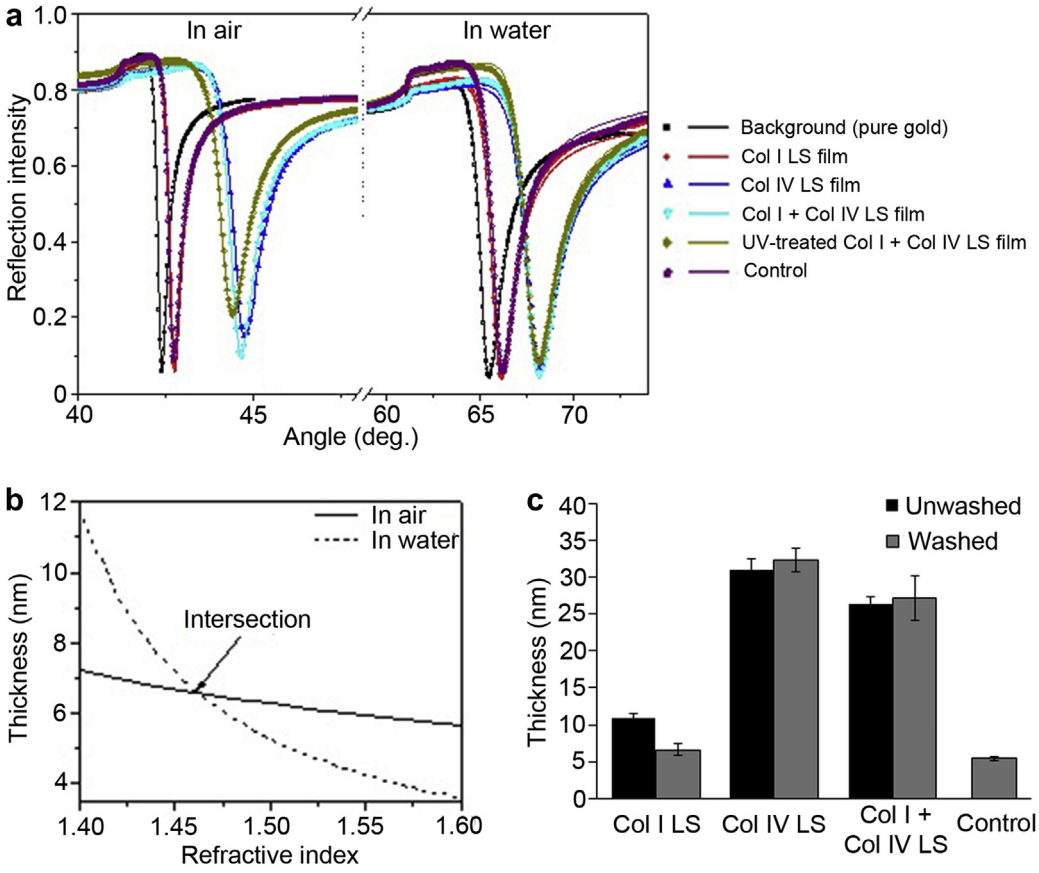

Fig. 3. SPR analysis of LS films. a) Measured MP-SPR angle scans (dots) and the fits (lines) in air and water phase (at 782 nm) of the pure MP-SPR sensor background and the washed deposited collagen LS films on the MP-SPR sensor surfaces. b) Example of the intersection points from the thickness (d) versus refractive index (n) plots for unwashed Col I LS film. c) Thicknesses of deposited collagen layers determined from the two-media (air and water) MP-SPR measurements. The error bars are the standard deviations (SD) from the thicknesses at four different wavelengths.

compared to cells on the dip-coated controls (Fig. 4(f,g)); 3.6- and 1.3-fold expression levels were confirmed for Regea 08/023 and Regea 11/013 hESC-RPE cells on double layer LS films, respectively.

3.5. Barrier properties of hESC-RPE cells on layered collagen LS films

The barrier properties of hESC-RPE cells on double layer LS films were examined with IF staining, TER measurements and permeability studies. hESC-RPE cells on LS films showed uniform expression of tight junction protein ZO-1, while more discontinuous and heterogeneous labeling against ZO-1 was detected on the dip-coated controls (Fig. 5(a,b)). The integrity of hESC-RPE epithelia on double layer LS films was investigated further with TER-measurements following 42 days of culture. In both studied hESC-lines, the TER-values were significantly higher ($P < 0.005$) on LS films compared to hESC-RPE cells grown on dip-coated controls (Fig. 5(c)). With Regea 08/023 hESC-RPE cells, measured TER-values reached 2.4 ± 0.6 −fold on LS films compared to the controls. Similar increase in TER-values was seen with Regea 11/013 hESC-RPE cells with 2.0 ± 0.4-fold higher relative TER on LS films.

Junctional integrity of hESC-RPE cells was assessed by measuring the flux of 700 Da fluorescent markers at the concentration of 0.0065 mM (Fig. 5(d–f)) after 64 days of culture when hESC-RPE at control conditions have usually reached highly polarized structures with tight junctions [27]. In both investigated cell lines, the hESC-RPE on double layer LS films resulted in significantly lower permeability ($p < 0.05$) compared to dip-coated controls, with P_{app}-values of $1.76 \times 10^{-6} \pm 5.78 \times 10^{-7}$ cm^2 s^{-1}and $2.48 \times 10^{-6} \pm 1.99 \times 10^{-6}$ cm^2 s^{-1}for Regea 08/023 and Regea 11/013 hESC-RPE cells, respectively (Fig. 5(d)). P_{app}-values for dip-coated control samples reached for $3.86 \times 10^{-6} \pm 2.49 \times 10^{-6}$ cm^2 s^{-1} for Regea 08/023 hESC-RPE cells and $4.93 \times 10^{-6} \pm 2.09 \times 10^{-6}$ cm^2 s^{-1} for Regea 11/013 hESC-RPE cells. After 5 h exposure time, the cumulative permeability for 700 Da molecules on double layer LS films was 0.10 ± 0.03% for Regea 08/023 hESC-RPE cells and 0.13 ± 0.06% for Regea 11/013 hESC-RPE cells, whereas 0.23 ± 0.04% and 0.28 ± 0.07% were measured for Regea 08/023 and 11/013 hESC-RPE cells on dip-coated controls (Fig. 5(e,f)).

3.6. Functionality of hESC-RPE cells on double layer collagen LS films

The functionality of hESC-RPE cells on double layer LS films was assessed with *in vitro* phagocytosis assay after 56 days of culture. Internalized POS were seen in both investigated cell lines on double layer LS films as well as on dip-coated controls, confirming that the hESC-RPE cells on studied collagen films possess phagocytic activity (Fig. 6(a,b)). It is known that PEDF secretion starts very early phase of RPE maturation [43]. Therefore, the PEDF secretion of hESC-RPE cells grown on double layer LS films was evaluated after 21 days of culture. Major differences were found in PEDF secretion of hESC-RPE cells on double layer LS films compared to the dip-coated controls. hESC-RPE cells on LS films showed highly significant ($p < 0.005$) increase in PEDF secretion with both studied cell lines after 21 days of culture (Fig. 6(e)). PEDF secretion was 1682 ± 167 ng ml^{-1} for Regea 08/023 hESC-RPE cells and 853 ± 146 ng ml^{-1} for Regea 11/013 hESC-RPE cells on LS films, whereas lower PEDF concentrations of 274 ± 118 ng ml^{-1} and

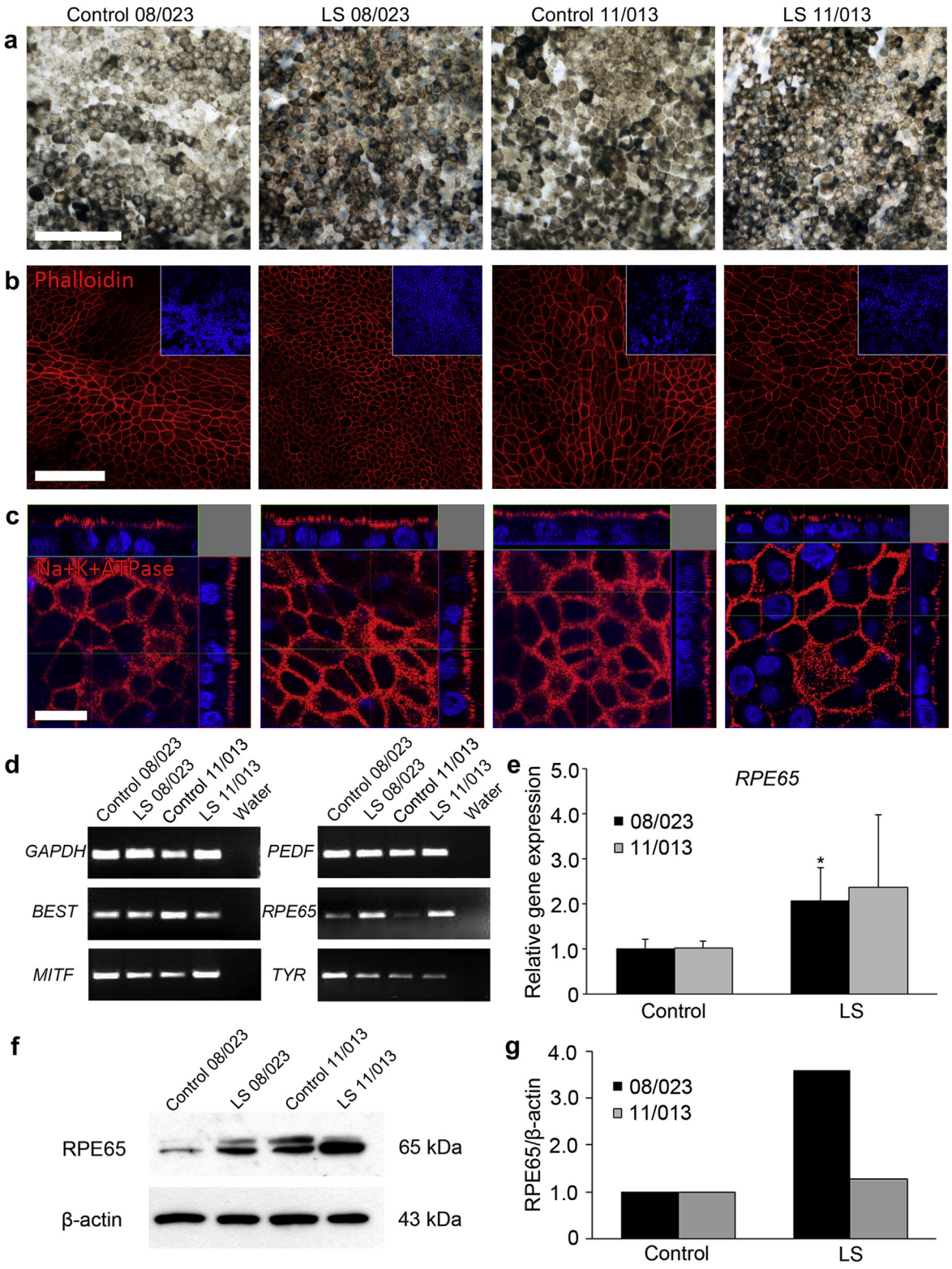

Fig. 4. Human ESC-RPE growth on collagen LS films after 42 days of culture. (a) Bright field images illustrating the degree of pigmentation of hESC-RPE cells on double layer collagen LS films. Immunofluorescent staining of (b) phalloidin (red) showing cell morphology and uniformity of the epithelium on collagen films and (c) Na^+K^+ATPase (red) confirming correct polarization of the epithelial monolayers with both investigated cell lines. The nuclei were counterstained with DAPI (blue). (d) Gene expression of mature RPE markers *BEST*, *MITF*, *PEDF*, *RPE65* and *TYR* on LS films. (e) Relative quantitative real-time polymerase chain reaction (qPCR) analysis of *RPE65*. (f–g) Western blot analysis of RPE65 protein expression of hESC-RPE cells on collagen double layer LS films. *$P < 0.05$ compared to the dip-coated sample. Scale bars (a) and (b) 100 μm and (c) 20 μm.

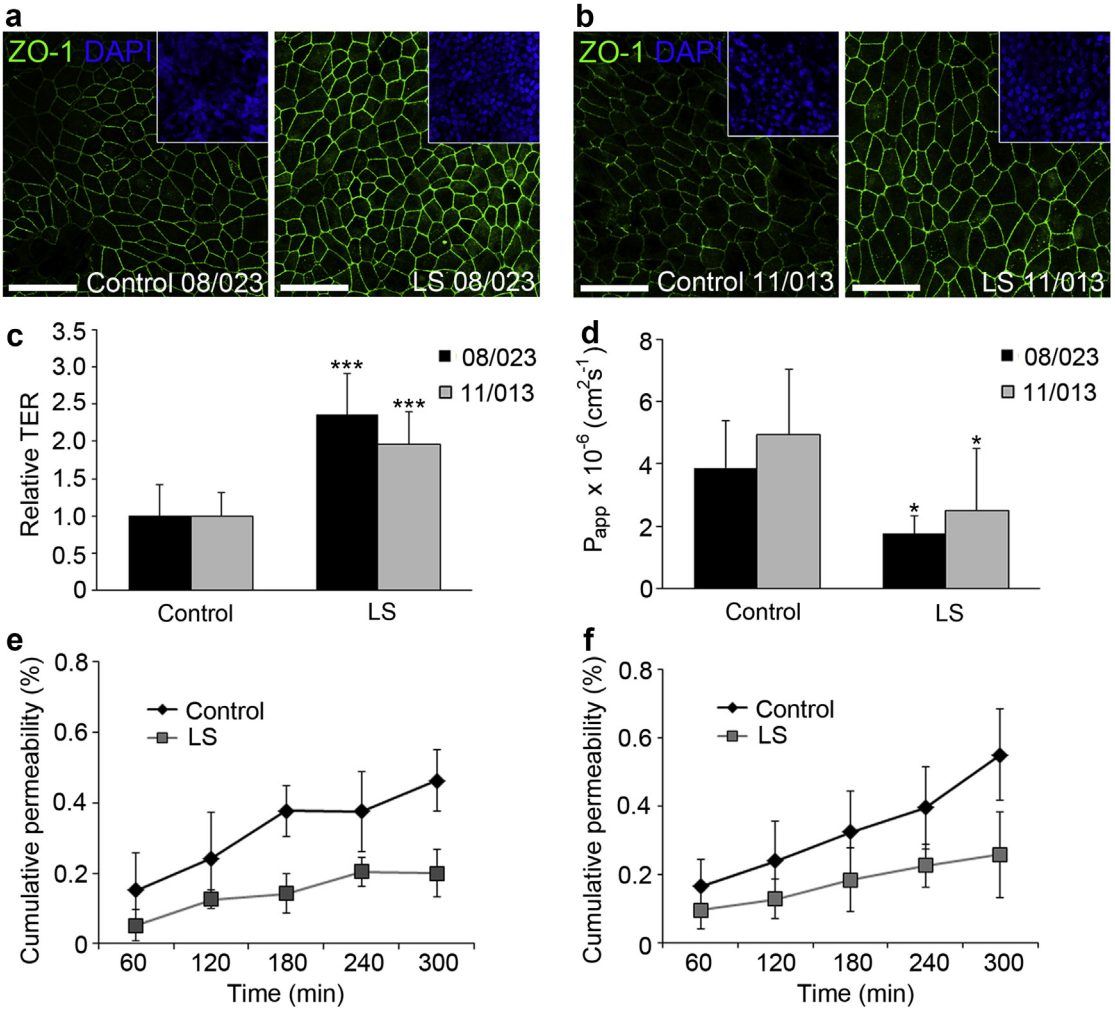

Fig. 5. Barrier properties of hESC-RPE cells on double layer collagen LS film. Expression of tight junction protein zonula occludens 1 (ZO-1) (green) in (a) Regea 08/023 hESC-RPE cells and (b) Regea 11/013 hESC-RPE cells. The nuclei were counterstained with DAPI (blue). Scale bars 50 μm. (c) Relative transepithelial resistance (TER) of hESC-RPE cells on double layer LS films after 42 days of culture. The apparent permeability coefficient P_{app} (d) and the cumulative permeability of small molecular weight fluorescent marker for (e) Regea 08/023 hESC-RPE cells and (f) Regea 11/013 hESC-RPE cells after 64 days of culture. (d) *P < 0.05 and ***P < 0.005 compared to the dip-coated Col IV control sample.

207 ± 155 ng ml^{-1} were measured for Regea 08/023 hESC-RPE cells and Regea 11/013 hESC-RPE cells on controls, respectively.

4. Discussion

The microenvironments where the cells reside in tissues affect the characteristics of cells including cell morphology, polarity and function [44]. Microenvironment of the cells *in vivo* is a combination of multiple complex factors. The surrounding extracellular matrix and the structural environment of the cells is one of them [45]. However, the classic cell culture substrates do not provide the natural environment for the cultured cells *in vitro*, potentially affecting the clinical outcome of cells in tissue engineering applications [7,44]. Furthermore, it is difficult to generate a substrate that possesses similar properties to the tissue environment and that can be produced in a reproducible manner [46]. In this study, we manufactured a microenvironment mimicking the layered structure and composition of the Bruch's membrane from human sourced collagens I and IV for the production of functional hESC-RPE cells. To our awareness, the present study is the first to demonstrate the preparation of oriented and fiber-like collagen type IV LS films as well as culture of hESC-RPE cells on thin layer by layer deposited double layer collagen films with oriented fiber-like structure.

Collagen molecules precipitate out of solution and form fibers at neutral pH [35]. Here, we demonstrated a steady increase in surface pressure upon compression of the interface between the Langmuir trough barriers for both Col I and Col IV LS films. This steady increase in surface pressure during compression indicates that both collagens resided at the air-subphase interface. These results are in good agreement with those previously reported for Col I LB films [30,34,47]. With both collagens, a clear increase in surface pressure was detected after the spreading of the collagens initially dissolved in acidic solution onto the neutral subphase. This increase in surface pressure during stabilization period could be caused by the potassium and phosphate ions in the DPBS subphase, both of which have been shown to affect the fiber formation and structure of the forming collagen fibrils [48]. Based on our observations, this self-assembly of collagens on the air-subphase interface was not an instant process. However, equilibrium was reached after 30 min stabilization period. The higher surface pressure of Col IV after the stabilization period as well as the brighter images seen with BAM during compression indicates that more Col IV remains at the air-subphase interface than that of Col I.

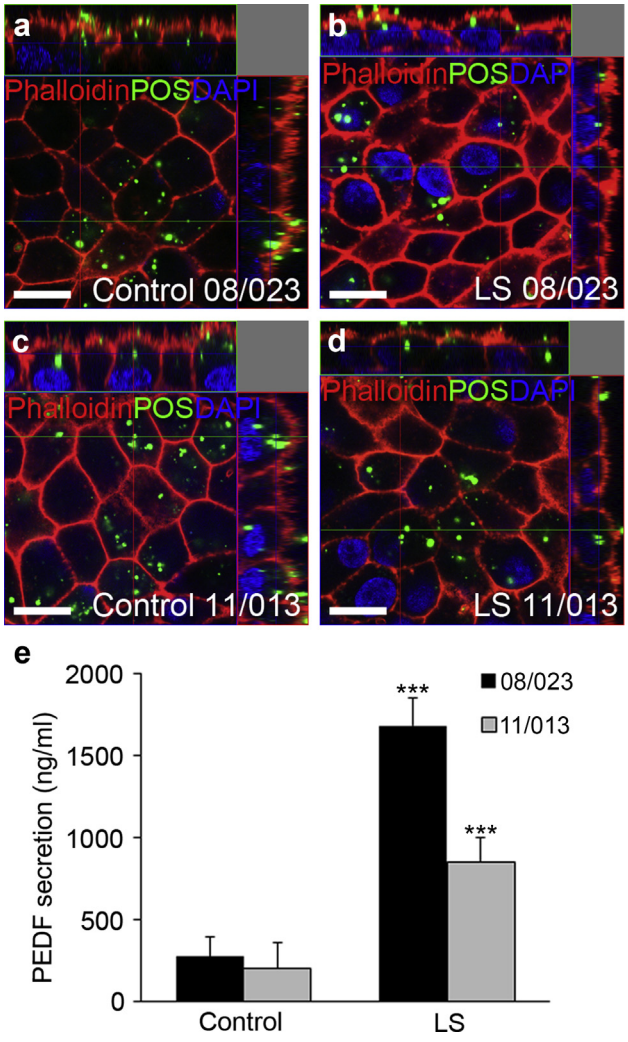

Fig. 6. Functionality of hESC-RPE cells on double layer collagen LS films. The phagocytosis of photoreceptor outer segments (POS) after 56 days of culture (a–d): Regea 08/023 hESC-RPE cells on (a) control and (b) LS film. Regea 11/013 hESC-RPE cells on (c) control and (d) LS films. Filament actin was visualized with phalloidin (red), and the nuclei were counterstained with DAPI (blue). Vertical confocal sections show internalization of POS (green) by hESC-RPE cells on LS films after 2 h culture with porcine POS. Scale bars 10 μm. (e) PEDF secretion of Regea 08/023 and Regea 11/013 hESC-RPE cells on layered LS films after 21 days of culture. ***$P < 0.005$ compared to the dip-coated Col IV control sample.

BAM analysis confirmed the formation of oriented structures during compression. Previously, the collagen type I fibers have been shown to orient parallel to the Langmuir trough barriers [34]. This is in accordance with our findings with Col I as well as with Col IV LS films. In contrast to LS films, no fiber-like oriented networks were detected with Col I and Col IV dip-coated controls in IF stainings, implying that the fiber-like organization of the collagen networks is due to the application of the collagen solution on the air-subphase interface and subsequent compression [33]. The presence of the Col I and Col IV LS films in double layer LS structures was confirmed with SEM and IF analysis, in which the two oriented collagen layers could be distinguished by the different angle between the oriented fiber layers. This is in line with previously reported results for layered Col I LB films [30].

High resolution AFM images allowed detailed analysis of the assembly of collagen molecules into fibrillar structures. The inner collagenous layer of Bruch's membrane consists of 60 nm thick striated fibers of collagen I, III and V [15]. In the present study, the average thickness for the fiber-like structures detected with AFM for Col I LS films was 4.5 nm, suggesting that the prepared film mainly consists of tropocollagen triple-helix structures with collagen I microfibrils [32]. The larger microfibril structures detected with AFM had the diameter of 65 nm, indicating that the manufactured Col I LS films had similar fiber-like structures compared to the native inner collagenous layer of Bruch's membrane. The collagen I diameter reported here is closer to its native equivalent compared to a previous study mimicking the inner collagenous layer of human Bruch's membrane, where electrospun collagen I fibers with diameters ranging from 200 to 500 nm were gained [22]. By comparison, the suprastructure of Col IV LS film resulted in a net-like structure formed by smaller 12.5 nm and larger 140 nm thick fibrils, resembling the sheet-like networks of Col IV found in basement membranes [49].

One important function of Bruch's membrane is allowing the reciprocal flow of small molecular substances through its layered structure [15]. Col I LB films have been previously reported to be non-porous and free of holes [30]. In contrast in the present study, both individual collagen LS layers as well as the double layer LS film were permeable for small molecular weight fluorescent marker. Interestingly, the barrier function was mainly formed by the Col IV LS layer, but the presence of Col I LS layer was clearly required in the double layer LS film to make the structure mechanically durable enough.

In theory, the thickness of the layered LS film should be equal to the sum of the thickness of the washed Col I and Col IV LS films, i.e. 38–39 nm. However, the measured thicknesses of the layered LS films in this study were almost 10 nm lower. Similar result has been established previously in a study for layered Col I LB films, where the mean thickness of monolayer Col I LB films was 20 nm, whereas ten-layer were reported to be 100 nm thick [30]. Likewise, the thicknesses of the washed Col I LS films were lower than the unwashed films. This reduction in expected thickness could be due to a lower binding affinity of the subsequent layers onto the preceding collagen layer governed by differences between the collagen–collagen interactions and those between collagen and the substrate [33,50]. Furthermore, loss of collagen during washing steps between the layer depositions as well as desorption of the salt crystals of the subphase during washing procedure could have also reduced the film thickness. In addition to the change in expected thickness, differences were also seen in the surface topography of the Col IV in the double layer LS film compared to the Col IV monolayer LS film. This indicates that the layer by layer deposited collagens influence the order of them, while deposited as Col I and IV, as is the case in the natural Bruch's membrane. Thus, our study confirms that the first layer affects the structure of the next layer, which is a well-known phenomenon in the field of LB films [51].

The arrangement and orientation of ECM dictate cell size, spreading and cell morphology [52]. LS technique enables low-cost and simple method to produce controlled and oriented substrates for tissue engineering applications [30,34]. In the present study, we hypothesized that the double layer LS films would be superior in supporting the hESC-RPE maturation and functionality compared to the conventional dip-coated controls. The hESC-RPE cells on LS films displayed RPE specific cobblestone morphology, pigmentation, gene expression, correct localization of RPE specific proteins, high degree of polarity, as well as phagocytic activity. Importantly, the hESC-RPE cells showed more homogenous epithelium on double layer LS films compared to the dip-coated controls. Moreover, hESC-RPE cells on LS films demonstrated increased expression of RPE specific protein RPE65 on both gene and protein level in comparison to the dip-coated controls, indicating that the double layer LS films provide more optimal cues for hESC-RPE cell maturation. Previous investigations have found that collagen nanofibers show improved degree of maturation for neural cells against

collagen protein coating [53]. Furthermore, Warnke et al. reported that human primary RPE cells cultured on nanofibrous bovine collagen type I membranes resemble the native human RPE [22]. Surprisingly, even though fibroblasts have been shown to align parallel to the Col I LB films [34,37], such orientation was not detected with hESC-RPE cells on double layer LS films. This data suggests that while Col IV LS films showed oriented structure seen in BAM, the netlike supramolecular organization of the Col IV LS films observed with AFM mimic the native organization of the basement membrane and promotes the formation of homogenous epithelium. Therefore, this study shows that Langmuir–Blodgett technology is a convenient method for the preparation of sophisticated biomimetic structures with intricate architecture, and has a potential in tissue engineering applications.

The principal function of RPE is to form a dynamic barrier between the neural retina and the choroid [54]. Previously, it has been shown that the ECM protein coating affects the barrier properties of the forming hESC-RPE epithelium [27]. The hESC-RPE cells on double layer LS films showed significantly increased TER-values as well as clear reduction in the permeability of small molecular weight particles, indicating that the double layer LS films provide a more favorable microenvironment for the development of barrier properties of hESC-RPE cells compared to the dip-coated controls. Moreover, a significant increase in PEDF secretion, another important hallmark of RPE functionality [55,56], was measured for hESC-RPE cells cultured on LS films against dip-coated controls. In a previous study, NB1-RGN cells grown on collagen-blended LB membranes showed increased interferon-β production [38].

In this study, variation in the functionality of hESC-RPE cells on double layer LS films was detected between the two investigated cell lines. Previously, it has been shown that there are differences between the individual hESC and hiPSC lines [57]. The Regea 08/023 hESC line produces pigmentation faster compared to the Regea 11/013 hESC line, and thus might reach the maturated state of the epithelium slightly earlier. This is the most obvious reason that might cause the differences seen between these two cell lines in this study. Although cell line dependent differences were seen in the maturation state of hESC-RPE cells on double layer LS films, hESC-RPE functionality was superior on the double layer LS films compared to the dip-coated controls regardless of the cell line. Hence, the results reported here demonstrate that double layer collagen LS films offer a more natural and appropriate environment for the production of mature and functional hESC-RPE cells. Extensive cell characterization results in this study suggest that hESC-RPE cells maturated on double layer LS films could be more suitable for sheet transplantation than cells cultivated in standard conditions. However, to be able to conclude the suitability of the double layer LS film for implant production and transplantation purposes, *in vivo* studies need to be conducted in the future.

5. Conclusions

In this study, we demonstrated a LS fabrication technique for generating a biomimetic microenvironment mimicking the structure and organization of native Bruch's membrane from human derived collagens without the use of bioincompatible substances. The prepared thin films showed layered structure with oriented fibers resembling the architecture of the inner collagenous layer and basement membrane of the Bruch's membrane. This study is the first to show successful preparation of organized collagen IV films with fiber-like networks using LS technique as well as the first study to successfully mimic the organized structure and composition of the two uppermost layers of the Bruch's membrane. Furthermore, the prepared double layer collagen LS films were superior in supporting the hESC-RPE maturation and functionality compared to the dip-coated collagen control. Hence, this study demonstrates that the prepared double layer collagen LS films provide a biomimetic microenvironment for the efficient production of hESC-RPE cells *in vitro* potentially increasing their functionality in tissue engineering applications.

Acknowledgments

The authors wish to thank the Finnish funding agency of innovation (Tekes), the Academy of Finland (grant numbers 218050, 272808 and 140357), the Finnish Cultural Foundation, Pirkanmaa Regional fund (grant number 50121465) and the Otto A. Malm Foundation. The funders had no role in study design, data collection and analysis, decision to publish, or preparation of the manuscript. Outi Melin, Hanna Pekkanen and Outi Heikkilä are thanked for technical assistance.

Appendix A. Supplementary data

Supplementary data related to this article can be found at http://dx.doi.org/10.1016/j.biomaterials.2015.02.005.

References

[1] Heino J. The collagen family members as cell adhesion proteins. Bioessays 2007;29:1001–10.
[2] Leitinger B, Hohenester E. Mammalian collagen receptors. Matrix Biol 2007;26:146–55.
[3] Hynes RO. The extracellular matrix: not just pretty fibrils. Science 2009;326:1216–9.
[4] Labat-Robert J. Cell-Matrix interactions, the role of fibronectin and integrins. A survey. Pathol Biol Paris 2012;60:15–9.
[5] Kim DH, Provenzano PP, Smith CL, Levchenko A. Matrix nanotopography as a regulator of cell function. J Cell Biol 2012;197:351–60.
[6] Shapira A, Kim DH, Dvir T. Advanced micro- and nanofabrication technologies for tissue engineering. Biofabrication 2014;6. 020301–5082/6/2/020301. Epub 2014 May 30.
[7] McCarthy JB, Vachhani B, Iida J. Cell adhesion to collagenous matrices. Biopolymers 1996;40:371–81.
[8] Gehrs KM, Anderson DH, Johnson LV, Hageman GS. Age-related macular degeneration–emerging pathogenetic and therapeutic concepts. Ann Med 2006;38:450–71.
[9] Ambati J, Fowler BJ. Mechanisms of age-related macular degeneration. Neuron 2012;75:26–39.
[10] Vazin T, Freed WJ. Human embryonic stem cells: derivation, culture, and differentiation: a review. Restor Neurol Neurosci 2010;28:589–603.
[11] Vaajasaari H, Ilmarinen T, Juuti-Uusitalo K, Rajala K, Onnela N, Narkilahti S, et al. Toward the defined and xeno-free differentiation of functional human pluripotent stem cell-derived retinal pigment epithelial cells. Mol Vis 2011;17:558–75.
[12] Idelson M, Alper R, Obolensky A, Ben-Shushan E, Hemo I, Yachimovich-Cohen N, et al. Directed differentiation of human embryonic stem cells into functional retinal pigment epithelium cells. Cell Stem Cell 2009;5:396–408.
[13] Schwartz SD, Hubschman JP, Heilwell G, Franco-Cardenas V, Pan CK, Ostrick RM, et al. Embryonic stem cell trials for macular degeneration: a preliminary report. Lancet 2012;379:713–20.
[14] Kamao H, Mandai M, Okamoto S, Sakai N, Suga A, Sugita S, et al. Characterization of human induced pluripotent stem cell-derived retinal pigment epithelium cell sheets aiming for clinical application. Stem Cell Rep 2014;2:205–18.
[15] Booij JC, Baas DC, Beisekeeva J, Gorgels TG, Bergen AA. The dynamic nature of Bruch's membrane. Prog Retin Eye Res 2010;29:1–18.
[16] Mollers S, Heschel I, Damink LH, Schugner F, Deumens R, Muller B, et al. Cytocompatibility of a novel, longitudinally microstructured collagen scaffold intended for nerve tissue repair. Tissue Eng A 2009;15:461–72.
[17] Wang HY, Wei RH, Zhao SZ. Evaluation of corneal cell growth on tissue engineering materials as artificial cornea scaffolds. Int J Ophthalmol 2013;6:873–8.
[18] Chajra H, Rousseau CF, Cortial D, Ronziere MC, Herbage D, Mallein-Gerin F, et al. Collagen-based biomaterials and cartilage engineering. Application to osteochondral defects. Biomed Mater Eng 2008;18:S33–45.
[19] Thumann G, Hueber A, Dinslage S, Schaefer F, Yasukawa T, Kirchhof B, et al. Characteristics of iris and retinal pigment epithelial cells cultured on collagen type I membranes. Curr Eye Res 2006;31:241–9.
[20] Thumann G, Viethen A, Gaebler A, Walter P, Kaempf S, Johnen S, et al. The in vitro and in vivo behaviour of retinal pigment epithelial cells cultured on ultrathin collagen membranes. Biomaterials 2009;30:287–94.

[21] Bhatt NS, Newsome DA, Fenech T, Hessburg TP, Diamond JG, Miceli MV, et al. Experimental transplantation of human retinal pigment epithelial cells on collagen substrates. Am J Ophthalmol 1994;117:214–21.
[22] Warnke PH, Alamein M, Skabo S, Stephens S, Bourke R, Heiner P, et al. Primordium of an artificial Bruch's membrane made of nanofibers for engineering of retinal pigment epithelium cell monolayers. Acta Biomater 2013;9:9414–22.
[23] Lu JT, Lee CJ, Bent SF, Fishman HA, Sabelman EE. Thin collagen film scaffolds for retinal epithelial cell culture. Biomaterials 2007;28:1486–94.
[24] Lai JY. The role of bloom index of gelatin on the interaction with retinal pigment epithelial cells. Int J Mol Sci 2009;10:3442–56.
[25] Del Priore LV, Tezel TH, Kaplan HJ. Survival of allogeneic porcine retinal pigment epithelial sheets after subretinal transplantation. Investig Ophthalmol Vis Sci 2004;45:985–92.
[26] Ho TC, Del Priore LV, Kaplan HJ. En bloc transfer of extracellular matrix in vitro. Curr Eye Res 1996;15:991–7.
[27] Sorkio A, Hongisto H, Kaarniranta K, Uusitalo H, Juuti-Uusitalo K, Skottman H. Structure and barrier properties of human embryonic stem cell derived retinal pigment epithelial cells are affected by extracellular matrix protein coating. Tissue Eng A 2013.
[28] Subrizi A, Hiidenmaa H, Ilmarinen T, Nymark S, Dubruel P, Uusitalo H, et al. Generation of hESC-derived retinal pigment epithelium on biopolymer coated polyimide membranes. Biomaterials 2012;33:8047–54.
[29] Rowland TJ, Blaschke AJ, Buchholz DE, Hikita ST, Johnson LV, Clegg DO. Differentiation of human pluripotent stem cells to retinal pigmented epithelium in defined conditions using purified extracellular matrix proteins. J Tissue Eng Regen Med 2012.
[30] Tenboll A, Darvish B, Hou W, Duwez AS, Dixon SJ, Goldberg HA, et al. Controlled deposition of highly oriented type I collagen mimicking in vivo collagen structures. Langmuir 2010;26:12165–72.
[31] Hynes SR, Lavik EB. A tissue-engineered approach towards retinal repair: scaffolds for cell transplantation to the subretinal space. Graefes Arch Clin Exp Ophthalmol 2010;248:763–78.
[32] Friess W. Collagen–biomaterial for drug delivery. Eur J Pharm Biopharm 1998;45:113–36.
[33] Chen Q, Xu S, Li R, Liang X, Liu H. Network structure of collagen layers absorbed on LB film. J Colloid Interface Sci 2007;316:1–9.
[34] Goffin AJ, Rajadas J, Fuller GG. Interfacial flow processing of collagen. Langmuir 2010;26:3514–21.
[35] Jiang F, Horber H, Howard J, Muller DJ. Assembly of collagen into microribbons: effects of pH and electrolytes. J Struct Biol 2004;148:268–78.
[36] Langmuir I. Overturning and anchoring of monolayers. Science 1938;87:493–500.
[37] Pastorino L, Dellacasa E, Scaglione S, Giulianelli M, Sbrana F, Vassalli M, et al. Oriented collagen nanocoatings for tissue engineering. Colloids Surf B Biointerfaces 2014;114:372–8.
[38] Higuchi A, Takanashi Y, Ohno T, Asakura T, Cho CS, Akaike T, et al. Production of interferon-beta by fibroblast cells on membranes prepared by extracellular matrix proteins. Cytotechnology 2002;39:131–7.
[39] Skottman H. Derivation and characterization of three new human embryonic stem cell lines in Finland. Vitro Cell Dev Biol Anim 2010;46:206–9.
[40] Livak KJ, Schmittgen TD. Analysis of relative gene expression data using real-time quantitative PCR and the 2(-delta delta C(T)) method. Methods 2001;25:402–8.
[41] Juuti-Uusitalo K, Delporte C, Gregoire F, Perret J, Huhtala H, Savolainen V, et al. Aquaporin expression and function in human pluripotent stem cell-derived retinal pigmented epithelial cells. Invest Ophthalmol Vis Sci 2013;54:3510–9.
[42] Liang H, Miranto H, Granqvist N, Sadowski JW, Viitala T, Wang B, et al. Surface plasmon resonance instrument as a refractometer for liquids and ultrathin films. Sens Actuators B Chem 2010;149:212–20.
[43] Kozulin P, Natoli R, Bumsted O'Brien KM, Madigan MC, Provis JM. The cellular expression of antiangiogenic factors in fetal primate macula. Invest Ophthalmol Vis Sci 2010;51:4298–306.
[44] Alamdari OG, Seyedjafari E, Soleimani M, Ghaemi N. Micropatterning of ECM proteins on glass substrates to regulate cell attachment and proliferation. Avicenna J Med Biotechnol 2013;5:234–40.
[45] Barthes J, Ozcelik H, Hindie M, Ndreu-Halili A, Hasan A, Vrana NE. Cell microenvironment engineering and monitoring for tissue engineering and regenerative medicine: the recent advances. Biomed Res Int 2014;2014:921905.
[46] Poole K, Khairy K, Friedrichs J, Franz C, Cisneros DA, Howard J, et al. Molecular-scale topographic cues induce the orientation and directional movement of fibroblasts on two-dimensional collagen surfaces. J Mol Biol 2005;349:380–6.
[47] Usha R, Dhathathreyan A, Mandal AB, Ramasami T. Behavior of collagen films in presence of structure modifiers at solid liquid interface. J Polym Sci B Polym Phys 2004;42:3859–65.
[48] Cooper A. Thermodynamic studies of the assembly in vitro of native collagen fibrils. Biochem J 1970;118:355–65.
[49] Kalluri R. Basement membranes: structure, assembly and role in tumour angiogenesis. Nat Rev Cancer 2003;3:422–33.
[50] Narayanan B, Gilmer GH, Tao J, De Yoreo JJ, Ciobanu CV. Self-assembly of collagen on flat surfaces: the interplay of collagen-collagen and collagen-substrate interactions. Langmuir 2014;30:1343–50.
[51] Lotta TI, Laakkonen LJ, Virtanen JA, Kinnunen PK. Characterization of Langmuir-Blodgett films of 1,2-dipalmitoyl-sn-glycero-3-phosphatidylcholine and 1-palmitoyl-2-[10-(pyren-1-yl)decanoyl]-sn-glycero-3-phosphat idylcholine by FTIR-ATR. Chem Phys Lipids 1988;46:1–12.
[52] Li N, Tourovskaia A, Folch A. Biology on a chip: microfabrication for studying the behavior of cultured cells. Crit Rev Biomed Eng 2003;31:423–88.
[53] Yin Y, Huang P, Han Z, Wei G, Zhou C, Wen J, et al. Collagen nanofibers facilitated presynaptic maturation in differentiated neurons from spinal-cord-derived neural stem cells through MAPK/ERK1/2-synapsin I signaling pathway. Biomacromolecules 2014.
[54] Rizzolo LJ. Barrier properties of cultured retinal pigment epithelium. Exp Eye Res 2014.
[55] Strauss O. The retinal pigment epithelium in visual function. Physiol Rev 2005;85:845–81.
[56] Steele FR, Chader GJ, Johnson LV, Tombran-Tink J. Pigment epithelium-derived factor: neurotrophic activity and identification as a member of the serine protease inhibitor gene family. Proc Natl Acad Sci U S A 1993;90:1526–30.
[57] Toivonen S, Ojala M, Hyysalo A, Ilmarinen T, Rajala K, Pekkanen-Mattila M, et al. Comparative analysis of targeted differentiation of human induced pluripotent stem cells (hiPSCs) and human embryonic stem cells reveals variability associated with incomplete transgene silencing in retrovirally derived hiPSC lines. Stem Cells Transl Med 2013;2:83–93.

TISSUE ENGINEERING: Part A
Volume 21, Numbers 17 and 18, 2015

DOI: 10.1089/ten.tea.2014.0640

termis
Tissue Engineering
& Regenerative Medicine
International Society

ORIGINAL ARTICLE

Surface Modified Biodegradable Electrospun Membranes as a Carrier for Human Embryonic Stem Cell-Derived Retinal Pigment Epithelial Cells

Anni Sorkio, MSc,[1,*] Patrick J. Porter, PhD,[2,*] Kati Juuti-Uusitalo, PhD,[1] Brian J. Meenan, PhD,[2] Heli Skottman, PhD,[1] and George A. Burke, PhD[2]

Human embryonic stem cell-derived retinal pigment epithelial (hESC-RPE) cells are currently undergoing clinical trials to treat retinal degenerative diseases. Transplantation of hESC-RPE cells in conjuction with a supportive biomaterial carrier holds great potential as a future treatment for retinal degeneration. However, there has been no such biodegradable material that could support the growth and maturation of hESC-RPE cells so far. The primary aim of this work was to create a thin porous poly (L-lactide-co-caprolactone) (PLCL) membrane that could promote attachment, proliferation, and maturation of the hESC-RPE cells in serum-free culture conditions. The PLCL membranes were modified by atmospheric pressure plasma processing and coated with collagen IV to enhance cell growth and maturation. Permeability of the membranes was analyzed with an Ussing chamber system. Analysis with scanning electron microscopy, contact angle measurement, atomic force microscopy, and X-ray photoelectron spectroscopy demonstrated that plasma surface treatment augments the surface properties of the membrane, which enhances the binding and conformation of the protein. Cell proliferation assays, reverse transcription–polymerase chain reaction, indirect immunofluoresence staining, trans-epithelial electrical resistance measurements, and *in vitro* phagocytosis assay clearly demonstrated that the plasma treated PLCL membranes supported the adherence, proliferation, maturation and functionality of hESC-RPE cells in serum-free culture conditions. Here, we report for the first time, how PLCL membranes can be modified with atmospheric pressure plasma processing to enable the formation of a functional hESC-RPE monolayer on a porous biodegradable substrate, which have a potential as a tissue-engineered construct for regenerative retinal repair applications.

Introduction

Irreversible damage of the retinal pigment epithelium (RPE), the polarized cellular monolayer between the retina and the underlying choroidal vasculature, is a fundamental factor in the pathophysiology of age-related macular degeneration (AMD). AMD is the leading cause of blindness in the elderly population worldwide[1] and phenotypically it can be divided into two main forms: dry (atrophic) and wet (exudative) type.[2] Currently, there are no effective preventative drug therapies nor cure for the dry form of AMD.[3]

A potential alternative therapeutic strategy for the treatment of AMD is the replacement of the dysfunctional RPE cells with a population of healthy cells.[4–6] Human embryonic stem cells (hESCs) represent an attractive cell source for these transplantation therapies owing to their limitless supply and ability to differentiate toward functional RPE cells.[7–10] Cell transplants of hESC-derived RPE (hESC-RPE) cells are currently used in clinical trials for the treatment of the dry AMD and related conditions such as Stargardt's disease.[5,6]

Bruch's membrane is a complex semi-permeable barrier located between the RPE and the choroid that ensures the healthy homeostasis of the retina and provides a structural support for the attachment, migration, and differentiation of RPE cells.[11] The natural aging process and the pathology of retinal diseases, such as AMD, have been shown to have a detrimental effect on the structure and function of the Bruch's membrane.[12] Previous studies have demonstrated that a potential treatment for AMD involving the delivery of RPE cells

[1]BioMediTech, University of Tampere, Tampere, Finland.
[2]Nanotechnology and Integrated Bioengineering Centre (NIBEC), School of Engineering, University of Ulster, Newtownabbey, Northern Ireland.
*These authors equally contributed to this work.

in suspension into the subretinal space on an aged or damaged Bruch's membrane showed poor RPE cell functionality and viability.[13,14] Hence, the use of a ''tissue engineering'' approach, whereby a biomaterial polymer substrate provides a support for the delivery of functional RPE to subretinal space, could improve surgical handling and cell survival and enhance cellular function and organization.[15,16]

A number of natural and synthetic biomaterials have been examined previously as potential delivery systems for the transplantation of RPE cells.[17–23] An approach where hiPSC-RPE cell sheets have been developed without an artificial scaffold has been also introduced.[24,25] Yet, it still needs to be proven that better integration and survival of the cells is achieved using this technique. The choice of synthetic carrier material to direct growth and maturation of human pluripotent stem cells (hPSCs) toward functional RPE is still poorly studied: only inert materials parylene-C and polyimide have been assessed for use as delivery systems with hPSC-RPE cells.[15,26–28]

By using a biodegradable scaffold with a slow *in vivo* degradation period, the scaffold provides physical support during the surgical procedure. While the polymer scaffold slowly degrades, the transplanted cells can conceivably generate their own matrix to replace the defects in the damaged Bruch's membrane. Candidate polymers for the fabrication of biodegradable membranes for RPE cell delivery include poly-α-hydroxy-acid-based polymers, such as poly(L-lactide acid) (PLLA) and poly(caprolactone) (PCL), with tunable properties that include mechanical strength and degradation rate.[29] The combination of both materials as a co-polymer poly(L-lactide-co-caprolactone) (PLCL) therefore offers a range of important features.

Electrospun membranes have been shown to mimic the cues and properties of the extracellular matrix (ECM), providing for transportation of nutrients and metabolic waste.[30] In a previous study, an electrospun PLCL fiber sheet showed elastic properties,[31] which are in a similar range as reported for native Bruch's membrane[32] therefore making it an attractive choice as a scaffold for subretinal implantations. Human RPE cells,[18,19] human fetal RPE cells,[21,33] and the immortalized cell line, ARPE-19[16] have been previously cultured on various polymeric electrospun membranes. To our knowledge, the culturing of clinically relevant hESC-RPE cells on a biodegradable porous carrier for cell transplantation therapies has not been previously assessed.

In this work we studied a thin electrospun PLCL membrane surface modified with dielectric barrier discharge (DBD) plasma processing technique as a carrier for the hESC-RPE cells for retinal repair applications in serum-free conditions. The structure and properties of the membranes; effects of DBD plasma treatment on the chemical and physical surface properties of the thin electrospun PLCL membranes; and the nature and scale of hESC-RPE cell attachment, proliferation, and maturation on various samples are reported.

Materials and Methods

Fabrication of PLCL polymer fibers

A 10% (w/v) solution of PLCL (PURAC) was prepared as a 9:1 v/v chloroform/dimethylformamide (DMF; Sigma-Aldrich) solution. Fibrous membranes were produced in an electrospinning chamber (IME Technologies). The polymer solution was fed into the system at a flow rate of 1 mL per hour and a high voltage DC current (18 kV) was applied to the 21 G dispensing needle to achieve the Taylor cone condition. The PLCL fiber membranes were deposited onto glass coverslips mounted on the collector at distance of 15 cm from the syringe tip. The chemical composition of the resulting fibers was confirmed as PLCL by Fourier Transform Infrared Spectroscopy (FTIR) and the (solvent free) purity checked by thermogravimetric analysis (TGA) (data not shown).

DBD plasma treatment

The DBD processing methodology has been described in detail elsewhere.[34–37] In this work two different plasma powers, 500 W and 750 W, were used. The transit speed of all the samples through the active plasma zone was fixed at 0.48 m/s and the number of cycles was 10. The processing conditions employed here are denoted: ES 5/10 for the 500 W, 10 cycle, 0.48 m/s condition, which results in a power density (P_d) of 52.91 W/cm^2, residence time (R) of 0.19 s, and a total dose (D) of 9.92 J/cm^2 and ES 7/10 for the 750 W, 10 cycle, 0.48 m/s condition, which results in a power density (P_d) of 79.37 W/cm^2, residence time (R) of 0.19 s, and a total dose (D) of 14.88 J/cm^2.

Collagen IV coating of electrospun PLCL membranes

Col IV is a major component of Bruch's membrane[11] and has previously been used for the enrichment and maturation of hPSC-RPE.[7,38] In this work, electrospun PLCL membranes were rinsed with Dulbecco's Phosphate Buffered Saline (DPBS) (Lonza Group Ltd.), and immersed in a solution of human placenta Col IV (Sigma-Aldrich) in DPBS at a concentration of 10 μg cm^{-2} over night at 4°C. Before cell seeding, the samples were rinsed twice with DPBS to remove any unbound protein.

Scanning electron microscopy

The diameter and morphology of electrospun PLCL fibers and the membrane thickness were determined by scanning electron microscopy (SEM) (Quanta 3D, FEI) operating at 5 kV. Samples were sputter coated with a thin ($\sim$20 nm) layer of gold, using an Emitech K500X (Quorum Technologies) to reduce charging and image distortion.

Contact angle analysis

Static contact angle (CAM2000, KSV Instrument Ltd.) was used to determine changes in the surface wettability after atmospheric pressure DBD plasma processing. Measurements were taken using glycerol[39] at time points 0.5, 168, and 336 h following treatment. Twenty readings were performed per sample type.

Atomic force microscopy

Atomic force microscopy (AFM) (Nanoscope Dimension 3100; Vecco) was used to analyze topographical changes on individual electrospun PLCL fibers before and after atmospheric pressure DBD plasma treatment. The instrument was equipped with a TESPA silicon tip (Vecco) mounted on a

cantilever of stiffness of 40 N/m^{-1}, operating at a resonance of 300 Hz and a scan rate of 1 Hz. Images were acquired in tapping mode and all samples were analyzed over a scan area of $2\,\mu m \times 1\,\mu m$ at a resolution of 512×512 pixels. Pseudo–3D false color images and associated line profiles were acquired using the Nanoscope 6.11r1 Software (Veeco). Three scans of each individual fiber were obtained for each experimental group and root mean square average (Rq) values were calculated.

X-ray photoelectron spectroscopy

A Kratos Axis Ultra DLD spectrometer (Kratos) was used to obtain X-ray photoelectron spectroscopy (XPS) spectra from the various sample surfaces of interest before and after atmospheric pressure DBD plasma treatment and after Col IV adsorption. Spectra were collected using monochromated AlKα X-ray source generating photons of energy 1486.6 eV. The vacuum condition was maintained at $<5 \times 10^{-8}$ torr during spectral analysis. Three separate areas of $\sim 300\,\mu m \times 700\,\mu m$ were analyzed per sample. Wide energy survey scans (WESS) were obtained in the binding energy range 0–1300 eV, at pass energy 160 eV. Corresponding high resolution spectra of the C1s, O1s, and as appropriate N1s regions were collected at pass energy 20 eV. Binding energies were corrected for surface charging by setting the adventitious hydrocarbon C1s peak to 285.0 eV.

The Kratos vision processing software was used to obtain quantitative data from the high resolution spectra and to carry out spectral peak fitting. In all cases, a linear background subtraction was applied to the spectra. Peak fitting of the C1s spectral envelope was carried out to take account of the 70PLA/30PCL co-polymer percentage ratio.

Permeability study

The ability of electrospun PLCL membranes to act as semipermeable barrier was assessed by measuring the flux of a small molecular weight (700 Da) Alexa Fluor® 568 Hydrazide sodium salt (Life Technologies) at a concentration of 0.0065 mM. The study was carried out in an Ussing chamber system (Physiologic Instruments) with P2300 chambers and P2307 sliders and in culture medium without KnockOut™ Serum Replacement (KO-SR). Samples were taken from the receptor chamber at 60, 120, 180, and 240 min. The fluorescence of the samples was analyzed using the Wallac Victor2™ 1420 Multilabel counter (Perkin Elmer-Wallace) at 590 nm excitation and 642 nm emission wavelengths.

The diffusion was characterized by calculating the apparent permeability coefficient (P_{app}, $cm^2 s^{-1}$) as $P_{app} = dC/dt/(60C_0A)$, where dC/dt is the slope of the linear portion of the permeability curve, C_0 is the initial concentration in the donor chamber, and A is the exposed surface area of the RPE monolayer (0.031 cm^2).

Human embryonic stem cell-derived retinal pigment epithelium cells

Two hESC lines, Regea 08/023 (46, XY) and Regea 11/013 (46, XY), were used in this study. Cell lines were derived as described previously.[40] Undifferentiated hESCs were maintained and differentiated into RPE cells in serum-free culture conditions as also previously described, with the modification of enzymatically passaging the undifferentiated hESCs using TrypLE Select (Invitrogen) onto fresh feeder cells at 10-day intervals.[7,41]

After 50–98 days of differentiation in suspension culture, the pigmented areas of the floating aggregates were manually cut. These pigmented cell clusters were dissociated with 1× Trypsin-EDTA (Lonza) and replated into Col IV coated 24-well culture plates (Corning® CellBIND®, Corning, Inc.) for enrichment. The pigmented cells were grown in adherent cultures for 180–210 days, during which the cells were replated once more onto fresh Col IV coated 24-well plates.

Electrospun PLCL films were cleaned in 70% ethanol for 1 h at room temperature and repeatedly washed with DPBS. For seeding on electrospun PLCL membranes, with and without Col IV coating, the cells were dissociated with TrypLE Select (Invitrogen). The cells were filtered through BD Falcon cell strainer (BD Biosciences) and seeded onto the fiber membranes at a density of 1.5×10^5 cells cm^2.

Analysis of cell number

The attachment and proliferation of hESC-RPE cells on untreated and DBD plasma-treated electrospun fibers with the Col IV adlayer were determined by cell counts after 7 and 42 days in culture. To get an objective estimation of the cell numbers on the samples four randomly chosen areas of each sample with DAPI-stained nuclei were captured with AxioScope A1 fluorescence microscope using a 10× objective lens. Two samples were analyzed for each experimental condition at both time points. The data for the cell number analysis was collected from two individual experiments, that is, a total 4 samples and at least 16 low magnification images. Representative low magnification images used for cell count analysis for each sample are shown in Supplementary Fig. S1 (Supplementary Data are available online at www.liebertpub.com/tea). The number of cells in each image was determined using Image J Image Processing and the Cell Counter plugin.

Proliferation assay

The proliferation of hESC-RPE cells on the various PLCL surfaces was studied after 21 days in culture using the alamarBlue® assay (Invitrogen) according to the manufacturer's instructions. The measured values were normalized against the untreated samples (relative cell proliferation for untreated samples equals 1).

Transepithelial resistance measurements

Transepithelial resistance (TER) of hESC-RPE monolayers formed after 42 days in culture on the Col IV coated untreated and plasma-treated PLCL membranes was determined as a measure of the integrity and barrier properties of the epithelium. Samples were clamped to a P2307 slider (Physiologic Instruments) before being placed in a custom-made Teflon chamber, as described previously.[41] Measurements were carried out in DBPS with a Millicell electrical resistance system equipped with a volt-ohm meter (Merck Millipore). TER values were calculated by subtracting the value for a similarly treated substrate without cells from the results. Values are reported in ohms per unit area ($\Omega\ cm^2$). TER values were obtained as an average of three samples of each membrane from three individual experiments. The data presented were

normalized to the value determined for the untreated PLCL fiber membranes.

Gene expression analysis

The expression of genes coding for the RPE-specific proteins bestrophin (*BEST*), microphthalmia-associated transcription factor (*MITF*), pigment epithelium-derived factor (*PEDF*), retinal pigment epithelium specific protein 65 kDa (*RPE65*), tyrosinase (*TYR*), and pluripotency marker octamer-binding transcription factor (*OCT*)3/4 was assessed with reverse transcription–polymerase chain reaction (RT-PCR) for hESC-RPE cells on the Col IV-coated PLCL fibers surfaces after 42 days in culture. Glyceraldehyde 3-phosphate dehydrogenase (*GAPDH*) was used as an endogenous control.

RNA was extracted using NucleoSpin RNA II kits (Macherey-Nagel, GmbH & Co) in accordance with the manufacturer's instructions. hESC-RPE cells grown on Col IV-coated cell culture inserts (Millipore) were used as a positive control and water was included as a control in RT-PCR analysis to detect any impurities in the reagents and procedure. Undifferentiated hESCs were used as a negative control. A detailed account of the RT-PCR protocol and primer sequences have been published previously.[7]

Immunofluorescence

Protein expression and localization on Col IV coated untreated and DBD plasma-treated electrospun PLCL fibers were further investigated using immunofluorescence staining after 42 days in culture as described previously.[38] The following primary antibodies and concentrations were used: bestrophin (1:200), cellular retinaldehyde-binding protein (CRALBP) (1:200), anti-Na^+/K^+ATPase (1:200), microphthalmia-associated transcription factor (MITF) (1:350) (all from Abcam), Mer Tyrosine Kinase (MERTK) 1:50 (Abnova), and zonula occludens 1 (ZO-1) (1:200) (Invitrogen). Alexa Fluor fluorescent-conjugated secondary antibodies (Molecular Probes, Life Technologies) were diluted at 1:800.

In addition, phalloidin-tetramethylrhodamine B isothiocyanate (Sigma-Aldrich) was used for labeling filamentous actin. Images of stained cells were taken with an AxioScope A1 fluorescence microscope (Carl Zeiss) or an LSM 700 confocal microscope (Carl Zeiss) using a 63× oil immersion objective lens. Images were edited using ZEN 2011 Light Edition (Carl Zeiss) and Adobe Photoshop CS4.

Phagocytosis

The phagocytic properties of hESC-RPE monolayers on Col IV coated untreated and DBD plasma-treated electrospun PLCL fibers after 92 days in culture were studied using isolated porcine photoreceptor outer segments (POS). The isolation of POS has been described previously.[7] Human foreskin fibroblasts (CRL-2429TM; ATCC) were used as a negative control.

For the *in vitro* phagocytosis assay, POS were labeled with fluorescein isothiocyanate (FITC) (0.04 μg μL^{-1}; Sigma-Aldrich) in 0.1 M $NaHCO_3$ (pH 9) for 1 h at RT, washed thrice with PBS, and resuspended in culture medium supplemented with 10% fetal bovine serum (FBS; Sigma-Aldrich). The hESC-RPE cells on the Col IV-coated electrospun PLCL membranes were then incubated with POS for 2 h at 37°C. Subsequently, the cells were washed twice with PBS and fixed with 4% paraformaldehyde for 10 min at RT. Cells were permeabilized using 0.1% Triton X-100 for 10 min at RT followed by repeated PBS washings. Filamentous actin was stained with phalloidin (Sigma-Aldrich) by incubating for 30 min at RT in the solution and washing in PBS. The nuclei were counterstained with DAPI present in the mounting media.

In addition, Regea 08/023 hESC-RPE cell controls were blocked with anti-MERTK antibody to demonstrate that the POS phagocytosis experiment is MERTK dependent and RPE-specific. For blocking, the samples were incubated with anti-MERTK antibody (1:40) for 1 h at 37°C prior applying the POS and POS incubation for 2 h. The images of the hESC-RPE cells with internalized POS fragments were taken using a confocal microscope (LSM 700, Carl Zeiss, 63× oil immersion objective lens).

Statistics

The Mann–Whitney *U*-test was used for determining statistical significance of cell number counts and TER-values. One-way analysis of variance (ANOVA) and Tukey's multiple comparison test were used to assess whether the data obtained were significantly different between samples. The mean values of various data are presented ± standard error. *p*-values ≤0.05 were considered statistically significant. All statistical analysis was carried out using the data analysis software package Prism (GraphPad Software, Inc.) or IBM SPSS Statistics software.

Results

Structure and surface morphology of electrospun PLCL membranes

SEM images for the untreated material showed an average fiber diameter of 3.1 ± 0.14 μm and an average pore size of the upper layer of the matrix of 58.3 ± 12 μm (Fig. 1A). The membranes had an unaligned fiber orientation over an average membrane thickness of 43.2 ± 1.95 μm. The P_{app} for small molecular weight (700 Da) molecule was $5.02 \times 10^{-4} \pm 2.1 \times 10^{-4}$ cm^2s^{-1} for the untreated electrospun PLCL membrane. Similar P_{app} of $4.12 \times 10^{-4} \pm 2.01 \times 10^{-4}$ cm^2s^{-1} was measured for the ES 5/10-treated PLCL membranes, whereas slightly lower P_{app} value of $1.82 \times 10^{-4} \pm 2.87 \times 10^{-6}$ cm^2s^{-1} was reached for ES 7/10 PLCL membranes.

The untreated PLCL membrane fibers appeared quite smooth, whereas the treated fibers clearly displayed surface features (Fig. 1B). In addition, the DBD plasma treatment had no significant effect on the fiber diameter (Fig. 1C). AFM data confirmed that the plasma treatment alters the topography of the PLCL electrospun fiber surface with the root mean square average surface roughness (Rq) values increasing from 18.00 ± 2.46 nm for the untreated sample to 31.40 ± 3.93 nm for the ES 5/10 and 24.93 ± 1.13 nm for ES 7/10-treated PLCL membranes (Fig. 1D, E).

A statistically significant reduction in contact angle ($p < 0.001$) was recorded at 0.5 h post DBD plasma treatment (Fig. 2A). The lowest average contact angle measured was 96 ± 1° for sample ES 7/10, while the ES 5/10 value was 105 ± 1°, which compare to the untreated sample value of 138 ± 1°. Relaxation (hydrophobic recovery) occurred for all DBD-processed samples with contact angle increasing over

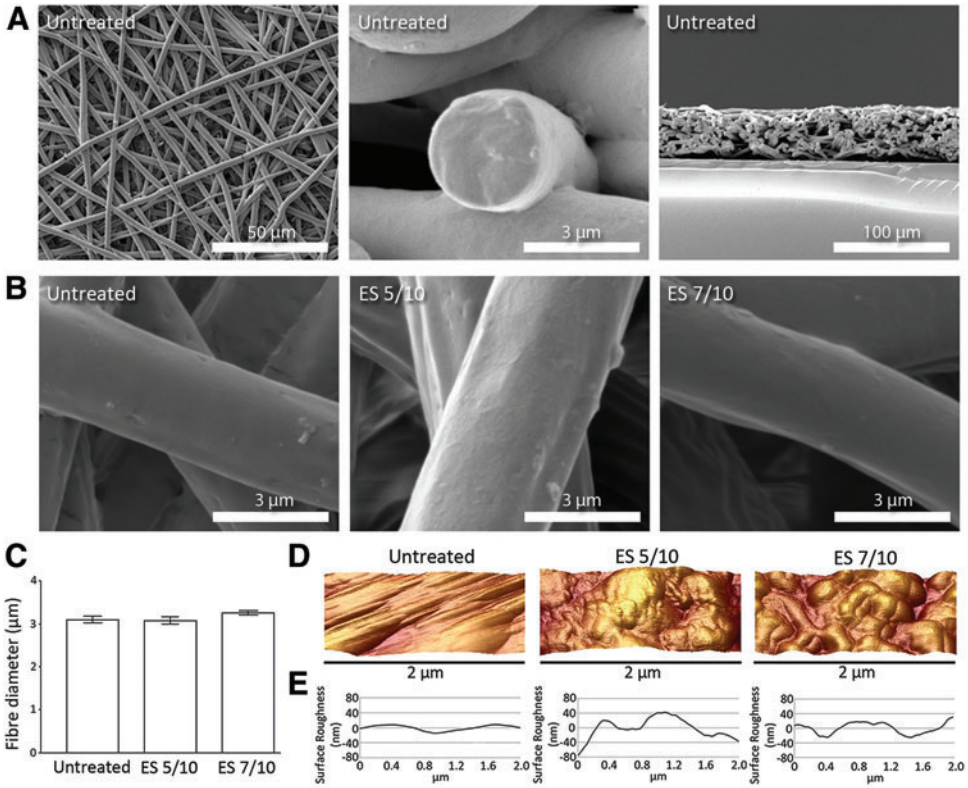

FIG. 1. Scanning electron microscopy (SEM) micrographs of **(A)** untreated poly (L-lactide-co-caprolactone) (PLCL) electrospun membranes, **(B)** untreated and dielectric barrier discharge (DBD) plasma-treated PLCL fiber topography, **(C)** SEM-derived average fiber diameter measurements of PLCL electrospun membranes, atomic force microscopy **(D)** 3D images, and **(E)** line profiles for fiber topography before and after atmospheric pressure plasma treatment. Color images available online at www.liebertpub.com/tea

the study period. However, the values did not recover to those of the untreated PLCL fiber indicating a permanent change in surface properties. Contact angle measurements of the Col IV-coated samples showed that DBD plasma treatment before Col IV coating significantly increased fiber wettability when compared with the equivalent untreated sample (Fig. 2B).

Surface chemistry of electrospun PLCL membranes

The atomic concentration (% at. conc.) values and O/C ratios obtained by quantification of the XPS spectral data (Fig. 3) revealed a decrease in carbon content and a significant increase ($p < 0.001$) in oxygen content on the PLCL surfaces after DBD plasma treatment (Table 1). This increase in oxygen content was dependent on the DBD plasma dose administered. XPS scans for the Col IV-coated plasma-treated PLCL samples showed an N1s (Nitrogen) peak associated with the protein layer (Fig. 3B). From the percentage atomic concentration values it can be seen that increasing the DBD plasma dose before Col IV adsorption has a substantial impact on the amount of nitrogen detected with the Col IV-coated ES 5/10 samples displaying significantly lower nitrogen content than Col IV-coated ES 7/10 membranes ($p < 0.05$) (Table 2). The amount of nitrogen on Col IV-coated DBD-treated membranes after both plasma doses was significantly higher compared with Col IV-coated untreated membranes (Table 2).

Distribution of collagen IV on electrospun PLCL membranes

Distribution of Col IV on porous PLCL membranes was assessed with immunofluorescence staining. Col IV adhered to the fibers of all the PLCL membranes under investigation, which was distributed in a uniform manner (Fig. 4).

Cell attachment and proliferation on biodegradable PLCL electrospun membranes

Without additional Col IV coating, hESC-RPE cells did not attach on any of the investigated PLCL membranes (data

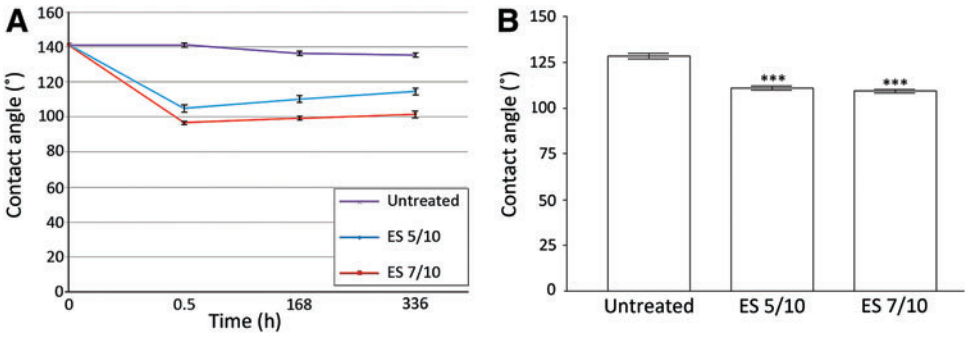

FIG. 2. Contact angle measurements of **(A)** PLCL electrospun membranes over time and **(B)** PLCL electrospun membranes coated with Col IV; *p*-value-< 0.001***. Color images available online at www.liebertpub.com/tea

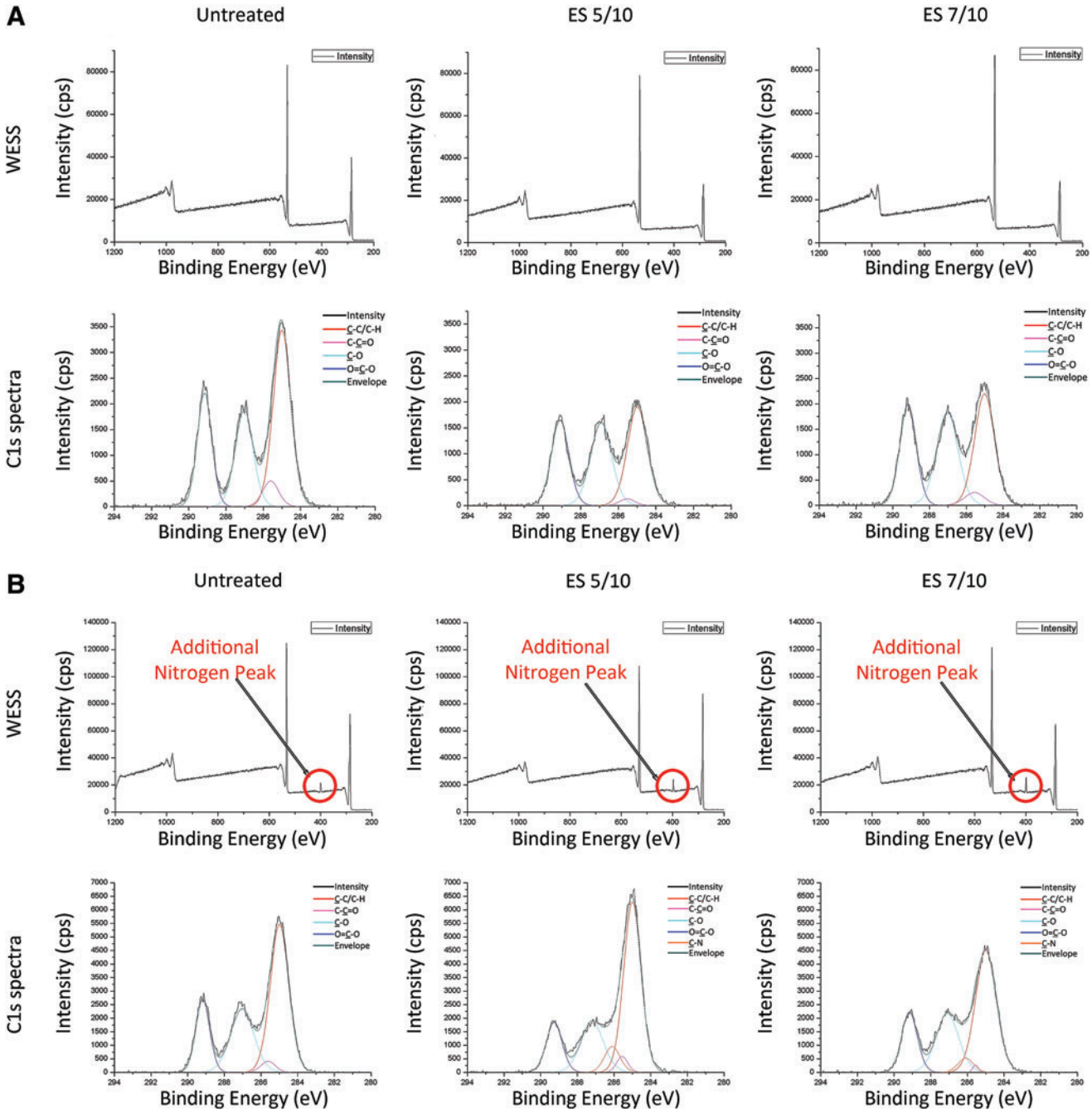

FIG. 3. XPS wide energy survey scan (WESS) and high-resolution C1s spectra for **(A)** electrospun PLCL membranes before and after DBD plasma treatment and **(B)** after coating untreated and plasma-treated surfaces with Col IV. Color images available online at www.liebertpub.com/tea

TABLE 1. % ATOMIC CONCENTRATION OF UNTREATED (CONTROL) AND DBD PLASMA-TREATED ELECTROSPUN PLCL MEMBRANES

Sample	*O1s AC%*	*O=C*	*O-C*	*C1s AC%*	*C-C/C-H*	*C-C=O*	*C-O*	*O=C-O*	*O/C ratio*
Untreated	31.7±0.10	14.5±0.27	17.2±0.18	68.3±0.10	30.5±0.16	3.8±0.22	17.2±0.20	16.8±0.42	0.46
ES 5/10	35.5±0.27	17.9±0.47	17.6±0.61	64.5±0.61	23.9±0.62	2.0±0.52	19.8±0.58	18.8±0.39	0.55
ES 7/10	37.2±0.65	17.9±0.76	19.3±0.30	62.8±0.30	23.2±0.34	2.4±0.19	20.4±0.75	16.8±0.12	0.59

O1s, oxygen; C1s, carbon; DBD, dielectric barrier discharge; PLCL, poly (L-lactide-co-caprolactone).

TABLE 2. % ATOMIC CONCENTRATION OF UNTREATED (CONTROL) AND DBD PLASMA-TREATED PLCL ELECTROSPUN MEMBRANES COATED WITH A COL IV LAYER

Sample	*O1s AC%*	*O=C*	*O-C*	*N1s AC%*	*N=C*	*C1s AC%*	*C-C/C-H*	*C-C=O*	*C-O*	*O=C-O*	*C-N*
Untreated	27.78±0.37	14.95±0.39	12.84±0.76	2.22±0.09	2.22±0.09	69.99±0.29	35.33±0.89	2.51±0.25	19.32±0.39	12.83±0.25	0.00
ES 5/10	25.10±0.48	15.50±0.32	9.60±0.41	3.29±0.20	3.29±0.20	71.47±0.62	37.87±0.70	2.35±0.02	15.50±0.17	10.88±0.21	4.87±0.26
ES 7/10	27.24±1.24	15.61±1.35	11.63±0.17	4.15±0.13	4.15±0.13	68.50±1.21	35.42±1.77	0.60±0.15	17.08±0.64	12.33±0.28	3.08±0.16

N1s, nitrogen.

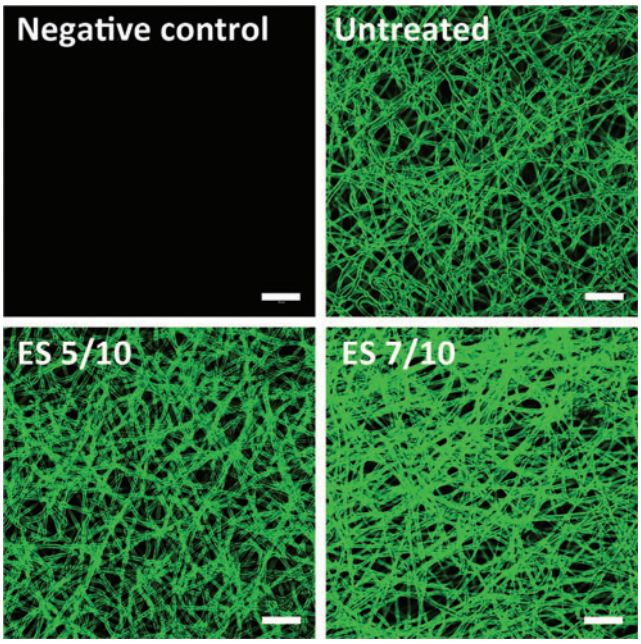

FIG. 4. Confocal microscopy images of immunostained Col IV-coated PLCL electrospun membranes. Scale bar 50 μm. Color images available online at www.liebertpub.com/tea

not shown). After the 7-day culture period, a significant ($p < 0.005$) increase was detected in hESC-RPE cell attachment on the Col IV-coated DBD plasma-treated PLCL membranes compared with the number on the untreated Col IV-coated samples in both investigated cell lines (Fig. 5A). The number of Regea 08/023 hESC-RPE cells present on ES 5/10 Col IV-coated membrane was higher ($p < 0.05$) compared with the number on ES 7/10 Col IV-coated membrane, whereas no significant difference was observed between the DBD plasma treatments with Regea 11/013 hESC-RPE cells.

After 42 days in culture, cell numbers were significantly higher on Col IV-coated DBD plasma-treated PLCL fiber membranes when compared with the untreated Col IV-coated sample (Fig. 5B). However, there was no difference between the numbers detected on the ES 5/10 and ES 7/10 Col IV-coated DBD plasma-treated membranes at this time point.

The results obtained from the cell proliferation analysis with alamarBlue® assay after 21 days in culture were consistent with the cell count data; higher cell proliferation was measured for both hESC-derived RPE cell lines on all of the Col IV-coated DBD plasma-treated samples compared with that on the Col IV-coated untreated membrane (Fig. 5C).

hESC-RPE cell maturation on biodegradable electrospun membranes

After 42 days in culture, the hESC-RPE cells on both the ES 5/10 and ES 7/10 Col IV-coated samples had formed a confluent and uniform RPE monolayer with abundant pigmentation and a typical hexagonal RPE cell morphology (Fig. 5D, E). By contrast, the hESC-RPE cells on Col IV-coated

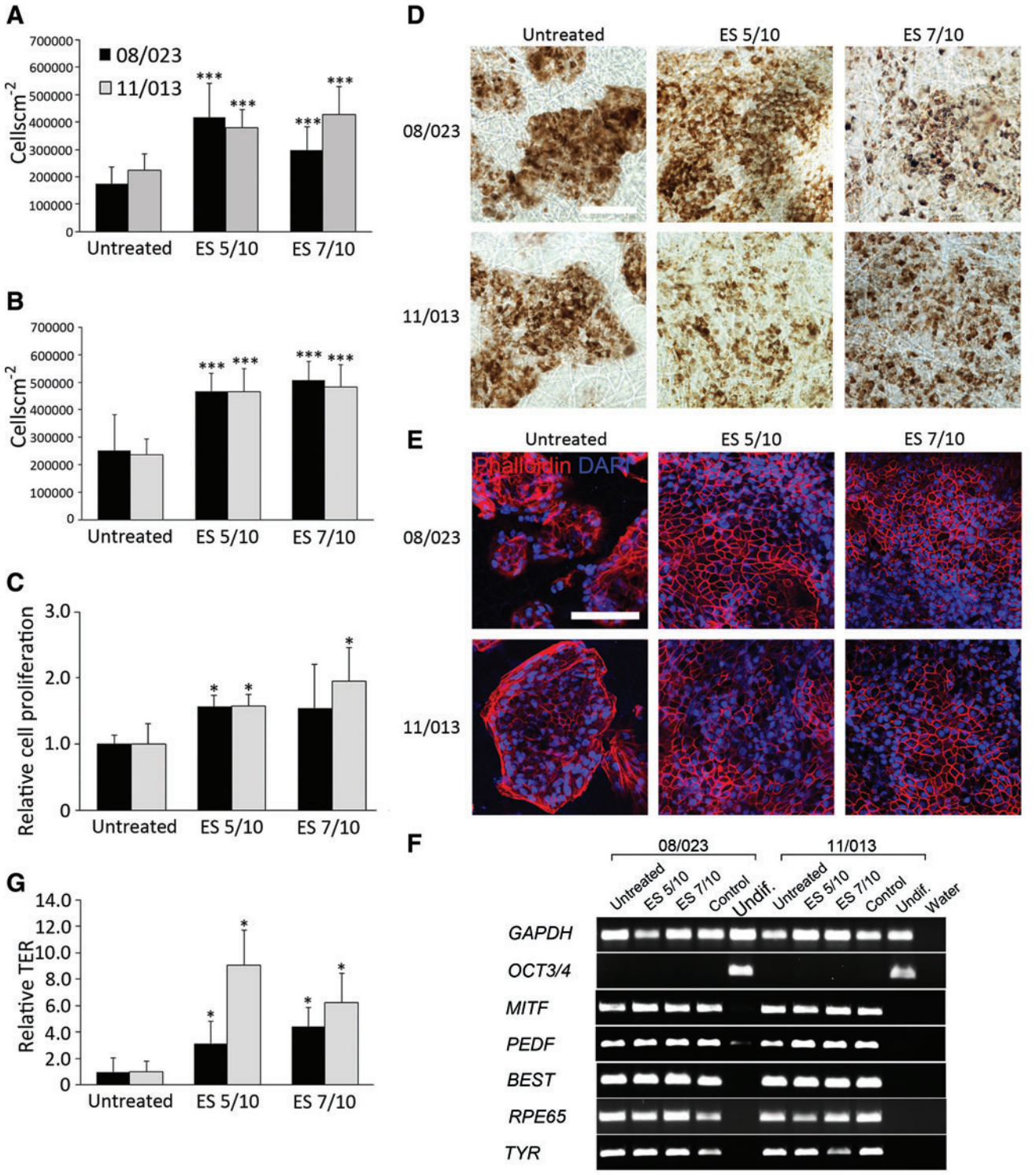

FIG. 5. Cell counts of hESC-RPE on electrospun untreated and atmospheric plasma-treated PLCL membranes with Col IV layer after **(A)** 7 days and **(B)** 42 days in culture. **(C)** Relative cell proliferation after 21 days in culture. **(D)** Light microscope images illustrating the degree of pigmentation on electrospun PLCL membranes. **(E)** Immunofluorescent staining of phalloidin showing cell morphology and uniformity of the epithelium on investigated substrates. Scale bars 100 μm. **(F)** Gene expression of mature RPE markers *BEST*, *MITF*, *PEDF*, *RPE65*, *TYR*, and pluripotency marker *OCT3/4* on studied membranes. **(G)** Barrier properties of maturate hESC-RPE cells after 42 days on electrospun PLCL membranes p-value < 0.05* and p-value < 0.005*** compared to untreated electrospun PLCL membrane. Color images available online at www.liebertpub.com/tea

untreated membranes grew as raft-like heterogeneous structures and comprised spherical cell clumps such that confluent layers were not attained during the 42-day culture period (Supplementary Fig. S2A). Gene expression analysis demonstrated the expression of mature RPE markers *BEST*, *MITF*, *PEDF*, *RPE 65*, and *TYR* on all investigated membranes (Fig. 5F). Furthermore, there was no expression of the pluripotency marker *OCT3/4* (Fig. 5F).

The hESC-RPE maturation on Col IV-coated DBD plasma-treated membranes was further examined using immunofluorescence staining.

The hESC-RPE cells on ES 5/10 and 7/10 Col IV-coated membranes showed homogenous expression of the RPE-specific markers MITF (Fig. 6A), bestrophin (Fig. 6B), CRALBP (Fig. 6C), and the tight junction marker ZO-1 (Fig. 6D). hESC-RPE cells on untreated Col IV-coated PLCL membranes expressed bestrophin, CRALBP, and MITF on protein level, however, cells failed to form homogenous monolayer (Supplementary Fig. S2A–D). The tight junction protein ZO-1 was localized on the apical membrane of hESC-RPE cells on Col IV-coated DBD plasma-treated PLCL membranes, which showed positive labeling for CRALBP, indicating that DBD plasma-treated PLCL membranes supported the growth of cells as an adherent RPE monolayer (Supplementary Fig. S3). Furthermore, Na^+/K^+ATPase was expressed on the apical membrane of the cells thereby demonstrating polarization of the epithelium (Fig. 6E).

Functionality of hESC-RPE cells on biodegradable PLCL electrospun membranes

For both hESC lines, the TER-values after 42 days in culture were significantly higher ($p < 0.05$) on the Col IV-coated DBD plasma-treated ES 5/10 and ES 7/10 samples compared with those on the Col IV-coated untreated sample (Fig. 5G). No notable differences were found between the ES 5/10 and 7/10 Col IV-coated electrospun PLCL membranes. Functionality of the hESC-RPE cells on the ES 5/10 and ES 7/10 Col IV samples was further assessed with an *in vitro* phagocytosis assay after 92 days in culture. Internalized POS was seen in both hESC-RPE cell lines on each of the DBD plasma-treated membranes (Fig. 7).

In addition, hESC-RPE cells on the DBD plasma-treated materials showed positive expression of MERTK at the

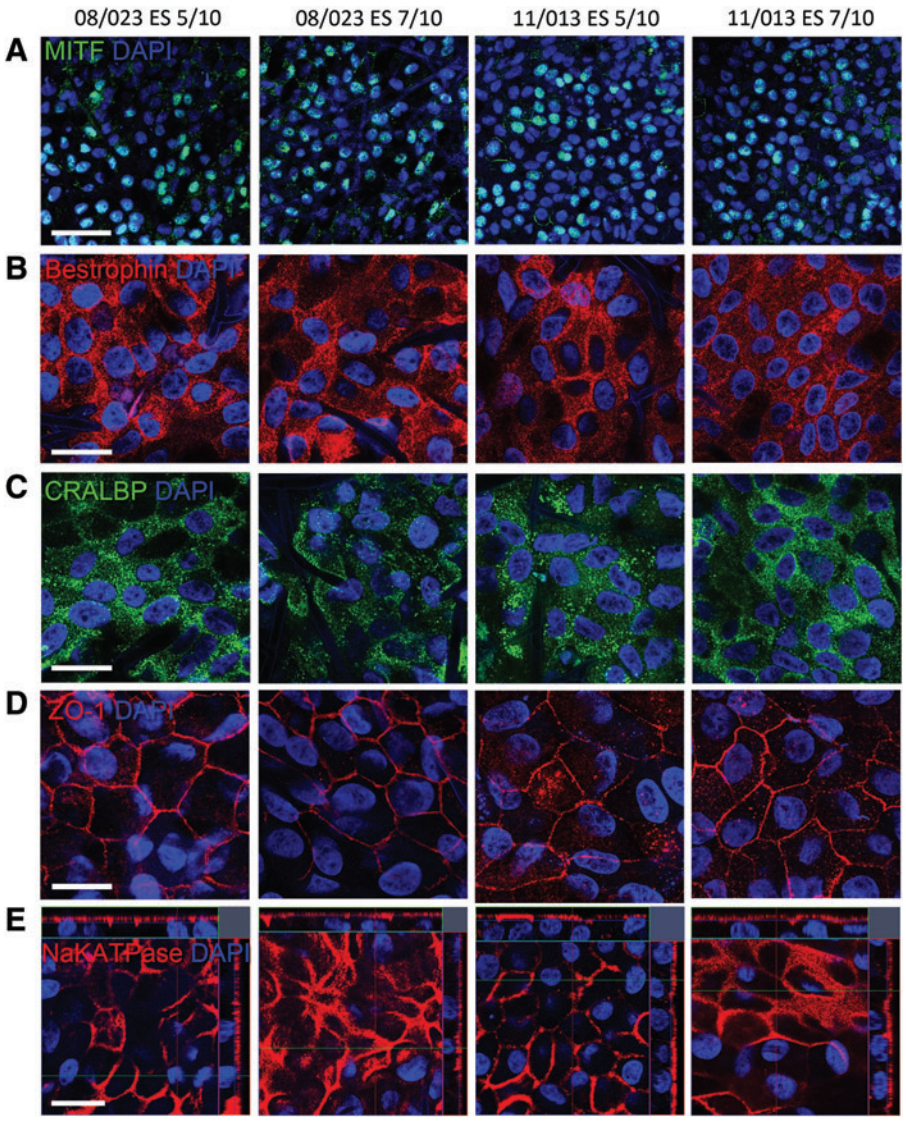

FIG. 6. Immunofluorescent (IF) staining showing expression and localization of RPE-specific proteins: **(A)** microphthalmia-associated transcription factor (MITF), **(B)** bestrophin (BEST), **(C)** cellular retinaldehyde-binding protein (CRALBP), and **(D)** tight junction protein zonula occludens 1 (ZO-1) after 42 days of culture. **(E)** Vertical confocal sections show apical localization of Na^+/K^+ATPase confirming correct polarization of the epithelial monolayers on Col IV-coated atmospheric plasma-treated materials with both investigated cell lines. Scale bars **(A)** 20 μm and **(B–E)** 10 μm. Color images available online at www.liebertpub.com/tea

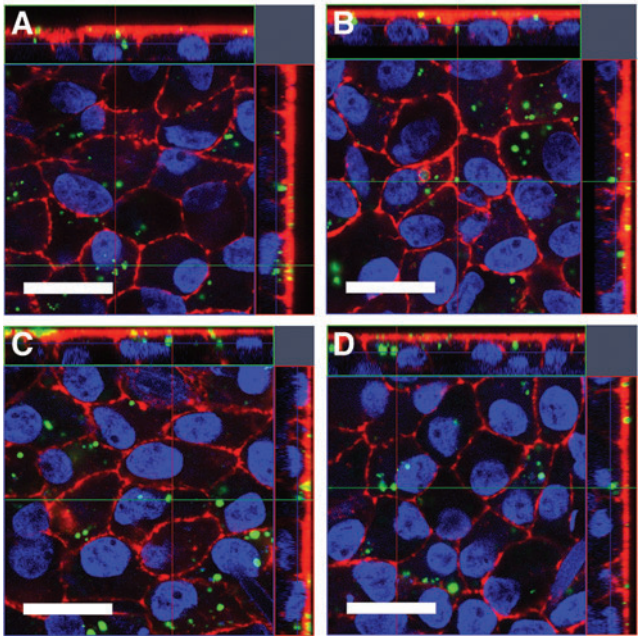

FIG. 7. The phagocytosis of photoreceptor outer segments (POS) after 92 days in culture on atmospheric plasma-treated electrospun PLCL membranes with Col IV layer: Regea 08/023 hESC-RPE cells on **(A)** ES 5/10 and **(B)** ES 7/10 membranes. Regea 11/013 hESC-RPE cells on **(C)** 5/10 and **(D)** ES 7/10 PLCL membranes. Filamentary actin was visualized with phalloidin, and the nuclei were counterstained with DAPI. Vertical confocal sections show internalization of POS by hESC-RPE cells on surface-treated membranes after 2 hr culture with porcine POS. Scale bars 10 μm. Color images available online at www.liebertpub.com/tea

apical side of the cells (Supplementary Fig. S4a). Internalized POS was not found in human foreskin fibroblasts, which were used as negative control (Supplementary Fig. S4b, c). Moreover, blocking hESC-RPE cells with anti-MERTK antibody reduced the amount of attached POS in the apical membrane and the amount of internalized POS (Supplementary Fig. S4b, c).

Discussion

Replacement of diseased RPE cells and Bruch's membrane with a healthy RPE cell layer on a thin membrane that can mimic the lost structure and function offers a viable regenerative transplantation treatment for retinal degeneration.

In this study, thin porous electrospun PLCL membranes coated with human Col IV were investigated as a carrier for the formation of a functional hESC-RPE cell monolayer. The primary aim of this work was to promote attachment, proliferation, and maturation of the hESC-RPE cells toward a functional RPE monolayer on a biodegradable thin membrane in serum-free culture conditions. Gaseous plasma-based processing is a widely utilized method for modifying a polymeric surface to enhance the cellular response thereon.[34]

The DBD plasma processing technique utilized here generates a gaseous plasma discharge in air at atmospheric pressure that is capable of permanently modifying the surface properties in a cost-effective manner. In this regard, DBD has been previously shown to enhance protein absorption and cellular responses of human lens epithelial cells.[34–36,42] Here, we assessed the impact of DBD treatment on the chemical and physical properties of the membranes and on the cellular response of hESC-RPE cells.

Biodegradable polymeric biomaterials provide the significant advantage of being able to be broken down or removed without surgical revision after they have served their 3D structural function.[43] Furthermore, they allow for the incorporation of therapeutic agents, such as anti-inflammatory drugs and growth factors, which can significantly improve cell survival in transplantation therapy.[44]

Biodegradable scaffolds fabricated from poly(α-hydroxy esters) have been investigated as potential substrates for human RPE cells and ARPE-19 cells[19,20] and Liu *et al.* have shown that electrospun PLCL fibers also support the growth of human fetal RPE cells[18,21] However, the lack of published data implies and our own empirical tests have shown that hESC-RPE cells do not adhere well on biodegradable scaffolds in serum-free conditions. Furthermore, comparison to studies carried out with immortalized RPE cell lines should be done carefully because hESC-RPE have been shown to differ, that is, in pigmentation and gene expression.[45]

hESC-RPE cells produce their own ECM including the major components of the uppermost layers of the native Bruch's membrane.[38] By using a biodegradable scaffold with a slow *in vivo* degradation time, the transplanted cells have a physical support during the transplantion. Thereafter, they can potentially generate their own matrix to replace the defects in the damaged Bruch's membrane while the scaffold is degrading.

Previous studies have indicated that electrospun PLCL fibrous membranes show no material degradation over 3-month cell culture period and demonstrate no detrimental effect on cellular response.[46] Our observations are in line with this study: hESC-RPE cells were cultured on DBD plasma-treated membranes up to 92 days without evidence of any degradation or harmful effects in the cells. In a previously reported *in vivo* study for highly porous PLCL scaffolds, the mass of the scaffold decreased to 81% after 15 weeks of subcutaneous implantation, indicating a slow degradation.[47] However, the *in vivo* degradation of electrospun PLCL membranes in intraocular tissue and subretinal space has not been studied and therefore *in vivo* experiments need to be carried out in the future to determine the suitability of these scaffolds for tissue-engineered retinal repair applications.

One important function of Bruch's membrane is allowing the reciprocal flow of small molecular substances through its layered structure.[11] Here, we showed that the prepared electrospun PLCL films had porous structure and were permeable for a small molecular weight fluorescent marker. The lowest DBD plasma dosage condition ES 5/10 did not affect the permeability of the electrospun PLCL membrane compared to the untreated membrane, whereas a slight reduction in membrane permeability was seen with the higher dosage condition ES 7/10.

In previous studies, inert PET carriers have been used as a support for electrospun poly(lactic-co-glycolic acid) (PLGA)[19] and PLCL[21] fibers in scaffolds designed for human fetal and primary RPE cells. In contrast, the manufactured electrospun films in this study were easy to handle and mechanically durable as such; no additional support was required for

the scaffold to maintain its porous fibrillar structure during handling and culture. Previously, a novel shooter instrument has been shown to enable transvitreal delivery of ultrathin rigid-elastic-carriers into the subretinal space of rabbits.[48] However, the feasibility of the instrument and surgical procedure with a biodegradable electrospun PLCL scaffold-hESC-RPE complex introduced in this study needs to be addressed in future experiments.

The polymers commonly used in tissue engineering applications are highly hydrophobic, which can hinder cellular attachment and proliferation.[34] The untreated electrospun PLCL fibers exhibited a highly hydrophobic surface, whereas atmospheric pressure DBD plasma treatment significantly increased fiber wettability, that is, increased hydrophilicity.

Moreover, XPS analysis indicated that DBD plasma treatment significantly increased the O/C ratio on the surface of electrospun PLCL fiber membranes compared with that for an untreated sample. This is attributed to the fact that DBD plasma treatment produces polar oxygen groups on the surface of the electrospun PLCL fibers and can also increase surface roughness, both of which effect the surface energy.[49] These data are consistent with the previous literature findings that also observed an increase in oxygen content on the surface of electrospun polymers after plasma treatment.[39,50]

Analysis by SEM here revealed that there was no thinning or destruction of the fibers compared between untreated and DBD plasma-treated PLCL electrospun fiber membranes, a phenomenon previously reported with low pressure (vacuum based) plasma treatment of electrospun fibers.[39] However, AFM analysis confirmed that the DBD plasma treatment increased the surface roughness of electrospun PLCL fiber membranes. Interestingly, the lower DBD plasma dosage condition ES 5/10 resulted in higher surface roughness compared with the larger DBD plasma dosage condition ES 7/10. These data support previous research, which illustrated that higher doses of plasma treatment produces a lower fiber surface roughness compared with the lower dose treatment.[50]

In this study, all the investigated membranes showed a good level of bound protein immunofluorescence staining, which uniformly dispersed across the fibers. However, XPS analysis indicated that the DBD plasma-treated electrospun PLCL membranes had a significantly higher level of nitrogen present, attributed to the introduction of the protein,[51] compared with that detected on the untreated membranes. XPS is a highly surface-sensitive quantitative spectroscopic technique that has been extensively used to determine the amount of protein on functionalized surfaces.[52] Thus, the increased nitrogen content reported in this study indicates enhanced protein binding of Col IV on DBD plasma-treated PLCL membranes compared with the untreated membranes. Furthermore, the Col IV-coated untreated electrospun PLCL membranes had an average contact angle only slightly lower than that of the untreated PLCL surface, whereas DBD plasma treatment before Col IV coating had a significant influence on the contact angle. Previously, Ai *et al.* observed a similar trend for plasma-treated poly(hydroxybutyrate-valerate) fibrous mats coated with collagen.[53]

In this study, electrospun PLCL fibers that were DBD plasma treated before deposition of a Col IV adlayer had a major beneficial effect on hESC-RPE cell attachment, proliferation, and maturation. By comparison, Col IV-coated untreated fibers failed to support an adequate response from the same hESC-RPE cells. These results are in line with previous studies that have investigated the effect of plasma treatment on immortalized RPE cells.[54,55]

In this study, the beneficial effects of the DBD plasma treatment on the hESC-RPE cell attachment and maturation were significant only with Col IV coating. It is suggested that the chemical and topographical surface conditions created by DBD plasma treatment of the PLCL fibers provides a Col IV protein conformation on the fiber surface that not only promotes attachment but also influences cell division in a way that results in the formation of a monolayer with mature epithelial function. It has been established previously that a more hydrophilic surface condition can induce the adsorption of a finer network of Col IV that enhances cellular response.[56,57]

A definite prerequisite for a biomaterial carrier intended for the clinical use of hESC-RPE cells is that it supports the formation of homogenous, mature and functional hESC-RPE monolayer. The Col IV-coated untreated PLCL membranes did not support the formation of a homogenous monolayer, and thus failed to support proper maturation of hESC-RPE. Instead, hESC-RPE monolayers on the Col IV-coated DBD plasma-treated PLCL membranes showed expression of RPE-specific markers at both gene and protein levels, abundant pigmentation, high degree of polarity, and uniform expression of tight junction protein ZO-1. Importantly, TER measurements of the hESC-RPE cells on Col IV-coated DBD plasma-treated electrospun PLCL membranes supported the formation of a tight and polarized cell monolayer, indicative of a functional RPE.

In addition, hESC-RPE cells on DBD plasma-treated electrospun PLCL membranes exhibited phagocytic activity. All of these functions are generally considered to be hallmarks of mature RPE.[4,58] Thus, this study shows that the DBD plasma-treated porous biodegradable membranes supported the growth of mature and functional hESC-RPE monolayer in serum-free culture conditions and are therefore suitable carrier candidates for retinal repair applications.

Conclusions

In this study, were produced a thin biodegradable electrospun PLCL membranes as a carrier for hESC-RPE cells for retinal cell therapy applications. The prepared membranes were modified by atmospheric pressure plasma processing and coated with Col IV to enhance cell growth and maturation. The DBD atmospheric pressure plasma treatment changed the surface charasteristics of the PLCL electrospun membranes, which led to enhanced Col IV protein binding. These DBD plasma-treated electrospun PLCL membranes had a porous structure and allowed the flow of small molecular substance through their structure. Here, we report for the first time, successful culture of mature and functional hESC-RPE cells on a porous biodegradable electrospun scaffold in serum-free culture conditions, which have potential as a tissue-engineered construct for regenerative retinal repair applications.

Ethical Issues

The National Authority for Medicolegal Affairs Finland has approved this research with human embryos (Dnro 1426/32/300/05). We also have a supportive statement from

the local ethics committee of the Pirkanmaa hospital district Finland to derive and expand hESC lines from surplus embryos not used in the treatment of infertility by the donating couples, and to use these cell lines for research purposes (R05116). No new lines were derived for this study.

Acknowledgments

The authors wish to thank the Academy of Finland (grant numbers 218050 and 137801), TEKES (the Finnish Funding Agency for Technology and Innovation), the Finnish Cultural Foundation, Pirkanmaa Regional fund (grant number 50121465), Invest Northern Ireland (grant number RD0212954), and the Northern Ireland Department for Employment and Learning (DEL) for their support. The funders had no role in study design, data collection and analysis, decision to publish, or preparation of the article. Outi Melin, Hanna Pekkanen, and Outi Heikkilä are thanked for technical assistance. Authors one and two equally contributed to this work.

Disclosure Statement

No competing financial interests exist.

References

1. Lim, L.S., Mitchell, P., Seddon, J.M., Holz, F.G., and Wong, T.Y. Age-related macular degeneration. Lancet **379,** 1728, 2012.
2. Ambati, J., and Fowler, B.J. Mechanisms of age-related macular degeneration. Neuron **75,** 26, 2012.
3. Fernndez-Robredo, P., Sancho, A., Johnen, S., Recalde, S., Gama, N., Thumann, G., Groll, J., and Garca-Layana, A. Current treatment limitations in age-related macular degeneration and future approaches based on cell therapy and tissue engineering. J Ophthalmol **2014,** 13, 2014.
4. Binder, S., Stanzel, B.V., Krebs, I., and Glittenberg, C. Transplantation of the RPE in AMD. Prog Retin Eye Res **26,** 516, 2007.
5. Schwartz, S.D., Hubschman, J.-P., Heilwell, G., Franco-Cardenas, V., Pan, C.K., Ostrick, R.M., Mickunas, E., Gay, R., Klimanskaya, I., and Lanza, R. Embryonic stem cell trials for macular degeneration: a preliminary report. Lancet **379,** 713, 2012.
6. Schwartz, S.D., Regillo, C.D., Lam, B.L., Eliott, D., Rosenfeld, P.J., Gregori, N.Z., Hubschman, J.-P., Davis, J.L., Heilwell, G., Spirn, M., Maguire, J., Gay, R., Bateman, J., Ostrick, R.M., Morris, D., Vincent, M., Anglade, E., Del Priore, L.V., and Lanza, R. Human embryonic stem cell-derived retinal pigment epithelium in patients with age-related macular degeneration and Stargardt's macular dystrophy: follow-up of two open-label phase 1/2 studies. Lancet 2014.
7. Vaajasaari, H., Ilmarinen, T., Juuti-Uusitalo, K., Rajala, K., Onnela, N., Narkilahti, S., Suuronen, R., Hyttinen, J., Uusitalo, H., and Skottman, H. Toward the defined and xeno-free differentiation of functional human pluripotent stem cell derived retinal pigment epithelial cells. Mol Vis **17,** 558, 2011.
8. Vugler, A., Lawrence, J., Walsh, J., Carr, A., Gias, C., Semo, M., Ahmado, A., da Cruz, L., Andrews, P., and Coffey, P. Embryonic stem cells and retinal repair. Mech Dev **124,** 807, 2007.
9. Carr, A.-J.F., Smart, M.J.K., Ramsden, C.M., Powner, M.B., da Cruz, L., and Coffey, P.J. Development of human embryonic stem cell therapies for age-related macular degeneration. Trends Neurosci **36,** 385, 2013.
10. Rowland, T.J., Blaschke, A.J., Buchholz, D.E., Hikita, S.T., Johnson, L.V., and Clegg, D.O. Differentiation of human pluripotent stem cells to retinal pigmented epithelium in defined conditions using purified extracellular matrix proteins. J Tissue Eng Regen Med **7,** 642, 2013.
11. Booij, J.C., Baas, D.C., Beisekeeva, J., Gorgels, T.G.M.F., and Bergen, A.A.B. The dynamic nature of Bruch's membrane. Prog Retin Eye Res **29,** 1, 2010.
12. Zarbin, M.A., Casaroli-Marano, R.P., and Rosenfeld, P.J. Age-related macular degeneration: clinical findings, histopathology and imaging techniques. Dev Ophthalmol **53,** 1, 2014.
13. Tezel, T.H., Kaplan, H.J., and Del Priore, L.V. Fate of human retinal pigment epithelial cells seeded onto layers of human Bruch's membrane. Invest Ophthalmol Vis Sci **40,** 467, 1999.
14. Sugino, I.K., Sun, Q., Wang, J., Nunes, C.F., Cheewatrakoolpong, N., Rapista, A., Johnson, A.C., Malcuit, C., Klimanskaya, I., Lanza, R., and Zarbin, M.A. Comparison of FRPE and human embryonic stem cell–derived RPE behavior on aged human Bruch's membrane. Invest Ophthalmol Vis Sci **52,** 4979, 2011.
15. Diniz, B., Thomas, P., Thomas, B., Ribeiro, R., Hu, Y., Brant, R., Ahuja, A., Zhu, D., Liu, L., Koss, M., Maia, M., Chader, G., Hinton, D.R., and Humayun, M.S. Subretinal implantation of retinal pigment epithelial cells derived from human embryonic stem cells: improved survival when implanted as a monolayer. Invest Ophthalmol Vis Sci **54,** 5087, 2013.
16. Treharne, A.J., Thomson, H.A.J., Grossel, M.C., and Lotery, A.J. Developing methacrylate-based copolymers as an artificial Bruch's membrane substitute. J Biomed Mater Res A **100A,** 2358, 2012.
17. Singh, S., Woerly, S., and McLaughlin, B.J. Natural and artificial substrates for retinal pigment epithelial monolayer transplantation. Biomaterials **22,** 3337, 2001.
18. Xiang, P., Wu, K.-C., Zhu, Y., Xiang, L., Li, C., Chen, D.-L., Chen, F., Xu, G., Wang, A., Li, M., and Jin, Z.-B. A novel Bruch's membrane-mimetic electrospun substrate scaffold for human retinal pigment epithelium cells. Biomaterials **35,** 9777, 2014.
19. Warnke, P.H., Alamein, M., Skabo, S., Stephens, S., Bourke, R., Heiner, P., and Liu, Q. Primordium of an artificial Bruch's membrane made of nanofibers for engineering of retinal pigment epithelium cell monolayers. Acta Biomater **9,** 9414, 2013.
20. McHugh, K.J., Tao, S.L., and Saint-Geniez, M. Porous poly(epsilon-caprolactone) scaffolds for retinal pigment epithelium transplantation. Invest Ophthalmol Vis Sci **55,** 1754, 2014.
21. Liu, Z., Yu, N., Holz, F.G., Yang, F., and Stanzel, B.V. Enhancement of retinal pigment epithelial culture characteristics and subretinal space tolerance of scaffolds with 200 nm fiber topography. Biomaterials **35,** 2837, 2014.
22. Shadforth, A.M.A., George, K.A., Kwan, A.S., Chirila, T.V., and Harkin, D.G. The cultivation of human retinal pigment epithelial cells on Bombyx mori silk fibroin. Biomaterials **33,** 4110, 2012.
23. Stanzel, B.V., Liu, Z., Somboonthanakij, S., Wongsawad, W., Brinken, R., Eter, N., Corneo, B., Holz, F.G., Temple,

S., Stern, J.H., and Blenkinsop, T.A. Human RPE stem cells grown into polarized RPE monolayers on a polyester matrix are maintained after grafting into rabbit subretinal space. Stem Cell Rep **2,** 64, 2014.

24. Kamao, H., Mandai, M., Okamoto, S., Sakai, N., Suga, A., Sugita, S., Kiryu, J., and Takahashi, M. Characterization of human induced pluripotent stem cell-derived retinal pigment epithelium cell sheets aiming for clinical application. Stem Cell Rep **2,** 205, 2014.
25. Kanemura, H., Go, M.J., Shikamura, M., Nishishita, N., Sakai, N., Kamao, H., Mandai, M., Morinaga, C., Takahashi, M., and Kawamata, S. Tumorigenicity studies of induced pluripotent stem cell (iPSC)-derived retinal pigment epithelium (RPE) for the treatment of age-related macular degeneration. PLoS One **9,** e85336, 2014.
26. Lu, B., Zhu, D., Hinton, D., Humayun, M.S., and Tai, Y.C. Mesh-supported submicron parylene-C membranes for culturing retinal pigment epithelial cells. Biomed Microdevices **14,** 659, 2012.
27. Subrizi, A., Hiidenmaa, H., Ilmarinen, T., Nymark, S., Dubruel, P., Uusitalo, H., Yliperttula, M., Urtti, A., and Skottman, H. Generation of hESC-derived retinal pigment epithelium on biopolymer coated polyimide membranes. Biomaterials **33,** 8047, 2012.
28. Hu, Y., Liu, L., Lu, B., Zhu, D., Ribeiro, R., Diniz, B., Thomas, P.B., Ahuja, A.K., Hinton, D.R., Tai, Y.C., Hikita, S.T., Johnson, L.V., Clegg, D.O., Thomas, B.B., and Humayun, M.S. A novel approach for subretinal implantation of ultrathin substrates containing stem cell-derived retinal pigment epithelium monolayer. Ophthalmic Res **48,** 186, 2012.
29. Thomson, H.A.J., Treharne, A.J., Walker, P., Grossel, M.C., and Lotery, A.J. Optimisation of polymer scaffolds for retinal pigment epithelium (RPE) cell transplantation. Br J Ophthalmol **95,** 563, 2011.
30. Zhang, Y.Z., Su, B., Venugopal, J., Ramakrishna, S., and Lim, C.T. Biomimetic and bioactive nanofibrous scaffolds from electrospun composite nanofibers. Int J Nanomedicine **2,** 623, 2007.
31. Lee, J., Tae, G., Kim, Y.H., Park, I.S., and Kim, S.H. The effect of gelatin incorporation into electrospun poly(L-lactide-co-epsilon-caprolactone) fibers on mechanical properties and cytocompatibility. Biomaterials **29,** 1872, 2008.
32. Ugarte, M., Hussain, A.A., and Marshall, J. An experimental study of the elastic properties of the human Bruch's membrane-choroid complex: relevance to ageing. Br J Ophthalmol **90,** 621, 2006.
33. Thieltges, F., Stanzel, B.V., Liu, Z., and Holz, F.G. A nanofibrillar surface promotes superior growth characteristics in cultured human retinal pigment epithelium. Ophthalmic Res **46,** 133, 2011.
34. D'Sa, R.A., Burke, G.A., and Meenan, B.J. Protein adhesion and cell response on atmospheric pressure dielectric barrier discharge-modified polymer surfaces. Acta Biomater **6,** 2609, 2010.
35. D'Sa, R.A., Raj, J., McMahon, M.A.S., McDowell, D.A., Burke, G.A., and Meenan, B.J. Atmospheric pressure plasma induced grafting of poly(ethylene glycol) onto silicone elastomers for controlling biological response. J Colloid Interface Sci **375,** 193, 2012.
36. D'Sa, R.A., Burke, G.A., and Meenan, B.J. Lens epithelial cell response to atmospheric pressure plasma modified poly(methylmethacrylate) surfaces. J Mater Sci Mater Med **21,** 1703, 2010.
37. Liu, C., Brown, N.M.D., and Meenan, B.J. Dielectric barrier discharge (DBD) processing of PMMA surface: optimization of operational parameters. Surf Coat Technol **201,** 2341, 2006.
38. Sorkio, A., Hongisto, H., Kaarniranta, K., Uusitalo, H., Juuti-Uusitalo, K., and Skottman, H. Structure and barrier properties of human embryonic stem cell derived retinal pigment epithelial cells are affected by extracellular matrix protein coating. Tissue Eng Part A **20,** 622, 2013.
39. Martins, A., Pinho, E.D., Faria, S., Pashkuleva, I., Marques, A.P., Reis, R.L., and Neves, N.M. Surface modification of electrospun polycaprolactone nanofiber meshes by plasma treatment to enhance biological performance. Small **5,** 1195, 2009.
40. Skottman, H. Derivation and characterization of three new human embryonic stem cell lines in Finland. In Vitro Cell Dev Biol Anim **46,** 206, 2010.
41. Juuti-Uusitalo, K., Delporte, C., Gregoire, F., Perret, J., Huhtala, H., Savolainen, V., Nymark, S., Hyttinen, J., Uusitalo, H., Willermain, F., and Skottman, H. Aquaporin expression and function in human pluripotent stem cell-derived retinal pigmented epithelial cells. Invest Ophthalmol Vis Sci **54,** 3510, 2013.
42. Jacobs, T., Declercq, H., De Geyter, N., Cornelissen, R., Dubruel, P., Leys, C., Beaurain, A., Payen, E., and Morent, R. Plasma surface modification of polylactic acid to promote interaction with fibroblasts. J Mater Sci Mater Med **24,** 469, 2013.
43. Ulery, B.D., Nair, L.S., and Laurencin, C.T. Biomedical applications of biodegradable polymers. J Polym Sci B Polym Phys **49,** 832, 2011.
44. Sakai, Y., Furukawa, K., Ushida, T., Tateishi, T., and Suzuki, M. *In vitro* organization of biohybrid rat liver tissue incorporating growth factor- and hormone-releasing biodegradable polymer microcapsules. Cell Transplant **10,** 479, 2001.
45. Klimanskaya, I., Hipp, J., Rezai, K.A., West, M., Atala, A., and Lanza, R. Derivation and comparative assessment of retinal pigment epithelium from human embryonic stem cells using transcriptomics. Cloning Stem Cells **6,** 217, 2004.
46. Dong, Y., Yong, T., Liao, S., Chan, C.K., Stevens, M.M., and Ramakrishna, S. Distinctive degradation behaviors of electrospun polyglycolide, poly(DL-lactide-co-glycolide), and poly(L-lactide-co-epsilon-caprolactone) nanofibers cultured with/without porcine smooth muscle cells. Tissue Eng Part A **16,** 283, 2010.
47. Jeong, S.I., Kim, B.S., Kang, S.W., Kwon, J.H., Lee, Y.M., Kim, S.H., and Kim, Y.H. *In vivo* biocompatibilty and degradation behavior of elastic poly(L-lactide-co-epsilon-caprolactone) scaffolds. Biomaterials **25,** 5939, 2004.
48. Stanzel, B.V., Liu, Z., Brinken, R., Braun, N., Holz, F.G., and Eter, N. Subretinal delivery of ultrathin rigid-elastic cell carriers using a metallic shooter instrument and biodegradable hydrogel encapsulation. Invest Ophthalmol Vis Sci **53,** 490, 2012.
49. Nandakumar, A., Birgani, Z.T., Santos, D., Mentink, A., Auffermann, N., Werf, K.v.d., Bennink, M., Moroni, L., Blitterswijk, C.v., and Habibovic, P. Surface modification of electrospun fibre meshes by oxygen plasma for bone regeneration. Biofabrication **5,** 015006, 2013.

50. Yan, D., Jones, J., Yuan, X.Y., Xu, X.H., Sheng, J., Lee, J.C.M., Ma, G.Q., and Yu, Q.S. Plasma treatment of electrospun PCL random nanofiber meshes (NFMs) for biological property improvement. J Biomed Mater Res A **101A,** 963, 2013.
51. Chu, P.K., Chen, J.Y., Wang, L.P., and Huang, N. Plasma-surface modification of biomaterials. Mater Sci Eng R Rep **36,** 143, 2002.
52. Baio, J.E., Weidner, T., Baugh, L., Gamble, L.J., Stayton, P.S., and Castner, D.G. Probing the orientation of electrostatically immobilized Protein G B1 by time-of-flight secondary ion spectrometry, sum frequency generation, and near-edge X-ray adsorption fine structure spectroscopy. Langmuir **28,** 2107, 2012.
53. Ai, J., Heidari, S., Ghorbani, F., Ejazi, F., Biazar, E., Asefnejad, A., Pourshamsian, K., and Montazeri, M. Fabrication of coated-collagen electrospun PHBV nanofiber film by plasma method and its cellular study. J Nanomater **2011,** 1, 2011.
54. Tezcaner, A., Bugra, K., and Hasırcı, V. Retinal pigment epithelium cell culture on surface modified poly(hydroxybutyrate-co-hydroxyvalerate) thin films. Biomaterials **24,** 4573, 2003.
55. Krishna, Y., Sheridan, C., Kent, D., Kearns, V., Grierson, I., and Williams, R. Expanded polytetrafluoroethylene as a substrate for retinal pigment epithelial cell growth and transplantation in age-related macular degeneration. Br J Ophthalmol **95,** 569, 2011.
56. Aumailley, M., and Timpl, R. Attachment of cells to basement membrane collagen type IV. J Cell Biol **103,** 1569, 1986.
57. Kalluri, R., and Cosgrove, D. Assembly of type IV collagen: insights from α3 (IV) collagen-deficient mice. J Biol Chem **275,** 12719, 2000.
58. Burke, J.M. Epithelial phenotype and the RPE: is the answer blowing in the Wnt? Prog Retin Eye Res **27,** 579, 2008.

Address correspondence to:
George A. Burke, PhD
Nanotechnology and Integrated
Bioengineering Centre (NIBEC)
School of Engineering
University of Ulster
Jordanstown Campus, Shore Road
Newtownabbey Co. Antrim BT37 0 QB
Northern Ireland

E-mail: g.burke@ulster.ac.uk

Received: November 19, 2014
Accepted: April 23, 2015
Online Publication Date: June 30, 2015